frontiers | Research Topics

Women in infectious agents and disease: 2022

Edited by
Beatrice Vitali, Svetlana Khaiboullina and Nayeli Alva-Murillo

Published in
Frontiers in Microbiology

ISSN 1664-8714
ISBN 978-2-83251-276-0
DOI 10.3389/978-2-83251-276-0

About Frontiers

Frontiers is more than just an open access publisher of scholarly articles: it is a pioneering approach to the world of academia, radically improving the way scholarly research is managed. The grand vision of Frontiers is a world where all people have an equal opportunity to seek, share and generate knowledge. Frontiers provides immediate and permanent online open access to all its publications, but this alone is not enough to realize our grand goals.

Frontiers journal series

The Frontiers journal series is a multi-tier and interdisciplinary set of open-access, online journals, promising a paradigm shift from the current review, selection and dissemination processes in academic publishing. All Frontiers journals are driven by researchers for researchers; therefore, they constitute a service to the scholarly community. At the same time, the *Frontiers journal series* operates on a revolutionary invention, the tiered publishing system, initially addressing specific communities of scholars, and gradually climbing up to broader public understanding, thus serving the interests of the lay society, too.

Dedication to quality

Each Frontiers article is a landmark of the highest quality, thanks to genuinely collaborative interactions between authors and review editors, who include some of the world's best academicians. Research must be certified by peers before entering a stream of knowledge that may eventually reach the public - and shape society; therefore, Frontiers only applies the most rigorous and unbiased reviews. Frontiers revolutionizes research publishing by freely delivering the most outstanding research, evaluated with no bias from both the academic and social point of view. By applying the most advanced information technologies, Frontiers is catapulting scholarly publishing into a new generation.

What are Frontiers Research Topics?

Frontiers Research Topics are very popular trademarks of the *Frontiers journals series*: they are collections of at least ten articles, all centered on a particular subject. With their unique mix of varied contributions from Original Research to Review Articles, Frontiers Research Topics unify the most influential researchers, the latest key findings and historical advances in a hot research area.

Find out more on how to host your own Frontiers Research Topic or contribute to one as an author by contacting the Frontiers editorial office: frontiersin.org/about/contact

Women in infectious agents and disease: 2022

Topic editors
Beatrice Vitali — University of Bologna, Italy
Svetlana Khaiboullina — University of Nevada, Reno, United States
Nayeli Alva-Murillo — University of Guanajuato, Mexico

Topic coordinator
Pragati Agnihotri — Advanced BioScience Laboratories, Inc (ABL), United States

Citation
Vitali, B., Khaiboullina, S., Alva-Murillo, N., eds. (2023). *Women in infectious agents and disease: 2022*. Lausanne: Frontiers Media SA. doi: 10.3389/978-2-83251-276-0

Table of contents

frontiers | Frontiers in Microbiology

TYPE Original Research
PUBLISHED 09 September 2022
DOI 10.3389/fmicb.2022.998849

OPEN ACCESS

EDITED BY
Svetlana Khaiboullina,
University of Nevada, Reno,
United States

REVIEWED BY
Sylvia Bruisten,
Public Health Service of
Amsterdam, Netherlands
Steven S. Witkin,
Cornell University, United States

*CORRESPONDENCE
Antonella Marangoni
antonella.marangoni@unibo.it

†These authors have contributed equally to this work and share first authorship
‡These authors have contributed equally to this work and share last authorship

SPECIALTY SECTION
This article was submitted to Infectious Agents and Disease, a section of the journal Frontiers in Microbiology

RECEIVED 20 July 2022
ACCEPTED 08 August 2022
PUBLISHED 09 September 2022

CITATION
Morselli S, Foschi C, Laghi L, Zagonari S, Patuelli G, Camboni T, Ceccarani C, Consolandi C, Djusse ME, Pedna MF, Marangoni A, Severgnini M and Sambri V (2022) Torquetenovirus in pregnancy: Correlation with vaginal microbiome, metabolome and pro-inflammatory cytokines. *Front. Microbiol.* 13:998849. doi: 10.3389/fmicb.2022.998849

Torquetenovirus in pregnancy: Correlation with vaginal microbiome, metabolome and pro-inflammatory cytokines

Sara Morselli[1†], Claudio Foschi[1,2†], Luca Laghi[3,4], Sara Zagonari[5], Giulia Patuelli[5], Tania Camboni[6], Camilla Ceccarani[6], Clarissa Consolandi[6], Marielle Ezekielle Djusse[1], Maria Federica Pedna[7], Antonella Marangoni[1*], Marco Severgnini[6‡] and Vittorio Sambri[1,7‡]

[1]Microbiology Unit, Department of Specialized, Experimental and Diagnostic Medicine (DIMES), University of Bologna, Bologna, Italy, [2]Microbiology Unit, IRCCS Azienda Ospedaliero-Universitaria di Bologna, Bologna, Italy, [3]Department of Agricultural and Food Sciences (DISTAL), Centre of Foodomics, University of Bologna, Cesena, Italy, [4]Interdepartmental Centre for Agri-Food Industrial Research (CIRI Agrifood), University of Bologna, Cesena, Italy, [5]Family Advisory Health Centres, Ravenna, Italy, [6]Institute of Biomedical Technologies, National Research Council, Segrate, Italy, [7]Great Romagna Hub Laboratory, Unit of Microbiology, Pievesestina di Cesena, Italy

Torquetenovirus (TTV) is a negative sense, single-stranded DNA virus present in many body fluids of apparently healthy individuals. At present, it is considered a non-pathogenic endogenous virus. TTV can be detected in the vagina of pregnant women, its abundance being modulated with the extent of immune system activation. Until now, there is only scarce information regarding the association between TTV and the composition of the vaginal environment. Therefore, this study aimed to assess the presence of TTV in the vaginal ecosystem of a cohort of white women with a normal pregnancy ($n = 60$) at different gestational stages (first, second and third trimester) and in 9 subjects suffering a first trimester miscarriage. For each woman, we determined (i) the presence and titer of TTV, (ii) the vaginal bacterial composition by means of Nugent score and 16S rRNA gene sequencing, (iii) the vaginal metabolic profiles through ^{1}H-NMR spectroscopy, and (iv) the vaginal concentration of two pro-inflammatory cytokines (IL-6 and IL-8). More than one third of women were found negative for TTV at all gestational stages. Although not statistically significant, the positivity for TTV dropped from 53.3% in the first to 36.6% in the third trimester. TTV loads varied greatly among vaginal samples, ranging between 2×10^1 and 2×10^5 copies/reaction. No difference in TTV prevalence and loads was observed between women with normal pregnancies and miscarriages. The presence of TTV was more common in women with a higher vaginal leucocyte count ($p = 0.02$). The levels of IL-6 ($p = 0.02$), IL-8 ($p = 0.03$), propionate ($p = 0.001$) and cadaverine ($p = 0.006$) were significantly higher in TTV-positive samples. TTV titer was positively correlated with the concentrations of 4-hydroxyphenyllactate ($p < 0.0001$), isoleucine ($p = 0.01$) and phenylalanine ($p = 0.04$). TTV-positive samples were characterized by a higher relative abundance of *Sneathia* ($p = 0.04$) and *Shuttleworthia*

($p = 0.0009$). In addition, a trend toward a decrease of *Lactobacillus crispatus* and *Lactobacillus jensenii*, and an increase of *Lactobacillus iners* was observed for TTV-positive samples. In conclusion, we found that TTV is quite common in women with normal pregnancy outcomes, representing a possible predictor of local immune status.

KEYWORDS

torquetenovirus, TTV, vaginal microbiome, pregnancy, vaginal metabolome, women's health

Introduction

Throughout a woman's lifespan, the vaginal microbiome undergoes major changes in response to various factors, such as hormonal levels, sexual habits, hygiene, pregnancy, pharmaceutical treatments, and urogenital infections (Kroon et al., 2018; Parolin et al., 2018; Ceccarani et al., 2019; Severgnini et al., 2022).

During healthy pregnancies, the vaginal microbiome is usually characterized by a significant decrease in overall bacterial diversity, an increased stability, and an enrichment of *Lactobacillus* spp. (Dall'Asta et al., 2021; Marangoni et al., 2021). A lactobacilli-dominated vaginal microbiota is associated with low inflammation and low immune system activation, thus contributing to the maintenance of maternal-fetal health (Witkin et al., 2019).

In the case of bacterial vaginosis (BV), a condition of vaginal dysbiosis characterized by a depletion of lactobacilli and an overgrowth of several anaerobes (e.g., *Gardnerella vaginalis*, *Fannyhessea vaginae*, *Prevotella* spp., *Megasphaera* spp.), an increased local inflammation is present, with the risk of pregnancy-related complications and preterm birth (Prince et al., 2014; Anahtar et al., 2015; Di Simone et al., 2020).

The changes in the vaginal bacterial communities are accompanied by profound alterations in the composition of vaginal metabolites. High concentrations of biogenic amines (e.g., putrescine, cadaverine, and trimethylamine) and short-chain fatty acids (SCFAs) are the most common fingerprints of BV (Srinivasan et al., 2015; Parolin et al., 2018).

Recently, it has been shown that Torquetenovirus (TTV), a non-pathogenic endogenous virus, can be detected in the vagina of pregnant women, its abundance being modulated with the extent of immune system activation (Maggi and Bendinelli, 2010; Tozetto-Mendoza et al., 2020, 2022). TTV has a worldwide distribution, and it can be transmitted by multiple routes, including bloodborne, oro-fecal, respiratory, and sexual transmission (Maggi and Bendinelli, 2010; Haloschan et al., 2014). This virus appears to replicate mainly in T lymphocytes, but the exact cellular receptors for TTV are still unknown. Anyway, even though TTV can be considered an orphan virus, TTV viremia may potentially be a simple and sensitive measure of immune system function of the host (Shibayama et al., 2001; Maggi et al., 2010).

Until now, there is only scarce information on the association between TTV titer and the microbial/metabolic composition of the vaginal environment (Tozetto-Mendoza et al., 2020, 2022). Moreover, the mechanisms associated with variations in vaginal TTV titer, as well as the relevance of monitoring TTV loads in pregnancy remain open questions.

Therefore, in this study we assessed the presence of TTV in the vaginal ecosystem of a cohort of white women with a normal pregnancy ($n = 60$) at different gestational stages (i.e., first, second and third trimester) and in 9 subjects suffering a first trimester miscarriage. For each woman, we determined (i) the presence and titer of TTV in the vaginal ecosystem by means of a real-time PCR assay, (ii) the vaginal bacterial composition by means of a microscopic scoring system (Nugent score) and by sequencing of the V3–V4 hypervariable regions of the 16S rRNA gene, (iii) the vaginal metabolic profiles through ^{1}H-NMR spectroscopy, and (iv) the vaginal concentration of two pro-inflammatory cytokines (IL-6 and IL-8).

Materials and methods

Study group and sample collection

From April 2019 all the white pregnant women attending the Family Advisory Health Centers of Ravenna (Italy) were considered eligible for the study. Exclusion criteria included the following: (i) age<18 years; (ii) being positive for HIV infection; (iii) obesity (body mass index >33); (iv) medically assisted procreation; (v) use of antimicrobials in the month prior the enrollment; (vi) use of vaginal topical agents in the 2 weeks before the enrollment; (vii) presence of chronic diseases (e.g., diabetes, autoimmune disorders, malignancies); (viii) drug addiction or heavy smokers (>15 cigarettes/day). Furthermore, women were excluded if a diagnosis of sexually transmitted infections (STIs) (i.e., *Chlamydia trachomatis, Neisseria gonorrhoeae, Trichomonas vaginalis, Mycoplasma genitalium*) or aerobic vaginitis was made. For each woman a clinical visit was performed at gestational stages 9–13 weeks (first trimester), 20–24 weeks (second trimester), and 32–34

weeks (third trimester). At each time point, two vaginal swabs were collected: the first one (E-swab, Copan, Brescia, Italy) was used for microbiological tests, while the second was collected with a sterile cotton bud, re-suspended in 1 ml of sterile saline, and stored at−80°C until use. Frozen vaginal swabs were thawed, vortexed for 1 min and removed from the liquid. After centrifugation (10,000 × g for 15 min) cell-free supernatants were used for metabolomic analysis and cytokine detection, whereas cell-pellets were employed both for TTV detection and vaginal microbiome profiling (see specific paragraphs).

Ethics statement

The study protocol was approved by the Ethics Committee of Romagna (CEROM) (no 2032 of 21st February 2018) and it was carried out in accordance with the Declaration of Helsinki. Each woman gave written informed consent to participate in the study.

Microbiological investigations

A commercial nucleic acid amplification technique (NAAT) was used to exclude the presence of STIs (Seeplex STI Master Panel 1, Seegene, Seoul, South Korea), whereas candidiasis and aerobic vaginitis diagnosis was performed by microscopic examination and microbial cultures, as described elsewhere (Donders et al., 2011; Yano et al., 2019).

Based on Nugent score, a Gram stain scoring system evaluating for the presence of different bacterial morphotypes (Nugent et al., 1991), women were categorized into 3 groups: 'H' (healthy; score 0–3; normal lactobacilli-dominated microbiota), 'I' (score 4–6; intermediate microbiota), 'BV' (score 7–10; bacterial vaginosis) (Zozaya-Hinchliffe et al., 2010).

The presence of vaginal leukocytes (white blood cells: WBCs) was evaluated after visualization of a minimum of five fields under light microscopy at 400×. Samples were categorized as 'minimal or no inflammation' in case of<5 WBCs in all visualized fields or as 'significant inflammation' in presence of ≥5 WBCs in at least one field visualized (Geisler et al., 2004).

Vaginal microbiome profiling

Nucleic acids were extracted from vaginal swabs by means of the Versant molecular system (Siemens Healthcare Diagnostics, Tarrytown, NY, USA) (Marangoni et al., 2015). Afterwards, the V3–V4 hypervariable regions of the bacterial 16S rRNA gene were amplified according to the 16S metagenomic sequencing library preparation protocol (Illumina, San Diego, CA, USA), as previously described (Severgnini et al., 2021). Raw reads were analyzed according to the procedure reported by (Severgnini et al., 2021).

Zero-radius Operational Taxonomic Units (zOTUs) creation, taxonomy assignments, and diversity analyses were performed using the QIIME suite (release 1.9.0) (Caporaso et al., 2010), unoise3 algorithm (Edgar, 2016), RDP classifier (Wang et al., 2007), and SILVA 16S rRNA database (release 132, https://www.arb/silva.de/fileadmin/silva_databases/qiime/Silva_132_release.zip).

As already reported, characterization of *Lactobacillus* spp. was performed by BLAST-aligning all reads belonging to that genus to a custom reference database (Ceccarani et al., 2019).

Alpha-diversity was evaluated according to several microbial diversity metrics (i.e., chao1, Shannon index, observed species, Good's coverage, and Faith's phylogenetic distance), whereas beta-diversity analysis was performed using both weighted and unweighted Unifrac metrics (Lozupone et al., 2011), and through the Principal Coordinates Analysis (PCoA).

Detection of TTV in the vaginal ecosystem

Starting from the remaining DNA eluate, all the vaginal swabs were tested for the presence of TTV as previously reported (Maggi et al., 2001; Tozetto-Mendoza et al., 2022).

The PCR reaction mixtures (final volume: 25 μL) included 12.5 μL of Platinum Quantitative PCR Supermix-UDG with ROX (Invitrogen, Waltham, MA, USA), 250 nM of primers, 62 nM of the probe, and 2.5 μL of template. All PCR reactions were performed with the following cycling conditions using a QuantStudio Real-Time PCR system (Applied Biosystems, Waltham, MA, USA): 2 min at 50°C, 15 s at 95°C, and 40 cycles of 15 s at 95°C and 60 s at 60°C.

A standard curve with known amounts of a synthetic oligonucleotide was used for TTV quantification (Tozetto-Mendoza et al., 2022). Results were expressed as log10 DNA copies/reaction.

Cytokine detection

The concentration of IL-6 (pg/ml) and IL-8 (pg/ml) was determined on the cell-free supernatants of the vaginal swabs by means of commercial ELISA assays (Simple Plex Human IL-6 and IL-8 Cartridges, R&D Systems, Minneapolis, MN, USA), following manufacturer's instructions (Brys et al., 2020).

Metabolomic analysis

Metabolomic analysis was performed by means of a ^{1}H-NMR spectroscopy starting from 700 μl of the cell-free

supernatants of the vaginal swabs, using an AVANCE III spectrometer (Bruker, Milan, Italy), as previously reported (Foschi et al., 2018; Zhu et al., 2019). The signals were assigned by comparing their multiplicity and chemical shift with Chenomx software data bank (ver 8.3, Chenomx Inc., Edmonton, Alberta, Canada).

Data analysis and statistics

Statistical analyses were conducted by using GraphPad Prism software (version 5.02; GraphPad Software, San Diego, CA, USA) and Matlab (Software version 7.7.0, Natick, MA, USA). Fisher's exact test was used to compare categorical data (i.e., presence of TTV stratified by the vaginal status), whereas ANOVA test, followed by Tukey's multiple comparisons test, was employed to compare TTV loads among the different categories. TTV loads were correlated to metabolite concentrations by calculating the Spearman correlation coefficient.

Statistical evaluation of the alpha-diversity indices was performed by non-parametric Monte Carlo-based tests, whereas beta-diversity differences were assessed by a permutation test with pseudo F-ratios ("adonis" function from R package "vegan", version 2.0-10 Oksanen et al., 2013). Pairwise relative abundance analysis was performed using a non-parametric Mann–Whitney U test.

Statistical significance (p-value <0.05) was assessed after adjustment for multiple comparisons (i.e., Benjamini-Hochberg correction, with a FDR of 0.25).

Correlation between microbial composition at the genus level and presence/absence of TTV was calculated using the point biserial correlation (Gupta, 1960), whereas the correlation between microbial profiles and TTV loads (log-transformed TTV copy number) was performed using Spearman's rank-based correlation coefficient. Only coefficients showing a p-value of the linear model <0.05 were considered.

Data availability

Raw sequencing data of 16S rRNA gene are available at NCBI Short-reads Archive (SRA) with BioProject accession number PRJNA766806 (https://www.ncbi.nlm.nih.gov/sra/PRJNA766806).

Results

Study population

A total of 60 pregnant women with a median age of 31 years (min–max: 21–44) completed the study. In addition, 9 women (median age: 35 years; min–max: 23–41) who had a spontaneous first trimester miscarriage (gestational age: 11–13 weeks) were also included.

Overall, excluding specimens from women with miscarriages, 118 vaginal samples (65.6%) were characterized by a lactobacilli-dominated flora (Nugent score 0–3), 43 (23.9%) by an intermediate microbiota (Nugent score: 4–6), and the remaining 19 (10.5%) harbored a BV-associated bacterial composition (Nugent score: 7–10).

It is noteworthy that a significant reduction of dysbiotic cases was noticed ($p = 0.002$) when moving from the first to the third trimester of pregnancy. Finally, women who suffered a first trimester miscarriage ($n = 9$) were mainly characterized by a condition of dysbiosis (i.e., 6 with an intermediate microbiota and 2 with a BV condition).

Detection of TTV

Overall, considering all the specimens belonging to the 60 women who completed the study, 42.7% (77/180) of the tested vaginal swabs were positive for TTV.

Stratifying the samples by the gestational age ($n = 60$ per time point), there was a non-significant decrease in TTV positivity between samples obtained in the first, second and third trimester. In fact, 32 (53.3%) were TTV-positive in the first trimester, 23 (38.3%) in the second, and 22 (36.6%) in the third. No difference in TTV prevalence was found when comparing normal pregnancies with miscarriages: in fact, TTV was detected in about half (5/9; 55.5%) of the women who suffered a first trimester miscarriage.

Considering each subject throughout the pregnancy, more than one third of women were found negative for TTV at all three trimesters of pregnancy (25/60; 41.6%). Conversely, 26.6% of women (16/60) were positive for TTV at each trimester. Thirteen of the remaining cases were characterized by a TTV positivity in the first and/or second trimester, with a negativity at the end of pregnancy.

TTV loads (expressed as log10 DNA copies/reaction) varied greatly among vaginal samples, ranging between 1.4 (about 26 copies/reaction) and 5.3 (about 209,000 copies), with a mean ($\pm$ standard deviation, SD) of 3.06 ± 0.96. No significant difference in TTV titer was found between women with a miscarriage and women with a normal pregnancy at the first trimester (2.8 ± 0.8 vs. 2.1 ± 0.5; $p = 0.06$).

Correlations between TTV and available variables

Considering only the first trimester of pregnancy, no difference in the median age among TTV-positive (30 years) and TTV-negative (32 years) women was found ($p = 0.36$).

Neither the presence of TTV ($p = 0.65$) nor TTV loads were associated with a condition of BV (BV: 2.7 ± 0.7; *I*: 2.8 ± 0.9; *H*: 3.2 ± 0.9; $p = 0.10$). Conversely, the presence of TTV was significantly more common in women with a higher vaginal WBC count (37.7 vs. 57.7%; $p = 0.02$). In line with these findings, the levels of IL-6 (median, range: 0.81, 0.01–57.8 vs. 0.41, 0.0–31.2 pg/mL; $p = 0.02$), as well as IL-8 (1,901, 34–35,783 vs. 652, 11.3–43,248; $p = 0.03$) were significantly higher in TTV-positive vaginal samples. Moreover, we observed a trend in the correlation between TTV loads and IL-8 levels ($R = 0.19$; $p = 0.09$). The detection of vaginal *Candida* spp. was not significantly associated with the vaginal presence of the virus nor with higher TTV loads ($p > 0.5$).

On the contrary, several correlations were observed between TTV presence/loads and the levels of particular vaginal metabolites. In relation to this, it is worth mentioning that a total of 63 metabolites were detected in the vaginal cell-free supernatants, mainly belonging to the groups of SCFAs, organic acids, amino acids, and biogenic amines (Supplementary Table S1).

In particular, TTV-positive samples were characterized by higher levels of propionate (median, range: 0.01, 0.001–0.36 vs. 0.007, 0.001–0.23 mM; $p = 0.001$) and cadaverine (0.008, 0.002–0.05 vs. 0.006, 0.001–0.06 mM; $p = 0.006$), compared to TTV-negative ones.

Moreover, TTV titer was positively correlated with the levels of 4-hydroxyphenyllactate ($p < 0.0001$), isoleucine ($p = 0.01$) and phenylalanine ($p = 0.04$). Vaginal molecules showing a negative correlation with TTV loads included benzoate ($p = 0.008$), inosine ($p = 0.002$), and creatine ($p = 0.004$) (the full list is displayed in Table 1).

TABLE 1 List of the vaginal molecules, whose concentration was found related to TTV loads.

	Spearman *r*	*p* -value
Xanthine	−0.276	0.01
Benzoate	−0.298	0.008
Phenylalanine	0.231	0.04
Tyramine	−0.259	0.02
4-Hydroxyphenyllactate	0.508	<0.0001
Inosine	−0.336	0.002
Uridine	−0.2285	0.04
Uracil	−0.265	0.02
Methanol	−0.256	0.02
Ethanolamine	−0.261	0.02
Creatinine	−0.2780	0.01
Creatine	−0.320	0.004
Asparagine	−0.288	0.01
TMA	−0.301	0.007
2,3-Butanediol	−0.285	0.01
Propionate	−0.366	0.001
Isoleucine	0.265	0.02

Statistical significance was searched by Spearman correlation coefficient.

Correlation between TTV and vaginal microbiome profiling

For microbiota analysis, only samples with a number of reads >5,000 ($n = 175$) were considered, in order to have a reliable picture of the microbial composition. TTV-positive and negative samples showed no statistical difference ($p > 0.05$) on both biodiversity (alpha-diversity) or microbial composition (beta-diversity) for all the metrics considered (Figure 1).

Moreover, the analysis of the bacterial relative abundances did not reveal any major changes in the bacterial groups between TTV+ and TTV- samples. Nevertheless, we noticed significant differences in two low-abundant taxa (average relative abundance <1%), such as a higher abundance of *Sneathia* (0.92 vs. 0.29%; $p = 0.04$) and *Shuttleworthia* (0.89 vs. <0.01%; $p = 0.0009$) in TTV-positive samples.

The point-biserial correlation confirmed the significant positive correlations between TTV presence and the abundance of *Sneathia* ($R = 0.123$) and *Shuttleworthia* ($R = 0.125$). Spearman analysis showed a significant correlation between TTV loads and the abundance of *Sneathia* ($R = 0.166$) and *Shuttleworthia* ($R = 0.313$).

Although not statistically significant, TTV-positive samples were characterized by a decrease of *L. crispatus* (32 vs. 41%) and *L. jensenii* (7 vs. 10%), as well as by an increase of *L. iners* (25 vs. 15%), compared to TTV-negative ones.

In this context, it is worth mentioning that we found a negative correlation between the levels of pro-inflammatory cytokines and both *L. crispatus* ($R = -0.354$ and $R = -0.277$ for IL-6 and IL-8, respectively) and *L. jensenii* ($R = -0.309$ and $R = -0.171$ for IL-6 and IL-8, respectively).

Discussion

The presence and role of TTV in pregnant women is still only scarcely available, so this study aimed to provide new insights into the dynamics of TTV in the vaginal ecosystem during pregnancy. We explored TTV presence and loads in a cohort of white pregnant women at different gestational stages and we assessed its correlation with the vaginal bacterial composition, with the vaginal metabolic profiles and with the vaginal concentration of two pro-inflammatory cytokines.

In line with previous findings (Tozetto-Mendoza et al., 2022), we observed that TTV is quite common in women with normal pregnancy outcomes, with a prevalence ranging from 53% at the first trimester to 36% at the third. This is not surprising if we consider that TTV has been identified both

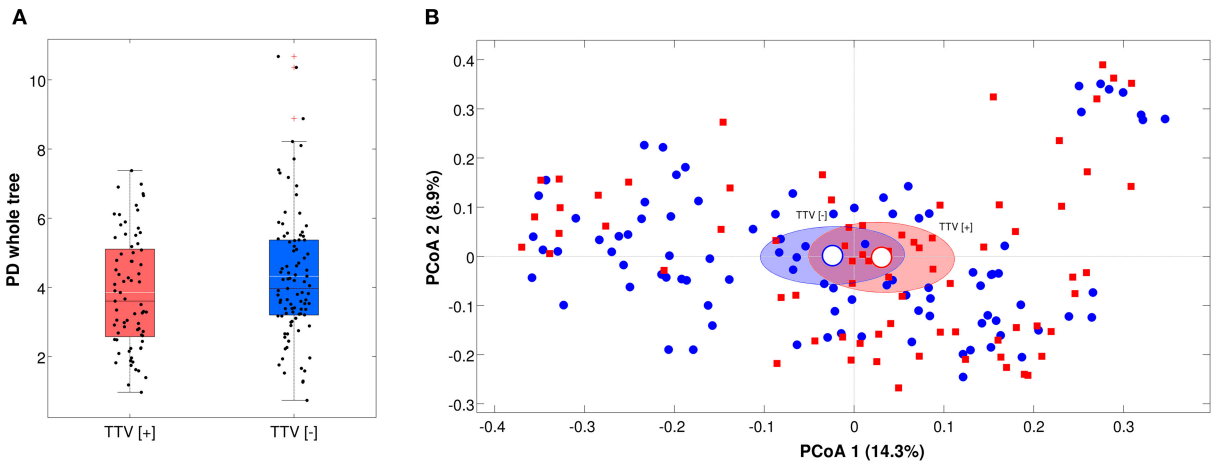

FIGURE 1
(A) Boxplot of the alpha-diversity according to Faith's phylogenetic diversity metric, grouped by TTV presence or absence. Each point represents a sample; median of the distributions are in black, whereas means are in white; **(B)** Principal Coordinate Analysis (PCoA) of the beta-diversity values according to unweighted Unifrac distances. Each point represents a sample; data points are colored according to the presence or absence of TTV; ellipses represent the 95% SEM-based confidence intervals; the first and the second coordinates are represented.

in peripheral blood and in cervical/vaginal fluids (Maggi and Bendinelli, 2010; Chen et al., 2011; Tozetto-Mendoza et al., 2020).

No difference in TTV prevalence and loads was observed between women with normal pregnancies and miscarriages. Even though further studies including a larger cohort of women are needed for a better comprehension of TTV role during pregnancy, these results seem to indicate that TTV does not have clinical outcome consequences.

Interestingly, TTV presence was positively related to the number of vaginal WBC, as well as to higher concentrations of vaginal proinflammatory cytokines (i.e., IL-6 and IL-8). This result is not surprising if we consider that TTV has been recognized as a predictor of local immune status (Focosi et al., 2016). It has been speculated that, in the vaginal ecosystem, TTV loads are related to the presence of activated lymphoid cells, being the vaginal TTV an additional indicator of the local "immune" status in pregnant women (Brundin et al., 2020; Tozetto-Mendoza et al., 2022).

Other interesting data emerged when TTV presence and loads were related to the vaginal bacterial composition. The most significant results included (i) the association between TTV and higher levels of *Sneathia* and *Shuttleworthia*, (ii) a trend toward a decrease of *L. crispatus* and *L. jensenii*, as well as an increase of *L. iners* in TTV-positive samples.

In this context, it is worth underlining that a significant negative correlation between *L. crispatus* and *L. jensenii* and both IL-6 and IL-8 was observed.

Since TTV replication preferentially occurs in activated lymphoid cells (Brundin et al., 2020), and immune system activation is at its lowest level in case of a *L. crispatus*-dominated vaginal microbiome (Witkin and Linhares, 2017), we can speculate that the absence/decrease of TTV is linked to the reduction of lymphoid cells or their pro-inflammatory molecules when *L. crispatus* is predominant. On the contrary, the presence of *L. iners* is associated with a higher expression of genes involved in leukocyte mediated immunity and activation (Mohd Zaki et al., 2022), being potentially associated with higher levels of TTV in the vaginal environment.

The association between TTV and higher levels of *Sneathia* and *Shuttleworthia* probably goes in the same direction. In fact, genital inflammation can be linked to specific BV-related microorganisms, including *Sneathia* (Kaelin et al., 2022). As reported by Lopez-Filloy et al., women with HPV infection are characterized by a significant increase in anaerobes, such as *Sneathia* and *Shuttleworthia*, their presence being in turn associated to a higher level of cervico-vaginal inflammation and a higher risk of BV recurrence (López-Filloy et al., 2022).

In this context, the association between TTV-positive samples and higher concentrations of propionate and cadaverine could reflect these findings. In fact, these two molecules (belonging respectively to SCFAs and biogenic amines) are common markers of vaginal dysbiosis, typically produced by BV-related anaerobes, when a reduction of vaginal lactobacilli is present (Laghi et al., 2021).

In addition, we observed a highly significant correlation between TTV loads and the levels of 4-hydroxyphenyllactate. This metabolite is produced by lactic acid bacteria and exerts both antifungal properties and radical scavenging activities (Mu et al., 2010; Suzuki et al., 2013).

Further studies are needed to understand the exact role and origin of 4-hydroxyphenyllactate and if this molecule can possess antiviral activities against TTV.

We are fully aware of some limitations of this study: (i) for TTV detection, we tested cell pellets after a low centrifugation step instead of supernatants; thus, we mainly detected the presence of the virus inside the host cells, (ii) the association between TTV and specific microbes of the vaginal ecosystem (i.e., *Sneathia* and *Shuttleworthia*) could be a coincidental finding. Additional studies are needed to understand if there is a real biological cooperation or if these microbes are simple bystanders.

In conclusion, in agreement with previous reports (Focosi et al., 2016; Tozetto-Mendoza et al., 2020), we found that TTV is commonly found in the vaginal ecosystem of pregnant women, representing a possible predictor of local immune status. In fact, its detection and loads vary with local vaginal conditions, being more common in presence of higher levels of leukocytes, higher levels of BV-related microbes, and lack of *L. crispatus* dominance.

Future perspectives include the assessment of the clinical role/utility of the vaginal TTV titer in the evaluation of the vaginal immune status, with the goal of opening new diagnostic/prognostic approaches for maternal-fetal health.

Data availability statement

The datasets presented in this study can be found in online repositories and in the Supplementary material. The names of the repository/repositories and accession number(s) can be found in the article.

Ethics statement

The studies involving human participants were reviewed and approved by Ethics Committee of Romagna (CEROM) (No. 2032 of 21st February 2018). The patients/participants provided their written informed consent to participate in this study.

Author contributions

AM, CF, and VS conceived and designed the study. SZ and GP recruited the patients. LL, MD, MP, SM, MS, CCo, CCe, and TC performed the experiments. CF, LL, and MS analyzed the data. AM and VS provided reagents, materials, and analysis tools. CF, AM, and MS wrote the paper. All the authors read, reviewed, and approved the final manuscript.

Funding

This study was supported by Fondazione del Monte di Bologna e Ravenna (Prot. No. 329bis/2017). The funder had no role in study design, data collection and analysis, decision to publish, or preparation of the manuscript.

Acknowledgments

We wish to thank all the enrolled volunteers and all staff involved in this study. Special thanks to Mrs. Oriana Gasperoni of the Family Advisory Health Centre in Ravenna for her skillful support during the study.

Conflict of interest

The authors declare that the research was conducted in the absence of any commercial or financial relationships that could be construed as a potential conflict of interest.

Publisher's note

Supplementary material

The Supplementary Material for this article can be found online at: https://www.frontiersin.org/articles/10.3389/fmicb.2022.998849/full#supplementary-material

References

Anahtar, M. N., Byrne, E. H., Doherty, K. E., Bowman, B. A., Yamamoto, H. S., Soumillon, M., et al. (2015). Cervicovaginal bacteria are a major modulator of host inflammatory responses in the female genital tract. *Immunity* 42, 965–976. doi: 10.1016/j.immuni.2015.04.019

Brundin, P. M. A., Landgren, B.-M., Fjallstrom, P., Johansson, A. P., and Nalvarte, I. (2020). Blood hormones and torque teno virus in peripheral blood mononuclear cells. *Heliyon* 6, e05535. doi: 10.1016/j.heliyon.2020.e05535

Brys, A., Stasio, E. D., Lenaert, B., Picca, A., Calvani, R., Marzetti, E., et al. (2020). Peridialytic serum cytokine levels and their relationship with postdialysis fatigue and recovery in patients on chronic haemodialysis—a preliminary study. *Cytokine* 135, 155223. doi: 10.1016/j.cyto.2020.155223

Caporaso, J. G., Kuczynski, J., Stombaugh, J., Bittinger, K., Bushman, F. D., Costello, E. K., et al. (2010). Correspondence QIIME allows analysis of high throughput community sequencing data Intensity normalization improves color calling in SOLiD sequencing. *Nat. Methods* 7, 335–336. doi: 10.1038/nmeth.f.303

Ceccarani, C., Foschi, C., Parolin, C., D'Antuono, A., Gaspari, V., Consolandi, C., et al. (2019). Diversity of vaginal microbiome and metabolome during genital infections. *Sci. Rep.* 9, 14095. doi: 10.1038/s41598-019-50410-x

Chen, P. K. S., Tam, W.-H., Yeo, W., Cheung, J. L. K., Zhong, S., and Chang, A. F. (2011). High carriage rate of TT virus in the cervices of pregnant women. *Clin. Infect. Dis.* 32, 1376–1377. doi: 10.1086/319983

Dall'Asta, M., Laghi, L., Morselli, S., Re, M. C., Zagonari, S., Patuelli, G., et al. (2021). Pre-pregnancy diet and vaginal environment in caucasian pregnant women: an exploratory study. *Front. Mol. Biosci.* 8, 702370. doi: 10.3389/fmolb.2021.702370

Di Simone, N., Santamaria Ortiz, A., Specchia, M., Tersigni, C., Villa, P., Gasbarrini, A., et al. (2020). Recent insights on the maternal microbiota: impact on pregnancy outcomes. *Front. Immunol.* 11, 528202. doi: 10.3389/fimmu.2020.528202

Donders, G., Bellen, G., and Rezeberga, D. (2011). Aerobic vaginitis in pregnancy. *BJOG* 118, 1163–1170. PMID: 21668769 doi: 10.1111/j.1471-0528.2011.03020.x

Edgar, R. C. (2016). UNOISE2: improved error-correction for Illumina 16S and ITS amplicon sequencing. *bioRxiv* 081257. doi: 10.1101/081257

Focosi, D., Antonelli, G., Pistello, M., and Maggi, F. (2016). Torquetenovirus: the human virome from bench to bedside. *Clin. Microbiol. Infect.* 22, 589–593. doi: 10.1016/j.cmi.2016.04.007

Foschi, C., Salvo, M., Laghi, L., Zhu, C., Ambretti, S., Marangoni, A., et al. (2018). Impact of meropenem on *Klebsiella pneumoniae* metabolism. *PLoS ONE* 13, e0207478. doi: 10.1371/journal.pone.0207478

Geisler, W. M., Yu, S., Venglarik, M., and Schwebke, J. R. (2004). Vaginal leucocyte counts in women with bacterial vaginosis: relation to vaginal and cervical infections. *Sex. Transm. Infect.* 80, 401–405. doi: 10.1136/sti.2003.009134

Gupta, S. D. (1960). Point biserial correlation coefficient and its generalization. *Psychometrika* 25, 393–408 doi: 10.1007/BF02289756

Haloschan, M., Bettesch, R., Görzer, I., Weseslindtner, L., Kundi, M., and Puchhammer-Stöckl, E. (2014). TTV DNA plasma load and its association with age, gender, and HCMV IgG serostatus in healthy adults. *Age (Dordr).* 36, 9716. doi: 10.1007/s11357-014-9716-2

Kaelin, E. A., Skidmore, P. T., Łaniewski, P., Holland, L. A., Chase, D. M., Herbst-Kralovetz, M. M., et al. (2022). Cervicovaginal DNA virome alterations are associated with genital inflammation and microbiota composition. *mSystems* 7, e0006422. doi: 10.1128/msystems.00064-22

Kroon, S. J., Ravel, J., and Huston, W. M. (2018). Cervicovaginal microbiota, women's health, and reproductive outcomes. *Fertil. Sterility* 110, 327–336. doi: 10.1016/j.fertnstert.2018.06.036

Laghi, L., Zagonari, S., Patuelli, G., Zhu, C., Foschi, C., Morselli, S., et al. (2021). Vaginal metabolic profiles during pregnancy: Changes between first and second trimester. *PLoS ONE* 16, e0249925. doi: 10.1371/journal.pone.0249925

López-Filloy, M., Cortez, F. J., Gheit, T., Cruz, Y., Cruz, O., Cruz-Talonia, F., et al. (2022). Altered vaginal microbiota composition correlates with human papillomavirus and mucosal immune responses in women with symptomatic cervical ectopy. *Front. Cell. Infect. Microbiol.* 12, 884272. doi: 10.3389/fcimb.2022.884272

Lozupone, C., Lladser, M. E., Knights, D., Stombaugh, J., and Knight, R. (2011). UniFrac: an effective distance metric for microbial community comparison. *ISME J.* 5, 169–172. doi: 10.1038/ismej.2010.133

Maggi, F., and Bendinelli, M. (2010). Human anelloviruses and the central nervous system. *Rev. Med. Virol.* 20, 392–407. PMID: 20925048. doi: 10.1002/rmv.668

Maggi, F., Focosi, D., Albani, M., Lanini, L., Vatteroni, M. L., Petrini, M., et al. (2010). Role of hematopoietic cells in the maintenance of chronic human torquetenovirus plasma viremia. *J Virol.* 84, 6891–6893. doi: 10.1128/JVI.00273-10

Maggi, F., Pistello, M., Vatteroni, M., Presciuttini, S., Marchi, S., Isola, P., et al. (2001). Dynamics of persistent TT virus infection, as determined in patients treated with alpha interferon for concomitant hepatitis C virus infection. *J. Virol.* 75, 11999–12004. doi: 10.1128/JVI.75.24.11999-12004.2001

Marangoni, A., Foschi, C., Nardini, P., Compri, M., and Cevenini, R. (2015). Evaluation of the versant CT/GC DNA 1.0 assay (kPCR) for the detection of extra-genital *Chlamydia trachomatis* and *Neisseria gonorrhoeae* infections. *PLoS ONE* 10, e0120979. doi: 10.1371/journal.pone.0120979

Marangoni, A., Laghi, L., Zagonari, S., Patuelli, G., Zhu, C., Foschi, C., et al. (2021). New insights into vaginal environment during pregnancy. *Front. Mol. Biosci.* 8, 656844. doi: 10.3389/fmolb.2021.656844

Mohd Zaki, A., Hadingham, A., Flaviani, F., Haque, Y., Mi, J. D., Finucane, D., et al. (2022). Neutrophils dominate the cervical immune cell population in pregnancy and their transcriptome correlates with the microbial vaginal environment. *Front. Microbiol.* 13, 904451. doi: 10.3389/fmicb.2022.904451

Mu, W., Yang, Y., Jia, J., Zhang, T., and Jiang, B. (2010). Production of 4-hydroxyphenyllactic Acid by *Lactobacillus* Sp. SK007 Fermentation. *J. Biosci. Bioeng.* 109, 369–371. doi: 10.1016/j.jbiosc.2009.10.005

Nugent, R. P., Krohn, M. A., and Hillier, S. L. (1991). Reliability of diagnosing bacterial vaginosis is improved by a standardized method of gram stain interpretation. *J. Clin. Microbiol.* 29, 297–301. doi: 10.1128/jcm.29.2.297-301.1991

Oksanen, J, Blanchet, F. G., Kindt, R., Legendre, P., Minchin. P. R., O'Hara. R. B., et al. (2013). *Package "Vegan". R Package Version 2.0–10.* Available online: https://cran.r-project.org/src/contrib/Archive/vegan/vegan_2.0-10.tar.gz

Parolin, C., Foschi, C., Laghi, L., Zhu, C., Banzola, N., Gaspari, V., et al. (2018). Insights into vaginal bacterial communities and metabolic profiles of *Chlamydia trachomatis* infection: positioning between eubiosis and dysbiosis. *Front. Microbiol.* 9, 600. doi: 10.3389/fmicb.2018.00600

Prince, A. L., Antony, K. M., Chu, D. M., and Aagaard, K. M. (2014). The microbiome, parturition, and timing of birth: more questions than answers. *J. Reprod. Immunol.* 104–105, 12–19. doi: 10.1016/j.jri.2014.03.006

Severgnini, M., Camboni, T., Ceccarani, C., Morselli, S., Cantiani, A., Zagonari, S., et al. (2021). Distribution of ermB, ermF, tet(W), and tet(M) resistance genes in the vaginal ecosystem of women during pregnancy and puerperium. *Pathogens* 10, 1546. doi: 10.3390/pathogens10121546

Severgnini, M., Morselli, S., Camboni, T., Ceccarani, C., Laghi, L., Zagonari, S., et al. (2022). A Deep Look at the Vaginal Environment During Pregnancy and Puerperium. *Front. Cell. Infect. Microbiol.* 12, 838405. doi: 10.3389/fcimb.2022.838405

Shibayama, T., Masuda, G., Ajisawa, A., Takahashi, M., Nishizawa, T., Tsuda, F., et al. (2001). Inverse relationship between the titre of TT virus DNA and the CD4 cell count in patients infected with HIV. *AIDS.* 15, 563–570. doi: 10.1097/00002030-200103300-00004

Srinivasan, S., Morgan, M. T., Fiedler, T. L., Djukovic, D., Hoffman, N. G., Raftery, D., et al. (2015). Metabolic signatures of bacterial vaginosis. *mBio* 6, e00204–15. doi: 10.1128/mBio.00204-15

Suzuki, Y., Kosaka, M., Shindo, K., Kawasumi, T., Kimoto-Nira, H., and Suzuki, C. (2013). Identification of antioxidants produced by *Lactobacillus plantarum*. *Biosci. Biotechnol. Biochem.* 77, 1299–1302. doi: 10.1271/bbb.121006

Tozetto-Mendoza, T. R., Bongiovanni, A. M., Minis, E., Linhares, I. M., Boester, A., Freire, W. S., et al. (2020). Torquetenovirus titer in vaginal secretions from pregnant and postpartum women: association with absence of *Lactobacillus crispatus* and levels of lactic acid and matrix metalloproteinase-8. *Reprod. Sci.* 27, 2075–2081. doi: 10.1007/s43032-020-00227-1

Tozetto-Mendoza, T. R., Mendes-Correa, M. C., Moron, A. F., Forney, L. J., Linhares, I. M., Ribeiro da Silva, A. Jr, Honorato, L., et al. (2022). The vaginal torquetenovirus titer varies with vaginal microbiota composition in pregnant women. *PLoS ONE* 17, e0262672. doi: 10.1371/journal.pone.0262672

Wang, Q., Garrity, G. M., Tiedje, J. M., and Cole, J. R. (2007). Naive bayesian classifier for rapid assignment of rRNA sequences into the new bacterial taxonomy. *Appl. Environ. Microbiol.* 73, 5261–5267. doi: 10.1128/AEM.00062-07

Witkin, S. S., and Linhares, I. M. (2017). Why do lactobacilli dominate the human vaginal microbiota? *BJOG* 1024, 606–611. doi: 10.1111/1471-0528.14390

Witkin, S. S., Moron, A. F., Ridenhour, B. J., Minis, E., Hatanaka, A., Sarmento, S. G. P., et al. (2019). vaginal biomarkers that predict cervical length and dominant bacteria in the vaginal microbiomes of pregnant women. *mBio* 10, e02242–19. doi: 10.1128/mBio.02242-19

Yano, J., Sobel, J. D., Nyirjesy, P., Sobel, R., Williams, V. L., Yu, Q., et al. (2019). Current patient perspectives of vulvovaginal candidiasis: incidence, symptoms, management and post-treatment outcomes. *BMC Womens Health.* 19, 48. doi: 10.1186/s12905-019-0748-8

Zhu, C., Vitali, B., Donders, G., Parolin, C., Li, Y., and Laghi, L. (2019). Univariate statistical analysis as a guide to 1 HNMR spectra signal assignment by visual inspection. *Metabolites* 9, 15. doi: 10.3390/metabo9010015

Zozaya-Hinchliffe, M., Lillis, R., Martin, D. H., and Ferris, M. J. (2010). Quantitative PCR assessments of bacterial species in women with and without bacterial vaginosis. *J. Clin. Microbiol.* 2010; 48, 1812–1819. doi: 10.1128/JCM.00851-09

frontiers | Frontiers in Microbiology

TYPE Original Research
PUBLISHED 23 September 2022
DOI 10.3389/fmicb.2022.990478

OPEN ACCESS

EDITED BY
Svetlana Khaiboullina,
University of Nevada, Reno,
United States

REVIEWED BY
Eveline M. Ibeagha-Awemu,
Agriculture and Agri-Food Canada (AAFC), Canada
Muhammad Zahoor Khan,
University of Agriculture, Dera Ismail Khan, Pakistan

*CORRESPONDENCE
Alejandra Ochoa-Zarzosa
ochoaz@umich.mx;
alejandra.ochoa@umich.mx

SPECIALTY SECTION
This article was submitted to Infectious Agents and Disease, a section of the journal Frontiers in Microbiology

RECEIVED 10 July 2022
ACCEPTED 30 August 2022
PUBLISHED 23 September 2022

CITATION
Barajas-Mendiola MA, Salgado-Lora MG, López-Meza JE and Ochoa-Zarzosa A (2022) Prolactin regulates H3K9ac and H3K9me2 epigenetic marks and miRNAs expression in bovine mammary epithelial cells challenged with *Staphylococcus aureus*. *Front. Microbiol.* 13:990478. doi: 10.3389/fmicb.2022.990478

Prolactin regulates H3K9ac and H3K9me2 epigenetic marks and miRNAs expression in bovine mammary epithelial cells challenged with *Staphylococcus aureus*

Marco Antonio Barajas-Mendiola, María Guadalupe Salgado-Lora, Joel Edmundo López-Meza and Alejandra Ochoa-Zarzosa*

Centro Multidisciplinario de Estudios en Biotecnología, Facultad de Medicina Veterinaria y Zootecnia, Universidad Michoacana de San Nicolás de Hidalgo, Morelia, Mexico

Epigenetic mechanisms are essential in the regulation of immune response during infections. Changes in the levels of reproductive hormones, such as prolactin, compromise the mammary gland's innate immune response (IIR); however, its effect on epigenetic marks is poorly known. This work explored the epigenetic regulation induced by bovine prolactin (bPRL) on bovine mammary epithelial cells (bMECs) challenged with *Staphylococcus aureus*. In this work, bMECs were treated as follows: (1) control cells without any treatment, (2) bMECs treated with bPRL (5 ng/ml) at different times (12 or 24 h), (3) bMECs challenged with *S. aureus* for 2 h, and (4) bMECs treated with bPRL at different times (12 or 24 h), and then challenged with *S. aureus* 2 h. By western blot analyses of histones, we determined that the H3K9ac mark decreased (20%) in bMECs treated with bPRL (12 h) and challenged with *S. aureus*, while the H3K9me2 mark was increased (50%) in the same conditions. Also, this result coincided with an increase (2.3-fold) in HDAC activity analyzed using the cellular histone deacetylase fluorescent kit FLUOR DE LYS®. ChIP-qPCRs were performed to determine if the epigenetic marks detected in the histones correlate with enriched marks in the promoter regions of inflammatory genes associated with the *S. aureus* challenge. The H3K9ac mark was enriched in the promoter region of *IL-1*β, *IL-10*, and *BNBD10* genes (1.5, 2.5, 7.5-fold, respectively) in bMECs treated with bPRL, but in bMECs challenged with *S. aureus* it was reduced. Besides, the H3K9me2 mark was enriched in the promoter region of *IL-1*β and *IL-10* genes (3.5 and 2.5-fold, respectively) in bMECs challenged with *S. aureus* but was inhibited by bPRL. Additionally, the expression of several miRNAs was analyzed by qPCR. Let-7a-5p, miR-21a, miR-30b, miR-155, and

miR-7863 miRNAs were up-regulated (2, 1.5, 10, 1.5, 3.9-fold, respectively) in bMECs challenged with *S. aureus*; however, bPRL induced a down-regulation in the expression of these miRNAs. In conclusion, bPRL induces epigenetic regulation on specific IIR elements, allowing *S. aureus* to persist and evade the host immune response.

KEYWORDS

prolactin, innate immunity, epigenetic, mastitis, *Staphylococcus aureus*

Introduction

Bovine mastitis is an inflammatory disease of the mammary gland that generates significant economic loss to dairy farming worldwide due to reduced milk quality, high treatment costs due to the infection, decrease in milk production, fertility problems, or the cull of animals with chronic mastitis (Huijps et al., 2008; Reshi et al., 2015; Ruegg, 2017; Dego, 2020). This disease usually results from microbial infections, and *Staphylococcus aureus* is the most prevalent causal pathogen in many regions (9–17% from milk samples) (Wilson et al., 1997; Pitkälä et al., 2004). In addition, *S. aureus* is isolated more frequently from subclinical mastitis than clinical mastitis (up to 75% of the cases in US herds) (Dego, 2020). This pathogen can internalize into the mammary gland's epithelial cells, evading the immune system, favoring chronic infections, and failure in antibiotic therapy (Barkema et al., 2006; Atalla et al., 2008; Barlow, 2011; Conlon, 2014; Josse et al., 2017; Lee et al., 2018; Zaatout et al., 2020).

Epigenetic mechanisms (for example, chemical modifications on the DNA and histones) have a relevant role in the regulation of differentiation, function, and health of the mammary gland (Devinoy and Rijnkels, 2010; Ivanova et al., 2021; Wang and Ibeagha-Awemu, 2021). For example, in bovines, the hypomethylation of α-casein gene favors its expression, while methylation represses its expression (Singh et al., 2010). Also, there is an increase in the DNA methylation in peripheral blood lymphocytes isolated from cows with mastitis naturally infected with *S. aureus* (Song et al., 2016). Besides, the histone H3K27me3 mark was up-regulated in isolated peripheral blood lymphocytes from cows with mastitis caused by *S. aureus*. It was related to a down-regulation in the expression of the inflammatory response genes (He et al., 2016). Recently, our research group reported that combined bovine prolactin (bPRL) and 17β-estradiol modulate the IIR during *S. aureus* infection using an *in vitro* model of bovine mastitis, and these effects were related to the regulation of H3 histone modifications, such as H3K9ac and H3K9me2 (Salgado-Lora et al., 2020).

The epigenetic regulation also may be achieved through micro RNAs (miRNAs), and several reports evidence its role in bovine bacterial infections (Do et al., 2021). For example, a miRNA transcriptional analysis of MAC-T cell line challenged with *S. aureus* and *Escherichia coli* revealed a single and differential pattern of miRNAs expression, where bta-miR-184, miR-24-3p, miR-148, mir-486, and Let-7a-5p were unique miRNAs expressed during *E. coli* infection, while bta-miR-2339, miR-499, miR-99a, and miR.23a only were expressed during *S. aureus* infection (Jin et al., 2014). In addition, the miRNA expression analysis of monocytes-derived macrophages infected with *Streptococcus agalactiae* showed that miRNAs promote an inflammatory phenotype in these cells regulating the expression of genes coding for *IL-6*, *IL-1*β, and *TNF*-α (Lewandowska-Sabat et al., 2018).

Mammary gland function is regulated by hormones (for example, prolactin, 17β-estradiol, progesterone, glucocorticoids). Abrupt hormone levels change during the peripartum and lactation has been associated with the risk of mastitis development due to an impaired IIR (Lamote et al., 2006; Brisken and O'Malley, 2010; Lacasse et al., 2019; Alhussien and Dang, 2020). Prolactin is a hormone of 23 kDa (199 amino acids) synthesized mainly by the lactotrophic cells of the anterior pituitary gland with a relevant role in lactation regulation; however, this hormone also is involved in the regulation of the immune response (Binart, 2017; Savino, 2017; Berczi and Nagy, 2019).

Previously, we reported that bPRL at physiological concentrations (5 ng/ml) induces the internalization of *S. aureus* into bovine mammary epithelial cells (bMECs) and modulates the IIR of these cells. Particularly, bPRL up-regulated the expression of *TNF*-α, *IL-1*β, and *IL-6* genes; however, cells pre-treated with this hormone inhibited the bacterial induction of these genes. Similarly, the expression of the anti-inflammatory cytokine *IL-10* gene was induced by bPRL (Medina-Estrada et al., 2015). Despite the epigenetic role of bPRL on the mammary gland and IIR, their effects on specific epigenetic modifications in the promoter region of IIR genes and miRNAs expression in intramammary infections caused by *S. aureus* are scarce. Thus, this work aimed to characterize if the effects of bPRL on IIR genes in bMECs occur through epigenetic modifications of the promoter region of inflammatory response

genes. Besides we evaluate if other elements, such as miRNA expression, were modulated by bPRL in cells challenged with *S. aureus*. This information is relevant to knowing the epigenetic mechanisms underlying bovine mastitis, considering that bPRL receptor signal pathways have been associated with this disease (Khan et al., 2020).

Materials and methods

Bovine prolactin

Purified bovine prolactin (bPRL) (AFP7170E) was provided by A. F. Parlow from National Hormone & Peptide Program (NHPP)-National Institute of Diabetes and Digestive and Kidney Diseases (NIDDK) (Torrance, CA, USA) (Parlow, 2002). The hormone was dissolved in sterile water. We used 5 ng/ml in all experiments, as reported (Gutiérrez-Barroso et al., 2008).

Antibodies

For western blot assays, mouse monoclonal antibody anti-H3K9Ac (1:2,000) (Sc36616, Santa Cruz, CA, USA) and mouse monoclonal antibody anti-H3K9me2 ChIP grade (1:1,000) (ab1220, Abcam, Cambridge, UK) were used as primary antibodies. The rabbit polyclonal antibody anti-H3-ChIP grade (1:5,000) (ab1791, Abcam, Cambridge, UK) was used as load control. Secondary antibodies (1:3,000) raised against mouse and rabbit antibodies coupled to radish peroxidase were purchased from Cell Signaling Technology (Danvers, MA, USA).

For the chromatin immunoprecipitation assay (ChIP), 3 μg of the mouse monoclonal antibody anti-H3K9me2-ChIP grade (ab1220, Abcam, Cambridge, UK) and rabbit polyclonal antibody anti-H3K9ac-grade ChIP (ab10812, Abcam, Cambridge, UK) were used in each assay. In addition, rabbit polyclonal antibody anti-H3-grade ChIP (Abcam, ab1791) and the mouse polyclonal antibody anti-IgG (Sigma-Aldrich, St. Louis, MO, USA) were used as reference control and negative isotype control, respectively.

Staphylococcus aureus strain

Staphylococcus aureus subsp. *aureus* Rosenbach (ATCC 27543) strain was used in this work. This strain was isolated from a case of clinic mastitis and can invade bovine mammary epithelial cells (Medina-Estrada et al., 2015). Bacteria were grown overnight in Luria-Bertani (LB) broth (BIOXON, Becton Dickinson-México, México) at 37°C. Colony-forming units (CFU) were adjusted by measuring the optical density at 600 nm (OD 0.2 = 9.2 × 10^7 CFU/ml).

Primary bovine mammary epithelial cell culture

Bovine mammary epithelial cell (bMECs) were isolated from alveolar tissue of the udder of healthy lactating cows (slaughtered for meat), according to Anaya-López et al. (2006). Cells from passages 2–8 were used in all the experiments. Cells were grown on 90 × 15 mm culture Petri dishes (NEST Biotechnology Co. Wuxi, Jiangsu, China) in Dulbecco's Modified Eagle's Medium/Nutrient Mixture F-12 Ham (DMEM/F12-Ham) (Sigma-Aldrich, St. Louis, MO, USA) supplemented with 10% of fetal bovine serum (FBS) (Equitech Bio, Kerrville, TX, USA), insulin 10 μg/ml (Sigma-Aldrich, St. Louis, MO, USA), hydrocortisone 5 μg/ml (Sigma-Aldrich, St. Louis, MO, USA), penicillin 100 U/ml (Gibco, Waltham, MA, USA) streptomycin 100 μg/ml (Gibco) and amphotericin B 1 μg/ml (Sigma Sigma-Aldrich, St. Louis, MO, USA) to obtain the complete medium. Prior to the challenge, cells were maintained in a 5% CO_2 atmosphere at 37°C. All the experiments were performed using cells synchronized in DMEM/F12-Ham medium without FBS and antibiotics (incomplete medium) for 24 h. bMECs were treated as follows: (1) control cells without any treatment, (2) bMECs treated with bPRL (5 ng/ml) at different times (12 or 24 h), (3) bMECs challenged with *S. aureus* for 2 h, and (4) bMECs treated with bPRL at different times (12 or 24 h), and then challenged with *S. aureus* 2 h. The interaction of *S. aureus* with bMECs for 2 h is based on previous studies from our research group (Anaya-López et al., 2006; Gutiérrez-Barroso et al., 2008; Medina-Estrada et al., 2015), which analyzed the IIR to *S. aureus* challenge after this time.

Invasion assays

For ChIP assays, monolayers of 10 × 10^6 bMECs were grown in complete medium on 60 × 15 mm cell culture Petri dishes (NEST Biotechnology Co. Wuxi, Jiangsu, China) previously coated with 500 μl of type 1 rat collagen (Sigma-Aldrich St. Louis, MO, USA). Cells were incubated until reaching 90% of confluence in a 5% CO_2 atmosphere at 37°C for 4 days. For the miRNAs expression assays, monolayers of 2.5 × 10^5 bMECs were grown in complete medium on 24-well plates (NEST Biotechnology Co., Wuxi, Jiangsu, China) previously coated with 200 μl of type 1 rat collagen. Cells were incubated until reaching 90% of confluence in a 5% CO_2 atmosphere at 37°C for 24 h. Previous to the challenge, cells were synchronized with the incomplete medium in a 5% CO_2 atmosphere at 37°C for 24 h. Then, cells were treated with bPRL (5 ng/ml) and incubated in a 5% CO_2 atmosphere at 37°C for 12 h or 24 h. The invasion assay was performed using the gentamicin protection assay previously described (Gutiérrez-Barroso et al., 2008; Alva-Murillo et al., 2014). Briefly, bMECs

treated with bPRL were challenged with *S. aureus* (OD = 0.2) at a multiplicity of infection (MOI) of 30:1 (bacteria: cell) in a 5% CO_2 atmosphere at 37°C for 2 h. Later, cells were washed three times with PBS (pH 7.4), and an incomplete medium supplemented with gentamicin 80 μg/ml was added to eliminate extracellular bacteria for 1 h. Finally, cells were washed three times with PBS (pH 7.4) and were employed for ChIP and miRNAs expression assays as indicated below.

Chromatin immunoprecipitation-qPCR assays

Enrichment of the epigenetic marks on the promoter region of the IIR genes was assessed by ChIP, as described by Carey et al. (2009), with some modifications. DNA-protein complexes of the bMECs (10×10^6 cells) were fixed by cross-linking with 1% of formaldehyde (Baker Analyzed, J. T. Baker) in agitation for 10 min, and the reaction was stopped with glycine 1.35 M (Sigma) for 5 min. Then, cells were washed three times with cold PBS (pH 7.4), detached with a sterile cell scraper (Corning, Manassas, VA, USA), and centrifuged at 1,500 rpm for 10 min at 4°C. The cell pellet was resuspended in 10 ml of cold lysis buffer for ChIP (50 mM HEPES-KOH pH 7.5, 140 mM NaCl, 1% Triton X-100, 0.1% sodium deoxycholate, 0.1% SDS) and incubated 10 min on ice. The nuclei were pelleted at 1,500 rpm for 10 min at 4°C, then resuspended in cold lysis buffer with 10 μl of a cocktail of protease inhibitors (Sigma-Aldrich St. Louis, MO, USA). The chromatin was sheared by sonication (6 × 15 s pulses followed by 60 s rest). 300 μl chromatin (100 μg/ml) diluted in cold dilution buffer for ChIP (1% Triton X-100, 2 mM EDTA pH 8, 20 mM Tris-HCl pH 8, 150 mM NaCl) were supplemented with 3 μl of a cocktail of protease inhibitors and 50 μl of a mixture of protein A agarose/protein G agarose beads (Invitrogen, Waltham, MA, USA) were added to preclear the chromatin in agitation at 4°C for 2 h. Next, the samples were centrifuged at 3,000 rpm for 5 min at 4°C, the supernatants were transferred to new microtubes, and 3 μg of the specific antibody was added and maintained in agitation overnight at 4°C. Again, 50 μl of a mixture of protein A agarose/protein G agarose beads were added to each sample and kept in agitation at 4°C for 2 h. Then, the samples were centrifuged at 3,000 rpm for 3 min at 4°C, and the supernatants were removed carefully. Further, 1 ml of cold wash buffer for ChIP (0.1% SDS, 1% Triton X-100, 2 mM EDTA pH 8, 20 mM Tris-HCl pH 8, 150 mM NaCl) was added to samples, maintained in agitation for 10 min at room temperature, and centrifuged at 3,000 rpm for 3 min at 4°C, three times. Then, 1 ml of cold final wash buffer for ChIP (0.1% SDS, 1% Triton X-100, 2 mM EDTA pH 8, 20 mM Tris-HCl pH 8, 500 mM NaCl) was added, maintained in agitation for 10 min at room temperature, and centrifuged at 3,000 rpm for 3 min at 4°C. The beads were resuspended in 300 μl of elution buffer for ChIP (1% SDS, 100 mM $NaHCO_3$) supplemented with 0.5 μl of proteinase K (20 μg/μl, Thermo Scientific, Waltham, MA, USA) and incubated at 55°C for 2 h. An additional incubation at 65°C for 4 h was performed to reverse the cross-linking. Finally, the samples were incubated for 5 min at room temperature and centrifuged at 13,000 rpm for 5 min. The supernatants were transferred to new microtubes, and the DNA was isolated by phenol/chloroform extraction and frozen at −80°C until use. The enrichment of epigenetic marks was analyzed by quantitative PCR using the comparative Ct method (ΔΔCt) in a StepOne Plus Real-Time PCR System (Applied Biosystems, Waltham, MA, USA) according to the manufacturer's instructions. The reactions were carried out with qPCRBIO SyGreen Blue Mix Hi-ROX master mix (Biosystems, Wayne, PA, USA) with specific primers (Invitrogen, Waltham, MA, USA) for the promoter region of the IIR genes. The primer sequences and the PCR conditions used to amplify the promoter region of the bovine IIR genes are described in **Table 1**. GAPDH was used as a positive control for the analysis of H3K9ac enrichment and negative control for studying enrichment in H3K9me2.

RNA isolation and miRNAs expression

To analyze the effect of bPRL and *S. aureus* on the miRNAs expression, monolayers of 2.5×10^5 cells were cultured in 24-well plates (NEST, Biotechnology Co., Wuxi, Jiangsu, China) and incubated with bPRL (5 ng/ml) for 12 h and challenged or not with *S. aureus* (MOI 30:1). The total RNA was extracted using the Trizol™Reagent (Invitrogen, Waltham, MA, USA) according to the manufacturer's instructions. The integrity of total RNA was verified by agarose gel electrophoresis, and the genomic DNA contamination was removed with DNAse I (Invitrogen, Waltham, MA, USA) according to the manufacturer's instructions. Then, the cDNA was synthesized according to Varkonyi-Gasic and Hellens (2011), with some modifications. Briefly, 1 μg of total RNA was reversed transcribed to cDNA using the M-MLV-Reverse Transcriptase (Invitrogen, Waltham, MA, USA) in a reaction of 20 μl containing 1 μM stem-loop RT primer and 10 μM dNTPs mix (Invitrogen, Waltham, MA, USA). The reaction was incubated at 65°C for 5 min and then transferred to ice. Further, 1X First-Strand Buffer, 10 mM dithiothreitol, and 2 U/μl of RNAseOUT™ (Invitrogen, Waltham, MA, USA) were added to the reaction mixture incubated at 37°C for 2 min. Finally, 5 U/μl of M-MLV reverse transcriptase was added, and the reaction mixture was incubated at 37°C for 50 min, followed by 70°C for 15 min. The RT-qPCR assay was performed by quantitative PCR using the comparative Ct method (ΔΔCt) in a StepOne Plus Real-Time PCR System (Applied Biosystems, Waltham, MA, USA) according to the manufacturer's instructions. The reactions were carried out with qPCRBIO SyGreen Blue Mix

TABLE 1 Primers used for the analysis of the promoter region of innate immune response genes.

Bovine (genes)[1]	Sequence (5′→3′)	Tm (°C)	Fragment (bp)	Reference
TNF-α	F-GCTCATGGGTTTCTCCACCCA	60	197	This work
	R-GGAGGTTATCTCCAGGGGGT			
IL-1β	F-TTGCCTGCCAGGTACAAGAT	60	154	This work
	R-ACCATTTGCCATGCCAGTCC			
IL-8	F-CAAAGCTTGGGTCACACAG	60	183	This work
	R-AGGGAACAAGTGCACCATC			
IL-10	F-GCGAAGGTTCAGCAAGAAG	60	129	This work
	R-TAATGAGGCTGGGGAAAACC			
LAP	F-GCTGAACTGACTGCCAGGAA	58.5	125	This work
	R-GGAGTGGCCTTCATAGCACA			
BNBD10	F-CAGGGGAAACAGGCAAGTCT	55.5	147	This work
	R-GGGGCAGTCACTTGTATGCT			
GAPDH	F-CTCTAATGTTCACCTTCCTC	58	191	This work
	R-CGACCACCCTATTCAGGTTC			

[1]TNF-α, tumor necrosis factor-alpha; IL-1β, interleukin 1-beta; IL-8, chemokine interleukin 8; IL-10, interleukin 10; LAP, lingual antimicrobial peptide; BNBD10, bovine neutrophil beta-defensin 10; GAPDH, glyceraldehyde 3-phosphate dehydrogenase.

TABLE 2 Primers used for the analysis of bovine miRNA expression.

Bovine miRNA		Sequence 5′ to 3′	Tm (°C)	Reference
Let-7a-5p	[a]Stem-Loop	GTTGGCTCTGGTGCAGGGTCCGAGG TATTCGCACCAGAGCCAAC	54	This study
	[b]Universal Reverse Primer	GTGCAGGGTCCGAGGT		
	[c]miRNA specific sequence	AACTAT		
	[d]Forward Primer	GGGTGAGGTAGTAGGTTGT		
miR-21a	[c]miRNA specific sequence	AGTCAA	56	This study
	[d]Forward Primer	GTTGTAGCTTATCAGACTGATG		
miR-30b	[c]miRNA specific sequence	AGCTGA	60	This study
	[d]Forward Primer	GTTTGGTGTAAACATCCTACAC		
miR-155	[c]miRNA specific sequence	ACCCCT	56	This study
	[d]Forward Primer	GTGGGTTAATGCTAATCGTGAT		
miR-23a	[c]miRNA specific sequence	TGGAAA	58	This study
	[d]Forward Primer	GTGATCACATTGCCAGGGA		
miR-7863	[c]miRNA specific sequence	TGGAAA	50	This study
	[d]Forward Primer	GTTGATGGACTGTCACCTG		
miR-146a	[c]miRNA specific sequence	ACAACC	52	This study
	[d]Forward Primer	GTGGTGAGAACTGAATTCCATA		
miR-144	[c]miRNA specific sequence	ACAACC	58	This study
	[d]Forward Primer	GTTGGGTACAGTATAGATGATG		
miR-451	[c]miRNA specific sequence	AAACTC	52	This study
	[d]Forward Primer	GTTGGAAACCGTTACCATTACT		
U6	Stem-Loop	CGCTTCACGAATTTGCGTGTCAT	50 to 60	(Han et al., 2020)
	Reverse Primer	GCTTCGGCAGCACATATACTAAAAT		
	Forward Primer	CGCTTCACGAATTTGCGTGTCAT		

[a]The Stem-Loop and the [b]Universal Reverse Primer sequences are the same for all miRNAs evaluated except for the [c]miRNA specific and [d]forward primer sequences. Primers were designed using the miRNA Primer Design Tool date base [miRNA Primer Design Tool | Login (dote.hu)].

Hi-ROX master mix (Biosystems, Wayne, PA, USA) with the specific primers (Elim Biopharm, Hayward, CA, USA) for the miRNAs. The stem-loop primer and the sequences of the primers used to amplify bovine miRNAs were designed using the miRNA Primer Design Tool[1]. The sequences and the PCR conditions used to amplify the bovine miRNAs are described in **Table 2**. U6 miRNA was used as an internal control of amplification.

Extraction and purification of histones

To analyze the effects of bPRL on the global epigenetics marks H3K9ac and H3K9me2 of bMECs, the histones were extracted according to the acidic extraction for histones protocol described by Shechter et al. (2007) and modified by Salgado-Lora et al. (2020). Briefly, 3×10^6 cells were cultured in Petri dishes at 90% of confluence, then bPRL (5 ng/ml) was added for 12 or 24 h, and then the cells were challenged with *S. aureus* for 2 h. Next, the cells were washed three times with PBS (pH 7.4), detached with trypsin (0.05%)-EDTA (0.02%) (Sigma-Aldrich, St. Louis, MO, USA), and centrifuged at 3,200 rpm at 4°C for 10 min. Next, the pellet was washed with PBS (pH 7.4) and resuspended in 1 ml of hypotonic lysis buffer (10 mM Tris-HCl pH 8.0, 1 mM KCl, 1.5 mM $MgCl_2$, 1 mM DTT), and cells were maintained in agitation at 4°C for 30 min. After, the intact nuclei were pelleted at 10,000 rpm for 10 min at 4°C, resuspended in 400 µl of 0.4 N H_2SO_4, and maintained in agitation overnight at 4°C. Next, the samples were centrifuged at 13,200 rpm for 10 min at 4°C; then, histones were precipitated with TCA (33%) and maintained in agitation at 4°C overnight. Next, histones were pelleted at 13,200 rpm for 10 min at 4°C, washed with cold acetone, and centrifugated at 13,200 for 10 min at 4°C; this last step was performed three times. Finally, histones were air-dried for 20 min at room temperature, and the pellet was dissolved in sterile distilled water and stored at −80°C until use. Finally, the histones were resolved on a 15% SDS-PAGE gel to verify the integrity before performing the western blot analysis.

Western blot assays

Histone proteins were transferred to PVDF membranes using a semi-dry transfer system (Fisher Scientific, Waltham, MA, United States). Membranes were blocked with 5% non-fat milk in PBS (pH 7.4) at 4°C for 4 h and then incubated with primary antibodies: anti-H3ac (1:1,000), anti-H3K9ac (1:200), anti-H3K9me2 (1:1,000), anti-H3 (1:5,000), at 4°C overnight. After this, the primary antibodies were removed, and the membranes were incubated with the mouse or anti-rabbit horseradish peroxidase coupled secondary antibodies (1:3,000) at 4°C for 2 h. Finally, the secondary antibody was removed and ECL western blotting substrate WesternsureT (Thermo Scientific, Waltham, MA, USA) was added and developed using the iBright CL1500 Imaging System (Thermo Scientific, Waltham, MA, USA). Signal intensity was quantified by densitometry using the iBright Analysis software (Thermo Scientific, Waltham, MA, USA). The data of the target histone mark were normalized to H3 expression.

Histone deacetylases activity assay

Histone deacetylases (HDACs) activity was evaluated using the cellular histone deacetylase fluorescent kit FLUOR DE LYS® (Enzo, Enzo Biochem, New York, NY, USA) according to the manufacturer's instructions. The kit measures the activity of the HDACs class I (HDAC 1, 2, 3, and 8), class IIa (HDAC 4, 5, 7, and 9), and class IIb (HDAC6 and 10). Briefly, 1×10^4 bMECs were grown on 96-well plates in a complete medium in a 5% CO_2 atmosphere at 37°C for 24 h. Then, the cells were synchronized for 16 h with the incomplete medium. Cells were treated with bPRL (5 ng/ml) and then were challenged with *S. aureus* (MOI 30:1) for 2 h, as control bMECs without any treatment were used. Next, the supernatant was removed, and 50 µl of acetylated FLUOR DE LYS® substrate was added and incubated at 37°C for 4 h. Later, the substrate was removed, the cells were washed with PBS (pH 7.4) three times, and 25 µl of the developer was added and incubated at 37°C for 5 min. A standard curve was generated using serial dilutions (1:10) of the deacetylated FLUOR DE LYS ® standard and the developer supplied with the kit. Finally, the relative fluorescence units (RFU) of both cells and the standard curve counts were acquired with a Varioskan (Thermo Fisher, Waltham, MA, USA) plate reader (360 nm emission and 460 nm excitation). Trichostatin A (TSA, 1 µM; Sigma-Aldrich, St. Louis, MO, USA) was used as an inhibitor of HDACs activity. The data of HDACs activity was calculated and normalized (to 1-fold) regarding the control condition.

Histone demethylases activity

Histone demethylases (HDMs) activity was evaluated using the Jumonji family demethylases activity kit (Invitrogen, Waltham, MA, USA). bMECs were grown on 96-well plates and treated as described for the HDACs assay, and cell lysates were obtained according to the manufacturer's instructions. The product of the enzymatic demethylation reactions is formaldehyde, which was quantitated directly by a fluorescent product with a Varioskan (Thermo Scientific, Waltham, MA, USA) plate reader (450 nm excitation, 510 nm emission). HDM activity was calculated and normalized (to 1-fold) regarding the

1 http://genomics.dote.hu:8080/mirnadesigntool/

control condition. According to the manufacturer's instructions, the assays were run in duplicate from two different experiments.

Statistics analysis

For western blot and ChIP-qPCR analysis, the data were obtained from at least three and four independent experiments, respectively, in triplicate and were compared with a *t*-student, and one-way analysis of variance (ANOVA) using the *post hoc* Tukey test, respectively. The results are reported as the mean ± standard error (SE) with a significance level of $p \leq 0.05$, $p \leq 0.01$, or $p \leq 0.001$. For HDACs and HDMs activity, the data were obtained from at least three and two independent experiments for duplicated, respectively, and were compared using *t*-student. The results are reported as the mean ± standard error (SE) with a significance level of $p \leq 0.05$, $p \leq 0.01$, or $p \leq 0.001$. Finally, for miRNAs analysis, the data were obtained from at least four experiments in triplicate and were compared with the *t*-student and Wilcoxon test. The results are reported as the mean ± SE with a significance level of $p \leq 0.05$, $p \leq 0.01$, or $p \leq 0.001$.

Results

Histone epigenetic marks are regulated by bovine prolactin in bovine mammary epithelial cells during *Staphylococcus aureus* challenge

Previously we reported the bPRL effects on IIR of bMECs. In this work, we analyzed the levels of several histone marks to determine if these effects could be related to epigenetic modulation. The results showed that the global acetylation of histone H3 of bMECs was not modified by bPRL at 12 h (**Figure 1A**). However, in bMECs treated with the hormone for 24 h and challenged with *S. aureus*, the global H3 acetylation decreased by 50% regarding control bMECs (**Figure 1B**). To determine if the hormone regulates specific H3 residues in bMECs, the H3K9ac and H3K9me2 marks were analyzed. The results showed that cells treated 12 h with bPRL and challenged with *S. aureus* significantly decreased the H3K9ac mark (20%) regarding control (**Figure 1C**). Interestingly, there were no significant changes in H3K9ac at 24 h (data not shown). Concerning the H3K9me2 mark, bMECs challenged with *S. aureus* increased significantly this mark (50%), as well as cells treated with bPRL (12 h) alone or together with the challenge (30%) (**Figure 1D**). Finally, bPRL at 24 h of treatment did not modify this mark (data not shown).

To explore if bPRL could be involved in the modulation of H3K9ac through regulating HDACs, the activity of two classes of HDACs (class I and II) was evaluated. The evaluations were performed at 6 and 12 h, considering that the effects of bPRL on the H3K9ac mark were detected at 12 h. Results showed that do not exist significant changes in the HDACs activity in both bMECs treated or not treated with bPRL, but when the bMECs were challenged with *S. aureus*, the HDACs activity was increased (2.3-fold) (**Figures 2A,B**). Also, we evaluated the HDMs activity (enzymes involved in the methyl group remotion), and the results showed a tendency to reduction in activity (10%) in bMECs treated with bPRL 12 h and challenged with *S. aureus* (**Figure 2C**); however, there were no significative differences.

Bovine prolactin regulates the expression of innate immune response elements through H3K9ac and H3K9me2 marks in bovine mammary epithelial cells challenged with *Staphylococcus aureus*

As indicated above, the epigenetic marks H3K9ac and H3K9me2 were modified in bMECs treated with bPRL and challenged with *S. aureus*. To determine the role of these marks in the expression of IIR elements regulated by bPRL, ChIP and quantitative qPCR assays were carried out. The results showed that the H3K9ac mark was enriched significantly in the promoter region of *IL-1β*, *IL-10*, and *BNBD10* genes (1.5, 2.5, and 7.5-fold, respectively) in bMECs treated 12 h with bPRL (**Figure 3A**). Still, this epigenetic mark was reduced significantly in both bMECs treated with bPRL and challenged and in cells only challenged (**Figure 3A**). Also, the promoter region of *TNF-α* gene showed an increase of the H3K9ac mark (5-fold) in bMECs challenged; however, in cells challenged and treated with bPRL this epigenetic mark decreased significantly (3-fold) (**Figure 3A**). Moreover, this mark was not modified in the promoter region of *IL-8* and *LAP* genes under the same conditions (**Figure 3A**). Additionally, we observed an inverse relationship between the H3K9me2 and H3K9ac marks for the *IL-1β* and *IL-10* genes. H3K9me2 mark was significantly enriched in the promoter region of *IL-1β* and *IL-10* (3.5, 2.5-fold, respectively) in bMECs only challenged. Still, it was reduced in bMECs treated with bPRL and challenged or not challenged (**Figure 3B**). A similar effect was observed for the *LAP* gene under the same conditions (**Figure 3B**). Interestingly, the H3K9me2 mark was enriched significantly in the promoter region of *TNF-α* and *IL-8* genes (1.3 and 3-fold, respectively) of bMECs treated with bPRL and challenged (**Figure 3B**). Altogether, these results indicate that bPRL, through epigenetic modifications mediated by H3K9ac and H3K9me2, allows the regulation of gene expression of IIR elements in bMECs. Moreover, this regulation is modified during *S. aureus* challenge. These marks correlate with the level

of the expression of these genes, as reported (Medina-Estrada et al., 2015).

miRNAs expression in bovine mammary epithelial cells is regulated by bovine prolactin during *Staphylococcus aureus* challenge

The expression of diverse miRNAs involved in the regulation of immune response of bMECs was evaluated by qPCR in cells treated with bPRL and challenged with *S. aureus*. The results showed an up-regulation in the expression of miRNAs Let-7a-5p, miR-21a, miR-30b, miR-155, and miR-7863 (2, 1.5, 10, 1.5, and 3.9-fold, respectively) in bMECs challenged with *S. aureus* (**Figure 4**). Also, bPRL (12 h) induced a down-regulation of these miRNAs in bMECs challenged or not challenged (**Figure 4**). Further, a significant increase in the miR-23a expression (3-fold) was observed in bMECs treated only with bPRL (12 h); however, *S. aureus* induced a significant decrease of this miRNA in bMECs treated or not treated with the hormone (**Figure 4F**). On the other hand, the expression of miR-451, miR-144, and miR146a miRNAs was not modified (**Figures 4G–I**). These findings show that bPRL, through the miRNA's expression, could participate in regulating immune response mounted in bMECs challenged with *S. aureus*.

Discussion

Bovine mastitis susceptibility has been associated with abrupt changes in the levels of reproductive hormones that induce an impaired immune response (Lamote et al., 2006; Lacasse et al., 2019; Alhussien and Dang, 2020). Previously we showed that bPRL induces a pro-inflammatory response in bMECs, which is down-regulated in cells challenged with *S. aureus* (Ochoa-Zarzosa et al., 2007; Gutiérrez-Barroso et al., 2008; Lara-Zárate et al., 2011; Medina-Estrada et al., 2015). In this work, we show evidence that this response is regulated by global and specific histone marks on the promoter region of IIR genes and the expression of regulatory miRNAs.

Several reports have shown the role of epigenetic regulation in mammary gland function. For example, the levels of DNA methylation are important for α-casein gene expression (Singh et al., 2010), and an increase in this mark has been reported in peripheral blood lymphocytes from cows with mastitis (Song et al., 2016), as well as in the histone H3K27me3 mark (He et al., 2016). Besides, combined hormones bPRL and 17β-estradiol regulate H3 histone marks during *S. aureus* infection (Salgado-Lora et al., 2020). In this work, bPRL (24 h) and *S. aureus* reduced H3 global acetylation of bMECs (**Figure 1B**), which is related to chromatin compaction that make difficult the access of the transcriptional machinery. This result agrees with the down-regulation of pro-inflammatory genes *TNF-α, IL-1β,* and *IL-8* in *S. aureus*-challenged bMECs and treated with bPRL previously reported (Medina-Estrada et al., 2015). Also, the H3K9ac mark was increased by *S. aureus* in bMECs, but it was reduced in the presence of bPRL (**Figure 1C**). These results agree with the up-regulation of this mark by *S. aureus* reported in a murine mastitis model (Modak et al., 2014). Noteworthy, the H3K9me2 mark was increased by *S. aureus* and bPRL in bMECs (**Figure 1D**), and it inversely correlated with the H3K9ac mark, which also agrees with light lysine demethylases (KDMs) activity reduction (**Figure 2C**). Interestingly, the H3K9ac mark reduction and H3K9me2 induction in bMECs treated with bPRL and challenged coincides with the increase in the HDACs activity (**Figures 2A,B**), which suggests differential regulation of these enzymes. A similar effect was reported by Báez-Magaña et al. (2020), who showed that *S. aureus* induced the HDACs activity in bMECs, which was enhanced by the antimicrobial peptide γ-thionin. However, an opposite effect was reported in bMECs challenged with *S. aureus* and treated with the combined hormones bPRL and 17β-estradiol, in this case, the histone acetylation was increased, but HDACs activity was down-regulated or inhibited (Salgado-Lora et al., 2020). Possibly, 17β-estradiol could be inhibiting the effect of bPRL; however, the cross-linking between both hormone signaling pathways needs further research (Rasmussen et al., 2010).

From those mentioned above, we hypothesized that prolactin could regulate the gene expression of elements of IIR in bMECs through the induction of specific epigenetic marks such as H3K9ac and H3K9me2. ChIP assays showed that bPRL favors the enrichment of the H3K9ac mark in the promoter region of *IL-1β* and *IL-10* genes (**Figure 3A**), which suggests chromatin decompaction that allows the transcriptional machinery access; however, *S. aureus* reduced this mark (**Figure 3A**), suggesting that the chromatin has been condensed. These results agree with a previous report of our group where it was shown that bPRL increased both gene expression and secretion of IL-1β and induced the expression of IL-10, while *S. aureus* downregulated the expression of both genes (Medina-Estrada et al., 2015). Similar findings were reported by Modak et al. (2014) in a murine mastitis model. Also, we observed an inverse relationship between the enrichment of the H3K9ac mark and the H3K9me2 mark in the promoter region of *IL-1β* and *IL-10* genes (**Figures 3A,B**) under the conditions mentioned above. Similar behavior was observed for the *BNBD10* gene concerning the H3K9ac mark (**Figure 3A**), which was consistent with this gene's expression level (personal communication). However, for this gene, even though there was a significant attenuation of the enrichment of the H3K9me2 mark (**Figure 3B**) in all of the conditions evaluated, suggesting the participation of other repressor marks in the negative regulation for the expression of *BNBD10* gene. In this sense, an opposite effect was observed on the *LAP* gene. bMECs only challenged with *S. aureus* showed significant enrichment of the H3K9me2 mark in the promoter region of

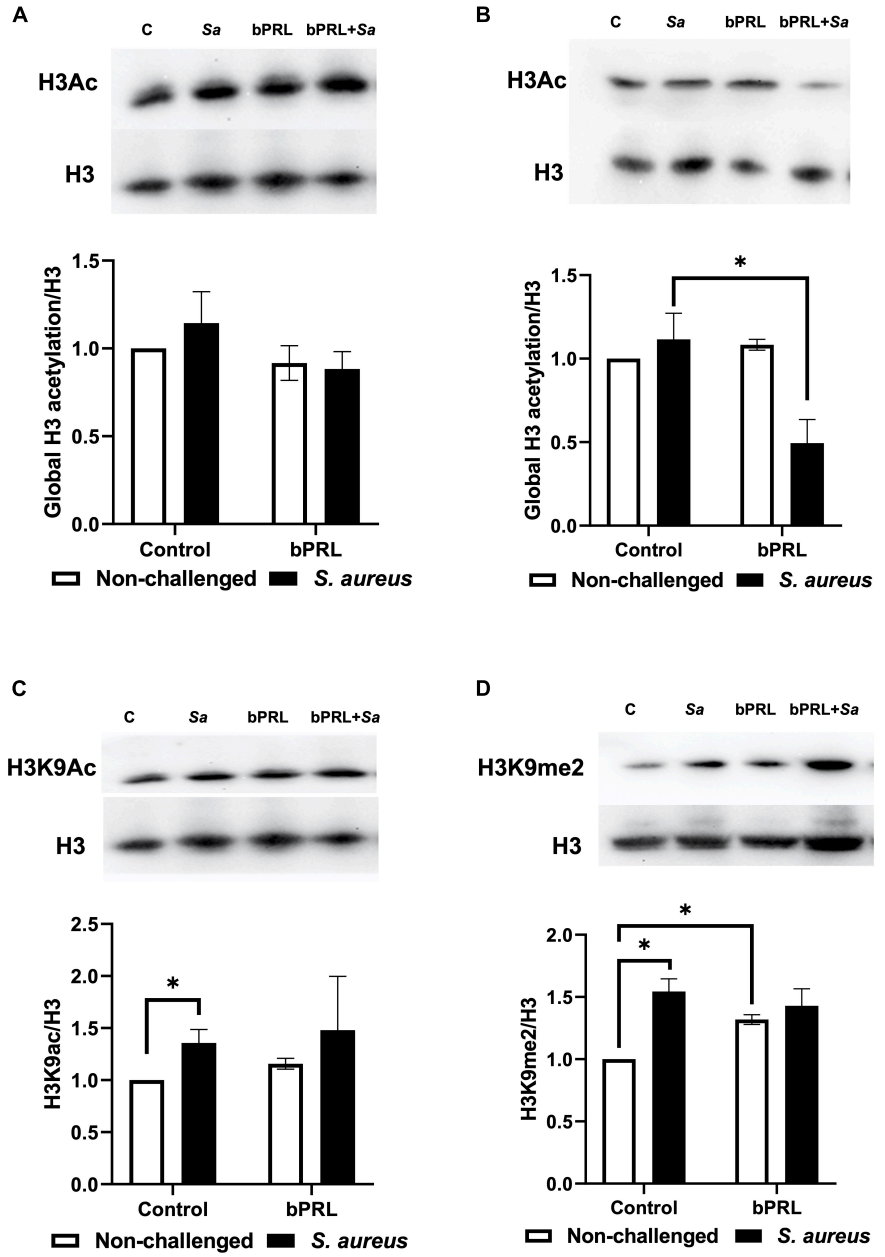

FIGURE 1
Regulation of histone H3 marks by bPRL in bMECs during *S. aureus* challenge. bMECs were treated with bPRL (5 ng/ml), and cells were or not challenged for 2 h with *S. aureus* (MOI 30:1). Densitometrical analysis of the immunoblots that shows the relative expression of global H3ac regarding the total H3 in bMECs treated 12 h **(A)** and 24 h **(B)** with bPRL and challenged or not challenged. Densitometrical analysis of immunoblots that shows the relative expression of H3K9ac mark **(C)** and H3K9me2 mark **(D)** regarding the total H3 in bMECs treated 12 h with bPRL and challenged or not challenged. C, bMECs without any treatment; bPRL, bMECs treated 12 h or 24 h with bPRL (5 ng/ml); bPRL + *Sa*, bMECs treated 12 or 24 h with bPRL (5 ng/ml) and challenged with *S. aureus* for 2 h (MOI = 30:1); *Sa*, bMECs only challenged with *S. aureus* (MOI = 30:1). Representative western blots are shown above each graph. Bars show the mean ± SE of optical density (arbitrary units, AU), considering the expression of control cells (bMECs without treatment) as 1 (data normalized) obtained from four independent experiments (n = 4). The symbol "*" indicates a significant change ($p \leq 0.05$).

this gene, which was attenuated in the presence of the hormone (Figure 3B), while there was no significant enrichment of the H3K9ac mark or inverse correlation concerning the H3K9me2 (Figure 3A); thus, probably the expression of this gene may be regulated for another epigenetic mark such as H3K14ac, H3K27ac, or H3K4me3, which are involved in the relaxing of chromatin and positive expression of genes (Modak et al., 2014). Further research is necessary to respond to these issues.

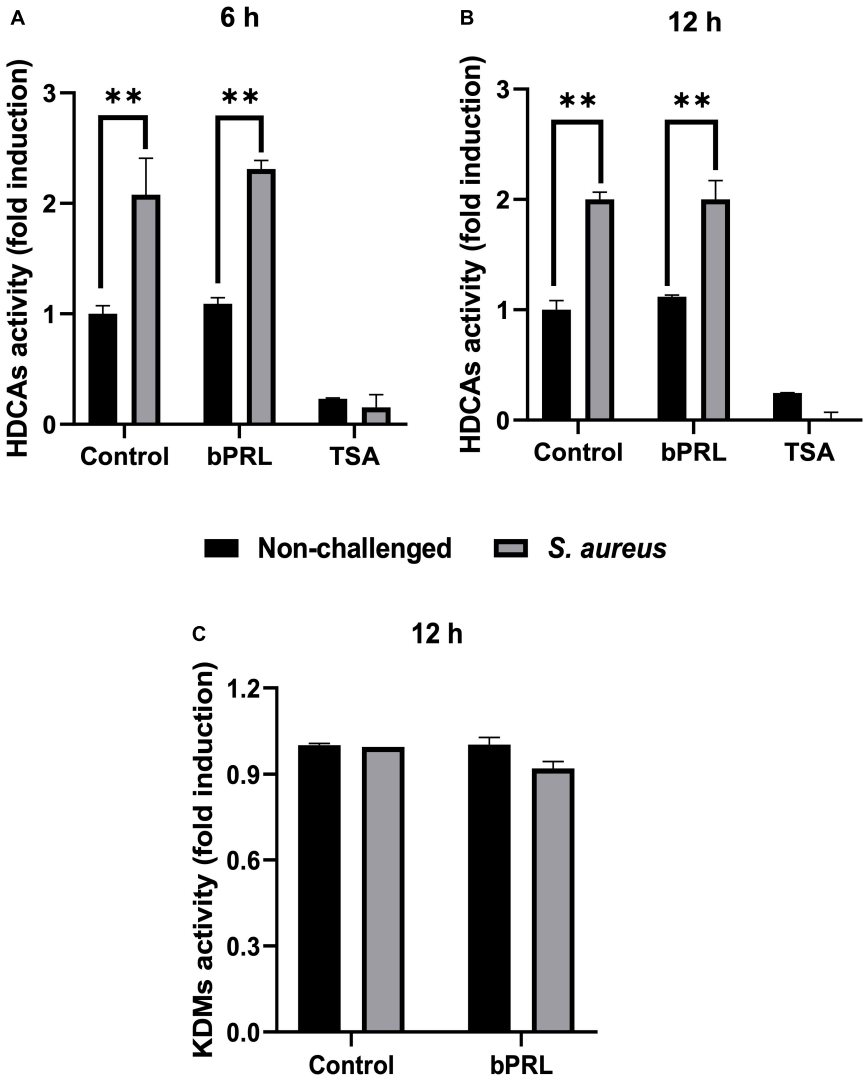

FIGURE 2
Activity of HDACs and HDMs in bMECs treated with bPRL and challenged with *S. aureus*. bMECs were treated **(A)** 6 and **(B)** 12 h with bPRL (5 ng/ml) and then were challenged or not 2 h with *S. aureus* (MOI 30:1). HDACs substrate was added and incubated according to the manufacturer's instructions. Total HDACs activity was determined using the HDAC fluorometric cellular activity assay FLUOR DE LYS®. Each bar shows the mean ± SE of HDAC activity of cells from three independent experiments for duplicates, considering the expression of control cells (bMECs without treatment) as 1 (data normalized). The symbol "**" ($p \leq 0.05$) indicates a significant change. Trichostatin (TSA, 1 μM) was used as an inhibitor of HDACs. **(C)** bMECs were treated 12 h with bPRL (5 ng/ml) and then were challenged or not 2 h with *S. aureus* (MOI 30:1), and were incubated with the substrates for Jumonji demethylases (HDMs). Each bar shows the mean of the HDM activity of cell lysates from two different experiments ± SE, which were run in duplicate ($n = 4$), considering the expression of control cells as 1 (data normalized).

Previously, our group reported that *S. aureus* induced both the gene expression and the secretion of TNF-α in bMECs, and this expression was downregulated by bPRL (Medina-Estrada et al., 2015). This is consistent with our results because the H3K9ac mark was increased on the promoter region of the *TNF*-α gene in bMECs only challenged and was reduced by bPRL (**Figure 3A**). Also, an inverse relationship was observed between the enrichment of the H3K9ac mark and the repressor H3K9me2 mark on the promoter region of the *TNF*-α gene (**Figure 3B**). A similar effect was observed in the promoter region of the *IL-8* gene concerning H3K9me2 (**Figure 3B**), except that an inverse correlation concerning the H3K9me2 mark only was observed in cells treated or not treated with the hormone and challenged with *S. aureus* (**Figure 3B**). To our knowledge, this is the first report that correlates epigenetics marks in the regulation of IIR by the lactogenic hormone bPRL in bMECs challenged with *S. aureus*.

On the other hand, small non-coding RNA molecules such as miRNAs are involved in regulating many physiologic processes; their role has been reported particularly in regulating

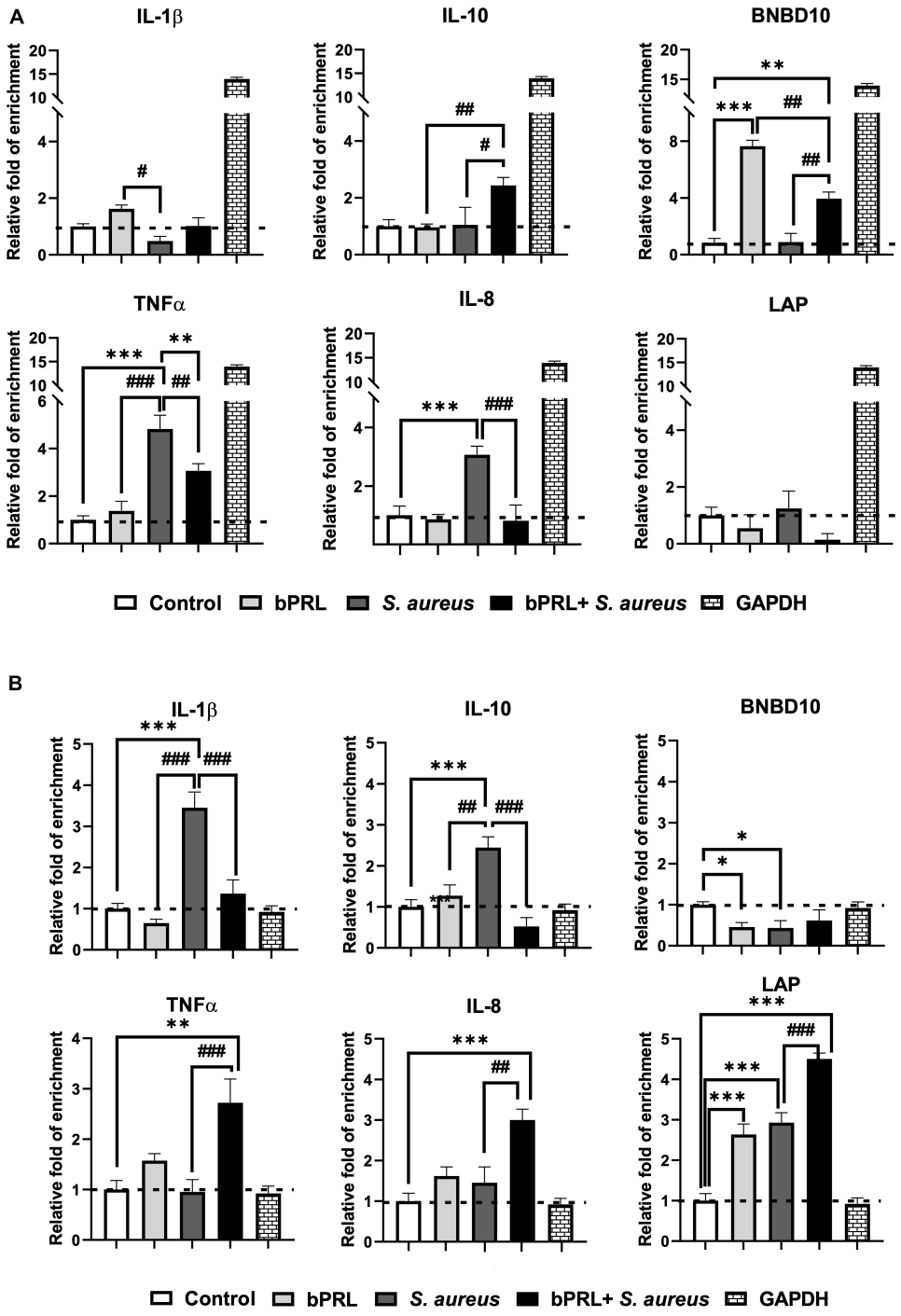

FIGURE 3
Analysis of epigenetic modulation of H3K9ac and H3K9me2 marks in the promoter region of IIR elements in bMECs treated with bPRL and challenged with *S. aureus*. bMECs were treated 12 h with bPRL (5 ng/ml), and cells were or not challenged for 2 h with *S. aureus* (MOI = 30:1). **(A)** The ChIP-qPCR assay was performed to evaluate the relative enrichment of the H3K9ac mark on the promoter region of *IL-1β*, *IL-10*, *BNBD10*, *TNF-α*, *IL-8*, and *LAP*. **(B)** Relative enrichment of the H3K9me2 mark on the promoter region of *IL-1β*, *IL-10*, *BNBD10*, *TNF-α*, *IL-8*, and *LAP*. Control, bMECs without any treatment; bPRL, bMECs treated 12 h with bPRL (5 ng/ml); bPRL + *S. aureus*: bMECs treated 12 h with bPRL (5 ng/ml) and challenged with *S. aureus* (MOI = 30:1); *S. aureus*, bMECs only challenged with *S. aureus* (MOI = 30:1). The data were normalized regarding IgG-Ab isotype control, and the expression of control cells (cells without treatment) was considered as one. The data correspond to the mean ± SE from four independent experiments ($n = 4$). "*" ($p \leq 0.05$), "**" ($p \leq 0.01$), and "***" ($p \leq 0.001$) indicate a significant change regarding control (bMECs without any treatment). "#" ($p \leq 0.05$), "##" ($p \leq 0.01$), and "###" ($p \leq 0.001$) indicate a significant change regarding bMECs+*S. aureus* condition. GAPDH was used as a positive control of enrichment (for H3K9ac) and not enrichment (for H3K9me2).

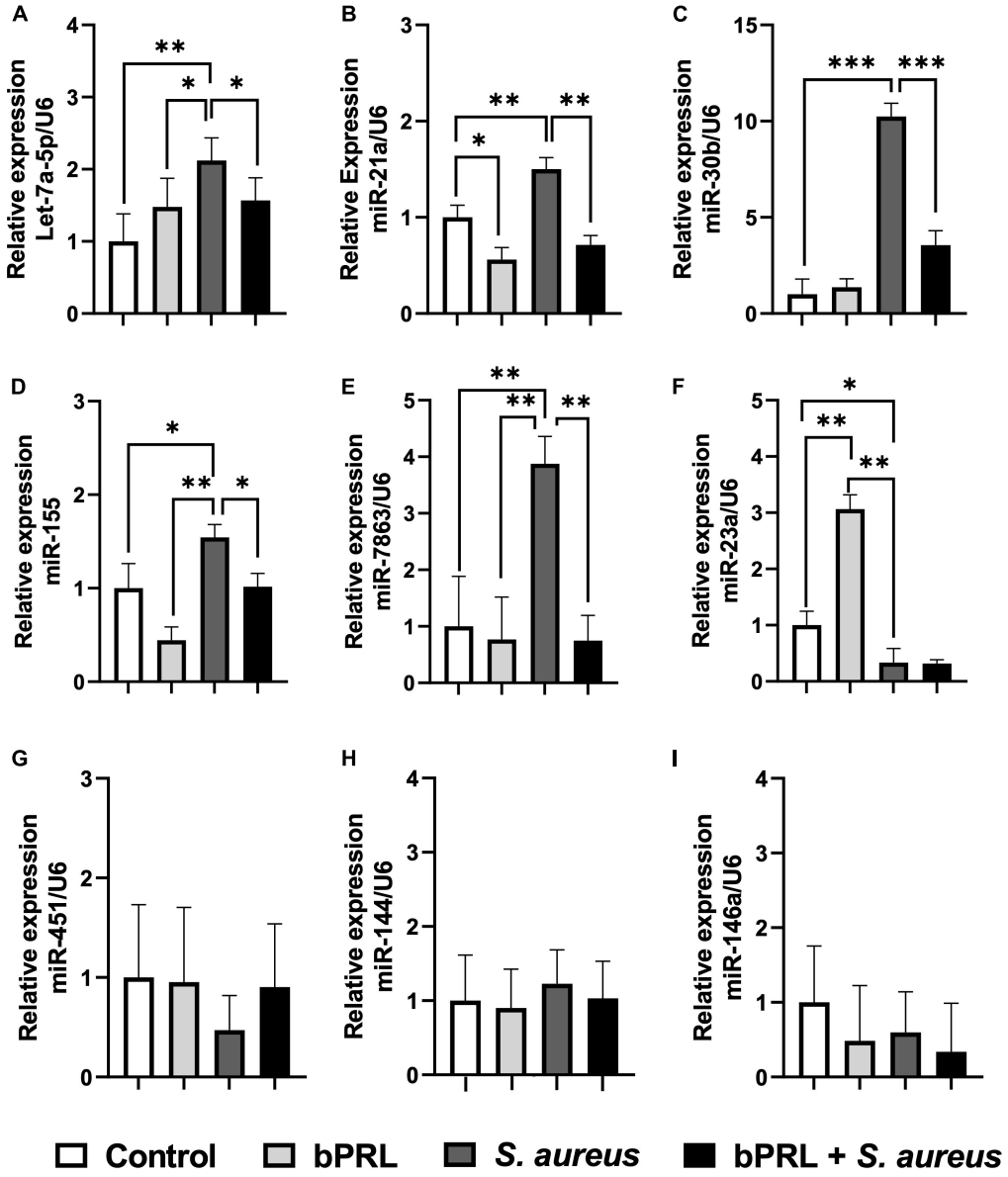

FIGURE 4
Bovine prolactin regulates the miRNAs expression in bMECs during *S. aureus* challenge. bMECs were treated 12 h with bPRL (5 ng/ml) and then were or not challenged for 2 h with *S. aureus* (MOI = 30:1). The RT-qPCR assay using the $\Delta\Delta$Ct comparative method was performed to evaluate the expression of miRNAs Let-7a-5p **(A)**, miR-21a **(B)**, miR-30b **(C)**, miR-155 **(D)**, miR-7863 **(E)**, miR-23a **(F)**, miR-451 **(G)**, miR-144 **(H)**, miR-146a **(I)**. Control, bMECs without any treatment; bPRL, bMECs treated 12 h with bPRL (5 ng/ml); bPRL + *S. aureus*, bMECs treated 12 h with bPRL (5 ng/ml) and challenged with *S. aureus* for 2 h (MOI = 30:1); *S. aureus*, bMECs only challenged with *S. aureus* (MOI = 30:1). Data were normalized regarding internal control U6. Each bar shows the mean ± SE and was analyzed using *t*-student and Wilcoxon tests from four independent experiments ($n = 4$). "*" ($p \leq 0.05$), "**" ($p \leq 0.01$), and "***" ($p \leq 0.001$) indicate significant differences.

the immune response during infectious diseases (Hirschberger et al., 2018; Nejad et al., 2018). To evaluate other epigenetics mechanisms modulated by bPRL, the expression of miRNAs involved in the regulation of IIR genes by *S. aureus* such as mir-21a, miR-30b, Let-7a-5p, miR-155, miR-23a, miR-7863, miR-144, miR-146a, and mi-451 was analyzed (Jin et al., 2014). Let-7a-5p, miR-21a, and mir-30b have a key role in the regulation of expression of IIR genes such as IL-6, IL-1β, and TNF-α through the direct interaction with elements downstream of the signaling pathway of Toll-like receptors (TLRs) and it has been reported that their overexpression promotes the internalization and persistence of intracellular bacteria in the cells host (Zhou et al., 2018). We showed that Let-7a-5p, miR-21a, and mir-30b were up-regulated in bMECs challenged with *S. aureus* and down-regulated significantly in the presence of bPRL (**Figures 4A–C**). This is in agreement with

Xu et al. (2021), who demonstrated that the pro-inflammatory response induced by bacterial lipopolysaccharide (LPS) is alleviated when miR-30b is silenced (Xu et al., 2021). In addition, Corsetti et al. (2018) reported that inhibition of expression of miR-21a induced the downregulation of TNF-α and promoted bacterial control in the host cell (Corsetti et al., 2018). In contrast to our results, Magryś and Bogut (2021) reported that a small variant colony (SVC) of *Staphylococcus epidermidis* down-regulated the expression of Let-7a-5p changing the pro-inflammatory profile to an anti-inflammatory environment that favors its intracellular persistence in macrophages THP-1. In this sense, Let-7a-5p could be key in the immune response of bMECs during *S. aureus* infection because the upregulation of this miRNA coincides with the downregulation of expression of IL-6 (Medina-Estrada et al., 2015; Zaatout et al., 2020). Further investigation is necessary to identify the molecular targets of miR-21a, and mir-30b and the key role in the immune response in bMECs challenged with *S. aureus* and treated or not with bPRL. On the other hand, miR-155 is the master regulator of pro-inflammatory genes, which are up-regulated through the signaling pathway of TLRs; this miRNA targets the IKKβ kinase, which is involved in the modulation of translocation of the transcription factor nuclear factor κ B (NF-κ B) to nuclei and promotes the expression of pro-inflammatory mediators (Zhou et al., 2018). In this sense, the interaction IKKβ k-miR-155 promotes in bacterial infections the escape to immune response mounted for the host through the downregulation of the expression of pro-inflammatory genes (Zhou et al., 2018). In this study, we showed that *S. aureus* promotes a significant upregulation of miR-155 in bMECs. This expression was attenuated in the presence of bPRL (**Figure 4D**). This supports the fact that miR-155 plays a key role in the success of the establishment and persistence of bacterial infection. Moreover, it has been reported that overexpression of miR-155 induces the expression and production of TNF-α in mycobacterial infection (Behrouzi et al., 2019). This is consistent with our results, where we showed an H3K9ac mark increased in the promotor gene of TNF-α (**Figure 3A**), which promotes the transcription of this gene and protein secretion (Medina-Estrada et al., 2015). Interestingly, the presence of bPRL attenuated the expression of miR-155 and coincides with the reduction of the H3K9ac mark in the promoter region of TNF-α and the reduction of gene expression and protein secretion (Medina-Estrada et al., 2015). A similar effect was reported by Rajaram et al. (2011), who demonstrated that lipomannan, a component of the cellular wall of *Mycobacterium tuberculosis,* blocks TNF-α synthesis mediated by mir-155 (Rajaram et al., 2011). In this sense, bPRL could be key for the downregulation of TNF-α through H3K9ac and miR-155. miR-23a is also a miRNA that regulates the inflammatory response by inhibiting the translocation of NF-κ B to nuclei and targeting PI3K kinase (Zhou et al., 2018). Recently, Cai et al. (2021) reported that short exposition of lipoteichoic acid (LTA), a component of the cellular wall of *S. aureus*, induced the overexpression of miR-23a, which targeted the PI3K kinase-TLR2-MyD88 axis and downregulated the pro-inflammatory response in the cell line MAC-T (bovine mammary epithelial cells), while the inhibition of expression of miR-23a or long exposition of LTA reversed this effect (Cai et al., 2021). Our results showed a similar effect in bMECs treated only with bPRL; we observed a significant increment of expression of miR-23a, but this expression was downregulated in the presence of the bacteria (**Figure 4F**). Possibly, short periods of the exposition of bMECs with *S. aureus* are sufficient to decrease the protective effect of bPRL through miR-23a-TLR2-MyD88-IP3K kinase. However, the regulatory mechanism of miR-23 related to the immune response is still poorly understood. We detected a significative level of expression of miR-7863 in bMECs challenged with *S. aureus*, which was down-regulated in the presence of bPRL (**Figure 4E**). This agrees with Luoreng et al. (2018). They reported through transcriptional analysis the expression of miR-7863 only in mastitis caused by *S. aureus* or *E. coli*. In this sense, miR-7863 could be a biomarker of bovine mastitis. Moreover, given that bPRL down-regulated the expression of miR-7863, it could be interesting to investigate the target of this miRNA and the molecular mechanism involved in the immune response during bacterial infection. Finally, even though miR-451, miR-144, and miR-146a are important regulators of the pro-inflammatory during bacterial infections (Zhou et al., 2018), we did not observe any changes in the expression level of these miRNAs in our model of study (**Figures 4G–I**). This suggests that miR-451, miR-144, and miR-146a are not key in regulating the immune response of bMECs during *S. aureus* challenge.

Conclusion

Bovine prolactin regulates the IIR of bMECs through modifications of H3K9ac and H3K9me2 marks and the expression of miRNAs. In general, we observed that bPRL induced an anti-inflammatory profile in bMECs through the regulation of epigenetic marks in promotor genes of key cytokines and in the induction of miRNAs that block the pro-inflammatory cytokine production, reverting the inflammatory response induced by *S. aureus*. To our knowledge, this is the first report that correlates epigenetic mechanisms in regulating elements of IIR modulated by lactogenic hormone bPRL in bMECs challenged with *S. aureus*.

Data availability statement

The raw data supporting the conclusions of this article will be made available by the authors, without undue reservation.

Author contributions

MB-M, MS-L, JL-M, and AO-Z conceptualized and designed the experiments and analyzed the data. MB-M and MS-L performed the experiments. MB-M, JL-M, and AO-Z wrote the manuscript. All authors read and approved the final manuscript.

Funding

This work was supported by grants from CONACyT (CB 2016-287210) and CIC 14.1 from Universidad Michoacana de San Nicolás de Hidalgo to AO-Z. MB-M obtained a Ph.D. Scholarship from CONACyT (743402).

Conflict of interest

The authors declare that the research was conducted in the absence of any commercial or financial relationships that could be construed as a potential conflict of interest.

Publisher's note

All claims expressed in this article are solely those of the authors and do not necessarily represent those of their affiliated organizations, or those of the publisher, the editors and the reviewers. Any product that may be evaluated in this article, or claim that may be made by its manufacturer, is not guaranteed or endorsed by the publisher.

References

Alhussien, M. N., and Dang, A. K. (2020). Interaction between stress hormones and phagocytic cells and its effect on the health status of dairy cows: a review. *Vet. World* 13:1837. doi: 10.14202/vetworld.2020.1837-1848

Alva-Murillo, N., López-Meza, J. E., and Ochoa-Zarzosa, A. (2014). Nonprofessional phagocytic cell receptors involved in *Staphylococcus aureus* internalization. *Biomed Res. Int.* 2014:538546. doi: 10.1155/2014/538546

Anaya-López, J. L., Contreras-Guzmán, O. E., Cárabez-Trejo, A., Baizabal-Aguirre, V. M., Lopez-Meza, J. E., Valdez-Alarcon, J. J., et al. (2006). Invasive potential of bacterial isolates associated with subclinical bovine mastitis. *Res. Vet. Sci.* 81, 358–361. doi: 10.1016/j.rvsc.2006.02.002

Atalla, H., Gyles, C., Jacob, C. L., Moisan, H., Malouin, F., and Mallard, B. (2008). Characterization of a *Staphylococcus aureus* small colony variant (SCV) associated with persistent bovine mastitis. *Foodborne Pathog. Dis.* 5, 785–799. doi: 10.1089/fpd.2008.0110

Báez-Magaña, M., Alva-Murillo, N., Medina-Estrada, I., Arceo-Martínez, M. T., López-Meza, J. E., and Ochoa-Zarzosa, A. (2020). Plant defensin γ-thionin induces MAPKs and activates histone deacetylases in bovine mammary epithelial cells infected with *Staphylococcus aureus*. *Front. Vet. Sci.* 7:390. doi: 10.3389/fvets.2020.00390

Barkema, H. W., Schukken, Y. H., and Zadoks, R. N. (2006). Invited review: the role of cow, pathogen, and treatment regimen in the therapeutic success of bovine *Staphylococcus aureus* mastitis. *J. Dairy Sci.* 89, 1877–1895. doi: 10.3168/jds.S0022-0302(06)72256-1

Barlow, J. (2011). Mastitis therapy and antimicrobial susceptibility: a multispecies review with a focus on antibiotic treatment of mastitis in dairy cattle. *J. Mamm. Gland Biol. Neoplasia* 16, 383–407. doi: 10.1007/s10911-011-9235-z

Behrouzi, A., Alimohammadi, M., Nafari, A. H., Yousefi, M. H., Riazi Rad, F., Vaziri, F., et al. (2019). The role of host miRNAs on *Mycobacterium tuberculosis*. *ExRNA* 1:40. doi: 10.1186/s41544-019-0040-y

Berczi, I., and Nagy, E. (2019). "Prolactin and other lactogenic hormones," in *Pituitary Function and Immunity*. eds B. Istvan and N. Eva (Boca Raton, FL: CRC Press), 161–184. doi: 10.1201/9780429279737-6

Binart, N. (2017). "Prolactin," in *The Pituitary*. ed. B. Nadine (London: Academic Press), 129–161. doi: 10.1016/B978-0-12-804169-7.00005-2

Brisken, C., and O'Malley, B. (2010). Hormone action in the mammary gland. *Cold Spring Harb Perspect. Biol.* 2:a003178. doi: 10.1101/cshperspect.a003178

Cai, M., Fan, W., Li, X., Sun, H., Dai, L., Lei, D., et al. (2021). The regulation of *Staphylococcus aureus*-induced inflammatory responses in bovine mammary epithelial cells. *Front. Vet. Sci.* 8:683886. doi: 10.3389/fvets.2021.683886

Carey, M. F., Peterson, C. L., and Smale, S. T. (2009). Chromatin immunoprecipitation (chip). *Cold Spring Harb. Protoc.* 2009:db–rot5279. doi: 10.1101/pdb.prot5279

Conlon, B. P. (2014). *Staphylococcus aureus* chronic and relapsing infections: evidence of a role for persister cells: an investigation of persister cells, their formation and their role in *S. aureus* disease. *Bioessays* 36, 991–996. doi: 10.1002/bies.201400080

Corsetti, P. P., de Almeida, L. A., Gonçalves, A. N. A., Gomes, M. T. R., Guimarães, E. S., Marques, J. T., et al. (2018). miR-181a-5p regulates TNF-α and miR-21a-5p influences gualynate-binding protein 5 and IL-10 expression in macrophages affecting host control of *Brucella abortus* infection. *Front. Immunol.* 9:1331. doi: 10.3389/fimmu.2018.01331

Dego, O. K. (2020). "Bovine Mastitis," in *Animal Reproduction in Veterinary Medicine*, Part I, eds F. Aral, R. Payan-Carreira, and M. Quaresma (London: IntechOpen), doi: 10.5772/intechopen.93483

Devinoy, E., and Rijnkels, M. (2010). Epigenetics in mammary gland biology and cancer. *J. Mamm. Gland Biol. Neoplasia* 15, 1–4. doi: 10.1007/s10911-010-9171-3

Do, D. N., Dudemaine, P. L., Mathur, M., Suravajhala, P., Zhao, X., and Ibeagha-Awemu, E. M. (2021). miRNA regulatory functions in farm animal diseases, and biomarker potentials for effective therapies. *Int. J. Mol. Sci.* 22:3080. doi: 10.3390/ijms22063080

Gutiérrez-Barroso, A., Anaya-López, J. L., Lara-Zárate, L., Loeza-Lara, P. D., López-Meza, J. E., and Ochoa-Zarzosa, A. (2008). Prolactin stimulates the internalization of Staphylococcus aureus and modulates the expression of inflammatory response genes in bovine mammary epithelial cells. *Vet. Immunol. Immunopathol.* 121, 113–122. doi: 10.1016/j.vetimm.2007.09.007

Han, S., Li, X., Liu, J., Zou, Z., Luo, L., Wu, R., et al. (2020). Bta-miR-223 Targeting CBLB contributes to resistance to *Staphylococcus aureus* mastitis through the PI3K/AKT/NF-κB pathway. *Front. Vet. Sci.* 7:529. doi: 10.3389/fvets.2020.00529

He, Y., Song, M., Zhang, Y., Li, X., Song, J., Zhang, Y., et al. (2016). Whole-genome regulation analysis of histone H3 lysin 27 trimethylation in subclinical mastitis cows infected by *Staphylococcus aureus*. *BMC Genomics* 17:565. doi: 10.1186/s12864-016-2947-0

Hirschberger, S., Hinske, L. C., and Kreth, S. (2018). MiRNAs: dynamic regulators of immune cell functions in inflammation and cancer. *Cancer Lett.* 431, 11–21. doi: 10.1016/j.canlet.2018.05.020

Huijps, K., Lam, T. J., and Hogeveen, H. (2008). Costs of mastitis: facts and perception. *J. Dairy Res.* 75:113. doi: 10.1017/S0022029907002932

Ivanova, E., Le Guillou, S., Hue-Beauvais, C., and Le Provost, F. (2021). Epigenetics: new insights into mammary gland biology. *Genes* 12:231. doi: 10.3390/genes12020231

Jin, W., Ibeagha-Awemu, E. M., Liang, G., Beaudoin, F., and Zhao, X. (2014). Transcriptome microRNA profiling of bovine mammary epithelial cells challenged with *Escherichia coli* or *Staphylococcus aureus* bacteria reveals pathogen directed microRNA expression profiles. *BMC Genomics* 15:181. doi: 10.1186/1471-2164-15-181

Josse, J., Laurent, F., and Diot, A. (2017). Staphylococcal adhesion and host cell invasion: fibronectin-binding and other mechanisms. *Front. Microbiol.* 8:2433. doi: 10.3389/fmicb.2017.02433

Khan, M. Z., Khan, A., Xiao, J., Ma, Y., Ma, J., Gao, J., et al. (2020). Role of the JAK-STAT pathway in bovine mastitis and milk production. *Animals* 1:2107. doi: 10.3390/ani10112107

Lacasse, P., Zhao, X., and Ollier, S. (2019). Effect of stage of lactation and gestation on milking-induced hormone release in lactating dairy cows. *Domestic Anim. Endocrinol.* 66, 72–85. doi: 10.1016/j.domaniend.2018.10.003

Lamote, I., Meyer, E., De Ketelaere, A., Duchateau, L., and Burvenich, C. (2006). Expression of the estrogen receptor in blood neutrophils of dairy cows during the periparturient period. *Theriogenology* 65, 1082–1098. doi: 10.1016/j.theriogenology.2005.07.017

Lara-Zárate, L., López-Meza, J. E., and Ochoa-Zarzosa, A. (2011). *Staphylococcus aureus* inhibits nuclear factor kappa B activation mediated by prolactin in bovine mammary epithelial cells. *Microb. Pathog.* 51, 313–318. doi: 10.1016/j.micpath.2011.07.010

Lee, A. S., de Lencastre, H., Garau, J., Kluytmans, J., Malhotra-Kumar, S., Peschel, A., et al. (2018). Methicillin-resistant *Staphylococcus aureus*. *Nat. Rev. Dis. Primers* 4, 1–23. doi: 10.1038/nrdp.2018.33

Lewandowska-Sabat, A. M., Hansen, S. F., Solberg, T. R., Østerås, O., Heringstad, B., Boysen, P., et al. (2018). MicroRNA expression profiles of bovine monocyte-derived macrophages infected in vitro with two strains of *Streptococcus agalactiae*. *BMC Genomics* 19:241. doi: 10.1186/s12864-018-4591-3

Luoreng, Z. M., Wang, X. P., Mei, C. G., and Zan, L. S. (2018). Comparison of microRNA profiles between bovine mammary glands infected with *Staphylococcus aureus* and *Escherichia coli*. *Int. J. Biol. Sci.* 14, 87–99. doi: 10.7150/ijbs.22498

Magryś, A., and Bogut, A. (2021). MicroRNA hsa-let-7a facilitates staphylococcal small colony variants survival in the THP-1 macrophages by reshaping inflammatory responses. *Int. J. Med. Microbiol.* 311:151542. doi: 10.1016/j.ijmm.2021.151542

Medina-Estrada, I., Alva-Murillo, N., López-Meza, J. E., and Ochoa-Zarzosa, A. (2015). Non-classical effects of prolactin on the innate immune response of bovine mammary epithelial cells: implications during *Staphylococcus aureus* internalization. *Microb. Pathog.* 89, 43–53. doi: 10.1016/j.micpath.2015.08.018

Modak, R., Mitra, S. D., Vasudevan, M., Krishnamoorthy, P., Kumar, M., Bhat, A. V., et al. (2014). Epigenetic response in mice mastitis: role of histone H3 acetylation and microRNA (s) in the regulation of host inflammatory gene expression during *Staphylococcus aureus* infection. *Clin. Epigenet.* 6:12. doi: 10.1186/1868-7083-6-12

Nejad, C., Stunden, H. J., and Gantier, M. P. (2018). A guide to miRNAs in inflammation and innate immune responses. *FEBS J.* 285, 3695–3716. doi: 10.1111/febs.14482

Ochoa-Zarzosa, A., Gutiérrez-Barroso, A., Lara-Zárate, L., Loeza-Lara, P. D., Anaya-López, J. L., and López-Meza, J. E. (2007). Prolactin stimulates endocytosis of *Staphylococcus aureus* in bovine mammary ephithelial cells. *Vet. México* 38, 455–465.

Parlow, A. F. (2002). National hormone & peptide program-NIDDK. *J. Clin. Endocrinol. Metab.* 87, 3514–3516. doi: 10.1210/jcem.87.7.0134

Pitkälä, A., Haveri, M., Pyörälä, S., Myllys, V., and Honkanen-Buzalski, T. (2004). Bovine mastitis in Finland 2001—prevalence, distribution of bacteria, and antimicrobial resistance. *J. Dairy Sci.* 87, 2433–2441. doi: 10.3168/jds.S0022-0302(04)73366-4

Rajaram, M. V., Ni, B., Morris, J. D., Brooks, M. N., Carlson, T. K., Bakthavachalu, B., et al. (2011). *Mycobacterium tuberculosis* lipomannan blocks TNF biosynthesis by regulating macrophage MAPK-activated protein kinase 2 (MK2) and microRNA miR-125b. *Proc. Natl. Acad. Sci. U.S.A.* 108, 17408–17413. doi: 10.1073/pnas.1112660108

Rasmussen, L. M., Frederiksen, K. S., Din, N., Galsgaard, E., Christensen, L., Berchtold, M. W., et al. (2010). Prolactin and oestrogen synergistically regulate gene expression and proliferation of breast cancer cells. *Endocr. Relat. Cancer* 17, 809–822. doi: 10.1677/ERC-09-0326

Reshi, A. A., Husain, I., Bhat, S. A., Rehman, M. U., Razak, R., Bilal, S., et al. (2015). Bovine mastitis as an evolving disease and its impact on the dairy industry. *Int. J. Curr. Res. Rev.* 7:48.

Ruegg, P. L. (2017). A 100-year review: mastitis detection, management, and prevention. *J. Dairy Sci.* 100, 10381–10397. doi: 10.3168/jds.2017-13023

Salgado-Lora, M. G., Medina-Estrada, I., López-Meza, J. E., and Ochoa-Zarzosa, A. (2020). Prolactin and estradiol are epigenetic modulators in bovine mammary epithelial cells during *Staphylococcus aureus* infection. *Pathogens* 9:520. doi: 10.3390/pathogens9070520

Savino, W. (2017). Prolactin: an immunomodulator in health and disease. *Endocr. Immunol.* 48, 69–75. doi: 10.1159/000452906

Shechter, D., Dormann, H. L., Allis, C. D., and Hake, S. B. (2007). Extraction, purification and analysis of histones. *Nat. Protoc.* 2, 1445–1457. doi: 10.1038/nprot.2007.202

Singh, K., Erdman, R. A., Swanson, K. M., Molenaar, A. J., Maqbool, N. J., Wheeler, T. T., et al. (2010). Epigenetic regulation of milk production in dairy cows. *J. Mamm. Gland Biol. Neoplasia* 15, 101–112. doi: 10.1007/s10911-010-9164-2

Song, M., He, Y., Zhou, H., Zhang, Y., Li, X., and Yu, Y. (2016). Combined analysis of DNA methylome and transcriptome reveal novel candidate genes with susceptibility to bovine *Staphylococcus aureus* subclinical mastitis. *Sci. Rep.* 6:29390. doi: 10.1038/srep29390

Varkonyi-Gasic, E., and Hellens, R. P. (2011). Quantitative stem-loop RT-PCR for detection of microRNAs. *Methods Mol. Biol.* 744, 145–157. doi: 10.1007/978-1-61779-123-9_10

Wang, M., and Ibeagha-Awemu, E. M. (2021). Impacts of epigenetic processes on the health and productivity of livestock. *Front. Genet.* 11:613636. doi: 10.3389/fgene.2020.613636

Wilson, D. J., Gonzalez, R. N., and Das, H. H. (1997). Bovine mastitis pathogens in New York and Pennsylvania: prevalence and effects on somatic cell count and milk production. *J. Dairy Sci.* 80, 2592–2598. doi: 10.3168/jds.S0022-0302(97)76215-5

Xu, J., Li, H., Lv, Y., Zhang, C., Chen, Y., and Yu, D. (2021). Silencing XIST mitigated lipopolysaccharide (LPS)-induced inflammatory injury in human lung fibroblast WI-38 cells through modulating miR-30b-5p/CCL16 axis and TLR4/NF-κB signaling pathway. *Open Life Sci.* 16, 108–127. doi: 10.1515/biol-2021-0005

Zaatout, N., Ayachi, A., and Kecha, M. (2020). *Staphylococcus aureus* persistence properties associated with bovine mastitis and alternative therapeutic modalities. *J. Appl. Microbiol.* 129, 1102–1119. doi: 10.1111/jam.14706

Zhou, X., Li, X., and Wu, M. (2018). miRNAs reshape immunity and inflammatory responses in bacterial infection. *Signal Transduct. Target. Ther.* 3:14. doi: 10.1038/s41392-018-0006-9

frontiers | Frontiers in Microbiology

TYPE Original Research
PUBLISHED 26 September 2022
DOI 10.3389/fmicb.2022.1009798

OPEN ACCESS

EDITED BY
Beatrice Vitali,
University of Bologna, Italy

REVIEWED BY
Noble K. Kurian,
Atmiya University, India
Sara Morselli,
Sant'Orsola-Malpighi Polyclinic, Italy

*CORRESPONDENCE
Fengyu Zhang
zfengyu@mail.sdu.edu.cn
Lichuan Gu
lcgu@sdu.edu.cn

SPECIALTY SECTION
This article was submitted to Infectious Agents and Disease, a section of the journal Frontiers in Microbiology

RECEIVED 02 August 2022
ACCEPTED 30 August 2022
PUBLISHED 26 September 2022

CITATION
Zhang K, Lu M, Zhu X, Wang K, Jie X, Li T, Dong H, Li R, Zhang F and Gu L (2022) Antibiotic resistance and pathogenicity assessment of various *Gardnerella* sp. strains in local China. *Front. Microbiol.* 13:1009798. doi: 10.3389/fmicb.2022.1009798

Antibiotic resistance and pathogenicity assessment of various *Gardnerella* sp. strains in local China

Kundi Zhang[1], Mengyao Lu[1], Xiaoxuan Zhu[1], Kun Wang[2], Xuemei Jie[2], Tan Li[3], Hongjie Dong[1], Rongguo Li[2], Fengyu Zhang[1]* and Lichuan Gu[1]*

[1]State Key Laboratory of Microbial Technology, Shandong University, Qingdao, China, [2]Jinan Key Laboratory of Female Reproductive Tract Infection, Jinan Genital Tract Microecological Clinical Laboratory, Jinan Maternity and Child Care Hospital Affiliated to Shandong First Medical University, Jinan, China, [3]Faculty of Health Sciences, Cumming School of Medicine, Calgary, AB, Canada

Gardnerella overgrowth is the primary cause of bacterial vaginosis (BV), a common vaginal infection with incidences as high as 23–29% worldwide. Here, we studied the pathogenicity, drug resistance, and prevalence of varying *Gardnerella* spp. We isolated 20 *Gardnerella* strains from vaginal samples of 31 women in local China. Ten strains were then selected *via* phylogenetic analysis of *cpn60* and *vly* gene sequences to carry out genome sequencing and comparative genomic analysis. Biofilm-formation, sialidase, and antibiotic resistance activities of the strains were characterized. All strains showed striking heterogeneity in genomic structure, biofilm formation and drug resistance. Two of the ten strains, JNFY3 and JNFY15, were classified as *Gardnerella swidsinskii* and *Gardnerella piotii*, respectively, according to their phenotypic characteristics and genome sequences. In particular, seven out of the ten strains exhibited super resistance (≥ 128 μg/mL) to metronidazole, which is the first line of treatment for BV in China. Based on the biochemical and genomic results of the strains, we proposed a treatment protocol of prevalent *Gardnerella* strains in local China, which provides the basis for accurate diagnosis and therapy.

KEYWORDS

***Gardnerella vaginalis*, prevalent strains, comparative genomics, antibiotic resistance, accurate diagnosis and therapy**

Introduction

Gardnerella vaginalis is a facultatively anaerobic bacterium of the *Bifidobacteriaceae* family and part of the normal vaginal microbiome. Often described as a Gram variable organism with a Gram-positive wall type, the genome size of the type strain ATCC 14018 is remarkably small compared to other facultative anaerobes (Greenwood and Pickett, 1980). At only 1.6 M, it is one-third and one-fifth that of *E. coli* and

Pseudomonas aeruginosa, respectively. In addition, no plasmids nor phages have been characterized in any identified strains thus far (Yeoman et al., 2010). As such, the metabolic pathway of *G. vaginalis* is also relatively simple, with only succinic acid dehydrogenase and malate dehydrogenase remaining in the TCA cycle (Greenwood and Pickett, 1980).

As a conditional pathogen, *G. vaginalis* has a very simple cell signaling system and a relatively rich virulence system, which leads to differences in pathogenicity amongst various strains. The type strain, for example, does not contain signaling molecules such as c-di-NMP and cNMP (He et al., 2016), thus lacking the second messenger system of cyclic nucleotides commonly used in most strains. It only has six pairs of two-component systems (TCS), which is rather simple compared to the 130 pairs of TCS in *Pseudomonas aeruginosa* (Francis et al., 2017). Regarding the virulence system, strain ATCC 14019 has no typical secretory system (Hood et al., 2010) and does not contain flagella, and its adhesion to the epithelial cell mainly relies on type I and type II pili (Punsalang and Sawyer, 1973). It secretes vaginolysin, a cholesterol-dependent cytotoxin (Rottini et al., 1990; Gelber et al., 2008). As for other genes associated with pathogenicity, it has two high-affinity iron transporters and is resistant to bleomycin, methicillin and lanthionine antibiotics (Berger-Bachi et al., 1989; Jarosik et al., 1998). The mechanism of immune escape mainly involves changing the molecular weight of its surface antigen (Lindahl et al., 2005). Previously, it has been observed that *G. vaginalis* can form a dense biofilm structure and stick to the surface of the vaginal epithelial cells, resulting in stubborn drug resistance (McGregor and French, 2000; Workowski et al., 2010; Rosca et al., 2020).

Although *G. vaginalis* commonly occurs in the vaginal microbiota of healthy individuals (Fredricks et al., 2005; Hyman et al., 2005; Kim et al., 2009), it is also one of the most frequent and predominant vaginal tract colonists in women diagnosed with bacterial vaginosis (BV) (Fredricks et al., 2005; Menard et al., 2010; Patterson et al., 2010). BV is the most common bacterial inflammatory reproductive tract disease amongst females of reproductive age, with incidence rates as high as 23–29% worldwide (Peebles et al., 2019). BV results in a range of symptoms such as vaginal itching, odor, and abnormal vaginal discharge, and it is caused by the disruption of the dynamic balance between the bacterial microflora in the vagina, the host, and the environment. This involves the overgrowth of various anaerobic bacteria in the vaginal microbiome relative to *Lactobacilli*, with *G. vaginalis* overgrowth in particular being implicated in the formation of a stubborn biofilm that is indicative of BV (Anahtar et al., 2018; Rosca et al., 2020). This biofilm can adhere to the vaginal epithelium, forming clue cells for the diagnostic basis of BV (Swidsinski et al., 2005). Additionally, *G. vaginalis* infections have been associated with various clinical presentations. Many *G. vaginalis* infections can cause pelvic inflammatory disease, salpingitis, infertility, and gynecological tumors. *G. vaginalis* infections have also been associated with adverse outcomes in pregnancy—incidences of premature rupture of membranes, premature delivery and intrauterine infection were 25, 31.67, and 32%, respectively, which were significantly higher than those in normal pregnant women (Cauci et al., 2008; Gelber et al., 2008; Fettweis et al., 2019).

In recent years, comparative genomics studies on *G. vaginalis* have emerged. Whole genome DNA-DNA hybridization of vaginal samples from women presenting varying phenotypes led to a reclassification of several *G. vaginalis* strains (UGent 06.41, UGent 18.01, GS9838-1). These strains have been reclassified to *G. leopoldii, G. piotii,* and *G. swidsinskii*, respectively (Vaneechoutte et al., 2019). Further genome sequencing and comparative analyses of three *G. vaginalis* strains (ATCC 14018, ATCC 14019, and 409-05) showed the high genetic diversity of this species, with only 846 genes out of more than 1,300 genes in the genome being identical. All three strains are able to thrive in vaginal environments, thus allowing the BV isolates ATCC 14018 and 14019 to occupy a niche that is unique from 409-05. Each strain has significant virulence potential, although genomic and metabolic differences, such as the ability to degrade mucin, indicate that the detection of *G. vaginalis* in the vaginal tract provides only partial information on the physiological potential of the organism (Yeoman et al., 2010). Comparative genomic analyses of strains 5-1 (from healthy hosts) and AMD (from bacterial vaginosis) showed that the copy number and amino acid sequence of vaginolysin in these two strains were almost identical, with only one amino acid difference. Strain AMD contains more toxin-antitoxin (TA) systems; Strain 5-1 lacks two key adhesion proteins, Rib, significantly reduced ability to adhere to epithelial cells, and is more sensitive to erythromycin, leading to weakened pathogenicity (Harwich et al., 2010). All these studies have provided a solid basis for the development of novel diagnostics and treatments against *Gardnerella* infections. However, given the high heterogenicity of *Gardnerella*, and the large population with high BV infection rates in China, the lack of in-depth research on varying *Gardnerella* strains poses a concern for the treatment of patients in China.

Therefore, this study investigates ten epidemic strains of *Gardnerella* in local China. First, we used molecular biology and biochemistry techniques to classify and determine the epidemic percentage of each subtype. Then, we analyzed both common and unique pathogenic genes of different *Gardnerella* strains through comparative genomics. Based on these results, we constructed a database of epidemic *Gardnerella* strains in local China, which may act as a foundation for developing accurate diagnostics and therapeutics for *Gardnerella*-induced BV.

Materials and methods

Selection of patients

Samples were obtained from 31 women who attended private gynecology clinics in Jinan Maternal and Child Health Care Hospital, China. The study was approved by the Jinan Health Committee (approval no. 2019-1-25). Written informed consent was obtained from all study participants prior to enrollment. All were Han Chinese > 18 years of age (range, 21–55 years; mean, 31.2 years). All had come to the clinic for a routine gynecological examination, with self-reported complaints of vaginal itching/burning sensations, or with increased and/or malodorous vaginal discharge. All participants were asked to complete a questionnaire on the current use of hormonal contraceptives, menstrual cycle, and frequency of vaginal infections. Exclusion criteria included menstruation at the time of enrollment, human immunodeficiency virus (HIV) infection, and antibiotic/antimicrobial treatment within 14 days of sampling.

Examination of vaginal samples, *Gardnerella vaginalis* isolation

All samples were subjected to Gram-staining and microscopy to assess their Nugent score (NS) (Nugent et al., 1991). BV diagnosis was also defined by the clinician. BV diagnosis included the mandatory satisfaction of three out of the four Amsel criteria (elevated pH, clue cells, fishy odor, and characteristic vaginal discharge); this was supplemented by chemical analysis results (H_2O_2 concentration, activity of leucocyte esterase, sialidase, coagulase and beta-glucosidase) (Amsel et al., 1983; Workowski et al., 2010). A sample was considered as BV-positive if the NS ranged from 7 to 10 and at least three Amsel criteria were present (Workowski et al., 2010). In the case of any inconsistency between the results of chemical analysis and morphology, it should be subjected to morphology. For *G. vaginalis* isolation, a swab taken near mid-vagina was placed in a BHI liquid medium and then the 10 × gradient dilution was spread on a Chocolate Agar Medium (Haibo, Qingdao, China). Chocolate agar plates were incubated at 37°C in 5% CO_2 for 48 h. Colonies of *G. vaginalis* were identified as described previously (Pleckaityte et al., 2012).

Growth condition

Planktonic cells were grown in sBHI [Brain-heart infusion supplemented with 2% (wt/wt) gelatin (Aladdin, Shanghai, China), 0.5% (wt/wt) yeast extract (Oxford, UK), 0.1% (wt/wt) glucose and 0.1% (wt/wt) soluble starch (Aladdin, Shanghai, China)] for 24 h at 37°C with 5% CO_2. For biofilm formation, the glucose was replaced by maltose, and 5% (v/v) goat blood was added. 2% mid-log phase seed was inoculated to a fresh medium for the following tests.

Gene-specific PCR assays and phylogeny construction

Gardnerella vaginalis identification was confirmed by PCR amplification of the 16S rRNA gene (Rainey et al., 1996) and sequencing of the obtained PCR product. *G. vaginalis* subtypes were classified through phylogenetic tree construction using *cpn60* and *vly* gene sequences according to previous studies (Janulaitiene et al., 2017, 2018). The primers are listed in **Supplementary Table 1**.

Sialidase assay

To further characterize the virulence factors of *Gardnerella* clinical isolates, we investigated the presence and expression of the sialidase gene. The presence of the sialidase gene in clinical isolates of *Gardnerella* was identified by PCR using specific primers (**Supplementary Table 1**). In addition, The *Gardnerella* cultures were diluted to an OD_{600} value of 0.8 with 50 mM MES buffer (pH 5.5). The reaction system contained 2.2 mM NBT (Nitrotetrazolium Blue chloride, Sigma-Aldrich, St. Louis, MO), 146 mM sucrose, 10.5 mM $MgCl_2$, 6.3 mM BCIN (5-Bromo-4-chloro-3-indolyl α-D-N-acetylneuraminic acid sodium salt, Sigma-Aldrich, St. Louis, MO), with 0.5% sulfonyl 440 added to avoid bubbles. The mixture was then incubated at 37°C for 20 min and 100 μL of the incubated mixture was added to the wells of black polystyrene microplates (Nunc, Thermo Fisher Scientific). The plates were sealed with an optically clear seal, and BCIN hydrolysis was monitored by measuring the fluorescence at a wavelength of 616 nm using a SynergyH4 hybrid multi-mode microplate reader (Biotek, Winooski, VT, USA) (Zhang and Rochefort, 2013; Janulaitiene et al., 2018). The fluorescence of each supernatant was analyzed in triplicate.

Biofilm assay

For biofilm formation, the cell concentration of 24 h-old cultures was assessed by measuring the optical density of the cultures at 600 nm (Model Sunrise, Tecan, Switzerland). The cultures were further diluted to obtain a final concentration of approximately 10^6 CFU/mL. After homogenization, 200 μL of *G. vaginalis* suspensions were dispensed into each well of three 96-well flat-bottom tissue culture plates (Orange Scientific, Braine L'Alleud, Belgium). The tissue culture plates were incubated at 37°C in 10% CO_2. After 24 h, the culture medium covering the biofilm was removed, then replaced by

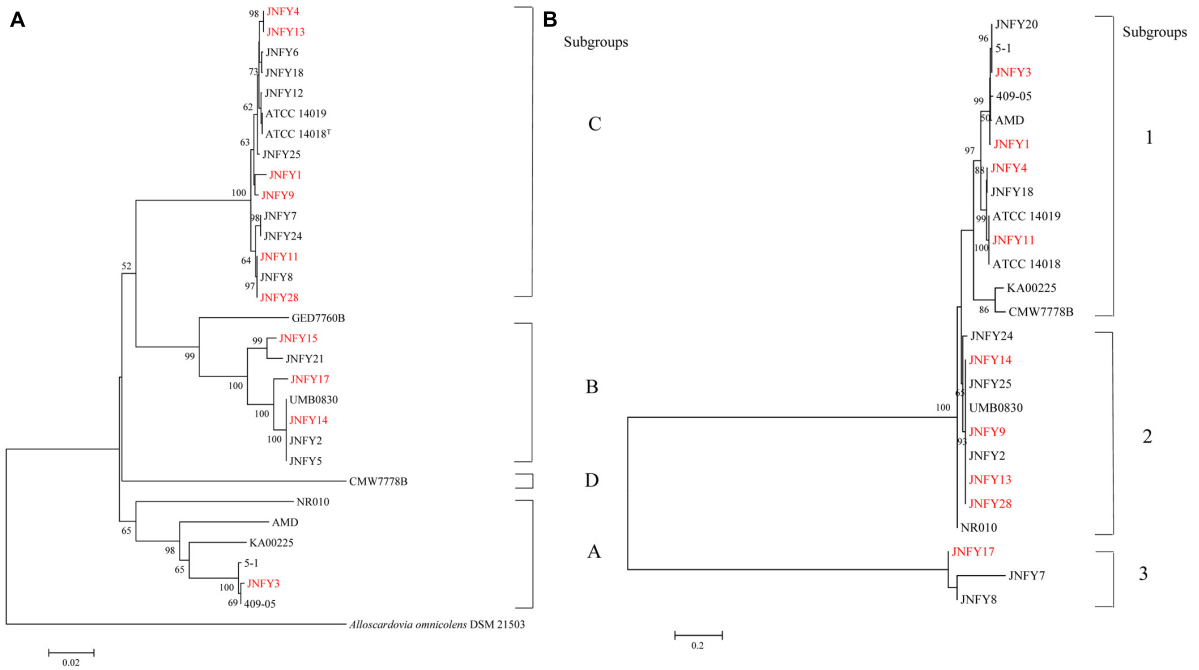

FIGURE 1
Phylogenetic analysis of *Gardnerella* strains based on *cpn60*(a) and *vly*(b) sequences. **(A)** Phylogenetic tree of *Gardnerella cpn60* sequences comprising four distinct clades: (A–D). Bootstrap values for each node are indicated. ATCC 14018^T, ATCC 14019, 41V, 101, 1500E, AMD, 409-05, JCP8066, and JCP7719 are *G. vaginalis* isolates with whole genome sequence information available in Genbank (Accession numbers ADNB00000000, CP002104, AEJE00000000, AEJD00000000, GCA_000263595, ADAM00000000, CP001849, GCA_000414565, and GCA_000414625, respectively). **(B)** Phylogenetic tree of *Gardnerella vly* sequences comprising four distinct clades: 1, 2, 3, and 4 (no *vly* gene).

fresh sBHI and allowed to grow under the same conditions for an additional 24 h. The biofilm produced was quantified by crystal violet staining and then scanned at OD 570 (Jayaprakash et al., 2012; Janulaitiene et al., 2018).

Antibiotic resistance

All antibiotic reserve fluids were prepared at a concentration of 5,120 μg/mL, filtered by a filter membrane to ensure sterility, and stored separately at −20°C. The final antimicrobial concentration was obtained by double dilution with sBHI broth, which was diluted to 512, 256, 128, 64, 32, 16, 8, 4, 2, 1, 0.5, 0.25, and 0.125 μg/mL, respectively. The microdilution plate was made of a 96-well plate with 100 μL of prepared working fluid added to each well. At least one well containing only 100 μL of the antimicrobial-free broth was used as a growth control for the test strain. At the same time, at least one well containing only 100 μL of antimicrobial-free broth was used as an unvaccinated negative control well. Three to five colonies were selected from the blood plate medium with a sterile inoculation loop and placed in a sBHI liquid medium. The broth was incubated at 37°C, until it reached a turbidity of at least 0.5 McFarland (spectrophotometer 625 nm wavelength, 1 cm path, absorption rate 0.08–0.13). To maintain the stability of the cell concentration in the inoculation suspension, the microdilution plate must be inoculated within 30 min after preparation of the inoculation suspension. In the microdilution plate containing 100 μL of diluted antimicrobial agents, 5 μL of cell suspension was added to each well so that the number of cells in each well was approximately 5×10^5 CFU/mL. The microdilution plate was placed in an incubator at 37°C and 5% CO_2 for 18 ± 2 h. When the bacteria in the growth control hole had sufficient growth and the negative control hole without inoculation did not grow, MIC was determined as the minimum drug concentration that could significantly inhibit bacterial growth (Clinical and Laboratory Standards Institute, 2020a,b).

Genome sequencing

The strains were cultured to the middle and late logarithmic stage, and cells were collected. The QIAGEN Genomic DNA extraction kit (QIAGEN, Dusseldorf, Germany) was used for Genomic DNA extraction of the samples according to the standard operating procedure provided by the manufacturer. The extracted genomic DNA was determined with the NanoDrop One UV-vis spectrophotometer (Thermo Fisher

Scientific, Massachusetts, USA). OD260/280 was within 1.8–2.0, and OD 260/230 was between 2.0 and 2.2. DNA was subsequently quantified using the Qubit 3.0 Fluorometer (Invitrogen, California, USA).

After quality inspection, the Blue Pippin automatic nucleic acid recycling instrument (Sage Science, Massachusetts, USA) was used to cut and recycle large fragments. Then, the connectors in the LSK108 linking kit (Oxford, UK) were used for the linkage reaction. Finally, the Qubit 3.0 Fluorometer (Invitrogen, California, USA) was used for accurate quantitative testing of the established DNA libraries. After completion of database construction, a DNA library of a certain concentration and volume was added into one flow cell, and the flow cell was transferred to the Nanopore GridION X5 (Oxford Nanopore Technologies, UK) for real-time single-molecule sequencing.

Genome analysis and phylogenomic tree construction of *Gardnerella* taxon

After quality control, the data was assembled with CANU[1] and corrected with PILON (Walker et al., 2014) combined with second-generation sequencing data. The corrected genome uses its own script to detect whether it is ringed or not. After the redundant parts are removed, the origin of the ringed sequence is moved to the replication starting site of the genome with Circlator (parameter: Fixstart) to obtain the final genome sequence.

The coding gene was predicted by Prodigal[2] and the complete CDS was retained. The tRNA gene was predicted by Transcan-SE, and the rRNA gene was predicted by RNAmmer. Other ncRNA searched the RFAM database for predictions using Infernal, retaining the predicted length (Kalvari et al., 2020). CRISPR was predicted with MinCED (Bland et al., 2007) and Islander was predicted with IslandViewer.[3]

Genome-encoded proteins were extracted and annotated with InterPro[4] to extract annotation information from TIGRFAMs, Pfam and GO databases. Blastp was used to compare the coded proteins to KEGG and Refseq databases, and the best result of the comparison coverage > 30% was kept as the annotation result. The encoding protein was compared with the COG database for COG annotation by RPSBLAST. ABRicate could obtain resistance genes from contig, which correlated with databases such as NCBI, CARD [The Comprehensive Antibiotic Resistance Database (mcmaster.ca)] and ARG-Annot (Gupta et al., 2014). ABRicate software was also used to predict the resistance genes in the genome. Sequencing strain genes were compared with the Pathogenic Bacteria Virulence factor database (VFDB).[5] The VFDB database, developed by the Chinese Academy of Medical Sciences, is widely used in the identification of virulence factor genes. VFDB collected the sequence information of bacterial virulence genes from 30 genera (74 pathogens). The bacterial genes were predicted using AntiSMASH.[6] AntiSMASH used a rules-based clustering method to identify 45 different types of secondary metabolite biosynthesis pathways through its core biosynthesis enzyme.

To assess genome differences between *Gardnerella* strains, a phylogenetic analysis involving 22 genome sequences retrieved from NCBI and our data was performed. For this purpose, the genome sequences were aligned using MAFFT, and the phylogenetic tree was constructed using the neighbor-joining method in Clustal W v2.1; the image was produced using FigTree software.[7]

Results

Collection and phylogenetic analysis of *Gardnerella* isolates

Twenty *Gardnerella* clinical strains were isolated from characterized vaginal samples of 31 women in local China. Each plate was inoculated from a single vaginal swab. *Gardnerella* strains were identified as described in Methods. Isolates from individual colonies were then subtyped by clade-specific PCR. Based on *cpn60* gene sequences, 13 isolates were defined as belonging to clade C, six isolates belonged to clade B, and one isolate belonged to clade A. We found no *Gardnerella* strains belonging to clade D (**Figure 1A**). Two isolates (JNFY3 and JNFY13) originated from vaginal samples with normal vaginal microflora (NS = 1 and 0, respectively), whereas the other 29 vaginal swabs with NS values ranging from 4-10 (**Table 1**). The 20 *Gardnerella* clinical strains were divided into four clades based on their *vly* gene sequences (**Figure 1B**), and strains without the *vly* gene (JNFY15 and JNFY21) were classified as subtype 4.

Biofilm, biomass, and sialidase activity in *Gardnerella* strains

The measurement of biofilm formation capacity of 10 strains showed that, except for JNFY3, JNFY15, and JNFY17, other prevalent strains could form biofilm with varied thickness. JNFY14 produced the largest amount of biofilm, and *cpn60* subtype C prevalent strains generally formed a certain amount

1 https://github.com/marbl/canu
2 https://github.com/hyattpd/Prodigal/wiki/introduction
3 http://www.pathogenomics.sfu.ca/islandviewer/upload/
4 http://www.ebi.ac.uk/interpro/search/sequence/
5 http://www.mgc.ac.cn/VFs/
6 http://antismash.secondarymetabolites.org/
7 http://tree.bio.ed.ac.uk/software/figtree/

10.3389/fmicb.2022.1009798

TABLE 1 Polyphasic comparison of the *Gardnerella* strains.

Strains	Nugent score	Biofilm intensity	Phylogenetic subgroups	to Mid-log phase (h)	Sialidase activity	Vaginolysin-encoding gene	Antibiotic resistance genes	MID = 16 μg/ml
ATCC 14019	ND	1.69	C1	10 h	ND	+	*lsaC*	GM, TO
JNFY1	4	1.42	C1	14 h	0.29±0.009	+	*ermX, lsaC*	CIP, TO, MTZ
JNFY3	1	0.48	A1	8 h	ND	+	*ermX*	AZM, CIP, GM, TO, MTZ
JNFY4	8	1.06	C1	9 h	ND	+	*ermX, lsaC, tetL, tetM*	AZM, TE, CIP, GM, ERM, TO, CLI, MTZ
JNFY9	7	1.03	C2	15 h	ND	+	*ermX, lsaC, tetL, tetM*	TE, CIP, TO
JNFY11	8	1.29	C1	10 h	ND	+	*ermX, lsaC*	CLI, CIP, TO, AZM
JNFY13	0	1.1	C2	12 h	ND	+	*lsaC, tetL, tetM*	GM, TE, TO, MTZ
JNFY14	8	2.57	B2	11 h	0.38±0.008	+	2*lsaC	CIP, GM, TO, MTZ
JNFY15	8	0.59	B4	20 h	ND	-	*ermX, lsaC*	CIP, GM, ERM, CLI, TO
JNFY17	4	0.52	B3	13 h	0.27±0.014	+	*lsaC*	CIP, GM, TO, MTZ
JNFY28	8	1.13	C2	14 h	ND	+	*lsaC*	GM, DNR, TO, MTZ

of biofilm (Table 1, Figure 2, and Supplementary Figure 2). Sialidase activity was detected in strains JNFY3, JNFY4, JNFY11, and JNFY17. Moreover, strain JNFY14 exhibited weak sialidase activity (Table 1).

General genome features and phylogenomic tree of *Gardnerella* strains

The genome size of *Gardnerella* was between 1.5 and 1.8 Mb, which was smaller than other members of the *Bifidobacteriaceae* family, one-third the size of *E. coli* and one-fifth the size of *P. aeruginosa*. The genomes of these ten strains contained about 1,300 genes, with a GC content of about 41–43%. The basic features of the ten prevalent GV strains were similar to those of the American strain ATCC 14019 isolated from BV patients (genome size 1,667,350 bp, GC content 41%). No obvious plasmid sequence was found in any of the ten strains. One genomic island was predicted in JNFY1, JNFY11, and JNFY17, and two genomic islands were predicted in JNFY3. No genomic island was predicted in other strains. A CRISPR sequence was predicted in JNFY1, JNFY3, JNFY4, JNFY13, and JNFY28, but not in other prevalent strains (Table 2). The phylogenomic tree showed that the *Gardnerella* strains were generally divided into four groups, which was similar to the *cpn60* phylogenetic tree (Figure 1A). Strains JNFY1, 4, 9, 11, 13, 28, and ATCC 14019 were located in the same group in both trees; likewise, strains 409-05, JNFY3, 5-1, and JNFY15, 17, UMB0830 located to the same groups. Strains JNFY3 and JNFY15 were classified as *Gardnerella swidsinskii* and *Gardnerella piotii,* respectively, according to their genome sequences (Supplementary Figure 1). On the basis of the distance from the position of each strain to the root of the phylogenomic tree (Supplementary Figure 1), we calculated that the evolutionary order of each strain is as follows: ATCC 14018, JNFY3, 409-05, 5-1, JNFY14, JNFY15, JNFY17, JNFY4, JNFY11, JNFY9, JNFY13, JNFY1, and ATCC 14019.

Carbohydrate transport and metabolism

In general, biofilm formation is tightly related to carbohydrate transport and metabolism. Compared with the biofilm-rich strain JNFY14, the biofilm-lacking strains JNFY3, JNFY15, JNFY17, and JNFY28 lacked many genes involved in polysaccharides synthesis and sugar transport. Absent genes included *afuC*, *araD*, *fucP*, *galM*, *galT*, *lacZ*, *mglA*, *xylB,* and *xylF*. In addition, there were fewer copies of *nagC*, *ugpA*, *ugpB,* and *ugpE* in biofilm-lacking strains, compared to the biofilm-rich strain JNFY14 (Supplementary Table 2). The

10.3389/fmicb.2022.1009798

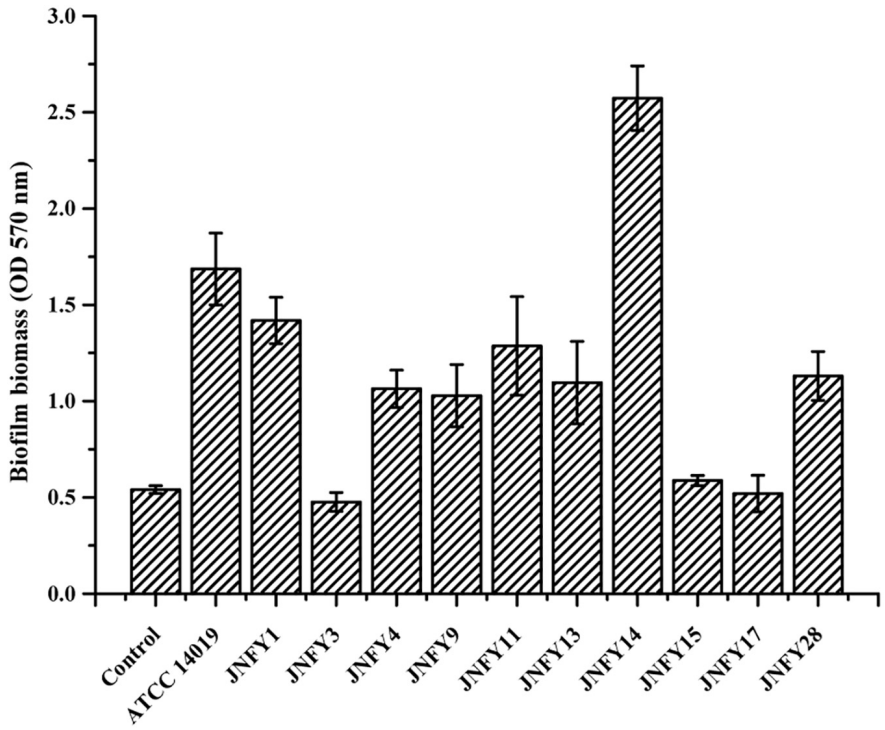

FIGURE 2
Biofilm formation by *Gardnerella* strains. Isolates were cultured in 96-well plate in BHI medium, stained at 48 h, after removal of planktonic cells.

TABLE 2 The general features of the 10 *Gardnerella* genomes.

Strains	Size (bp)	CDS number	Plasmid	Island	GC %	tRNA	rRNA	CRISPR	Accession No.
JNFY1	1,711,437	1,316	NO	1	41.61	45	6	1	CP083177
JNFY3	1,602,355	1,245	NO	2	42.02	45	6	1	CP083176
JNFY4	1,742,450	1,359	NO	NO	41.56	45	6	1	CP083175
JNFY9	1,640,523	1,243	NO	NO	41.41	45	6	NO	CP083174
JNFY11	1,743,456	1,357	NO	1	41.82	45	6	NO	CP083173
JNFY13	1,682,566	1,290	NO	NO	41.64	45	6	1	CP083172
JNFY14	1,680,963	1,290	NO	NO	41.67	45	6	NO	CP083171
JNFY15	1,541,442	1,164	NO	NO	42.55	45	6	NO	CP083170
JNFY17	1,595,814	1,236	NO	1	42.74	45	6	NO	CP083169
JNFY28	1,542,082	1,392	NO	NO	42.23	45	6	1	CP083168

absence and reduced copy numbers of these genes may explain why the strains of this group cannot form normal biofilm.

Antibiotic resistance

According to the genomic data, all of the ten *Gardnerella* isolates contained antibiotic resistance genes, with a total of four detected antibiotic resistance genes. JNFY1, JNFY3, JNFY4, JNFY9, JNFY11, and JNFY15 contained the macrolide erythromycin resistance gene *ermX*. Strains JNFY1, JNFY4, JNFY9, JNFY11, JNFY13, JNFY14, JNFY15, JNFY17, and JNFY28 contained the lincosamide antibiotic resistance gene *lsaC*, while strains JNFY4, JNFY9, and JNFY13 contained the tetracycline resistance genes *tetL* and *tetM*. The comparative genomics data also showed that all strains contain the daunorubicin resistance protein (Table 3).

Resistance tests showed that *Gardnerella* strains containing erythromycin resistance genes were resistant to macrolide azithromycin. Similarly, prevalent strains containing tetracycline resistance genes were resistant to tetracycline. Strains JNFY13 and JNFY28 showed weak resistance to erythromycin, despite their lack of *ermX*. Alternatively,

TABLE 3 Antibiotic-resistance genes predicted in genome of the *Gardnerella* strains.

Strains	Macrolides-resistant		Tetracyclines-resistant	
	ermX	*lsaC*	*tetL*	*tetM*
ATCC 14019	0	1	0	0
JNFY1	1	1	0	0
JNFY3	1	0	0	0
JNFY4	1	1	1	1
JNFY9	1	1	1	1
JNFY11	1	1	0	0
JNFY13	0	1	1	1
JNFY14	0	2	0	0
JNFY15	1	1	0	0
JNFY17	0	1	0	0
JNFY28	0	1	0	0

strain JNFY3 showed strong resistance to lincosamide, despite its lack of *lsaC*. YadH (ABC-type multidrug transport system) and McrA (5-methylcytosine-specific restriction endonuclease) existed only in metronidazole-resistant strains JNFY3, JNFY4, JNFY14, JNFY17, and JNFY28 (**Table 4**), thus these genes are likely involved in metronidazole resistance.

Virulence

Typically, epithelial cell adhesion is mediated by pili. All ten strains of *Gardnerella* contained *ppK*, a gene encoding for type IV pili. Some *Gardnerella* strains share virulence factors involved in pathogenic mechanisms like epithelial cell adhesion, iron absorption, secretion, acting as toxins and endotoxins, and immune escape; virulence factors can also have regulatory functions (**Supplementary Table 3**). Strains lacking these virulence factors such as JNFY3, JNFY15, and JNFY17 have the common feature of impaired biofilm formation. *Gardnerella* produces vaginolysin, which plays a critical role in BV pathogenesis. The gene encoding vaginolysin was detected in nine strains, with the exception of JNFY15 (**Supplementary Table 4**). Strains JNFY3 and JNFY4 exhibited nine and one unique virulence factor(s), respectively, with virulence factors having roles in allantoin utilization, adhesion, secretion and iron uptake (**Supplementary Table 5**). The TA components and other competitive exclusion genes of the *Gardnerella* strains are listed in **Table 5**. There are mainly four TA systems in *Gardnerella* genomes including HicAB family, PHD-RelE family, ParE family, and RelB-Txe family, with various distribution in the 11 strains. However, the other genes related to competitive exclusion showed a similar pattern in each strain.

Secondary metabolites biosynthesis

Analysis of secondary metabolite gene clusters in ten isolates of *Gardnerella* demonstrated the presence of polyketosynthase (PKS)-related secondary metabolite gene clusters in the *Gardnerella* genome. PKS genes encode an enzyme, or enzyme complex with multiple domains, capable of synthesizing polyketo compounds, including common antibiotics such as erythromycin, tetracycline and so on. Type I, type II, and type III PKS synthesize T1PKS, T2PKS, and T3PKS, respectively. The T3PKS gene cluster was predicted in all strains except JNFY3.

Discussion

Bacterial vaginosis (BV) is a common vaginal infection in women of child-bearing age, with *Gardnerella* spp. being the main pathogen of BV. Alongside BV, *Gardnerella* spp. has also been associated with vertebral osteomyelitis and discitis (Graham et al., 2009), retinal vasculitis (Neri et al., 2009), acute hip arthritis (Sivadon-Tardy et al., 2009), and bacteremia (Chen et al., 2018). While the vaginal overgrowth of several anaerobic bacteria has been associated with BV, *Gardnerella* spp. has a stronger adhesion to vaginal epithelium and a stronger tendency to form biofilm compared to other BV-related microorganisms. It can be used as a scaffold to attach other anaerobic bacteria and is associated with the onset and recurrence of BV (Anahtar et al., 2018). The treatment of recurrent BV is difficult, and existing treatment measures include the prolongation of an antibiotic course and consolidation treatment. However, due to biofilm formation and strain differences in *Gardnerella*, antibiotics cannot eliminate the bacteria, making the current treatment of BV unable to achieve ideal therapeutic effect (Cohen et al., 2020; Laniewski et al., 2020). Therefore, it is of great significance to construct a database detailing prevalent *Gardnerella* strains in local China, which can provide the basis for the accurate diagnosis and therapy of BV and allow for the development of more effective antibacterial drugs targeting prevalent strains.

In this study, 20 prevalent strains of *Gardnerella* from local China were collected from clinical specimens to study the differences in their pathogenicity and drug resistance. This would provide a theoretical basis for the accurate diagnosis and treatment of BV. First, based on *cpn60* sequence genotyping, the 20 prevalent strains were divided into subtypes A, B, and C. Based on *vly* sequence genotyping, prevalent strains were divided into subtypes 1, 2, 3, and 4. Ten strains of subtypes C1 (JNFY9, 13 and 28), C2 (JNFY1,4 and 11), B1 (JNFY14 and 17), A1 (JNFY3), and B4 (JNFY15) were selected for comparative genomics. The genome size of the 10 strains ranged from 1.54 to 1.74 Mb, and the GC content was about 41–43%. No plasmid was observed, and 1–2 gene islands were predicted in 4 strains. The phylogenomic tree of the *Gardnerella* strains showed that strains JNFY3, JNFY15,17, and JNFY1,4,9,11,13,14,28 were

TABLE 4 MIC (minimum inhibitory concentration) of the *Gardnerella* strains on common antibiotics in clinic.

Antibiotics-resistant genes	MIC(μg/mL)											
	First-line								Second-line			Third-line
	Beta-lactam	Tetracycline	Macrolide			Quinolone	Nitroimidazole	Aminoglycoside	Macrolide	Aminoglycoside	Beta-lactam	Glycopeptide
	AMP	TE	AZM	ERM	CLI	CIP	MTZ	GM	DNR	TO	CMR	VA
ATCC 14019	<0.25	<0.25	<0.25	0	0	2	8	16	2	64	0.25	1
JNFY1	0.5	0.25	4	0.5	0	16	128	8	0	16	0.25	1
JNFY3	0.5	0.25	16	0.125	0.0625	16	>128	16	8	32	0.5	1
JNFY4	0.5	16	16	32	128	16	>128	16	2	32	0.5	1
JNFY9	0.25	16	8	0	0	16	4	4	0.125	16	0.5	1
JNFY11	1	0.25	64	0.125	16	16	2	8	1	32	1	1
JNFY13	0.25	32	0.25	0.125	0	1	>128	16	2	128	1	1
JNFY14	4	0·125	0.5	0	0.0625	32	>128	32	0·5	32	1	1
JNFY15	0.5	<0.25	8	128	128	16	16	32	1	128	0.5	0.5
JNFY17	4	0.5	0.5	0	0	32	>128	32	0	64	2	1
JNFY28	0.5	0.25	0.25	0.25	0	8	>128	16	32	128	0.5	1

AMP, ampicillin; TE, tetracycline; AZM, azithromycin; ERM, erythromycin; CLI, clindamycin; CIP, ciprofloxacin; MTZ, metronidazole; GM, gentamicin; DNR, daunorubicin; TO, tobramycin; CMR, chloramphenicol; VA, vancomycin.

10.3389/fmicb.2022.1009798

TABLE 5 TA system components and other competitive exclusion genes.

TA system	ATCC 14019	JNFY1	JNFY3	JNFY4	JNFY9	JNFY11	JNFY13	JNFY14	JNFY15	JNFY17	JNFY28
HicA-family TA system toxin HicB-family TA system antitoxin	1	2	HicB only	n/a	1	2	n/a	2	1	1	n/a
PHD/YefM family TA system antitoxin RelE/StbE family TA system toxin	1	n/a	PHD only	PHD only	n/a	PHD only	n/a	PHD only	1	PHD only	n/a
ParE-family TA system toxin TA system antitoxin	3	1	1	n/a	1	n/a	1	ParE only	1	2	n/a
RelB/DinJ family TA system antitoxin Txe/YoeB family TA system toxin	5	1	3	RelB only	RelB only	1	RelB only	1	n/a	RelB only	1
Other genes with potential roles in competitive exclusion											
Abi-like protein	n/a	3	1	n/a	n/a	n/a	n/a	n/a	2	2	2
CHAP domain protein	2	2	2	2	2	2	2	2	2	2	3
GH25 enzyme	1	1	1	1	1	1	1	1	1	1	1
SalY-family antimicrobial peptide ABC transport system, ATP-binding protein	4	5	5	5	5	5	5	5	6	5	5

n/a indicates protein was not identified within the genome.

10.3389/fmicb.2022.1009798

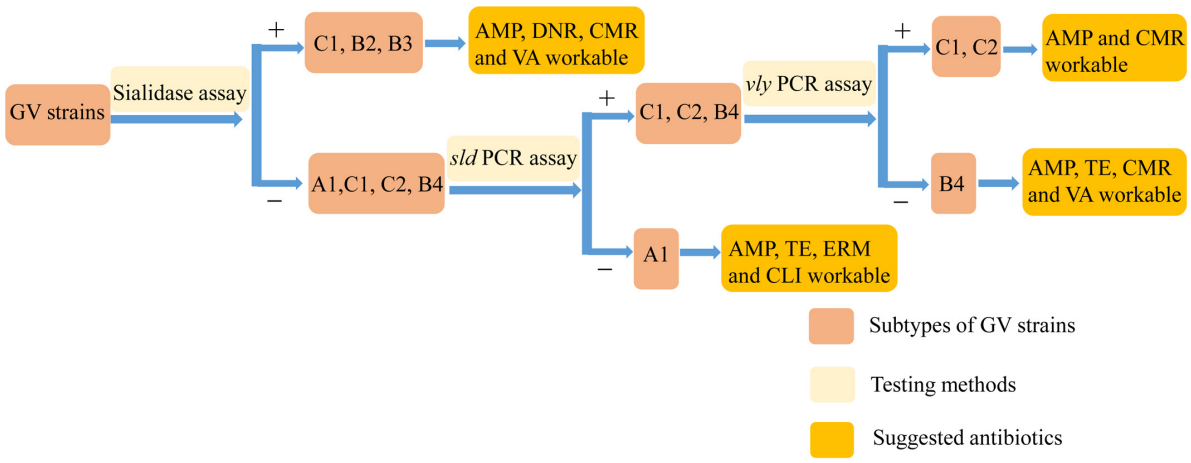

FIGURE 3
The diagnose pathway of *Gardnerella* strains.

located in three different branches. This was almost identical to the *cpn60* phylogenetic tree, except for the position of strain JNFY14. Therefore, the *cpn60* distribution could represent genomic classification to some extent. The *G. vaginalis* strains 5-1, 409-05 and JNFY3 were grouped in the same branch in all three trees, further indicating the weak pathogenicity of these strains in healthy hosts.

Virulence factors associated with microbial pathogenesis were found in the genome of prevalent strains, including factors for adhesion, secretion, iron and magnesium absorption, immune escape, and toxins. Common virulence factors were found in the ten prevalent strains, although differences also exist amongst the strains. It is worth noting that JNFY3 had nine specific virulence factors while JNFY4 had one. In addition, JNFY3, JNFY15, and JNFY17 had severely hindered abilities in biofilm formation. These three strains not only lacked certain carbohydrate metabolism genes (**Supplementary Table 2**), but also lacked virulence factors related to adhesion, iron absorption and toxins, which might be conductive to biofilm formation in the comparative genomic analysis.

Subsequent biochemical experiments were conducted to preliminarily investigate the pathogenic mechanism of *Gardnerella*. Experiments on the biofilm-forming capabilities of *Gardnerella* showed variable abilities to form biofilm amongst different prevalent strains with *cpn60* subtype C displaying weak to moderate biofilm-forming abilities. Sialidases are enzymes associated with bacterial invasion of the host and are implicated as virulence factors in diseases such as meningitis, glomerulonephritis, and periodontal disease (Corfield, 1992). Previous studies have shown that BV-associated bacteria produce sialidase, and its activity is inversely related to vaginal IgA response against vaginolysin produced by *Gardnerella* (Cauci et al., 2003). The sialidase assay showed that most strains lacked sialidase activity despite some strains having a higher NS; thus, there is no association between sialidase and pathogenicity.

Resistance tests showed that *Gardnerella* was sensitive to antibiotics, including tetracycline, nitroimidazoles, macrolide and aminoglycosides. Meanwhile, the macrolide erythromycin resistance genes *ermX* and *lsaC*, and the tetracycline resistance genes *tetL* and *tetM* were also predicted in the ten strains. It is worth noting that seven out of the ten strains exhibited strong resistance ($\geq$ 128 μg/mL) to metronidazole, which is the first line of treatment for BV in China. In addition to nitroreductase, YadH and McrA may also have roles in metronidazole resistance, with YadH involved in metronidazole excretion and McrA hydrolyzing the methyl-nitryl group from metronidazole (Lorca et al., 2007; Lubelski et al., 2007).

Additionally, we compared pathogenic genes of the prevalent strain in local China and the American type strain ATCC 14019. According to the phylogenetic analysis, strain ATCC 14019 belonged to the subtype C1, and possessed fairly thick biofilm and tobramycin resistance. Compared to strain ATCC 14019, the Chinese prevalent strains contained poor and incomplete TA systems with only antitoxin genes included, suggesting that the antitoxins may be essential to neutralize the toxins secreted by other microbes in the vaginal biome. The strains JNFY4, JNFY9, JNFY11, JNFY13, and JNFY14 without Abi-like proteins lack means of defense to a broad-range of bacteriocins produced by opponents, which probably is complemented by the single antitoxins (Kjos et al., 2010). Although there was no intact secretion system in *Gardnerella*, it was speculated that *Gardnerella* secreted toxic proteins to injure other bacteria, such as *Lactobacillus*, to enhance their survivability and displace the balance of the normal vaginal microflora. Strain ATCC 14019 encodes a methicillin resistance protein not found in the ten Chinese prevalent strains. Carbohydrate transport and

metabolism genes of the 11 *Gardnerella* strains, including the genes associated with biofilm formation, were also analyzed and combined with biofilm thickness data (**Figure 2** and **Supplementary Figure 2**). AraD, GalM, and GalT may be responsible for constructing biofilm, while FucP, MalA, and XylF are involved in monosaccharide transport. The additional monosaccharide units in the biofilm of strain JNFY14, arabinose and galactose hydrochloride, may play the role of connective elements which help to build a thicker biofilm.

Previous treatment standards involving clindamycin and metronidazole cannot account for all prevalent strains with sufficient efficacy to achieve complete recovery. Therefore, we need targeted treatments for diseases caused by different prevalent strains of *Gardnerella* to obtain the best results. Although the pathogenic genes of *Gardnerella* were previously characterized, the pathogenesis of BV is not yet understood. Through genomic and biochemical data analysis, we found that strains of subtype C could generally form biofilm, with varying degrees of antibiotic resistance (apart from invariable tobramycin resistance). Strain *G. swidsinskii* JNFY3 had a NS of 1, impaired ability to form biofilm, and lacked the *sld* and *lsaC* genes. *G. vaginalis* JNFY14 had the thickest biofilm, whereas strains JNFY17 and *G. piotii* JNFY15 rarely produced biofilm. On the whole, with the exception of strain JNFY14, the evolutionary trend appears to be the development of a progressively thicker biofilm from JNFY3 to ATCC 14019. All three strains (JNFY14, JNFY17, and JNFY15) showed some resistance to ciprofloxacin, gentamicin and tobramycin. Additionally, *G. piotii* JNFY15 lacked the *vly* gene and grew slower than other *Gardnerella* strains (**Table 1**). Based on this study, we constructed an initial database of *Gardnerella* prevalent strains in local China, which can be used as a reference to elucidate more accurate diagnostic pathways and treatments for BV (**Table 1** and **Figure 3**).

Data availability statement

The datasets presented in this study can be found in online repositories. The names of the repository/repositories and accession number(s) can be found in the article/**Supplementary material**.

Ethics statement

The studies involving human participants were reviewed and approved by the Medical Ethics Committee of Jinan Maternity and Child Care Hospital. The patients/participants provided their written informed consent to participate in this study.

Author contributions

LG, KZ, and RL conceptualized and designed the study. KZ and XZ analyzed the data. ML, KZ, KW, and HD accessed and verified the data. XJ collected samples from participants. KZ, FZ, and TL wrote the first draft of the manuscript. All authors contributed to drafting of the manuscript and read and approved the final version of the manuscript for submission, had full access to all data in the study, and had final responsibility for the decision to submit for publication.

Funding

This study was funded by the China Postdoctoral Science Foundation (No. 2018M642648), the State Key Laboratory of Microbial Technology Open Projects Fund (No. M2021-17), the Natural Science Foundation of Shandong Province (No. ZR2021MC038), and the Science and Technology Project of Jinan Municipal Health Commission (No. 2019-1-25).

Acknowledgments

We thank Dr. Xiaodi Chen from the Jinan Maternal and Child Health Care Hospital for providing references about therapy of bacterial vaginosis cited in this article and Carina Muyao Gu at CBe-Learn School for proofreading.

Conflict of interest

The authors declare that the research was conducted in the absence of any commercial or financial relationships that could be construed as a potential conflict of interest.

Publisher's note

Supplementary material

The Supplementary Material for this article can be found online at: https://www.frontiersin.org/articles/10.3389/fmicb.2022.1009798/full#supplementary-material

References

Amsel, R., Totten, P. A., Spiegel, C. A., Chen, K. C. S., Eschenbach, D., and Holmes, K. K. (1983). Nonspecific vaginitis - diagnostic-criteria and microbial and epidemiologic associations. *Am. J. Med.* 74, 14–22.

Anahtar, M. N., Gootenberg, D. B., Mitchell, C. M., and Kwon, D. S. (2018). Cervicovaginal microbiota and reproductive health: The virtue of simplicity. *Cell Host Microbe* 23, 159–168. doi: 10.1016/j.chom.2018.01.013

Berger-Bachi, B., Barberis-Maino, L., Strassle, A., and Kayser, F. H. (1989). FemA, a host-mediated factor essential for methicillin resistance in *Staphylococcus aureus*: Molecular cloning and characterization. *Mol. Gen. Genet.* 219, 263–269. doi: 10.1007/BF00261186

Bland, C., Ramsey, T. L., Sabree, F., Lowe, M., Brown, K., Kyrpides, N. C., et al. (2007). CRISPR recognition tool (CRT): A tool for automatic detection of clustered regularly interspaced palindromic repeats. *BMC Bioinformatics* 8:209. doi: 10.1186/1471-2105-8-209

Cauci, S., Culhane, J. F., Di Santolo, M., and McCollum, K. (2008). Among pregnant women with bacterial vaginosis, the hydrolytic enzymes sialidase and prolidase are positively associated with interleukin-1 beta. *Am. J. Obstet. Gynecol.* 198, 132.e1–132.e7.

Cauci, S., Thorsen, P., Schendel, D. E., Bremmelgaard, A., Quadrifoglio, F., and Guaschino, S. (2003). Determination of immunoglobulin A against *Gardnerella vaginalis* hemolysin, sialidase, and prolidase activities in vaginal fluid: Implications for adverse pregnancy outcomes. *J. Clin. Microbiol.* 41, 435–438. doi: 10.1128/JCM.41.1.435-438.2003

Chen, Y., Han, X., Guo, P., Huang, H., Wu, Z., and Liao, K. (2018). Bacteramia caused by *Gardnerella vaginalis* in a cesarean section patient. *Clin. Lab.* 64, 379–382.

Clinical and Laboratory Standards Institute (2020a). *Methods for dilution antimicrobial susceptibility tests for bacteria that grow aerobically. Approved standard-eleventh edition, Document M07-A11*. Wayne, PA: CLSI.

Clinical and Laboratory Standards Institute (2020b). *Performance standards for antimicrobial susceptibility testing: Twenty-eighth informational supplement M100-S30*. Wayne, PA: CLSI.

Cohen, C. R., Wierzbicki, M. R., French, A. L., Morris, S., Newmann, S., Reno, H., et al. (2020). Randomized trial of lactin-V to prevent recurrence of bacterial vaginosis. *N. Engl. J. Med.* 382, 1906–1915.

Corfield, T. (1992). Bacterial sialidases - roles in pathogenicity and nutrition. *Glycobiology* 2, 509–521.

Fettweis, J. M., Serrano, M. G., Brooks, J. P., Edwards, D. J., Girerd, P. H., Parikh, H. I., et al. (2019). The vaginal microbiome and preterm birth. *Nat. Med.* 25, 1012–1021.

Francis, V. I., Stevenson, E. C., and Porter, S. L. (2017). Two-component systems required for virulence in *Pseudomonas aeruginosa*. *FEMS Microbiol. Lett.* 364:fnx104. doi: 10.1093/femsle/fnx104

Fredricks, D. N., Fiedler, T. L., and Marrazzo, J. M. (2005). Molecular identification of bacteria associated with bacterial vaginosis. *N. Engl. J. Med.* 353, 1899–1911.

Gelber, S. E., Aguilar, J. L., Lewis, K. L., and Ratner, A. J. (2008). Functional and phylogenetic characterization of Vaginolysin, the human-specific cytolysin from *Gardnerella vaginalis*. *J. Bacteriol.* 190, 3896–3903. doi: 10.1128/JB.01965-07

Graham, S., Howes, C., Dunsmuir, R., and Sandoe, J. (2009). Vertebral osteomyelitis and discitis due to *Gardnerella vaginalis*. *J. Med. Microbiol.* 58, 1382–1384. doi: 10.1099/jmm.0.007781-0

Greenwood, J. R., and Pickett, M. J. (1980). Transfer of *Hemophilus vaginalis* gardner and dukes to a new genus, *Gardnerella*, *G. vaginalis* (gardner and dukes) comb nov. *Int. J. Syst. Bacteriol.* 30, 170–178.

Gupta, S. K., Padmanabhan, B. R., Diene, S. M., Lopez-Rojas, R., Kempf, M., Landraud, L., et al. (2014). ARG-ANNOT, a new bioinformatic tool to discover antibiotic resistance genes in bacterial genomes. *Antimicrob. Agents Chemother.* 58, 212–220. doi: 10.1128/AAC.01310-13

Harwich, M. D., Alves, J. M., Buck, G. A., Strauss, J. F., Patterson, J. L., Oki, A. T., et al. (2010). Drawing the line between commensal and pathogenic *Gardnerella vaginalis* through genome analysis and virulence studies. *BMC Genomics* 11:375. doi: 10.1186/1471-2164-11-375

He, Q., Wang, F., Liu, S. H., Zhu, D. Y., Cong, H. J., Gao, F., et al. (2016). Structural and biochemical insight into the mechanism of Rv2837c from *Mycobacterium tuberculosis* as a c-di-NMP phosphodiesterase (vol 291, pg 3668, 2016). *J. Biol. Chem.* 291, 14386–14387. doi: 10.1074/jbc.M115.699801

Hood, R. D., Singh, P., Hsu, F., Guvener, T., Carl, M. A., Trinidad, R. R., et al. (2010). A type VI secretion system of *Pseudomonas aeruginosa* targets a toxin to bacteria. *Cell Host Microbe* 7, 25–37. doi: 10.1016/j.chom.2009.12.007

Hyman, R. W., Fukushima, M., Diamond, L., Kumm, J., Giudice, L. C., and Davis, R. W. (2005). Microbes on the human vaginal epithelium. *Proc. Natl. Acad. Sci. U.S.A.* 102, 7952–7957.

Janulaitiene, M., Gegzna, V., Baranauskiene, L., Bulavaite, A., Simanavicius, M., and Pleckaityte, M. (2018). Phenotypic characterization of *Gardnerella vaginalis* subgroups suggests differences in their virulence potential. *PLoS One* 13:e0200625. doi: 10.1371/journal.pone.0200625

Janulaitiene, M., Paliulyte, V., Grinceviciene, S., Zakareviciene, J., Vladisauskiene, A., Marcinkute, A., et al. (2017). Prevalence and distribution of *Gardnerella vaginalis* subgroups in women with and without bacterial vaginosis. *BMC Infect. Dis.* 17:394. doi: 10.1186/s12879-017-2501-y

Jarosik, G. P., Land, C. B., Duhon, P., Chandler, R. Jr., and Mercer, T. (1998). Acquisition of iron by *Gardnerella vaginalis*. *Infect. Immun.* 66, 5041–5047.

Jayaprakash, T. P., Schellenberg, J. J., and Hill, J. E. (2012). Resolution and characterization of distinct cpn60-based subgroups of *Gardnerella vaginalis* in the vaginal microbiota. *PLoS One* 7:e43009. doi: 10.1371/journal.pone.0043009

Kalvari, I., Nawrocki, E. P., Ontiveros-Palacios, N., Argasinska, J., Lamkiewicz, K., Marz, M., et al. (2020). Rfam 14: Expanded coverage of metagenomic, viral and microRNA families. *Nucleic Acids Res.* 49, D192–D200. doi: 10.1093/nar/gkaa1047

Kim, T. K., Thomas, S. M., Ho, M. F., Sharma, S., Reich, C. I., Frank, J. A., et al. (2009). Heterogeneity of vaginal microbial communities within individuals. *J. Clin. Microbiol.* 47, 1181–1189.

Kjos, M., Snipen, L., Salehian, Z., Nes, I. F., and Diep, D. B. (2010). The abi proteins and their involvement in bacteriocin self-immunity. *J. Bacteriol.* 192, 2068–2076. doi: 10.1128/JB.01553-09

Laniewski, P., Ilhan, Z. E., and Herbst-Kralovetz, M. M. (2020). The microbiome and gynaecological cancer development, prevention and therapy. *Nat. Rev. Urol.* 17, 232–250.

Lindahl, G., Stalhammar-Carlemalm, M., and Areschoug, T. (2005). Surface proteins of *Streptococcus agalactiae* and related proteins in other bacterial pathogens. *Clin. Microbiol. Rev.* 18, 102–127.

Lorca, G. L., Barabote, R. D., Zlotopolski, V., Tran, C., Winnen, B., Hvorup, R. N., et al. (2007). Transport capabilities of eleven gram-positive bacteria: Comparative genomic analyses. *Biochim. Biophys. Acta* 1768, 1342–1366.

Lubelski, J., Konings, W. N., and Driessen, A. J. (2007). Distribution and physiology of ABC-type transporters contributing to multidrug resistance in bacteria. *Microbiol. Mol. Biol. Rev.* 71, 463–476. doi: 10.1128/MMBR.00001-07

McGregor, J. A., and French, J. I. (2000). Bacterial vaginosis in pregnancy. *Obstet. Gynecol. Surv.* 55(5 Suppl. 1), S1–S19.

Menard, J. P., Mazouni, C., Salem-Cherif, I., Fenollar, F., Raoult, D., Boubli, L., et al. (2010). High vaginal concentrations of *Atopobium vaginae* and *Gardnerella vaginalis* in women undergoing preterm labor. *Obstet. Gynecol.* 115, 134–140. doi: 10.1097/AOG.0b013e3181c391d7

Neri, P., Salvolini, S., Giovannini, A., and Mariotti, C. (2009). Retinal vasculitis associated with asymptomatic *Gardnerella vaginalis* infection: A new clinical entity. *Ocul. Immunol. Inflamm.* 17, 36–40. doi: 10.1080/09273940802491876

Nugent, R. P., Krohn, M. A., and Hillier, S. L. (1991). Reliability of diagnosing bacterial vaginosis is improved by a standardized method of gram stain interpretation. *J. Clin. Microbiol.* 29, 297–301. doi: 10.1128/jcm.29.2.297-301.1991

Patterson, J. L., Stull-Lane, A., Girerd, P. H., and Jefferson, K. K. (2010). Analysis of adherence, biofilm formation and cytotoxicity suggests a greater virulence potential of *Gardnerella vaginalis* relative to other bacterial-vaginosis-associated anaerobes. *Microbiology* 156, 392–399. doi: 10.1099/mic.0.034280-0

Peebles, K., Velloza, J., Balkus, J. E., McClelland, R. S., and Barnabas, R. V. (2019). High global burden and costs of bacterial vaginosis: A systematic review and meta-analysis. *Sex. Transm. Dis.* 46, 304–311.

Pleckaityte, M., Janulaitiene, M., Lasickiene, R., and Zvirbliene, A. (2012). Genetic and biochemical diversity of *Gardnerella vaginalis* strains isolated from women with bacterial vaginosis. *FEMS Immunol. Med. Microbiol.* 65, 69–77. doi: 10.1111/j.1574-695X.2012.00940.x

Punsalang, A. P. Jr., and Sawyer, W. D. (1973). Role of pili in the virulence of *Neisseria gonorrhoeae*. *Infect. Immun.* 8, 255–263.

Rainey, F. A., Ward-Rainey, N., Kroppenstedt, R. M., and Stackebrandt, E. (1996). The genus *Nocardiopsis* represents a phylogenetically coherent taxon and

a distinct actinomycete lineage: Proposal of *Nocardiopsaceae* fam. nov. *Int. J. Syst. Bacteriol.* 46, 1088–1092. doi: 10.1099/00207713-46-4-1088

Rosca, A. S., Castro, J., Sousa, L. G. V., and Cerca, N. (2020). *Gardnerella* and vaginal health: The truth is out there. *FEMS Microbiol. Rev.* 44, 73–105. doi: 10.1093/femsre/fuz027

Rottini, G., Dobrina, A., Forgiarini, O., Nardon, E., Amirante, G. A., and Patriarca, P. (1990). Identification and partial characterization of a cytolytic toxin produced by *Gardnerella vaginalis*. *Infect. Immun.* 58, 3751–3758. doi: 10.1128/iai.58.11.3751-3758.1990

Sivadon-Tardy, V., Roux, A. L., Piriou, P., Herrmann, J. L., Gaillard, J. L., and Rottman, M. (2009). *Gardnerella vaginalis* acute hip arthritis in a renal transplant recipient. *J. Clin. Microbiol.* 47, 264–265. doi: 10.1128/JCM.01854-08

Swidsinski, A., Mendling, W., Loening-Baucke, V., Ladhoff, A., Swidsinski, S., Hale, L. P., et al. (2005). Adherent biofilms in bacterial vaginosis. *Obstet. Gynecol.* 106(5 Pt 1), 1013–1023.

Vaneechoutte, M., Guschin, A., Van Simaey, L., Gansemans, Y., Van Nieuwerburgh, F., and Cools, P. (2019). Emended description of *Gardnerella vaginalis* and description of *Gardnerella leopoldii* sp. nov., *Gardnerella piotii* sp. nov. and *Gardnerella swidsinskii* sp. nov., with delineation of 13 genomic species within the genus *Gardnerella*. *Int. J. Syst. Evol. Microbiol.* 69, 679–687. doi: 10.1099/ijsem.0.003200

Walker, B. J., Abeel, T., Shea, T., Priest, M., Abouelliel, A., Sakthikumar, S., et al. (2014). Pilon: An integrated tool for comprehensive microbial variant detection and genome assembly improvement. *PLoS One* 9:e112963. doi: 10.1371/journal.pone.0112963

Workowski, K. A., Berman, S., and Centers for Disease Control and Prevention. (2010). Sexually transmitted diseases treatment guidelines, 2010. *MMWR Recomm. Rep.* 59, 1–110.

Yeoman, C. J., Yildirim, S., Thomas, S. M., Durkin, A. S., Torralba, M., Sutton, G., et al. (2010). Comparative genomics of *Gardnerella vaginalis* strains reveals substantial differences in metabolic and virulence potential. *PLoS One* 5:e12411. doi: 10.1371/journal.pone.0012411

Zhang, Y., and Rochefort, D. (2013). Fast and effective paper based sensor for self-diagnosis of bacterial vaginosis. *Anal. Chim. Acta* 800, 87–94. doi: 10.1016/j.aca.2013.09.032

frontiers | Frontiers in Microbiology

TYPE Original Research
PUBLISHED 29 September 2022
DOI 10.3389/fmicb.2022.1023083

OPEN ACCESS

EDITED BY
Nayeli Alva-Murillo,
University of Guanajuato,
Mexico

REVIEWED BY
Guodong Zhao,
Zhejiang University Kunshan Innovation Institute, China
Anita Hafner,
University of Zagreb,
Croatia

*CORRESPONDENCE
Nataša Škalko-Basnet
natasa.skalko-basnet@uit.no

SPECIALTY SECTION
This article was submitted to Infectious Agents and Disease, a section of the journal Frontiers in Microbiology

RECEIVED 19 August 2022
ACCEPTED 15 September 2022
PUBLISHED 29 September 2022

CITATION
Hemmingsen LM, Panchai P, Julin K, Basnet P, Nystad M, Johannessen M and Škalko-Basnet N (2022) Chitosan-based delivery system enhances antimicrobial activity of chlorhexidine. *Front. Microbiol.* 13:1023083. doi: 10.3389/fmicb.2022.1023083

Chitosan-based delivery system enhances antimicrobial activity of chlorhexidine

Lisa Myrseth Hemmingsen[1], Pimmat Panchai[1], Kjersti Julin[2], Purusotam Basnet[3], Mona Nystad[3,4], Mona Johannessen[2] and Nataša Škalko-Basnet[1]*

[1]Drug Transport and Delivery Research Group, Department of Pharmacy, University of Tromsø The Arctic University of Norway, Tromsø, Norway, [2]Research Group for Host-Microbe Interaction, Department of Medical Biology, University of Tromsø The Arctic University of Norway, Tromsø, Norway, [3]Women's Health and Perinatology Research Group, Department of Clinical Medicine, University of Tromsø The Arctic University of Norway, Tromsø, Norway, [4]IVF Clinic, Women's Clinic, University Hospital of North Norway, Tromsø, Norway

Infected chronic skin wounds and other skin infections are increasingly putting pressure on the health care providers and patients. The pressure is especially concerning due to the rise of antimicrobial resistance and biofilm-producing bacteria that further impair treatment success. Therefore, innovative strategies for wound healing and bacterial eradication are urgently needed; utilization of materials with inherent biological properties could offer a potential solution. Chitosan is one of the most frequently used polymers in delivery systems. This bioactive polymer is often regarded as an attractive constituent in delivery systems due to its inherent antimicrobial, anti-inflammatory, anti-oxidative, and wound healing properties. However, lipid-based vesicles and liposomes are generally considered more suitable as delivery systems for skin due to their ability to interact with the skin structure and provide prolonged release, protect the antimicrobial compound, and allow high local concentrations at the infected site. To take advantage of the beneficial attributes of the lipid-based vesicles and chitosan, these components can be combined into chitosan-containing liposomes or chitosomes and chitosan-coated liposomes. These systems have previously been investigated for use in wound therapy; however, their potential in infected wounds is not fully investigated. In this study, we aimed to investigate whether both the chitosan-containing and chitosan-coated liposomes tailored for infected wounds could improve the antimicrobial activity of the membrane-active antimicrobial chlorhexidine, while assuring both the anti-inflammatory activity and cell compatibility. Chlorhexidine was incorporated into three different vesicles, namely plain (chitosan-free), chitosan-containing and chitosan-coated liposomes that were optimized for skin wounds. Their release profile, antimicrobial activities, anti-inflammatory properties, and cell compatibility were assessed *in vitro*. The vesicles comprising chitosan demonstrated slower release rate of chlorhexidine and high cell compatibility. Additionally, the inflammatory responses in murine macrophages treated with these vesicles were reduced by about 60% compared to non-treated cells. Finally, liposomes containing both chitosan and chlorhexidine demonstrated the strongest antibacterial effect against *Staphylococcus aureus*. Both chitosan-containing and

chitosan-coated liposomes comprising chlorhexidine could serve as excellent platforms for the delivery of membrane-active antimicrobials to infected wounds as confirmed by improved antimicrobial performance of chlorhexidine.

KEYWORDS

chitosan, chlorhexidine, lipid-based vesicles, membrane-active antimicrobials, skin wound healing, bioactive polymer, antibacterial activity

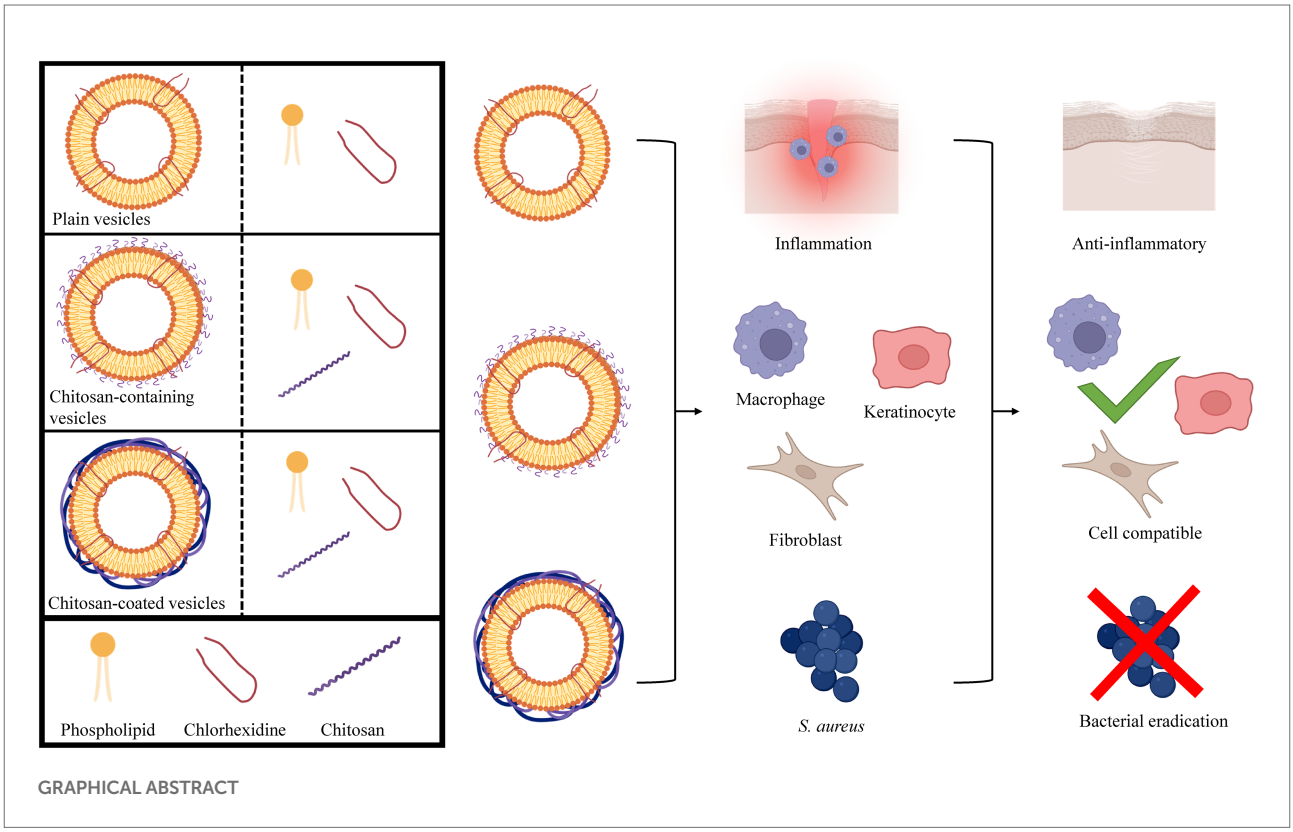

GRAPHICAL ABSTRACT

Introduction

Skin wounds, and particularly chronic wounds, are placing an enormous strain on health care systems worldwide; in 2018 the prevalence of chronic wounds was estimated to be approximately 1–2% in the general population (Kaiser et al., 2021). There is a solid consensus that one of the most important factors permitting wounds to heal properly is the ability to lower the microbial burden and inflammation in the wound bed (Eriksson et al., 2022). However, the rising antimicrobial resistance (AMR) and bacteria's production of biofilms are making this undertaking more challenging, therefore innovative strategies are urgently needed to mend the situation (Barrigah-Benissan et al., 2022). In this scenario, chitosan could play an important role both because of its inherent biological properties, but also its ability to improve efficacy of antimicrobial compounds (Hemmingsen et al., 2021a). Chitosan is among the most frequently used polymers in pharmaceutical technology and drug delivery systems (Pramanik and Sali, 2021). The interest in chitosan emanates from its many beneficial attributes, such as antimicrobial, anti-inflammatory, anti-oxidative, and hemostatic properties (Iacob et al., 2021). Additionally, this polymer, derived from deacetylated chitin found in crab, shrimp, krill shells, and fungi, is biodegradable and biocompatible with generally low toxicity (Bakshi et al., 2020). Numerous studies have confirmed its potential in skin therapy, especially against skin infections (Hemmingsen et al., 2021c). However, lipid-based systems are more frequently used in skin delivery; liposomes are often considered attractive because of their ability to closely interact

Abbreviations: AMR, Antimicrobial resistance; CCK-8, Cell counting kit-8; CFU, Colony-forming units; CHX, chlorhexidine; DMEM-hg, Dulbecco's Modified Eagle Medium high glucose; EE, Entrapment efficiency; FBS, Fetal bovine serum; LPS, Lipopolysaccharide; MAA, Membrane-active antimicrobial; M_w, Molecular weight; NO, Nitric oxide; PBS, Phosphate buffered-saline; PEG, Polyethylene glycol; PI, Polydispersity index; RMPI, Roswell park memorial institute medium.

with the skin structure (Matei et al., 2021). Additionally, liposomes and lipid-based vesicles provide prolonged release, protect the entrapped antimicrobial, and allow high local drug concentrations at the infected site (Nwabuife et al., 2021). To utilize the advantageous attributes from both lipid-based systems and chitosan, they can be combined, as, e.g., in chitosomes (chitosan-containing liposomes) with chitosan on the surface and in the interior of the liposomes or chitosan-coated liposomes (Sebaaly et al., 2021). These vesicles have been investigated for several applications, however, mainly for mucosal delivery (Sebaaly et al., 2021). Additionally, their role in wound healing has also been investigated (Mengoni et al., 2017; Eid et al., 2022), yet their role in antimicrobial wound therapy is not fully explored. We propose that by tailoring chitosan's availability on vesicle surface we could improve the antimicrobial potential of chitosan-comprising vesicles for wound therapy.

Taking advantage of the antimicrobial properties and potentially elevate the effect of chitosan, chitosan-containing or chitosan-coated drug delivery systems could be further combined with membrane-active antimicrobials (MAAs); their combination could generate a synergetic antimicrobial effect (Hemmingsen et al., 2021b). Among antiseptics that are often used to treat skin and soft tissue infections, the MAA chlorhexidine (CHX), is one of the most common (Hoang et al., 2021). Its main mechanism of action is proposed to be a destruction of the bacterial membranes; however, precipitation of the cytoplasm has been observed at higher doses (Hubbard et al., 2017). Unfortunately, studies show growing resistance towards CHX which might affect its future effectiveness in the clinics (Fritz et al., 2013; Cieplik et al., 2019; Abdel-Sayed et al., 2020). Here, the drug delivery systems could play a valuable role. Carefully tailored delivery systems could improve the antimicrobial efficacy of antimicrobial compounds by increasing their local concentration and retention time, protect antimicrobial compounds, and improve interaction with bacterial membranes (Osman et al., 2022). Furthermore, in chronic wounds, the additional beneficial biological properties of chitosan could improve wound healing by directly affecting the healing cascade or reducing inflammation and oxidative radicals (Iacob et al., 2021).

In our previous study, we investigated the effect of medium molecular weight (M_w) chitosan combined with liposomes on inflammatory responses and antimicrobial potential (Hemmingsen et al., 2021b). In the current study, we assessed whether the insertion of chitosan into lipid vesicles, as in chitosan-containing liposomes or chitosomes, or chitosan-coating of pre-made lipid carriers, influenced the CHX release and biological properties of the novel system. Furthermore, we investigated the ability of low M_w chitosan to improve the anti-inflammatory and antimicrobial properties of CHX. The antimicrobial activity of chitosan is not fully elucidated, however, the most common explanations for its antimicrobial properties are proposed to be linked to the interaction between positively charged chitosan and the slightly negatively charged bacterial membrane (Khan et al., 2020; Xia et al., 2022). However, chitosan's biological properties are coupled to its M_w and degree of deacetylation. Chitosans of higher M_w are proposed to form an envelope around the bacterial membrane, limiting nutrient uptake and growth, while chitosans of lower M_w are more prone to penetrate the bacterial membrane and interact with intracellular components (Matica et al., 2019). We aimed to exploit the latter mechanism to improve the antimicrobial potential of CHX.

Materials and methods

Materials

Chitopharm™ S-Chitosan with low M_w (50–1000 kDa), degree of deacetylation >70% was kindly provided by Chitinor (Tromsø, Norway). Lipoid S100 was kindly provided by Lipoid GmbH (Ludwigshafen, Germany). Methanol ≥99.9%, HiPerSolv CHROMANORM® for LC–MS, phosphate buffered-saline (PBS, pH 7.4) tablets and acetic acid glacial were procured from VWR International (Fontenay-sous-Bois, France). Chlorhexidine ≥99.5%, glycerol solution (86–89%), glycine hydrochloride ≥99% (HPLC), sodium chloride, hydrochloric acid, Cell Counting Kit-8 (CCK-8), and Kollisolv® polyethylene glycol (PEG) E 400 were obtained from Sigma-Aldrich (St. Louis, MO, United States). Cibacron Brilliant Red 3BA was a product from Santa Cruz Biotechnology (Dallas, TX, United States). Ortho-phosphoric acid ≥85% was purchased from Kebo Lab Ab (Oslo, Norway). Penicillin–streptomycin and Roswell Park Memorial Institute (RPMI) medium 1640 were purchased from Sigma-Aldrich (Steinheim, Germany). Lipopolysaccharide (LPS, from *Escherichia coli* 055:B5), sulfanilamide ≥98% and N-(1-Naphthyl)ethylenediamine dihydrochloride ≥98% were obtained from Sigma Life Science Norway AS (Oslo, Norway). Dulbecco's Modified Eagle Medium high glucose w/ l-glutamine (DMEM-hg) and sodium pyruvate and fetal bovine serum (FBS) were purchased from Biowest (Nuaillé, France). Blood agar plates, saline solution, and Mueller–Hinton broth were supplied by University Hospital of North Norway (Tromsø, Norway). Murine macrophage RAW 264.7 cells were ordered from ATCC (Manassas, VA, United States). Human Dermal Fibroblasts, Neonatal (NHDF-neo) were obtained from Lonza (Basel, Switzerland), and HaCaT cell line (immortalized human keratinocytes) from CLS Cell Lines Service GmbH (Eppelheim, Germany). *Staphylococcus aureus* (ATCC® BAA-1721™) MSSA476 was ordered from LGC standards AB (Borås, Sweden).

Preparation of vesicles

Preparation of plain lipid carriers or chitosan-containing liposomes

Vesicles were produced by the thin film method as described previously (Shukla et al., 2020; Hemmingsen et al., 2021a). In

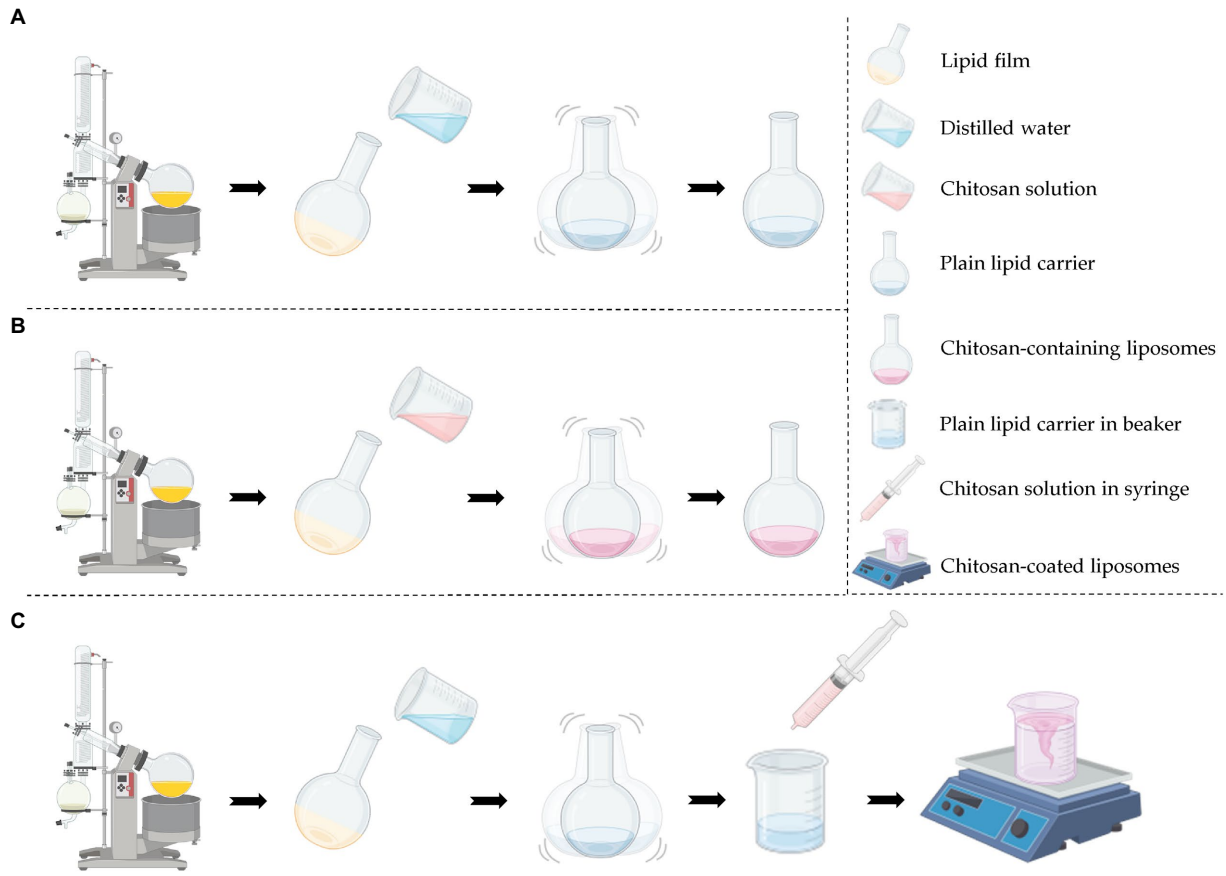

FIGURE 1
Production procedure of the different vesicles. **(A)** Production of plain lipid carrier with or without chlorhexidine. **(B)** Production of chitosan-containing liposomes with or without chlorhexidine. **(C)** Production of chitosan-coated liposomes with or without chlorhexidine. Created with BioRender.com.

brief, Lipoid S100 (200 mg) and CHX (10 mg) were dissolved in methanol; the solvent was removed by evaporation (Büchi rotavapor R-124 with vacuum controller B-721, Büchi Vac® V-500, Büchi Labortechnik, Flawil, Switzerland) at 60 mBar and 45°C for at least 1 h. The lipid film was dislodged with 10 ml distilled water to create plain (chitosan-free) lipid carriers or 10 ml 0.2% (w/v) chitosan solution in 0.1 M acetic acid, to form chitosan-containing liposomes. Both formulations were shaken to anneal vesicles. Empty lipid carriers were prepared in the same manner without CHX present. The vesicles were stored in the refrigerator (4°C) prior to size reduction.

Vesicle coating with chitosan

Plain lipid carriers with or without CHX were coated with 0.2% (w/v) chitosan solution in 0.1 M acetic acid (1:1, v/v, Jøraholmen et al., 2014). The chitosan solution was added dropwise (1.22 min/ml) under continuous stirring (250 rpm). The suspensions were stirred for another hour at 24°C before refrigeration (4°C). The lipid and chitosan concentrations were adjusted to be comparable prior to all further experiments. The production of the different vesicles is depicted in Figure 1.

Vesicle size reduction

The size of the vesicles was reduced using probe sonication and manual extrusion. The amplitude of the probe (SONICS high intensity ultrasonic processor, 500-watt model, 13 mm probe diameter, Sonics & Materials Inc., Newtown, CT, United States) was set to 40% and the samples were kept on ice bath to avoid extensive heating. Extrusion was performed with polycarbonate membranes (Nuclepore Track-Etch Membrane, Whatman House, Maidstone, United Kingdom) with average pore size of 0.4 µm (Cauzzo et al., 2020). The size of the different formulations was reduced as described in Table 1 to attain vesicles of similar sizes.

Vesicle characterization

Vesicle size and zeta potential measurements

The size of vesicles was measured with NICOMP Submicron particle sizer (NICOMP Particle Sizing System, Santa Barbara, CA, United States) at an intensity of 250–350 kHz reached by dilution in filtered (0.2 µm) distilled water (Hemmingsen et al., 2021b). The vesicles were measured in three rounds of 15–20 min

TABLE 1 Vesicle type, designation, and size reduction procedure.

	Sonication time (s)	Sonication intervals	Rounds of extrusion
PL	10	10	3
PL-CHX	5	1	–
CH	10	10	3
CH-CHX	5	2	–
CO	10	18	–
CO-CHX	5	1	–

PL, Plain, empty lipid carrier; PL-CHX, Plain CHX-lipid carrier; CH, Chitosan-containing empty liposomes; CH-CHX, Chitosan-containing CHX-liposomes; CO, Chitosan-coated empty liposomes; CO-CHX, Chitosan-coated CHX-liposomes.

(to attain stable readings) at 22–24°C, and the weight-intensity distribution was recorded (as cumulative size of 80% of the population).

The zeta potential was measured with Zetasizer Nano Zen 2,600 (Malvern, Worcestershire, United Kingdom). The samples were diluted in filtered (0.2 µm) tap water (assuring counter ions) to an appropriate concentration (according to attenuation) and measured at 25°C in three cycles using a DTS1070 cell (Malvern, Worcestershire, United Kingdom, Jøraholmen et al., 2015).

The pH of vesicle suspensions was measured using sensION+ PH31 pH benchtop meter (Hach, Loveland, CO, United States).

Entrapment efficiency

Unentrapped CHX was removed from the vesicle suspension using dialysis tubing with M_w cut-off 12–14 kDa (Spectra/Por®4, Spectrum®, VWR International, Fontenay-sous-Bois, France). An aliquot of 1 ml of vesicle suspension was dialyzed against 1 l distilled water under stirring for 4 h at room temperature. The CHX incorporated in the liposomes was quantified using Spark M10 multimode plate reader (Tecan Trading AG, Männedorf, Switzerland) at 261 nm (Hemmingsen et al., 2021a).

Surface-available chitosan determination

Quantification of surface-available chitosan was performed as previously described (Muzzarelli, 1998; Jøraholmen et al., 2015). In short, glycine buffer (250 ml, pH 3.2) was prepared in distilled water using 1.87 g glycine and 1.46 g NaCl. This buffer (81 ml) was further diluted to a total volume of 100 ml in 0.1 M HCl. To quantify chitosan, a dye solution was prepared. An aliquot of 150 mg Cibacron Brilliant Red 3B-A was dissolved in distilled water (100 ml). The glycine buffer was used to dilute 5 ml of the dye solution to a total volume of 100 ml. An aliquot of 300 µl of diluted vesicle suspensions (distilled water, 1:1, v/v) were mixed with 3 ml of the diluted Cibacron dye and surface-available chitosan was quantified using Spark M10 multimode plate reader (Tecan Trading AG, Männedorf, Switzerland) at 575 nm (Jøraholmen et al., 2015).

Vesicle stability

The stability of the vesicles was evaluated after 2- and 4-week storage at 4°C. The parameters evaluated were the vesicle size, zeta potential, and pH as described in the section Vesicle size and zeta potential measurements.

In vitro chlorhexidine release

In vitro CHX release studies were performed using a Franz cell diffusion system (PermeGear, Hellertown, PA, United States). Pre-soaked cellophane membranes (Max Bringmann KG, Wendelstein, Germany) were used as diffusion barriers with area of 1.77 cm^2 (Jøraholmen et al., 2014). Due to the low water solubility of CHX base (Farkas et al., 2001), the acceptor chamber was filled with PEG E 400 (10%, v/v) in distilled water (12 ml acceptor volume, Hemmingsen et al., 2021b). The temperature was maintained at 32°C with heated circulating water. Vesicle suspensions (600 µl) were added to the donor chamber. Samples were withdrawn after 1, 2, 3, 4, 5, 8, and 24 h, and the sample volume was replaced with fresh medium to maintain sink conditions. The release from vesicles was compared to non-formulated CHX (dissolved in release media). Quantitative analysis was carried out using Spark M10 multimode plate reader (Tecan Trading AG, Männedorf, Switzerland) at 261 nm (Hemmingsen et al., 2021b).

Evaluation of cell viability and anti-inflammatory responses

Assessment of cell viability

Assessment of cell viability was accomplished using the CCK-8 kit according to methods previously described (Hemmingsen et al., 2021b). The cells (HaCaT; Cauzzo et al., 2020, NHDF-neo; Domiński et al., 2022, and murine macrophages RAW 264.7; Basnet et al., 2012; Cauzzo et al., 2020) in complete RPMI medium [containing 10% (v/v) FBS and penicillin–streptomycin; RAW 264.7] or complete DMEM-hg (HaCaT and NHDF-neo) were plated on 96-well plates (90 µl, 1×10^5 cells/ml) and incubated (37°C, 5% CO_2) for 24 h. Diluted vesicle suspensions (10 µl) were added to the wells (final lipid concentration of 1, 10, and 50 µg/ml) and the plates incubated for another 24 h (37°C, 5% CO_2). Next, an aliquot of 10 µl CCK-8 reagent was added to each well and the plates were incubated for 4 h. The cell viability was measured using Spark M10 multimode plate reader (Tecan Trading AG, Männedorf, Switzerland) at 450 nm with the reference set to 650 nm. Treated cells were compared to non-treated cells (only complete RPMI or DMEM-hg).

Anti-inflammatory activity

The anti-inflammatory activity of the vesicles was assessed by inducing nitric oxide (NO) production in murine macrophages using

LPS as previously described (Schulte-Werning et al., 2021). RAW 264.7 cells (Basnet et al., 2012) in complete RPMI medium [containing 10% (v/v) FBS and penicillin–streptomycin] were plated on 24-well plate (1,000 µl, 5×10^5 cells/ml) and incubated (37°C, 5% CO_2) for 24 h. The complete medium was aspirated and LPS (1 µg/ml, 990 µl) in complete RPMI added to each well. Next, diluted vesicle suspensions (10 µl) were added to the wells at final lipid concentration of 1, 10, and 50 µg/ml, and the plates incubated for another 24 h (37°C, 5% CO_2). The NO production was assessed by mixing the cell medium and Griess reagent [1:1, v/v; 2.5% phosphoric acid with 1% sulphanilamide and 0.1% N-(−1-naphthyl)ethylenediamine] and analyzing the mixture with Spark M10 multimode plate reader (Tecan Trading AG, Männedorf, Switzerland) at 560 nm. Only complete medium or LPS (1 µg/ml) in complete RPMI served as controls. The LPS-induced cells treated with vesicles were compared to non-treated LPS-induced cells (100%).

Antimicrobial evaluation

The broth microdilution method was utilized to evaluate the antibacterial properties of the vesicles with or without CHX (Balouiri et al., 2016). Overnight cultures of *S. aureus* MSSA476 were diluted in saline solutions (0.85%, w/w) to a turbidity of 0.5 McFarland; these bacterial suspensions were further diluted (1:150, v/v) in Mueller-Hinton broth. Vesicle suspensions were 2-fold diluted with Mueller-Hinton broth in 96-well plates and the diluted bacterial suspensions added (1:1, v/v). The plates were incubated at 37°C with shaking (100 rpm) for 24 h. Non-treated or treated (with different vesicles) bacteria in suspensions were serially diluted (10-fold) in PBS, plated on blood agar plates and incubated at 37°C overnight. The colony-forming units (CFUs) were counted to evaluate the activity of the tested formulations as compared to non-treated bacteria. Lipid concentrations of 0.3125 mg/ml were used to compare the different vesicle formulations (Ternullo et al., 2019).

Statistical analyses

The results are generally expressed as means ± SD. Statistical significance was evaluated by student's *t*-test or one-way ANOVA followed by Turkey's correction (p at least 0.05). All statistical analyses were performed in GraphPad Prism version 9.3.1 for Windows (GraphPad Software LLC, San Diego, CA, United States).

Results and discussion

Vesicle characteristics

Size is an important parameter in the development of drug delivery systems; considering the dermal administration route it has been proposed that size around 300 nm might be beneficial assuring that the vesicles are able to reach the deeper layers of the skin without advancing too deep (du Plessis et al., 1994). In our previous studies, we have shown that the vesicles in a size range between 250 and 350 nm provide good eradication of common skin pathogens (Hemmingsen et al., 2021a,b). Furthermore, reports indicate that nanoparticles smaller than 350 nm can diffuse through biofilm pores (Makabenta et al., 2021). Therefore, we aimed for the size range of 250–350 nm for our plain and chitosan-comprising formulations (Table 2). We assessed the vesicle size as cumulative size of 80% of the vesicle populations since some of the vesicles exhibited the bi- or multi-modal distributions that were difficult to directly compare. Most vesicles were slightly over 300 nm in diameter; however, the chitosan-coated liposomes displayed a larger size likely due to the coating procedure. Even though the optimal polydispersity index (PI) is suggested to be about 0.3 for lipid-based vesicles destined for skin delivery (Danaei et al., 2018), our vesicles had a PI below 0.4 and that was deemed acceptable. The vesicle size of chitosan-coated liposomes is often larger and harder to control as compared to non-coated liposomes (Jøraholmen et al., 2015).

TABLE 2 Chitosan-containing liposomes and chitosan-coated liposomes characteristics: mean diameter (≤80%, nm), polydispersity index (PI), zeta potential, entrapment efficacy (EE%), and pH in aqueous medium.

	Size (≤80%, nm)	PI	Zeta potential (mV)	EE%	pH
PL	308 ± 22	0.37 ± 0.04	−1.6 ± 1.4	–	5.8 ± 0.5
PL-CHX	305 ± 14	0.38 ± 0.03	42.9 ± 5.9	63.2 ± 4.8	8.5 ± 0.1
CH	303 ± 18	0.32 ± 0.01	12.4 ± 0.4	–	3.6 ± 0.0
CH-CHX	300 ± 24	0.34 ± 0.07	94.9 ± 2.2	65.7 ± 4.8	3.7 ± 0.0
CO	325 ± 23	0.35 ± 0.01	13.0 ± 0.4	–	3.7 ± 0.0
CO-CHX	393 ± 23	0.39 ± 0.02	83.3 ± 3.1	70.4 ± 3.9	3.8 ± 0.0

Results of size measurements are expressed as means of cumulative size ≤ 80% of vesicle populations (weight-intensity distribution) with their respective SD, while the rest of the results are expressed as means with their respective SD ($n = 3$). PL, Plain, empty lipid carrier; PL-CHX, Plain CHX-lipid carrier; CH, Chitosan-containing empty liposomes; CH-CHX, Chitosan-containing CHX-liposomes; CO, Chitosan-coated empty liposomes; and CO-CHX, Chitosan-coated CHX-liposomes.

Tailoring vesicles with chitosan have previously shown to increase the zeta potential of the delivery system (Mady et al., 2009; Park et al., 2014). The increase in surface charge is an indication of successful addition (coating or insertion) of chitosan indicating that chitosan is available on the surface of the vesicles (Jøraholmen et al., 2014). Additionally, nanoparticles with a cationic character are able to distribute within the biofilm after penetration into the matrix (Makabenta et al., 2021). The surface charge increased even more upon incorporation of CHX in the formulations; the fact that both chitosan and CHX are available on the vesicle surface and able to interact with the bacteria is highly encouraging considering antimicrobial potential of novel system. The entrapment of CHX was relatively high; however, lower than the entrapment achieved when

10.3389/fmicb.2022.1023083

TABLE 3 Surface-available chitosan on chitosan-containing liposomes and chitosan-coated liposomes.

	Surface-available chitosan (%)[1]
CH	86.2 ± 16.0
CH-CHX	92.2 ± 3.2
CO	55.1 ± 7.4
CO-CHX	84.4 ± 4.2

Results are expressed as means with their respective SD ($n = 3$). CH, Chitosan-containing empty liposomes; CH-CHX, Chitosan-containing CHX-liposomes; CO, Chitosan-coated empty liposomes; and CO-CHX, Chitosan-coated CHX-liposomes.
[1]Percentage of initial chitosan concentration.

TABLE 4 Chitosan-containing liposomes and chitosan-coated liposomes stability after 2 and 4 weeks of storage: mean diameter (≤80%, nm), polydispersity index (PI), zeta potential, and pH in aqueous medium.

	Week	Size (80%, nm)	PI	Zeta potential (mV)	pH
PL	2	326 ± 54	0.44 ± 0.05	−2.6 ± 0.6	6.0 ± 0.2
	4	298 ± 25	0.39 ± 0.05	−3.9 ± 0.1	5.7 ± 0.3
PL-CHX	2	272 ± 11	0.41 ± 0.02	40.2 ± 7.6	7.7 ± 0.2
	4	259 ± 8	0.40 ± 0.01	42.2 ± 10.5	7.8 ± 0.4
CH	2	307 ± 19	0.32 ± 0.00	11.1 ± 0.9	3.6 ± 0.0
	4	307 ± 24	0.31 ± 0.01	11.1 ± 0.9	3.7 ± 0.0
CH-CHX	2	285 ± 5	0.28 ± 0.01	92.1 ± 7.8	3.8 ± 0.0
	4	280 ± 6	0.29 ± 0.02	91.9 ± 3.3	3.8 ± 0.0
CO	2	316 ± 17	0.36 ± 0.01	12.5 ± 1.0	3.7 ± 0.0
	4	328 ± 25	0.37 ± 0.01	11.8 ± 0.6	3.7 ± 0.0
CO-CHX	2	375 ± 44	0.39 ± 0.02	83.3 ± 3.2	3.8 ± 0.0
	4	371 ± 40	0.42 ± 0.03	78.6 ± 0.9	3.8 ± 0.0

Vesicle stability after 2 and 4 weeks of storage at 4°C. Results of size measurements are expressed as means of cumulative size ≤80% of vesicle populations (weight-intensity distribution) with their respective SD, while the rest of the results are expressed as means with their respective SD ($n = 3$), while the rest of the results are expressed as means with their respective SD ($n = 3$). PL, Plain, empty lipid carrier; PL-CHX, Plain CHX-lipid carrier; CH, Chitosan-containing empty liposomes; CH-CHX, Chitosan-containing CHX-liposomes; CO, Chitosan-coated empty liposomes; and CO-CHX, Chitosan-coated CHX-liposomes.

utilizing the one-pot method which provided a CHX entrapment efficiency of 74% in chitosomes (Hemmingsen et al., 2021b). Nonetheless, a high entrapment and surface-available chitosan and CHX are assuring features for successful antimicrobial therapy. Both compounds are available to interact with the bacteria; moreover, the cationic nature of delivery system will improve the interaction between the vesicles and bacteria since bacterial membranes are slightly negatively changed (Epand and Epand, 2009).

Surface-available chitosan

To confirm that chitosan was available on the vesicle surface and determine to which extent it was available, we quantified the amount of surface-available chitosan on the vesicles using a colorimetric protocol first described by Muzzarelli (Muzzarelli, 1998). The quantity of surface-available chitosan on the vesicles was found to be rather high for all formulations (Table 3). For the empty, chitosan-coated liposomes the amount was comparable to the study of Jøraholmen et al. (2015). However, for the chitosan-containing liposomes, the amount of chitosan that was available on the surface was greater than the amount achieved for the chitosomes prepared with the one-pot method by Andersen et al. (2015). Additionally, contrary to our previous finding (Hemmingsen et al., 2021b), the addition of CHX seemed to increase the amount of surface-available chitosan on the vesicles; however, it was significant only for the chitosan-coated liposomes. Again, it is important to consider the chitosan origin and its M_w when comparing the results. Using a different method, Li et al. reported surface-available chitosan in quantities of up to 89.5% (Li et al., 2009). The surface availability is important not only for potential antimicrobial effects but also considering chitosan's bioadhesive properties that can be beneficial in wound treatment (Hamedi et al., 2022).

Vesicle stability

To assess the vesicle stability the size, PI, zeta potential, and pH of each formulation were evaluated after 2 and 4 weeks of storage at 4°C (Table 4). The size of all vesicles was relatively stable over the 4-week period; however, plain CHX-lipid carriers exhibited a small decrease in size between production and week 2 ($p = 0.0109$) that was not considered as an issue. Furthermore, the size did not change significantly between week 2 and 4; probably due to the surface charge (above 40 mV) and its stabilizing effect. All other parameters remained stable for the entire period. The addition of chitosan to liposomal formulations is often considered to improve the stability of the suspensions, both as a physical measure to maintain the integrity of the bilayers and due to electrostatic effects; however, this seems to be affected by the chitosan concentration (Sebaaly et al., 2021).

In vitro chlorhexidine release

As a result of the physical presence of chitosan and its physiochemical properties, chitosan could affect the release rate of active compounds from the vesicles (Gibis et al., 2016). Therefore, we investigated the CHX release from the plain lipid carriers, chitosan-containing, and chitosan-coated liposomes (Figure 2). Non-formulated CHX, dissolved in the release medium, was used as a control. After 24 h, the plain CHX-lipid carrier had released significantly more CHX than the chitosan-containing liposomes ($p = 0.0371$). However, no difference in the release was observed between the chitosan-containing and chitosan-coated liposomes. All vesicles significantly decreased the rate of release compared with non-formulated CHX at all time points. This prolonged release profile with gradual, long-lasting release of the compounds is highly beneficial for a drug delivery

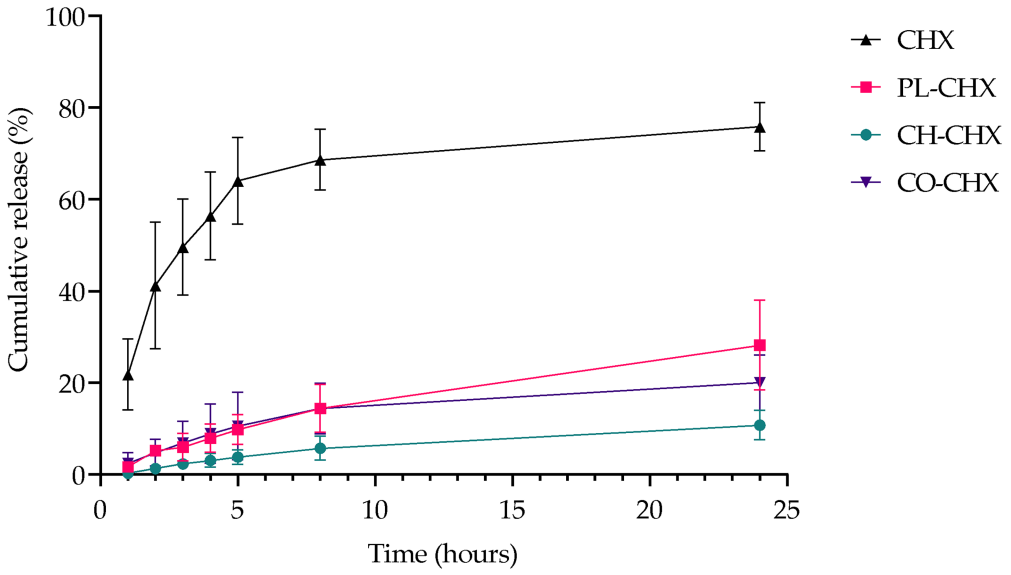

FIGURE 2
Cumulative *in vitro* release of CHX from non-formulated and formulated CHX over 24 h at 32°C. Results are expressed as release percentage compared to entrapped amount of CHX and means with their respective SD (n=3). Chlorhexidine (CHX), non-formulated CHX in media; PL-CHX, Plain CHX-lipid carrier; CH-CHX, Chitosan-containing CHX-liposomes; and CO-CHX, Chitosan-coated CHX-liposomes.

system intended for topical, antimicrobial therapy. First, these delivery systems could provide a high local concentration important for the therapeutic outcome; however, this is depending on whether the concentration reaches an effective concentration limit (Allen and Cullis, 2013). To prove the effect, biological assays are required. Second, drug delivery systems with prolonged release of the antimicrobial compound could help prevent regrowth of bacteria as well as ensure long-lasting antimicrobial effects (Piras et al., 2015). Third, as the compounds are retained onto/in the skin assuring local depot, the potential for reaching the systemic circulation is limited (Cui et al., 2021). The latter is highly relevant when limiting AMR.

Polymyxin B, another MAA, has previously displayed slower release rate from chitosan-modified liposomes. The vesicles released polymyxin B over a period of 24 h, while the non-formulated polymyxin B was completely released already after 12 h (Fu et al., 2019). On the other hand, Park et al. reported faster permeation rate of the MAA nisin from coated liposomes than uncoated liposomes; however, this study was conducted with mouse skin (Park et al., 2014). It is rather challenging to compare the release data from different studies due to the differences in physicochemical properties of active compounds and experimental settings.

Cell viability and anti-inflammatory responses

Liposomes and many other lipid-based delivery systems are generally regarded to be highly biocompatible, biodegradable, and safe. Furthermore, the toxicity of certain pharmaceutical compounds is often reduced when they are entrapped in these drug delivery systems (Liu et al., 2022). Nevertheless, the systems' effect on relevant cells is a critical parameter to be assessed in the development of new carriers or upon entrapment of new pharmaceutical compounds. The safety of these carriers is highly influenced by different features of the systems, such as the composition, size, size distribution, and surface properties (Liu et al., 2022). Consequently, we investigated cell compatibility in relevant cells, namely keratinocytes, fibroblasts, and macrophages, as well as the system's influence on inflammatory responses in macrophages.

Cell viability

As previously mentioned, liposomes can reduce the toxicity of pharmaceutical compounds (Nwabuife et al., 2021). Similarly, chitosan is also regarded biocompatible and biodegradable (Rashki et al., 2021). However, it is known that several alternations could change the properties of the materials, especially in the nano-range. For instance, the safety of chitosan is often considered to be linked to its degree of deacetylation and M_w (Rashki et al., 2021). The MAA, CHX, has in previous studies displayed toxicity in different cells, e.g., macrophages, keratinocytes, and fibroblasts (Li et al., 2014; Borges et al., 2017). Therefore, the potential toxicity of empty and CHX-loaded vesicles was assessed in these cells (Figure 3). In HaCaT and NHDF-neo cells, the viability of cells was unaffected by the treatment with both empty and CHX-loaded vesicles with or without chitosan. This is highly beneficial, as the viability of these cells is crucial for the successful therapy by therapeutics

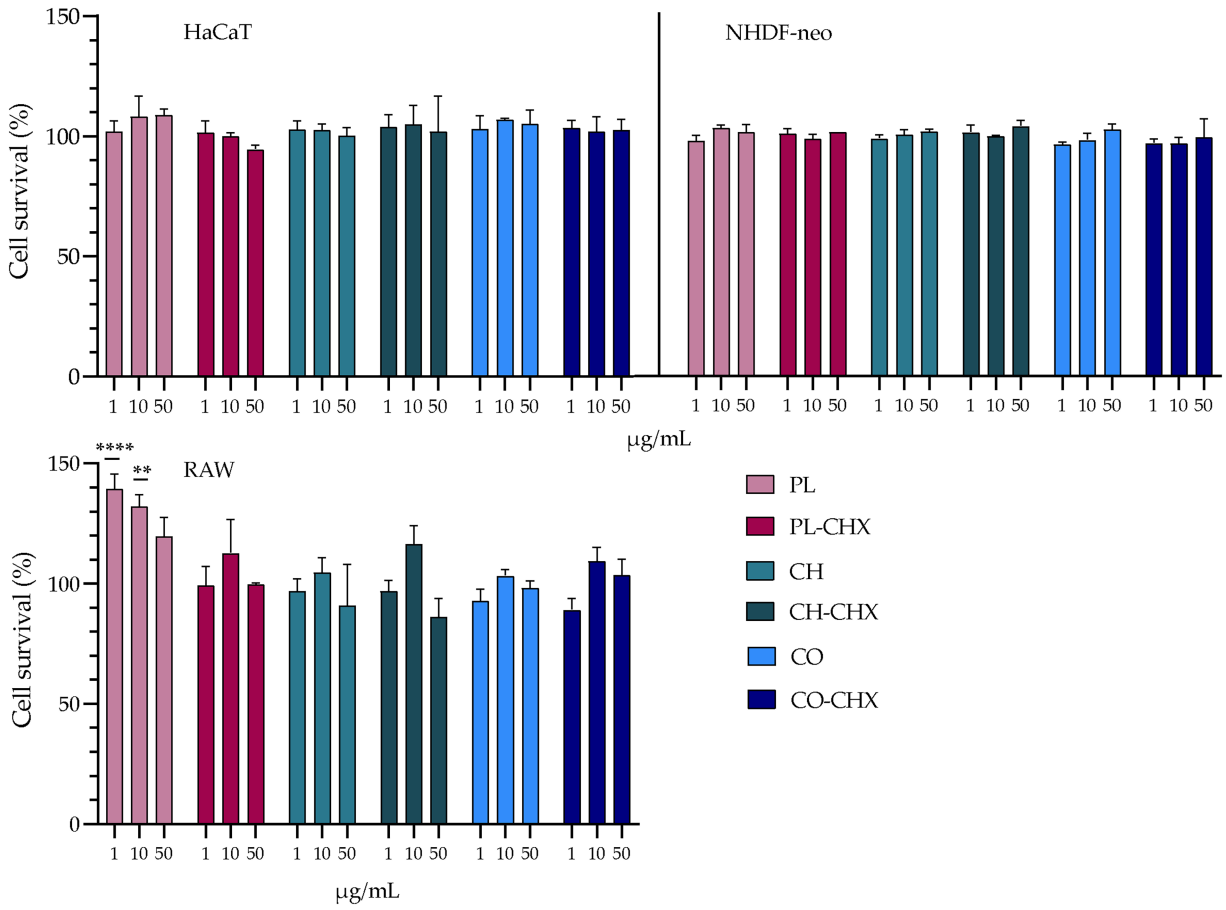

FIGURE 3
Evaluation of cell toxicity of chitosan-containing liposomes and chitosan-coated liposomes in HaCaT, NHDF-neo cells, and RAW 264.7. Three different concentrations were tested, namely 1, 10, and 50 μg/ml lipid, and the results are presented as cell viability of treated cells compared to control (100%). Control cells were only supplemented with complete medium; the cell viability is thereof considered as 100%. The results are expressed as means with their respective SD (n=3). PL, plain, empty lipid carrier; PL-CHX, plain CHX-lipid carrier; CH, chitosan-containing empty liposomes; CH-CHX, chitosan-containing CHX-liposomes; CO, chitosan-coated empty liposomes; and CO-CHX, chitosan-coated CHX-liposomes. **$p \leq 0.01$, ****$p \leq 0.0001$.

intended for wounds. Both keratinocytes and fibroblasts play active roles in the inflammatory phase in wounds; their release of cytokines and growth factors maintains hemostasis and influences other cells to participate in the process of wound closure (Wojtowicz et al., 2014). Moreover, keratinocytes are especially important in our defense against bacterial invasion due to their ability to release the antimicrobial peptides with antibacterial, antifungal, and antiviral activities (Chessa et al., 2020).

In the murine macrophages, no negative effects were observed in the treated cells; however, the empty, plain lipid carriers seemed to improve the viability of the cells, suggesting a proliferative effect. At lipid concentrations of 1 and 10 μg/ml, the viability or cell proliferation was significantly improved compared to control ($p < 0.0001$ and 0.0013, respectively). The proliferative effects of liposomes have previously been demonstrated by Ye et al. (2019); however, in significantly higher concentrations than in the current study. Macrophages play several pivotal roles in the wound healing cascade, for instance, cleaning of pathogens and debris from the wound, activation of immune cells, promotion of migration of other cells, such as keratinocytes and fibroblasts, and breaking down the temporary extracellular matrix (Krzyszczyk et al., 2018). Therefore, their presence and retained viability are of high importance. Furthermore, Hilițanu et al. confirmed the biocompatibility of chitosan-coated liposomes containing erythromycin after oral administration in mice. The authors investigated erythrocyte counts, liver enzyme activity, serum urea plasma levels, immunological biomarkers, and histopathological examinations of liver or kidney, and found no significant changes in the mice (Hilițanu et al., 2021).

Anti-inflammatory activity

Macrophages bear crucial attributes in wound healing; however, in chronic wounds these cells might also be a part of the problem. Chronic wounds are arrested in a state of

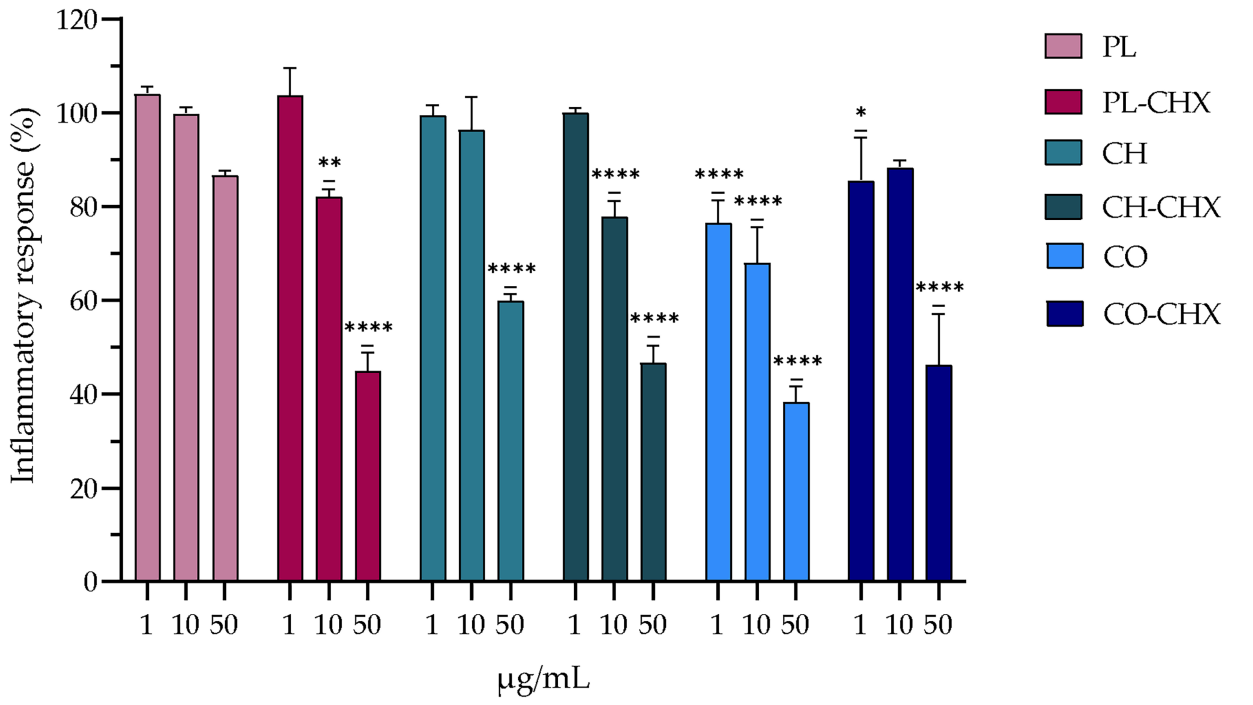

FIGURE 4
Evaluation of anti-inflammatory activity of chitosan-containing and chitosan-coated liposomes expressed as reduction of nitric oxide (NO) production in RAW 264.7 cells. Three different concentrations were tested, namely 1, 10, and 50 µg/ml lipid, and the results are presented as NO production of treated cells compared to control (100%). Control cells were non-treated lipopolysaccharide (LPS)-induced cells; their production is thereof considered as 100%. The results are expressed as means with their respective SD (n=3). PL, Plain, empty lipid carrier; PL-CHX, Plain CHX-lipid carrier; CH, Chitosan-containing empty liposomes; CH-CHX, Chitosan-containing CHX-liposomes; CO, Chitosan-coated empty liposomes; CO-CHX, Chitosan-coated CHX-liposomes. *$p \leq 0.05$, **$p \leq 0.01$, ****$p \leq 0.0001$, compared to control.

inflammation and unable to progress in the healing cascade. This is linked to the presence of pro-inflammatory macrophages (M1-type macrophages) at the site of injury that leads to elevated levels of cytokines and reactive oxygen species, and apoptosis of keratinocytes and fibroblasts (Shamiya et al., 2022). This prolonged state of inflammation is undesirable in wounds as it hinders healing. To evaluate whether novel formulations can act on inflammatory response, we assessed the anti-inflammatory effects in murine macrophages. In macrophages, LPS is recognized by toll-like receptor 4, its binding leading to expression of pro-inflammatory genes. In mice, this leads to overexpression of inducible nitric oxide synthase and subsequent high levels of NO that could serve as an indicator of anti-inflammatory responses. This effect is far greater in mice than in humans, and therefore murine macrophages were utilized to assess the potential anti-inflammatory activity (Krzyszczyk et al., 2018). The results of the inflammatory assessments are presented in Figure 4 and demonstrate a clear dose-dependent anti-inflammatory effect the formulations had on treated cells. The anti-inflammatory activities of the vesicles with chitosan and/or CHX were significantly higher as compared to non-treated LPS-induced macrophages. However, the effects did not seem to be synergetic, namely the presence of both chitosan and CHX did not enhance the effects in synergy. The determined threshold was at about 55–65% reduction. Interestingly, the empty, plain lipid carriers also induced a dose-dependent reduction in inflammatory response; however, this effect was not significant.

Antimicrobial evaluation

In recent years, more focus has been placed on drug delivery systems and nanostructured materials in the development of new therapeutic options for microbial eradication and prevention. These systems and materials, both organic and inorganic, have demonstrated superior antimicrobial activities against a wide variety of microbial strains (Baranwal et al., 2018). Liposomes are among the most frequently used systems while chitosan has generated interest due to its inherent antimicrobial properties (Baranwal et al., 2018). Considering liposomes, their structure and composition is similar to the bacterial membrane; this could lead to a fusion between liposomes and bacteria resulting in delivery of higher antimicrobial payloads. Additionally, liposomes that possess a positively charged surface could interact with bacteria and further improve the antimicrobial effects (Wang et al., 2020). All of this is expected to improve the therapeutic index and make bacteria more susceptible to antimicrobials associated with delivery system as compared to non-formulated antimicrobials (Wang et al., 2020). To further improve the antimicrobial properties of drug delivery systems,

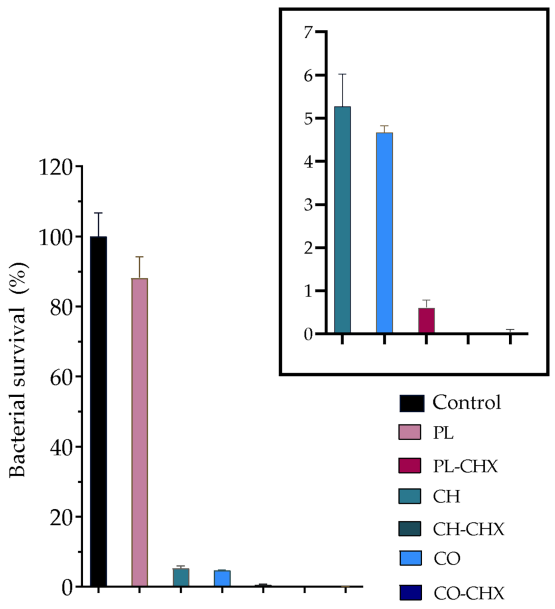

FIGURE 5
Bacterial survival (%) of *Staphylococcus aureus* MSSA476 (ATCC® BAA-1721™) in the presence of non-formulated and formulated chlorhexidine (CHX) at a lipid concentration of 0.3125 mg/ml. The boxed area is enlarged to depict the chitosan- and/or CHX-containing and/or coated vesicles. The results are expressed as means with their respective SD (n=3). PL, Plain, empty lipid carrier; PL-CHX, Plain CHX-lipid carrier; CH, Chitosan-containing empty liposomes; CH-CHX, Chitosan-containing CHX-liposomes; CO, Chitosan-coated empty liposomes; and CO-CHX, Chitosan-coated CHX-liposomes. ****$p \leq 0.0001$, compared to control.

chitosan is often utilized together with other delivery systems. In the current study, we were using an MAA, postulating that chitosan and MAA could act in synergy and enhance the effect on the bacteria. We assessed the antimicrobial activity of our vesicles against *S. aureus*, one of the most common pathogens found in chronic wounds (Alves et al., 2021). As seen in Figure 5, the empty, plain lipid carriers did not display any antimicrobial activity, as expected; however, upon inclusion of chitosan in vesicles, the bacterial survival was dramatically reduced to 5.3 and 4.7% for the chitosan-containing and chitosan-coated liposomes, respectively. Jøraholmen et al. have previously proven that chitosan-coated liposomes exhibit antimicrobial activity against *S. aureus*, even when their corresponding non-coated liposomes did not possess any activities (Jøraholmen et al., 2020).

We were also interested in the activity of plain and chitosan-comprising vesicles with CHX. The plain CHX-lipid carriers reduced the bacterial survival by 99.4%; even more than chitosan-vesicles without CHX. However, the combination of chitosan and CHX in vesicles demonstrated the strongest antimicrobial activity. Chitosan-containing CHX-liposomes completely eradicated *S. aureus*, while the bacterial survival after treatment with chitosan-coated CHX-liposomes was reduced to only 0.03%. These results are in agreement with the results from our previous study where we utilized one-pot method for the production of vesicles; however, chitosan of different M_w (higher M_w) was utilized in that study (Hemmingsen et al., 2021b). Wang et al. also demonstrated improved antimicrobial activity against *S. aureus* of cinnamaldehyde, a MAA, when the compound was entrapped in chitosan-coated liposomes. Furthermore, they also demonstrated that the mechanism behind this action was membrane disruption (Wang et al., 2021). In another study, Hassan et al., proved lowered MIC and faster antimicrobial action of vancomycin when it was entrapped in lipid-chitosan hybrid vesicles. They also established that the effect was due to membrane destruction. Moreover, the authors demonstrated eradication of pre-formed MRSA biofilms (Hassan et al., 2020). These encouraging results highlight the potential of systems combining lipid-based vesicles and chitosan for successful microbial eradication.

Conclusion

In an era of lowered microbial susceptibility to conventional antimicrobial compounds and higher prevalence of chronic wounds, often with high microbial burden, innovative strategies for microbial eradication and improved wound healing are crucially needed. We proposed that combinations of lipid-based vesicles and chitosan could serve as promising delivery systems for MAAs, such as CHX, as confirmed by successful bacterial eradication of the common skin pathogen *S. aureus*. Indeed, we showed that both chitosan-containing liposomes and chitosan-coated liposomes destined to treat infected wounds could successfully improve antimicrobial activity of CHX against *S. aureus*, highlighting their potential in antimicrobial wound therapy.

Data availability statement

The raw data supporting the conclusions of this article will be made available by the authors, without undue reservation.

Author contributions

LH and NŠ-B: conceptualization, formal analysis, and writing—original draft preparation. LH, KJ, PB, MJ, and NŠ-B: methodology. LH, KJ, and NŠ-B: validation. LH and PP: investigation and data curation. MN, MJ, and NŠ-B: resources. LH, PP, KJ, PB, MN, MJ, and NŠ-B: writing—review and editing. LH: visualization. NŠ-B: supervision, project administration, and funding acquisition. All authors contributed to the article and approved the submitted version.

Funding

UiT The Arctic University of Norway, Norway funded this study (project no. 235569). The publication fund of UiT The Arctic

University of Norway funded the publication charges of this article.

Acknowledgments

The authors would like to acknowledge Chitinor (Tromsø, Norway) and Lipoid GmbH (Ludwigshafen, Germany) for providing chitosan and phospholipid, respectively, for this study. The authors would also like to thank Maddhusja Sritharan Nalliah and Nora Hersoug Nedberg at Department of Clinical Medicine, UiT The Arctic University of Norway. Figure 1 and graphical abstract were created with BioRender.com.

Conflict of interest

The authors declare that the research was conducted in the absence of any commercial or financial relationships that could be construed as a potential conflict of interest.

Publisher's note

References

Abdel-Sayed, P., Tornay, D., Hirt-Burri, N., De Buys Roessingh, A., Raffoul, W., and Applegate, L. A. (2020). Implications of chlorhexidine use in burn units for wound healing. *Burns* 46, 1150–1156. doi: 10.1016/j.burns.2019.12.008

Allen, T. M., and Cullis, P. R. (2013). Liposomal drug delivery systems: from concept to clinical applications. *Adv. Drug Deliv. Rev.* 65, 36–48. doi: 10.1016/j.addr.2012.09.037

Alves, P. J., Barreto, R. T., Barrois, B. M., Gryson, L. G., Meaume, S., and Monstrey, S. J. (2021). Update on the role of antiseptics in the management of chronic wounds with critical colonisation and/or biofilm. *Int. Wound J.* 18, 342–358. doi: 10.1111/iwj.13537

Andersen, T., Bleher, S., Flaten, G. E., Tho, I., Mattsson, S., and Škalko-Basnet, N. (2015). Chitosan in mucoadhesive drug delivery: focus on local vaginal therapy. *Mar. Drugs* 13, 222–236. doi: 10.3390/md13010222

Bakshi, P. S., Selvakumar, D., Kadirvelu, K., and Kumar, N. S. (2020). Chitosan as an environment friendly biomaterial – a review on recent modifications and applications. *Int. J. Biol. Macromol.* 150, 1072–1083. doi: 10.1016/j.ijbiomac.2019.10.113

Balouiri, M., Sadiki, M., and Ibnsouda, S. K. (2016). Methods for in vitro evaluating antimicrobial activity: a review. *J. Pharm. Anal.* 6, 71–79. doi: 10.1016/j.jpha.2015.11.005

Baranwal, A., Srivastava, A., Kumar, P., Bajpai, V. K., Maurya, P. K., and Chandra, P. (2018). Prospects of nanostructure materials and their composites as antimicrobial agents. *Front. Microbiol.* 9:422. doi: 10.3389/fmicb.2018.00422

Barrigah-Benissan, K., Ory, J., Sotto, A., Salipante, F., Lavigne, J. P., and Loubet, P. (2022). Antiseptic agents for chronic wounds: a systematic review. *Antibiotics* 11:350. doi: 10.3390/antibiotics11030350

Basnet, P., Hussain, H., Tho, I., and Škalko-Basnet, N. (2012). Liposomal delivery system enhances anti-inflammatory properties of Curcumin. *J. Pharm. Sci.* 101, 598–609. doi: 10.1002/jps.22785

Borges, G. Á., Elias, S. T., Da Silva, S. M. M., Magalhães, P. O., Macedo, S. B., Ribeiro, A. P. D., et al. (2017). In vitro evaluation of wound healing and antimicrobial potential of ozone therapy. *J. Craniomaxillofac. Surg.* 45, 364–370. doi: 10.1016/j.jcms.2017.01.005

Cauzzo, J., Nystad, M., Holsæter, A. M., Basnet, P., and Škalko-Basnet, N. (2020). Following the fate of dye-containing liposomes in vitro. *Int. J. Mol. Sci.* 21:4847. doi: 10.3390/ijms21144847

Chessa, C., Bodet, C., Jousselin, C., Wehbe, M., Lévêque, N., and Garcia, M. (2020). Antiviral and Immunomodulatory properties of antimicrobial peptides produced by human keratinocytes. *Front. Microbiol.* 11:1155. doi: 10.3389/fmicb.2020.01155

Cieplik, F., Jakubovics, N. S., Buchalla, W., Maisch, T., Hellwig, E., and Al-Ahmad, A. (2019). Resistance toward Chlorhexidine in Oral bacteria–is there cause for concern? *Front. Microbiol.* 10:587. doi: 10.3389/fmicb.2019.00587

Cui, M., Wiraja, C., Chew, S. W. T., and Xu, C. (2021). Nanodelivery Systems for Topical Management of skin disorders. *Mol. Pharm.* 18, 491–505. doi: 10.1021/acs.molpharmaceut.0c00154

Danaei, M., Dehghankhold, M., Ataei, S., Hasanzadeh Davarani, F., Javanmard, R., Dokhani, A., et al. (2018). Impact of particle size and Polydispersity index on the clinical applications of Lipidic Nanocarrier systems. *Pharmaceutics* 10:57. doi: 10.3390/pharmaceutics10020057

Domiński, A., Domińska, M., Skonieczna, M., Pastuch-Gawołek, G., and Kurcok, P. (2022). Shell-Sheddable micelles based on poly(ethylene glycol)-hydrazone-poly[RS]-3-hydroxybutyrate copolymer loaded with 8-Hydroxyquinoline Glycoconjugates as a dual tumor-targeting drug delivery system. *Pharmaceutics* 14:290. doi: 10.3390/pharmaceutics14020290

du Plessis, J., Ramachandran, C., Weiner, N., and Müller, D. G. (1994). The influence of particle size of liposomes on the deposition of drug into skin. *Int. J. Pharm.* 103, 277–282. doi: 10.1016/0378-5173(94)90178-3

Eid, H. M., Ali, A. A., Ali, A. M. A., Eissa, E. M., Hassan, R. M., Abo El-Ela, F. I., et al. (2022). Potential use of tailored Citicoline chitosan-coated liposomes for effective wound healing in diabetic rat model. *Int. J. Nanomedicine* 17, 555–575. doi: 10.2147/ijn.S342504

Epand, R. M., and Epand, R. F. (2009). Lipid domains in bacterial membranes and the action of antimicrobial agents. *Biochim. Biophys. Acta Biomembr.* 1788, 289–294. doi: 10.1016/j.bbamem.2008.08.023

Eriksson, E., Liu, P. Y., Schultz, G. S., Martins-Green, M. M., Tanaka, R., Weir, D., et al. (2022). Chronic wounds: treatment consensus. *Wound Repair Regen.* 30, 156–171. doi: 10.1111/wrr.12994

Farkas, E., Zelkó, R., Török, G., Rácz, I., and Marton, S. (2001). Influence of chlorhexidine species on the liquid crystalline structure of vehicle. *Int. J. Pharm.* 213, 1–5. doi: 10.1016/S0378-5173(00)00575-5

Fritz, S. A., Hogan, P. G., Camins, B. C., Ainsworth, A. J., Patrick, C., Martin, M. S., et al. (2013). Mupirocin and Chlorhexidine resistance in Staphylococcus aureus in patients with community-onset skin and soft tissue infections. *Antimicrob. Agents Chemother.* 57, 559–568. doi: 10.1128/AAC.01633-12

Fu, Y. Y., Zhang, L., Yang, Y., Liu, C. W., He, Y. N., Li, P., et al. (2019). Synergistic antibacterial effect of ultrasound microbubbles combined with chitosan-modified polymyxin B-loaded liposomes on biofilm-producing Acinetobacter baumannii. *Int. J. Nanomedicine* 14, 1805–1815. doi: 10.2147/IJN.S186571

Gibis, M., Ruedt, C., and Weiss, J. (2016). In vitro release of grape-seed polyphenols encapsulated from uncoated and chitosan-coated liposomes. *Food Res. Int.* 88, 105–113. doi: 10.1016/j.foodres.2016.02.010

Hamedi, H., Moradi, S., Hudson, S. M., Tonelli, A. E., and King, M. W. (2022). Chitosan based bioadhesives for biomedical applications: a review. *Carbohydr. Polym.* 282:119100. doi: 10.1016/j.carbpol.2022.119100

Hassan, D., Omolo, C. A., Fasiku, V. O., Mocktar, C., and Govender, T. (2020). Novel chitosan-based pH-responsive lipid-polymer hybrid nanovesicles (OLA-LPHVs) for delivery of vancomycin against methicillin-resistant Staphylococcus aureus infections. *Int. J. Biol. Macromol.* 147, 385–398. doi: 10.1016/j.ijbiomac.2020.01.019

Hemmingsen, L. M., Giordani, B., Pettersen, A. K., Vitali, B., Basnet, P., and Škalko-Basnet, N. (2021a). Liposomes-in-chitosan hydrogel boosts potential of chlorhexidine in biofilm eradication in vitro. *Carbohydr. Polym.* 262:117939. doi: 10.1016/j.carbpol.2021.117939

Hemmingsen, L. M., Julin, K., Ahsan, L., Basnet, P., Johannessen, M., and Škalko-Basnet, N. (2021b). Chitosomes-in-chitosan hydrogel for acute skin injuries: prevention and infection control. *Mar. Drugs* 19:269. doi: 10.3390/md19050269

Hemmingsen, L. M., Škalko-Basnet, N., and Jøraholmen, M. W. (2021c). The expanded role of chitosan in localized antimicrobial therapy. *Mar. Drugs* 19:697. doi: 10.3390/md19120697

Hiliţanu, L. N., Mititelu-Tarţău, L., Popa, G. E., Buca, B. R., Pavel, L. L., Pelin, A. M., et al. (2021). The analysis of chitosan-coated Nanovesicles containing erythromycin–characterization and biocompatibility in mice. *Antibiotics* 10:1471. doi: 10.3390/antibiotics10121471

Hoang, T. P., Ghori, M. U., and Conway, B. R. (2021). Topical antiseptic formulations for skin and soft tissue infections. *Pharmaceutics* 13:558. doi: 10.3390/pharmaceutics13040558

Hubbard, A. T. M., Coates, A. R., and Harvey, R. D. (2017). Comparing the action of HT61 and chlorhexidine on natural and model Staphylococcus aureus membranes. *J. Antibiot.* 70, 1020–1025. doi: 10.1038/ja.2017.90

Iacob, A. T., Lupascu, F. G., Apotrosoaei, M., Vasincu, I. M., Tauser, R. G., Lupascu, D., et al. (2021). Recent biomedical approaches for chitosan based materials as drug delivery Nanocarriers. *Pharmaceutics* 13:587. doi: 10.3390/pharmaceutics13040587

Jøraholmen, M. W., Bhargava, A., Julin, K., Johannessen, M., and Škalko-Basnet, N. (2020). The antimicrobial properties of chitosan can be tailored by formulation. *Mar. Drugs* 18:96. doi: 10.3390/md18020096

Jøraholmen, M. W., Škalko-Basnet, N., Acharya, G., and Basnet, P. (2015). Resveratrol-loaded liposomes for topical treatment of the vaginal inflammation and infections. *Eur. J. Pharm. Sci.* 79, 112–121. doi: 10.1016/j.ejps.2015.09.007

Jøraholmen, M. W., Vanić, Ž., Tho, I., and Škalko-Basnet, N. (2014). Chitosan-coated liposomes for topical vaginal therapy: assuring localized drug effect. *Int. J. Pharm.* 472, 94–101. doi: 10.1016/j.ijpharm.2014.06.016

Kaiser, P., Wächter, J., and Windbergs, M. (2021). Therapy of infected wounds: overcoming clinical challenges by advanced drug delivery systems. *Drug Deliv. Transl. Res.* 11, 1545–1567. doi: 10.1007/s13346-021-00932-7

Khan, F., Pham, D. T. N., Oloketuyi, S. F., Manivasagan, P., Oh, J., and Kim, Y. M. (2020). Chitosan and their derivatives: Antibiofilm drugs against pathogenic bacteria. *Colloids Surf. B: Biointerfaces* 185:110627. doi: 10.1016/j.colsurfb.2019.110627

Krzyszczyk, P., Schloss, R., Palmer, A., and Berthiaume, F. (2018). The role of macrophages in acute and chronic wound healing and interventions to promote pro-wound healing phenotypes. *Front. Physiol.* 9:419. doi: 10.3389/fphys.2018.00419

Li, Y. C., Kuan, Y. H., Lee, S. S., Huang, F. M., and Chang, Y. C. (2014). Cytotoxicity and genotoxicity of chlorhexidine on macrophages in vitro. *Environ. Toxicol.* 29, 452–458. doi: 10.1002/tox.21771

Li, N., Zhuang, C., Wang, M., Sun, X., Nie, S., and Pan, W. (2009). Liposome coated with low molecular weight chitosan and its potential use in ocular drug delivery. *Int. J. Pharm.* 379, 131–138. doi: 10.1016/j.ijpharm.2009.06.020

Liu, P., Chen, G., and Zhang, J. (2022). A review of liposomes as a drug delivery system: current status of approved products, regulatory environments, and future perspectives. *Molecules* 27:1372. doi: 10.3390/molecules27041372

Mady, M. M., Darwish, M. M., Khalil, S., and Khalil, W. M. (2009). Biophysical studies on chitosan-coated liposomes. *Eur. Biophys. J.* 38, 1127–1133. doi: 10.1007/s00249-009-0524-z

Makabenta, J. M. V., Nabawy, A., Li, C. H., Schmidt-Malan, S., Patel, R., and Rotello, V. M. (2021). Nanomaterial-based therapeutics for antibiotic-resistant bacterial infections. *Nat. Rev. Microbiol.* 19, 23–36. doi: 10.1038/s41579-020-0420-1

Matei, A. M., Caruntu, C., Tampa, M., Georgescu, S. R., Matei, C., Constantin, M. M., et al. (2021). Applications of Nanosized-lipid-based drug delivery Systems in Wound Care. *Appl. Sci.* 11:4915. doi: 10.3390/app11114915

Matica, M. A., Aachmann, F. L., Tøndervik, A., Sletta, H., and Ostafe, V. (2019). Chitosan as a wound dressing starting material: antimicrobial properties and mode of action. *Int. J. Mol. Sci.* 20:5889. doi: 10.3390/ijms20235889

Mengoni, T., Adrian, M., Pereira, S., Santos-Carballal, B., Kaiser, M., and Goycoolea, F. M. (2017). A chitosan—based liposome formulation enhances the in vitro wound healing efficacy of substance P neuropeptide. *Pharmaceutics* 9:56. doi: 10.3390/pharmaceutics9040056

Muzzarelli, R. R. A. (1998). Colorimetric determination of chitosan. *Anal. Biochem.* 260, 255–257. doi: 10.1006/abio.1998.2705

Nwabuife, J. C., Pant, A. M., and Govender, T. (2021). Liposomal delivery systems and their applications against Staphylococcus aureus and methicillin-resistant Staphylococcus aureus. *Adv. Drug Deliv. Rev.* 178:113861. doi: 10.1016/j.addr.2021.113861

Osman, N., Devnarain, N., Omolo, C. A., Fasiku, V., Jaglal, Y., and Govender, T. (2022). Surface modification of nano-drug delivery systems for enhancing antibiotic delivery and activity. *Wires Nanomed. Nanobi.* 14:e1758. doi: 10.1002/wnan.1758

Park, S. N., Jo, N. R., and Jeon, S. H. (2014). Chitosan-coated liposomes for enhanced skin permeation of resveratrol. *J. Ind. Eng. Chem.* 20, 1481–1485. doi: 10.1016/j.jiec.2013.07.035

Piras, A. M., Maisetta, G., Sandreschi, S., Gazzarri, M., Bartoli, C., Grassi, L., et al. (2015). Chitosan nanoparticles loaded with the antimicrobial peptide temporin B exert a long-term antibacterial activity in vitro against clinical isolates of Staphylococcus epidermidis. *Front. Microbiol.* 6:372. doi: 10.3389/fmicb.2015.00372

Pramanik, S., and Sali, V. (2021). Connecting the dots in drug delivery: a tour d'horizon of chitosan-based nanocarriers system. *Int. J. Biol. Macromol.* 169, 103–121. doi: 10.1016/j.ijbiomac.2020.12.083

Rashki, S., Asgarpour, K., Tarrahimofrad, H., Hashemipour, M., Ebrahimi, M. S., Fathizadeh, H., et al. (2021). Chitosan-based nanoparticles against bacterial infections. *Carbohydr. Polym.* 251:117108. doi: 10.1016/j.carbpol.2020.117108

Schulte-Werning, L. V., Murugaiah, A., Singh, B., Johannessen, M., Engstad, R. E., Škalko-Basnet, N., et al. (2021). Multifunctional Nanofibrous dressing with antimicrobial and anti-inflammatory properties prepared by needle-free electrospinning. *Pharmaceutics* 13:1527. doi: 10.3390/pharmaceutics13091527

Sebaaly, C., Trifan, A., Sieniawska, E., and Greige-Gerges, H. (2021). Chitosan-coating effect on the characteristics of liposomes: a focus on bioactive compounds and essential oils: a review. *Processes* 9:445. doi: 10.3390/pr9030445

Shamiya, Y., Ravi, S. P., Coyle, A., Chakrabarti, S., and Paul, A. (2022). Engineering nanoparticle therapeutics for impaired wound healing in diabetes. *Drug Discov. Today* 27, 1156–1166. doi: 10.1016/j.drudis.2021.11.024

Shukla, S. K., Chan, A., Parvathaneni, V., and Gupta, V. (2020). Metformin-loaded chitosomes for treatment of malignant pleural mesothelioma – a rare thoracic cancer. *Int. J. Biol. Macromol.* 160, 128–141. doi: 10.1016/j.ijbiomac.2020.05.146

Ternullo, S., Gagnat, E., Julin, K., Johannessen, M., Basnet, P., Vanić, Ž., et al. (2019). Liposomes augment biological benefits of curcumin for multitargeted skin therapy. *Eur. J. Pharm. Biopharm.* 144, 154–164. doi: 10.1016/j.ejpb.2019.09.016

Wang, X., Cheng, F., Wang, X., Feng, T., Xia, S., and Zhang, X. (2021). Chitosan decoration improves the rapid and long-term antibacterial activities of cinnamaldehyde-loaded liposomes. *Int. J. Biol. Macromol.* 168, 59–66. doi: 10.1016/j.ijbiomac.2020.12.003

Wang, D. Y., Van Der Mei, H. C., Ren, Y., Busscher, H. J., and Shi, L. (2020). Lipid-based antimicrobial delivery-Systems for the Treatment of bacterial infections. *Front. Chem.* 7:872. doi: 10.3389/fchem.2019.00872

Wojtowicz, A. M., Oliveira, S., Carlson, M. W., Zawadzka, A., Rousseau, C. F., and Baksh, D. (2014). The importance of both fibroblasts and keratinocytes in a bilayered living cellular construct used in wound healing. *Wound Repair Regen.* 22, 246–255. doi: 10.1111/wrr.12154

Xia, Y., Wang, D., Liu, D., Su, J., Jin, Y., Wang, D., et al. (2022). Applications of chitosan and its derivatives in skin and soft tissue diseases. *Front. Bioeng. Biotechnol.* 10:894667. doi: 10.3389/fbioe.2022.894667

Ye, J., Yang, Y., Dong, W., Gao, Y., Meng, Y., Wang, H., et al. (2019). Drug-free mannosylated liposomes inhibit tumor growth by promoting the polarization of tumor-associated macrophages. *Int. J. Nanomedicine* 14, 3203–3220. doi: 10.2147/IJN.S207589

frontiers | Frontiers in Microbiology

TYPE Original Research
PUBLISHED 29 September 2022
DOI 10.3389/fmicb.2022.986326

OPEN ACCESS

EDITED BY
George Grant,
University of Aberdeen,
United Kingdom

REVIEWED BY
António Machado,
Universidad San Francisco de Quito,
Ecuador
Antonio Simone Laganà,
University of Palermo,
Italy

*CORRESPONDENCE
Xiaoying Liu
liuxiaoying@ahmu.edu.cn
Gang Liu
liugang8966@163.com

SPECIALTY SECTION
This article was submitted to Infectious Agents and Disease, a section of the journal Frontiers in Microbiology

RECEIVED 05 July 2022
ACCEPTED 16 August 2022
PUBLISHED 29 September 2022

CITATION
Sun M, Geng H, Bai J, Feng J, Xu N, Liu Y, Liu X and Liu G (2022) Characterization of cervical canal and vaginal bacteria in pregnant women with cervical incompetence.
Front. Microbiol. 13:986326.
doi: 10.3389/fmicb.2022.986326

Characterization of cervical canal and vaginal bacteria in pregnant women with cervical incompetence

Meiguo Sun[1], Huiwu Geng[2], Jingjing Bai[1], Jiahui Feng[2], Na Xu[2], Yunlong Liu[1], Xiaoying Liu[2,3]* and Gang Liu[2]*

[1]Department of Obstertrics and Gynecology, The First Affiliated Hospital of Anhui Medical University, Hefei, Anhui, China, [2]School of Life Sciences, Anhui Medical University, Hefei, Anhui, China, [3]Translational Research Institute of Henan Provincial People's Hospital and People's Hospital of Zhengzhou University, Henan International Joint Laboratory of Non-coding RNA and Metabolism in Cancer, Henan Provincial Key Laboratory of Long Non-coding RNA and Cancer Metabolism, Zhengzhou, Henan, China

Vaginal and cervical canal bacteria are associated with women's health and pregnancy outcomes. Here, we compared their composition and characteristics in 37 reproductive-aged Chinese women including 24 pregnant women with cervical incompetence (vaginal and cervical canal bacteria formed Groups A and B, respectively) and 13 healthy pregnant women (vaginal and cervical canal bacteria formed Groups C and D, respectively) using high-throughput sequencing of the V4 region of 16S rRNA gene. The results of alpha and beta diversity analysis, respectively, indicated no statistical differences between Groups A and B (p =0.32, 0.06), nor Groups B and D (p =0.69, 0.74); however, differences were found between Groups C and D (p =0.02, 0.01) and between Groups A and C (p =0.04, 0.02). PLS-DA analysis showed that the individuals from each group were irregularly distributed according to their clade. *Lactobacillus*, *Bifidobacterium* and *Ureaplasma* were the dominant genera in all groups. Phylogenetic Investigation of Communities by Reconstruction of Unobserved States (PICRUSts) analysis identified 31 Kyoto Encyclopedia of Genes and Genomes (KEGG) orthologs associated with the bacterial communities from the four groups, including membrane transport, folding, sorting and degradation, xenobiotics biodegradation and metabolism, and nucleotide metabolism. We further determined relationships between pregnancy outcomes (Apgar scores) and certain bacterial species. A significant positive correlation was found between Apgar scores and *Actinomyces neuii* and *Anoxybacillus flavithermus* in the vagina and cervical canal of pregnant women with cervical incompetence while *Bacteroides plebeius*, *Bifidobacterium pseudopodium* and *Staphylococcus petrasii* in the cervical canal displayed negative correlations with Apgar scores. Moreover, *Clostridium fimetarium*, *Methanobacterium congolense*, *Pseudomonas chlororaphis,* and *Psychrobacter nivimaris* in the vagina were negatively correlated with Apgar scores. These bacteria may serve as potential biomarkers, however, additional research is warranted to verify their role in clinical outcomes.

KEYWORDS

cervical incompetence, bacteria, biomarker, OTUs, vagina and cervical canal

Introduction

The female genital tract is home to trillions of bacteria that usually exist in a mutualistic relationship with their host (Younge et al., 2017; Elovitz et al., 2019). Intriguingly, the characteristics of vaginal and cervical canal bacterial communities are even more conspicuous and different from gut bacteria, displaying a high relative abundance of *Lactobacillus* and low bacterial diversity (Kervinen et al., 2019; Villani et al., 2022). Individual differences in the bacterial landscape of the vaginal and cervical canals are dramatically influenced by host genetics and environment, also being impacted by lifestyle factors (Moosa et al., 2020). Recent evidence supports the notion that the bacterial communities of the vagina and cervix are strongly associated with health status, with changes associated with pH, urinary tract infections, sexually transmitted infections including bacterial and viral infections such as HIV (human immunodeficiency virus) along with pregnancy outcomes (Watts et al., 2005; Flaviani et al., 2021; Lykke et al., 2021). Moreover, certain bacterial profiles are associated with adverse obstetric outcomes such as preterm birth, potentially leading to neonatal morbidity and mortality (Elovitz et al., 2019; Torcia, 2019; Tsonis et al., 2020; Tu et al., 2020; Flaviani et al., 2021).

In the female reproductive system, the vagina, cervical canal, fallopian tubes and uterus form the reproductive tract (McDonald, 1980; Chen et al., 2017). In general, the fallopian tubes and uterus are believed to be sterile, which requires the cervix to be a perfect barrier (Chen et al., 2017). The cervix does indeed provide a physical barrier to pathogens, and for example, the fetus is protected from the vaginal pathogens during healthy pregnancies (Hein et al., 2002; Goldenberg, et al., 2008; Aagaard et al., 2014; Liu et al., 2015; Kindinger et al., 2016). However, in some cases bacteria and other pathogens can ascend along the mucosal surfaces of the vagina to the fallopian tubes or the uterus (Liu et al., 2015; Chen et al., 2017; Brown et al., 2019).

Cervical incompetence is defined as the inability of the uterine cervix to retain a pregnancy in the second trimester in the absence of uterine contractions (Boelig et al., 2019). About 1% of females experience painless cervical dilation causing preterm birth in the second trimester, making this one of the most common diseases in reproductive-aged women (Brown et al., 2019; Pilarski et al., 2021). Building evidence over recent years implicates bacteria as the major cause of cervical incompetence, especially the composition and structures of bacteria which are highly correlated with preterm birth (Ravel et al., 2011; Smith and Ravel, 2017; Brown et al., 2019). Nonetheless, the bacterial composition and structures of the vagina and cervical canal in pregnant women suffering from cervical incompetence are yet to be fully characterized (Koedooder et al., 2019; Hao et al., 2021). Focusing on pregnant women with cervical incompetence, this study aimed to expand the current knowledgebase regarding the bacterial profiles of the vagina and cervical canal compared to normal pregnant woman using a high throughput sequencing approach. The results uncover potential new insights into the pathogenesis of cervical incompetence with implications for the prevention and treatment of the associated complications.

Materials and methods

Study population

Thirty-seven reproductive-aged Chinese women including 24 pregnant women with cervical incompetence and 13 healthy pregnant women were recruited at the First Affiliated Hospital of Anhui Medical University in 2021, China. We excluded subjects with vaginal inflammation, any acute inflammation, cancer, severe pelvic adhesion, endocrine or autoimmune disorders. Further exclusions were made regarding subjects treated with any vaginal medicine, antibiotics or hormones within one month, other cervical treatment or flushing within one month and sexual intercourse in the prior month (Chen et al., 2017; Tu et al., 2020). This study was approved by the institutional review board of Anhui Medical University (No. PJ2022-09012).

Sample collection

On the day of the prenatal visit, both vaginal lavage fluid and cervical canal swabs were collected. All collection materials and devices used were strictly sterilized. Cervical canal swabs were used to collect bacteria using a vaginal dilator, while the vaginal samples were performed with 10 ml of vaginal lavage fluid (saline solution). All samples were transferred to the lab within 2 h of collection and stored at −80°C.

DNA extraction and 16S rRNA ampliconsequencing

One millilitre of sterile phosphate-buffered saline was added to each cervical canal swab and rigorously vortexed for 1 min before 500 µl was collected, centrifuged and disrupted by enzymatic treatment. The vaginal lavage fluids were centrifuged at 2,000 rpm for 15 min. Total DNA of vaginal and cervical canal samples were determined using the Qubit high sensitivity kit follow the manufacturer's instructions. The V4 variable region of 16S rRNA gene was amplified used the 515F/806R primers (515F: 5′- GTG CCA GCM GCC GCG GTA A -3′; 806R 5′-GGA CTA CHV GGG TWT CTA AT -3′) followed by DNA extraction. The PCR products were purified and then subjected to high-throughput sequencing using the Illumina HiSeq 2,500 at BGI Genomics Co., Ltd. (Shenzhen, China). The raw data of all samples were submitted to the SRA (Sequence Read Archive) under accession numbers SRR19631963 at the NCBI database.

Bioinformatics, statistical analysis

Raw high-throughput sequencing data provided in FASTA format were subject to pre-processing (quality-trimmed, demultiplexed, and chimera-reduced) using QIIME Version 1.8.0

tools to remove short and poor-quality sequences (Caporaso et al., 2010). The clean reads were clustered to generate Operational Taxonomic Units (OTUs) with 97% similarity cutoff by Vsearch 2.4.2 (Rognes et al., 2016). Representative OUT sequences were given a taxonomic assignment based on the SILVA bacterial database using BLAST Version 2.60 (Altschul et al., 1997). Alpha diversity is a measure of bacteria diversity applicable to a single sample, and it is calculated by Chao1 index in this study. Beta diversity is a measure of similarity or dissimilarity of two communities, which is performed by calculating the UniFrac index by using R (v3.4.1; R Core Team, 2017). Differences between the two populations of the bacterial compositions were analyzed based on Partial Least Squares Discrimination Analysis (PLS-DA) by using the mixOmics package in R (v3.2.1; Rohart et al., 2017). Linear Discriminant Analysis Effect Size (LEfSe) analysis was used between or among groups to determine the differentially abundant taxonomic features by using the non-parametric Kruskal-Wallis rank sum test. Venn analysis diagrams were performed to categorize the core bacteria by using the VennDiagram package in R (v3.2.1; Chen and Boutros, 2011). All statistical analyses and plots were performed by GraphPad Prism v7.0.

Results

Sample groups and general sequencing information

We collected and sequenced the 16S rRNA gene from 74 vaginal and cervical canal samples from 37 pregnant women. The vaginal and cervical canal samples from pregnant women with cervical incompetence were designated as Group A (n = 24, sample no. A1-24) and Group B (n = 24, sample no. B1-24), respectively. The samples of the vagina and cervical canal of normal pregnant women were designated as Group C (n = 13, sample no. C1-13) and Group D (n = 13, sample no. D1-13), respectively. After removing low quality reads, a total of 4,825,697 clean reads were retained, which corresponding to 5,537 OTUs, the average reads were 63,496 ± 933 (range, 59,803–64,910 per sample) per sample. An average of 73 OTUs were contained in each sample, which ranged from 18 to 299 OTUs per sample. Samples from Groups A, B, C, and D had 1.06, 3.30, 0.38, and 3.61% unique OTUs with 12.44% of all OTUs common to the four groups (Supplementary Figure S1).

Alpha and beta diversity

Alpha and beta diversities were compared to determine the bacterial composition shift in patients of the four groups. There was no significant differences in Chao1 diversity indexes between Group A and Group B (Figure 1A; $p = 0.32$) and similarly there were no differences between Groups B and D (Figure 1D; $p = 0.69$). However, the Chao1 diversity index showed a significant difference between vaginal samples (Group C) and cervical canal samples (Group D) of healthy pregnant women (Figure 1B; $p = 0.02$), and also between Group A and Group C (Figure 1C; $p = 0.04$).

For the results of beta diversity, there was no significant differences between Groups A and B (Figures1E; $p = 0.06$), and between Groups B and D, respectively (Figure 1H; $p = 0.74$). However, beta diversity was significantly different between Groups C and D (Figure 1F, $p = 0.01$), and beta diversity was also significantly different between Group A and Group C (Figure 1G; $p = 0.02$). PLS-DA analysis results showed that individuals from Group C and D were irregularly distributed according to their clade, and the results of Groups A *vs* C were similar to Groups C *vs* D (Supplementary Figure S2).

Bacterial community compositions of vaginal and cervical canal

Fourteen phyla, 23 classes, 43 orders, 70 families and 138 genera of bacteria were identified in the four groups. Firmicutes, Actinobacteria and Tenericutes were the dominant bacterial phyla, accounting for 93.97, 4.91, and 0.44% of the OTUs, respectively. Bacteroidetes, Proteobacteria, Cyanobacteria, Fusobacteria, Deinococcus-Thermus, and Verrucomicrobia accounted for less than 0.02% of all bacteria (Figure 2A). Bacilli, Actinobacteria, Mollicutes, Clostridia, Erysipelotrichia, Bacteroidia, Negativicutes, Gammaproteobacteria, Betaproteobacteria and Cyanobacteria were the dominant bacterial classes, Bacilli and Actinobacteria are the dominant bacteria, accounting for 90.89 and 63.48%, respectively (Figure 2B). Lactobacillales, Bifidobacteriales, Mycoplasmatales, Clostridiales, Erysipelotrichales, Selenomonadales, Bacteroidales, Bacillales, Actinomycetales and Burkholderiales were the dominant bacterial orders, and Lactobacillales were the dominant bacteria, accounting for 91.13% (Figure 2C). *Lactobacillaceae*, *Bifidobacteriaceae*, *Mycoplasmataceae*, *Veillonellaceae*, *Prevotellaceae*, *Lachnospiraceae*, *Clostridiales*, *Porphyromonadaceae*, *Peptoniphilaceae* and *Ruminococcaceae* were the dominant bacterial families, *Lactobacillales* were the dominant bacteria, accounting for 88.72% (Figure 2D). The dominant genus was *Lactobacillus* (87.96%; Figure 2E).

Differences in taxa of the bacteria for vaginal and cervical canal samples

The relative abundance of several taxa was compared with each other for the four groups using LEfSe analysis (Figures 3A-D). A total of 42 species of the bacteria were identified from all the vaginal and cervical canal samples of 24 pregnant women with cervical incompetence and 13 healthy pregnant women. There were 11 differences in bacterial abundance found comparing between Groups A and B, the OUT was much lower in Group A than that in Group B (Figure 4A). Five differences were found between the abundance of bacteria in Group A and C, involving much higher

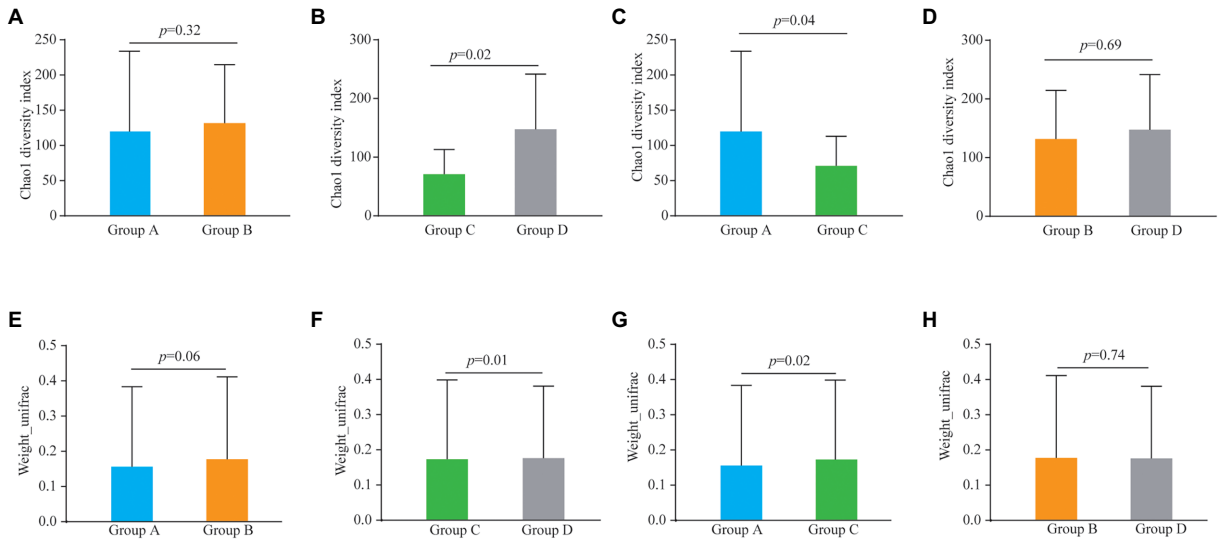

FIGURE 1
Alpha diversity analysis (Chao1 diversity index) of the bacteria from vaginal and cervical canal samples between Group A and Group B **(A)**, Group C and Group D **(B)**, Group A and Group C **(C)**, and Group C and Group D **(D)**, respectively. Beta diversity analysis of the bacteria from vaginal and cervical canal samples between Group A and Group B **(E)**, Group C and Group D **(F)**, Group A and Group C **(G)**, and Group C and Group D **(H)**, respectively.

abundance of *Actinomyces neuii*, *Anoxybacillus flavithermus*, *Bifidobacterium pseudolongum*, and *Staphylococcus petrasii* in Group A and higher abundance of *Bacteroides plebeius* in Group C (Figure 4B). Nine different species were identified between Groups B and D (Figure 4C), and 18 different species were found between Groups C and D (Figure 4D), respectively. In addition, Group D has significantly higher abundance of OUTs than that in Groups B and C, respectively.

Functional analysis of KEGG

To further explore the influence of the bacteria on the microenvironment of the vagina and cervical canal, KEGG pathway analyses were conducted. Overall, 31 orthologs were found by PICRUSts predictive exploration tool based on the KEGG database for each group (Figure 5). Half of the KEGG functions were classified into membrane transport, nucleotide metabolism and glycan biosynthesis and metabolism, xenobiotics biodegradation and metabolism, folding, sorting and degradation, etc. We also compared differences in KEGG bacterial function. The digestive system in Group A was significantly different from that in Group B (Figure 6A; $p = 0.037$) and signal transduction was significantly different between Groups A with C (Figure 6B; $p = 0.006$). Moreover, significant differences were found between Groups B with D involving replication and repair ($p = 0.010$), translation ($p = 0.018$), folding, sorting and degradation ($p = 0.019$), nucleotide metabolism ($p = 0.021$), and cell growth and death (Figure 6C; $p = 0.025$). Furthermore, digestive system ($p = 0.008$), signal transduction ($p = 0.018$), immune diseases ($p = 0.013$), environmental adaptation ($p = 0.031$), xenobiotics biodegradation and metabolism ($p = 0.024$) were dramatically different between Groups C and D (Figure 6D).

Analysis of pregnancy outcomes

We next analyzed pregnancy outcomes of the 37 subjects. The 24 women with cervical incompetence received an intervention during pregnancy involving cervical cerclage. The fetal survival rate was 100% for both groups and there was no significant differences in Apgar scores between healthy pregnant women and those with cervical incompetence (Table 1). However, some complications occurred after the intervention. Five cases of premature rupture of the membrane were diagnosed in women with cervical incompetence, representing 21.74%, higher than that of the normal pregnant women (15.38%; Table 1). Notably, the prematurity rate (defined as birth before 37 weeks) in the cervical incompetence group was 8.70%, which was much higher than that in healthy pregnant women, while one case of abortion was recorded at week 18 of pregnancy (Table 1).

We also analyzed the relationships between pregnancy outcomes and marker bacteria of the vagina and cervical canal from pregnant women with cervical incompetence receiving cervical cerclage (Supplementary Table 1). Statistical analysis showed that *Actinomyces neuii* and *Anoxybacillus flavithermus* were positively correlated with the pregnancy outcomes (Apgar score). Conversely, there were significant negative correlations between the Apgar score in the cervical canal and *Bacteroides plebeius*, *Bifidobacterium pseudolongum* and *Staphylococcus petrasii*. *Clostridium fimetarium*, *Methanobacterium congolense*, *Pseudomonas Chlororaphis*, and *Psychrobacter nivimaris* was

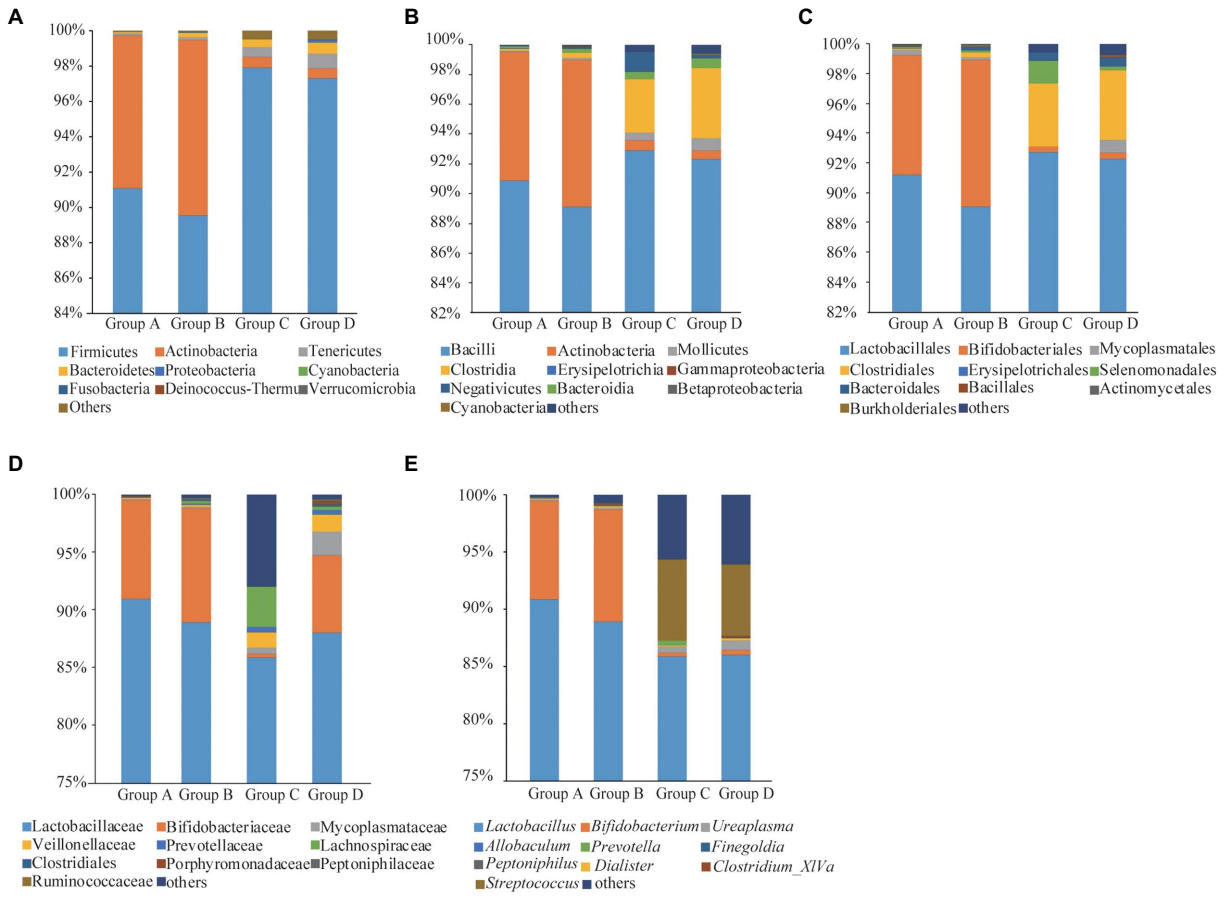

FIGURE 2
Taxonomic analyses for Groups A, B, C, and D at phyla **(A)**, classes **(B)**, orders **(C)**, families **(D)**, and genera **(E)** levels.

negatively correlated with the Apgar score of pregnancy outcomes in the vagina, while *Allobaculum stercoricanis*, *Fusobacterium nucleatum*, *Methylobacterium tardum*, *Nocardioides pacificus* and *Senegalimassilia anaerobia* were positively correlated.

Discussion

The human body contains trillions of bacteria inhabiting body surfaces and cavities which can be exchanged with those in the external environment (Ravel et al., 2011). Recent studies have indicated that the bacteria from vaginal and cervical canal play important roles in maintaining a healthy female reproductive system, and moreover, may be mechanistically linked to the pathogenesis of preterm birth (Ansari et al., 2021; Villani et al., 2022). Different bacterial communities or abnormal levels of bacteria populating the vaginal tract and cervical canal during late pregnancy can produce infections or dysfunction, which can adversely affect pregnancy outcomes (Perino et al., 2011; Ravel et al., 2011; Villani et al., 2022). Here, we compared the vaginal and cervical canal bacterial communities between healthy pregnant women and those with cervical incompetence, a condition which may disrupt the distribution of bacteria in the female reproductive tract. Our analysis results for alpha and beta diversity were similar to that of previous studies (Chen et al., 2017).

The bacteria inhabiting the vagina are considered to originate from the upper genital tract (Khan et al., 2016; Tu et al., 2020). In normal pregnant women, the vaginal and cervical canal bacterial communities were different due to the obstruction of the cervix (Chen et al., 2017). In this study we found the bacterial communities of the cervical canal in pregnant women with cervical incompetence were significantly different from that in the normal pregnant women. However, we found no differences in bacterial composition between the vagina and cervical canal of the pregnant women with cervical incompetence, suggesting cervical incompetence promotes bacterial exchange between the vaginal and cervical canal communities. One of the most important risk factors for preterm birth is cervical incompetence in the second trimester of pregnancy. In support of a prior study (Kindinger et al., 2016), we found associations between vaginal and cervical bacteria diversity with preterm delivery. However, larger sample size is needed if we aim to understand the relationships between the vaginal and cervical bacteria diversity and preterm birth.

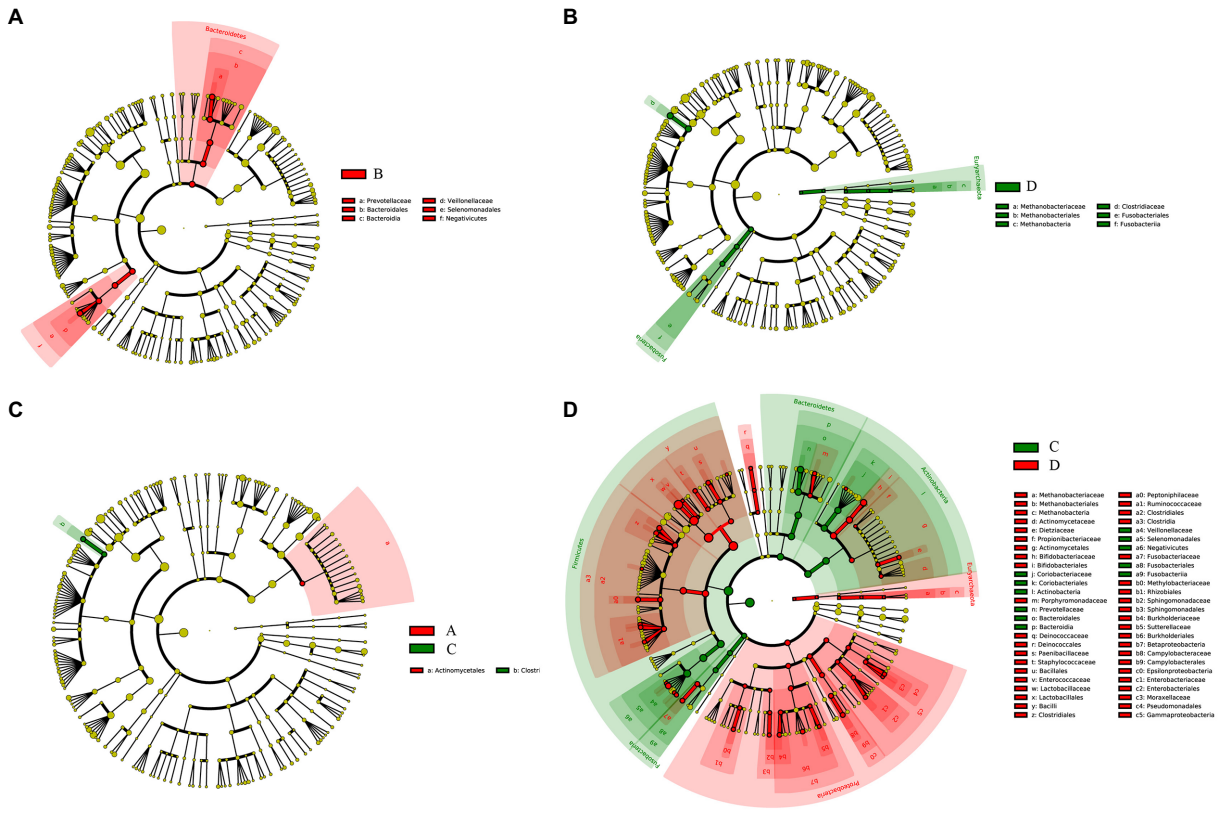

FIGURE 3
Taxa difference analyses between Group A and Group B **(A)**, Group C and Group D **(B)**, Group A and Group C **(C)**, and Group C and Group D **(D)** by LEfSe analysis, respectively.

Lactobacillus are the unequivocal dominant bacteria in the vaginal and cervical canal of healthy women. Their production of lactic acid serves to maintain the acidic pH of the vagina and cervical canal, acting as a barrier against pathogens and protects them from genital infection (Petricevic et al., 2014; Chen et al., 2017; Pace et al., 2021). Deficiencies in *Lactobacillus* could disturb the vaginal bacterial balance, resulting in the syndrome of bacterial vaginosis (Petricevic et al., 2014; Lozano et al., 2021). Nonetheless, *Lactobacillus* was reported to remain as the dominant species in pregnant women with cervical incompetence, and no differences were found in the abundance of OTUs compared to healthy pregnant women (Lozano et al., 2021). The vaginal and cervical canal bacteria are dynamic communities owing to physiological, pathological, environmental, and nutritional factors (D'Alterio et al., 2021). Bacterial dysbiosis may contribute to an inflammatory response in the vagina and cervical canal, also predisposing pregnant woman to a higher risk of infection (D'Alterio et al., 2021). Bacterial imbalance of the vaginal and cervical canal is correlated with higher genital pro-inflammatory cytokine concentrations and increased APC (antigen-presenting cell) activation through LPS pathways. Notably, triggering local immunity to increase the concentration of inflammatory factors including TNF-α, NF-κB and COX-2 may affect pregnancy outcomes (Ravel et al., 2011; Smith and Ravel, 2017; D'Alterio et al., 2021).

Similar to the results of previous studies we found differential genera in pregnant women with cervical incompetence including *Staphylococcus*, *Actinomyces*, *Aerococcus*, *Clostridium_sensu_stricto,* and *Anoxybacillus* (Flynn et al., 2013; Chen et al., 2017; Brown et al., 2019; Lozano et al., 2021). We identified Groups A and C -specific shifts in bacterial composition reflected by the enrichment of five species, including *Staphylococcus petrasii*, *Bacteroides plebeius*, *Bifidobacterium pseudolongum*, *Anoxybacillus flavithermus,* and *Actinomyces neuii*. *Bacteroides plebeius* has been found to be more significantly frequent in HPV-positive women, and *Actinomyces neuii* was reported in bacterial vaginosis (Chao et al., 2019; Castro et al., 2019) while the other species are unique to this study. Furthermore, we found the abundances of *Sutterella stercoricanis*, *Methanobacterium congolense*, *Pseudomonas chlororaphis*, *Psychrobacter nivimaris*, *Nocardioides pacificus*, *Senegalimassilia anaerobia*, *Fusobacterium nucleatum*, *Clostridium fimetarium*, *Methylobacterium tardum* were dramatically different between Groups B and D. Collectively, these results suggest that these species represent "biomarker" bacteria for differences between healthy pregnant women and those with cervical incompetence (Agarwal et al., 2020).

As an important potential anaerobic pathogen and Gram-negative bacterium, *Fusobacterium nucleatum* colonizes the female reproductive tract, digestive tract and oral cavity (Agarwal

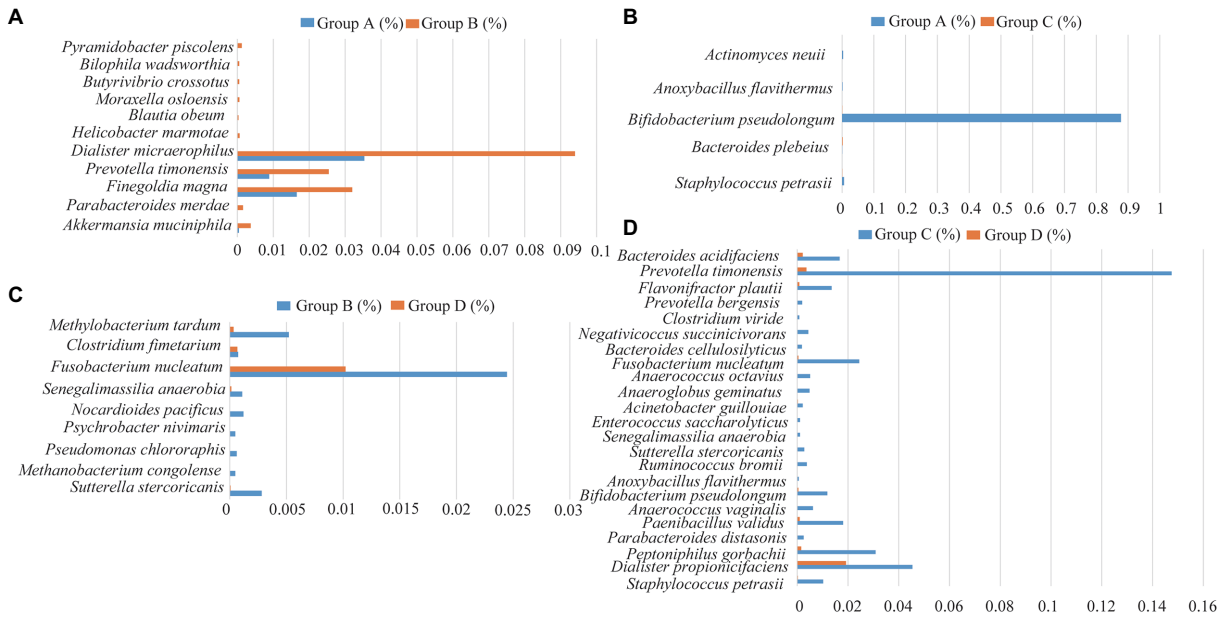

FIGURE 4
Differences in the species of the bacteria between Group A and Group B **(A)**, Group C and Group D **(B)**, Group A and Group C **(C)**, and Group C and Group D **(D)**, respectively.

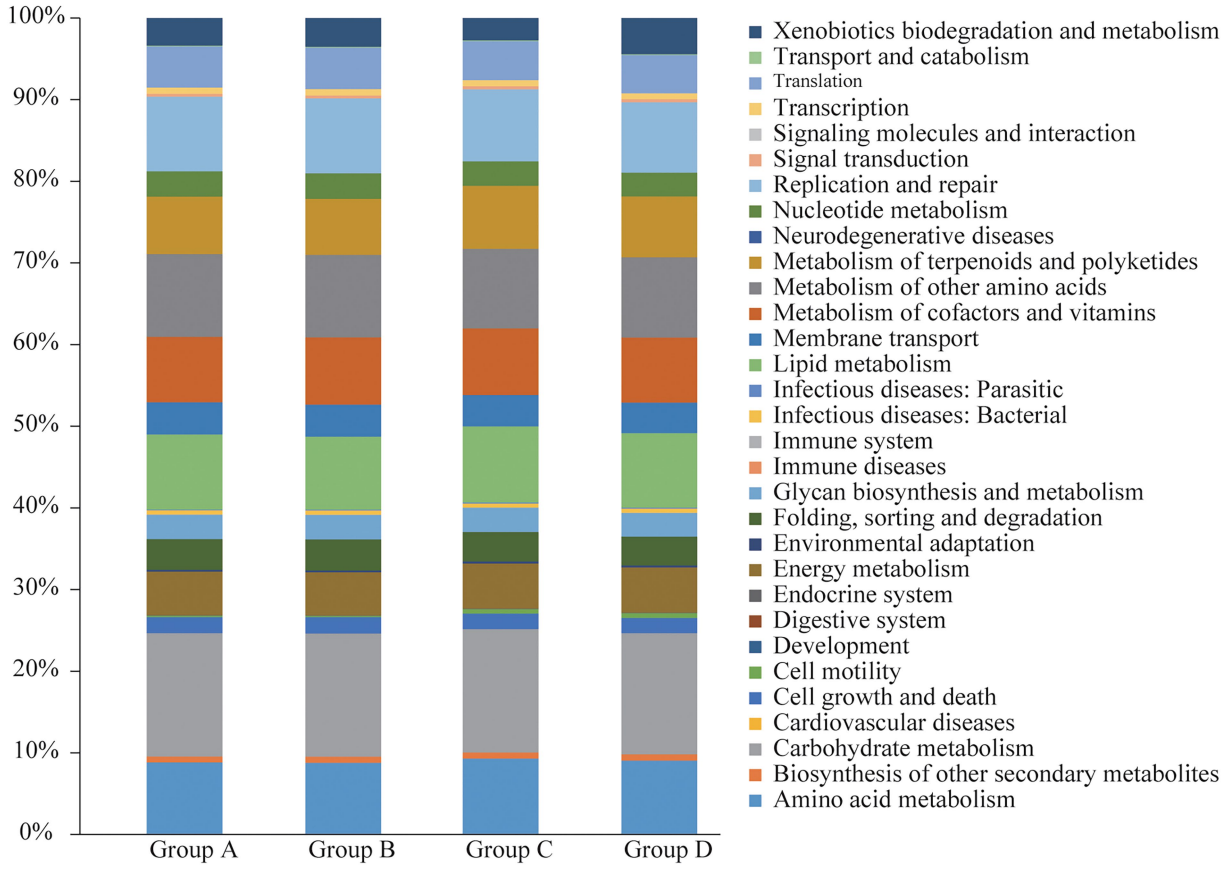

FIGURE 5
Functional analyses of bacterial composition from Groups A, B, C, and D, respectively.

FIGURE 6
Differences of KEGG bacterial functions between Group A and Group B **(A)**, Group C and Group D **(B)**, Group A and Group C **(C)**, and Group C and Group D **(D)**, respectively.

et al., 2020). This species has been associated with numerous human diseases, including oral infections, colorectal cancer, respiratory tract infections, and Alzheimer's disease (Allen-Vercoe et al., 2011; Liu et al., 2014; Han, 2015; Agarwal et al., 2020). *Fusobacterium nucleatum* was also detected in a wide spectrum of fetal membranes, amniotic fluid, neonatal gastric aspirates, chorioamnionitis, and was frequently detected in the cord blood and amniotic fluid of premature infants, being associated with intrauterine infection and preterm birth (Han et al., 2010; Wang et al., 2013; Han, 2015). Additional research also indicated that the mother's subgingival plaque in oral cavity may transfer *Fusobacterium nucleatum* to the placenta or fetus during pregnancy period, leading to acute inflammation, even leading to fetal stillbirth (Han, 2011; Wang et al., 2013). However, further validation is still needed to confirm the utility of the biomarker bacteria identified here and in other studies.

Preterm birth occurs in 5–20% of pregnant women and is defined as delivery before 37 weeks of gestation. Preterm birth is influenced by maternal, fetal and environmental factors, and is associated with a high risk of neonatal morbidity and mortality (Terzic et al., 2021). Some researches have indicated that cervical incompetence is related to preterm birth, although other potential risk factors can influence the incidence of preterm delivery, including diabetes, hypertension, thyroid disease, chronic renal disease and tobacco smoking (Guerra et al., 2006; Goldenberg et al., 2008; Vogel et al., 2018; Miklavcic et al., 2021). In addition, pre-pregnancy body mass index, advanced maternal age (more than 35 years old), endometriosis, polycystic ovary syndrome, and pre-pregnancy diabetes are also considered possible risk factors to preterm birth (Molin, 1993; Vyas et al., 2006; Ciancimino et al., 2014; Miklavcic et al., 2021; Pilarski et al., 2021). Other studies suggest that bacterial vaginal infection and maternal periodontal diseases increase the risk

TABLE 1 Analyses of the pregnancy outcomes from normal pregnant women and pregnant women with cervical incompetence.

Indicator types	Group A/B	Group C/D	*Value of p*
Sex rate	Male = 40%	Male = 41.7%	
	Female = 60%	Female = 58.3%	
Weight (g)	3037.2 ± 812.3	2465.4 ± 764.2	$p < 0.01$
Survival rate	100%	100%	
Premature rupture of membrane rate	21.74%	15.38%	$p < 0.01$
Prematurity rate	8.70%	0	$p < 0.05$
Abortion individuals	1	1	
Apgar score	9.375 ± 1.317	9.556 ± 1.257	

Group A/B and Group C/D are normal pregnant women and pregnant women with cervical incompetence, respectively.

of preterm birth, with bacterial transfer from the vagina to the uterus through the cervix (D'Alterio et al., 2021; Terzic et al., 2021). Pregnant women with intrauterine infection could also spread bacteria to the amniotic cavity to cause preterm birth (Angioni et al., 2015). Some studies reported that periodontal diseases of pregnant women were associated with preterm birth, the proposed reason being gingival bacterium transfer to the uterine cavity and placenta *via* the bloodstream, resulting in an intra-amniotic infection (Offenbacher et al., 2006; Ren and Du, 2017).

In summary, we investigated the bacterial compositions and structures of the vagina and cervical canal from healthy pregnant women and pregnant women with cervical incompetence by high-throughput sequencing technology. The overall bacteria were not significantly different in *Lactobacillus* in the vaginal and cervical canal of healthy pregnant women and pregnant women with cervical incompetence. However, the alpha and beta diversities were significantly different between vaginal samples and cervical canal samples of normal pregnant women. We also found differences in the bacterial communities of cervical canal samples between normal pregnant women and those with cervical incompetence. Several specific bacteria were identified, suggesting that these bacteria may act as potential biomarkers. However, we must also acknowledge certain limitations regarding our study. First, the sample size is relatively small. Second, further investigations are required to elaborate the functional consequences of the "biomarker" bacteria. Third, more experimental technologies are necessary to reveal the correlation between bacteria and clinical features and elucidate the molecular mechanism.

Data availability statement

The datasets presented in this study can be found in online repositories. The names of the repository/repositories and The datasets presented in this study can be found in online repositories. The names of the repository/repositories and accession number(s) can be found in the article/Supplementary material.

Ethics statement

The studies involving human participants were reviewed and approved by Anhui Medical University. Written informed consent for participation was not required for this study in accordance with the national legislation and the institutional requirements.

Author contributions

MS, GL and XL designed the experiments of this manuscript. MS, HG, JF, and GL performed the experiments. MS, NX, YL, and GL analyzed the data. MS, YL, and GL wrote the manuscript. All authors contributed to the article and approved the submitted version.

Funding

This research was supported by the National Natural Science Foundation of China (grant nos. 31702030 and 81772908) and the Natural Science Foundation for the Higher Education Institutions of Anhui Province of China (grant no. KJ2021A0246).

Acknowledgments

The authors thank Zhizhong Gong for data analysis, we also thank. Rick F. Thorne (The University of Newcastle, Newcastle) for polishing our English.

Conflict of interest

The authors declare that the research was conducted in the absence of any commercial or financial relationships that could be construed as a potential conflict of interest.

Publisher's note

Supplementary material

The Supplementary material for this article can be found online at: https://www.frontiersin.org/articles/10.3389/fmicb.2022.986326/full#supplementary-material

References

Aagaard, K., Ma, J., Antony, K. M., Ganu, R., Petrosino, J., and Versalovic, J. (2014). The placenta harbors a unique microbiome. *Sci. Transl. Med.* 6:237ra65. doi: 10.1126/scitranslmed.3008599

Agarwal, K., Robinson, L. S., Aggarwal, S., Foster, L. R., Hernandez-Leyva, A., Lin, H., et al. (2020). Glycan cross-feeding supports mutualism between *Fusobacterium* and the vaginal microbiota. *PLoS Biol.* 18:e3000788. doi: 10.1371/journal.pbio.3000788

Ansari, A., Bose, S., You, Y., Park, S., and Kim, Y. (2021). Molecular mechanism of microbiota metabolites in preterm birth: pathological and therapeutic insights. *Int. J. Mol. Sci.* 22:8145. doi: 10.3390/ijms22158145

Angioni, S., Cela, V., Sedda, F., Stochino Loi, E., Cofelice, V., Pontis, A., et al. (2015). Focusing on surgery results in infertile patients with deep endometriosis. *Gynecol. Endocrinol.* 31, 595–598. doi: 10.3109/09513590.2015.1062868

Altschul, S. F., Madden, T. L., Schäffer, A. A., Zhang, J., Zhang, Z., Miller, W., et al. (1997). Gapped BLAST and PSI-BLAST: a new generation of protein database search programs. *Nucleic Acids Res.* 25, 3389–3402. doi: 10.1093/nar/25.17.3389

Allen-Vercoe, E., Strauss, J., and Chadee, K. (2011). *Fusobacterium nucleatum*: an emerging gut pathogen? *Gut Microbes* 2, 294–298. doi: 10.4161/gmic.2.5.18603

Brown, R. G., Chan, D., Terzidou, V., Lee, Y. S., Smith, A., Marchesi, J. R., et al. (2019). Prospective observational study of vaginal microbiota pre- and post-rescue cervical cerclage. *BJOG* 126, 916–925. doi: 10.1111/1471-0528.15600

Boelig, R. C., Dugoff, L., Roman, A., Berghella, V., and Ludmir, J. (2019). (2019). Predicting asymptomatic cervical dilation in pregnant patients with short mid-trimester cervical length: a secondary analysis of a randomized controlled trial. *Acta Obstet. Gynecol. Scand.* 98, 761–768. doi: 10.1111/aogs.13545

Caporaso, J. G., Kuczynski, J., Stombaugh, J., Bittinger, K., Bushman, F. D., Costello, E. K., et al. (2010). QIIME allows analysis of high-throughput community sequencing data. *Nat. Methods* 7, 335–336. doi: 10.1038/nmeth.f.303

Castro, J., Machado, D., and Cerca, N. (2019). Unveiling the role of gardnerella vaginalis in polymicrobial bacterial vaginosis biofilms: the impact of other vaginal pathogens living as neighbors. *ISME J.* 13, 1306–1317. doi: 10.1038/s41396-018-0337-0

Chao, X. P., Sun, T. T., Wang, S., Fan, Q. B., Shi, H. H., Zhu, L., et al. (2019). Correlation between the diversity of vaginal microbiota and the risk of high-risk human papillomavirus infection. *Int. J. Gynecol. Cancer* 29, 28–34. doi: 10.1136/ijgc-2018-000032

Chen, C., Song, X., Wei, W., Zhong, H., Dai, J., Lan, Z., et al. (2017). The microbiota continuum along the female reproductive tract and its relation to uterine-related diseases. *Nat. Commun.* 8:875. doi: 10.1038/s41467-017-00901-0

Chen, H., and Boutros, P. C. (2011). Venn diagram: a package for the generation of highly-customizable Venn and Euler diagrams in R. *BMC Bioinformatics.* 12:35. doi: 10.1186/1471-2105-12-35

Ciancimino, L., Laganà, A. S., Chiofalo, B., Granese, R., Grasso, R., and Triolo, O. (2014). Would it be too late? A retrospective case-control analysis to evaluate maternal-fetal outcomes in advanced maternal age. *Arch. Gynecol. Obstet.* 290, 1109–1114. doi: 10.1007/s00404-014-3367-5

D'Alterio, M. N., Giuliani, C., Scicchitano, F., Laganà, A. S., Oltolina, N. M., Sorrentino, F., et al. (2021). Possible role of microbiome in the pathogenesis of endometriosis. *Minerva Obstet Gynecol.* 73, 193–214. doi: 10.23736/S2724-606X.21.04788-2

Elovitz, M. A., Gajer, P., Riis, V., Brown, A. G., Humphrys, M. S., Holm, J. B., et al. (2019). Cervicovaginal microbiota and local immune response modulate the risk of spontaneous preterm delivery. *Nat. Commun.* 10:1305. doi: 10.1038/s41467-019-09285-9

Flaviani, F., Hezelgrave, N. L., Kanno, T., Prosdocimi, E. M., Chin-Smith, E., Ridout, A. E., et al. (2021). Cervicovaginal microbiota and metabolome predict preterm birth risk in an ethnically diverse cohort. *JCI Insight.* 6:e149257. doi: 10.1172/jci.insight.149257

Flynn, A. N., Lyndon, C. A., and Church, D. L. (2013). Identification by 16S rRNA gene sequencing of an *Actinomyces hongkongensis* isolate recovered from a patient with pelvic actinomycosis. *J. Clin. Microbiol.* 51, 2721–2723. doi: 10.1128/JCM.00509-13

Goldenberg, R. L., Culhane, J. F., Iams, J. D., and Romero, R. (2008). Epidemiology and causes of preterm birth. *Lancet* 371, 75–84. doi: 10.1016/S0140-6736(08)60074-4

Guerra, B., Ghi, T., Quarta, S., Morselli-Labate, A. M., Lazzarotto, T., Pilu, G., et al. (2006). Pregnancy outcome after early detection of bacterial vaginosis. *Eur. J. Obstet. Gynecol. Reprod. Biol.* 128, 40–45. doi: 10.1016/j.ejogrb.2005.12.024

Han, Y. W. (2015). *Fusobacterium nucleatum*: a commensal-turned pathogen. *Curr. Opin. Microbiol.* 23, 141–147. doi: 10.1016/j.mib.2014.11.013

Han, Y. W., Fardini, Y., Chen, C., Iacampo, K. G., Peraino, V. A., Shamonki, J. M., et al. (2010). Redline RW: term stillbirth caused by oral *Fusobacterium nucleatum*. *Obstet. Gynecol.* 115, 442–445. doi: 10.1097/AOG.0b013e3181cb9955

Han, Y. W. (2011). Can oral bacteria cause pregnancy complications? *Women's Health (Lond. Engl.)* 7, 401–404. doi: 10.2217/whe.11.37

Hao, X., Li, P., Wu, S., and Tan, J. (2021). Association of the cervical microbiota with pregnancy outcome in a subfertile population undergoing in vitro fertilization: a case-control study. *Front. Cell. Infect. Microbiol.* 11:654202. doi: 10.3389/fcimb.2021.654202

Hein, M., Valore, E. V., Helmig, R. B., Uldbjerg, N., and Ganz, T. (2002). Antimicrobial factors in the cervical mucus plug. *Am. J. Obstet. Gynecol.* 187, 137–144. doi: 10.1067/mob.2002.123034

Kervinen, K., Kalliala, I., Glazer-Livson, S., Virtanen, S., Nieminen, P., and Salonen, A. (2019). Vaginal microbiota in pregnancy: role in induction of labor and seeding the neonate's microbiota? *J. Biosci.* 44:116. doi: 10.1007/s12038-019-9925-z

Khan, K. N., Fujishita, A., Masumoto, H., Muto, H., Kitajima, M., Masuzaki, H., et al. (2016). Molecular detection of intrauterine microbial colonization in women with endometriosis. *Eur. J. Obstet. Gynecol. Reprod. Biol.* 199, 69–75. doi: 10.1016/j.ejogrb.2016.01.040

Kindinger, L. M., MacIntyre, D. A., Lee, Y. S., Marchesi, J. R., Smith, A., McDonald, J. A., et al. (2016). Relationship between vaginal microbial dysbiosis, inflammation, and pregnancy outcomes in cervical cerclage. *Sci. Transl. Med.* 8:350ra102. doi: 10.1126/scitranslmed.aag1026

Koedooder, R., Singer, M., Schoenmakers, S., Savelkoul, P. H. M., Morré, S. A., de Jonge, J. D., et al. (2019). The vaginal microbiome as a predictor for outcome of in vitro fertilization with or without intracytoplasmic sperm injection: a prospective study. *Hum. Reprod.* 34, 1042–1054. doi: 10.1093/humrep/dez065

Liu, L., Oza, S., Hogan, D., Perin, J., Rudan, I., Lawn, J. E., et al. (2015). Global, regional, and national causes of child mortality in 2000-13, with projections to inform post-2015 priorities: an updated systematic analysis. *Lancet* 385, 430–440. doi: 10.1016/S0140-6736(14)61698-6

Liu, P., Liu, Y., Wang, J., Guo, Y., Zhang, Y., and Xiao, S. (2014). Detection of *Fusobacterium nucleatum* and fad A adhesin gene in patients with orthodontic gingivitis and non-orthodontic periodontal inflammation. *PLoS One* 9:e85280. doi: 10.1371/journal.pone.0085280

Lozano, F. M., Bernabeu, A., Lledo, B., Morales, R., Diaz, M., Aranda, F. I., et al. (2021). Characterization of the vaginal and endometrial microbiome in patients with chronic endometritis. *Eur. J. Obstet. Gynecol. Reprod. Biol.* 263, 25–32. doi: 10.1016/j.ejogrb.2021.05.045

Lykke, M. R., Becher, N., Haahr, T., Boedtkjer, E., Jensen, J. S., and Uldbjerg, N. (2021). Vaginal, cervical and uterine ph in women with normal and abnormal vaginal microbiota. *Pathogens.* 10:90. doi: 10.3390/pathogens10020090

McDonald, I. A. (1980). Cervical cerclage. *Clin. Obstet. Gynaecol.* 7, 461–479. doi: 10.1016/S0306-3356(21)00250-8

Miklavcic, J., Laganà, A. S., Premru Srsen, T., Korosec, S., and Ban Frangež, H. (2021). Effect of hysteroscopic septum resection on preterm delivery rate in singleton pregnancies. *Minim. Invasive Ther. Allied Technol.* 30, 377–383. doi: 10.1080/13645706.2020.1743721

Molin, A. (1993). Risk of damage to the cervix by dilatation for first-trimester-induced abortion by suction aspiration. *Gynecol. Obstet. Investig.* 35, 152–154. doi: 10.1159/000292688

Moosa, Y., Kwon, D., de Oliveira, T., and Wong, E. B. (2020). Determinants of vaginal microbiota composition. *Front. Cell. Infect. Microbiol.* 10:467. doi: 10.3389/fcimb.2020.00467

Offenbacher, S., Boggess, K. A., Murtha, A. P., Jared, H. L., Lieff, S., McKaig, R. G., et al. (2006). Progressive periodontal disease and risk of very preterm delivery. *Obstet. Gynecol.* 107, 29–36. doi: 10.1097/01.aog.0000190212.87012.96

Pace, R. M., Chu, D. M., Prince, A. L., Ma, J., Seferovic, M. D., and Aagaard, K. M. (2021). Complex species and strain ecology of the vaginal microbiome from pregnancy to postpartum and association with preterm birth. *Med (NY).* 2, 1027–1049.e7. doi: 10.1016/j.medj.2021.06.001

Perino, A., Giovannelli, L., Schillaci, R., Ruvolo, G., Fiorentino, F. P., Alimondi, P., et al. (2011). Human papillomavirus infection in couples undergoing in vitro fertilization procedures: impact on reproductive outcomes. *Fertil. Steril.* 95, 1845–1848. doi: 10.1016/j.fertnstert.2010.11.047

Petricevic, L., Domig, K. J., Nierscher, F. J., Sandhofer, M. J., Fidesser, M., Krondorfer, I., et al. (2014). Characterisation of the vaginal *lactobacillus* microbiota associated with preterm delivery. *Sci. Rep.* 4:5136. doi: 10.1038/srep05136

Pilarski, N., Hodgetts-Morton, V., and Morris, R. K. (2021). Is cerclage safe and effective in preventing preterm birth in women presenting early in pregnancy with cervical dilatation? *BMJ* 375:e067470. doi: 10.1136/bmj-2021-067470

R Core Team (2017). A language and environment for statistical computing. R foundation for statistical computing, Vienna, Austria, https://www.R-project.org.

Ravel, J., Gajer, P., Abdo, Z., Schneider, G. M., Koenig, S. S., McCulle, S. L., et al. (2011). Vaginal microbiome of reproductive-age women. *Proc. Natl. Acad. Sci. U. S A.* 108, 4680–4687. doi: 10.1073/pnas.1002611107

Ren, H., and Du, M. (2017). Role of maternal periodontitis in preterm birth. *Front. Immunol.* 8:139. doi: 10.3389/fimmu.2017.00139

Rognes, T., Flouri, T., Nichols, B., Quince, C., and Mahé, F. (2016). VSEARCH: a versatile open source tool for metagenomics. *Peer J.* 4:e2584. doi: 10.7717/peerj.2584

Rohart, F., Gautier, B., Singh, A., and Lê Cao, K. A. (2017). Mix Omics: An R package for 'omics feature selection and multiple data integration. *PLoS Comput. Biol.* 13:e1005752. doi: 10.1371/journal.pcbi.1005752

Smith, S. B., and Ravel, J. (2017). The vaginal microbiota, host defence and reproductive physiology. *J. Physiol.* 595, 451–463. doi: 10.1113/JP271694

Terzic, M., Aimagambetova, G., Terzic, S., Radunovic, M., Bapayeva, G., and Laganà, A. S. (2021). Periodontal pathogens and preterm birth: current knowledge and further interventions. *Pathogens.* 10:730. doi: 10.3390/pathogens10060730

Torcia, M. G. (2019). Interplay among vaginal microbiome, immune response and sexually transmitted viral infections. *Int. J. Mol. Sci.* 20:266. doi: 10.3390/ijms20020266

Tsonis, O., Gkrozou, F., Harrison, E., Stefanidis, K., Vrachnis, N., and Paschopoulos, M. (2020). Female genital tract microbiota affecting the risk of preterm birth: what do we know so far? A review. *Eur. J. Obstet. Gynecol. Reprod. Biol.* 245:168–173. doi: 10.1016/j.ejogrb.2019.12.005

Tu, Y., Zheng, G., Ding, G., Wu, Y., Xi, J., Ge, Y., et al. (2020). Comparative analysis of lower genital tract microbiome between PCOS and healthy women. *Front. Physiol.* 11:1108. doi: 10.3389/fphys.2020.01108

Villani, A., Fontana, A., Barone, S., de Stefani, S., Primiterra, M., Copetti, M., et al. (2022). Identifying predictive bacterial markers from cervical swab microbiota on pregnancy outcome in woman undergoing assisted reproductive technologies. *J. Clin. Med.* 11:680. doi: 10.3390/jcm11030680

Vogel, J. P., Chawanpaiboon, S., Moller, A. B., Watananirun, K., Bonet, M., and Lumbiganon, P. (2018). The global epidemiology of preterm birth. *Best Pract. Res. Clin. Obstet. Gynaecol.* 52, 3–12. doi: 10.1016/j.bpobgyn.2018.04.003

Vyas, N. A., Vink, J. S., Ghidini, A., Pezzullo, J. C., Korker, V., Landy, H. J., et al. (2006). Risk factors for cervical insufficiency after term delivery. *Am. J. Obstet. Gynecol.* 195, 787–791. doi: 10.1016/j.ajog.2006.06.069

Wang, X., Buhimschi, C. S., Temoin, S., Bhandari, V., Han, Y. W., and Buhimschi, I. A. (2013). Comparative microbial analysis of paired amniotic fluid and cord blood from pregnancies complicated by preterm birth and early-onset neonatal sepsis. *PLoS One* 8:e56131. doi: 10.1371/journal.pone.0056131

Watts, D. H., Fazzari, M., Minkoff, H., Hillier, S. L., Sha, B., Glesby, M., et al. (2005). Effects of bacterial vaginosis and other genital infections on the natural history of human papillomavirus infection in HIV-1-infected and high-risk HIV-1-uninfected women. *J. Infect. Dis.* 191, 1129–1139. doi: 10.1086/427777

Younge, N., Yang, Q., and Seed, P. C. (2017). Enteral high fat-polyunsaturated fatty acid blend alters the pathogen composition of the intestinal microbiome in premature infants with an enterostomy. *J. Pediatr.* 181, 93–101. doi: 10.1016/j.jpeds.2016.10.053

frontiers | Frontiers in Microbiology

TYPE Opinion
PUBLISHED 20 October 2022
DOI 10.3389/fmicb.2022.1031683

OPEN ACCESS

EDITED BY
Axel Cloeckaert,
Institut National de Recherche pour L'Agriculture, L'Alimentation et L'Environnement (INRAE), France

REVIEWED BY
Joel E. Lopez-Meza,
Michoacana University of San Nicolás de Hidalgo, Mexico

*CORRESPONDENCE
Daniela Fusco
fusco@bnitm.de

†These authors share last authorship

SPECIALTY SECTION
This article was submitted to Infectious Agents and Disease, a section of the journal Frontiers in Microbiology

RECEIVED 30 August 2022
ACCEPTED 20 September 2022
PUBLISHED 20 October 2022

CITATION
Fusco D, Martínez-Pérez GZ, Remkes A, De Pascali AM, Ortalli M, Varani S and Scagliarini A (2022) A sex and gender perspective for neglected zoonotic diseases.
Front. Microbiol. 13:1031683.
doi: 10.3389/fmicb.2022.1031683

A sex and gender perspective for neglected zoonotic diseases

Daniela Fusco[1,2]*, Guillermo Z. Martínez-Pérez[3], Aaron Remkes[1,2], Alessandra Mistral De Pascali[4], Margherita Ortalli[4], Stefania Varani[4,5†] and Alessandra Scagliarini[4†]

[1]Department of Infectious Diseases Epidemiology, Bernhard Nocht Institute for Tropical Medicine, Hamburg, Germany, [2]German Center for Infection Research (DZIF), Hamburg, Germany, [3]African Women's Research Observatory (AfWORO), Barcelona, Spain, [4]Section of Microbiology, Department of Experimental, Diagnostic and Specialty Medicine, Alma Mater Studiorum University of Bologna, Bologna, Italy, [5]Microbiology Unit, IRCCS Azienda Ospedaliero-Universitaria di Bologna, Bologna, Italy

KEYWORDS

neglected zoonotic diseases, gender, sex, schistosomiasis, leishmaniasis, monkeypox

Introduction

Individuals are affected differently by infectious diseases depending on their sex and gender identity, as well as the gender- and sex-specific values and norms held by society and healthcare providers (Ingersoll, 2017; Scully, 2022).

Among all the infectious diseases, neglected tropical diseases (NTDs) is a group of diseases of poverty, prevalent in tropical areas but not limited to them (Hotez, 2021; Molyneux et al., 2021). The acronym NTD suggests that these are diseases of populations living in the tropics, leading to a scarcity of data, treatment and diagnostic solutions. However, NTDs are also present among the socioeconomically-disadvantaged populations living in non-tropical regions, such as Europe and North America (Hotez and Gurwith, 2011). Most NTDs are zoonoses, i.e., infections transmitted from animals to humans and vice versa, which contributes to the complex epidemiology of these diseases.

Zoonotic NTDs are defined as neglected zoonotic diseases (NZDs) (King, 2011). The impact of sex and gender in populations affected by NZDs has been scarcely explored, but is imperative for their effective control, as NZDs can in most instances be prevented and controlled by public health interventions (King, 2011). A stronger emphasis on the integration of sex and gender perspectives in NZD research could help stakeholders and policy makers to conceptualize transformative solutions for most burdened populations.

The term sex refers to biological differences between males, females, and intersex persons. Sex-specific anatomical-physiological and hormonal differences influence the course of infectious diseases (World Health Organization, 2007). Studies have highlighted that hormonal and chromosomal factors contribute to sex-specific differences in host responses to some infections. For example, the ability of a parasite to affect female or male individuals differently may be due to the regulation of the immune response by sex hormones (Nava-Castro et al., 2012).

On the other hand, the term gender refers to the norms, values, functions, responsibilities or expectations that society imposes on people according to their assigned sex at birth (Connell, 2021). As gender affects individuals' cosmovision of

health and disease, NZD research needs to take gender into account since it impacts demand, access and utilization of NZD prevention and control. In addition, a One Health perspective should be adopted as NZDs occur at human/animal/environment interfaces with different gender-related exposure risks.

This opinion paper argues that considering sex- and gender-based differences and commonalities is crucial in the prevention and control of NZDs. Mainstreaming sex and gendered perspectives can guide research, clinical management and public health strategies that pursue the achievement of the Sustainable Development Goal 3: Good Health and Wellbeing for all, regardless of peoples' sex and gender (Manandhar et al., 2018).

In this paper, we will examine schistosomiasis, leishmaniasis and monkeypox as case studies where a sex- and gender-transformative approach could reduce the burden of these diseases.

Sex and gender barriers in the control of schistosomiasis

Human schistosomiasis is a parasitic disease with a zoonotic intermediate host, the freshwater snail, and is mainly caused by the species *Schistosoma mansoni* and *S. haematobium*, which infect humans through contact with contaminated water (McManus et al., 2018). The most typical chronic manifestations of schistosomiasis are hepatic fibrosis and urogenital schistosomiasis (McManus et al., 2018).

From a sex perspective, schistosomiasis infections cause a stronger pro-inflammatory response in men (Klein, 2004; Schneider-Crease et al., 2021). From a gender perspective, research suggests that men may be at a higher risk of contracting schistosomiasis due to their more frequent engagement, in comparison to women, in occupations that involve contact with contaminated waters (Ayabina et al., 2021). However, the occupational risk also exists for women living in high-burdened schistosomiasis environments, as they come into contact with water for household-related activities and fishing practices not often associated to women (Standley et al., 2011; Munisi et al., 2016; Sevilimedu et al., 2017; Pouramin et al., 2020; Ayabina et al., 2021).

Genital schistosomiasis is a chronic manifestation of the disease that affects all sexes (Christinet et al., 2016). Chronic infections with *S. haematobium* can lead to genital lesions, damage of reproductive organs and infertility (Kayuni et al., 2019). While sex-disaggregated data exists describing the burden of disease, the imbalanced number of studies on Male Genital Schistosomiasis (MGS), compared to those on Female Genital Schistosomiasis (FGS) makes it difficult to estimate whether more males than females are affected by the disease (Kayuni et al., 2019; Bustinduy et al., 2022). Task forces have been established to study and implement health programs aimed at managing FGS while MGS has received little attention (Bustinduy et al., 2022; Schistosomiasis. COR-NTD. 2022, 2022).

However, certain societal considerations of infertility as a community and family problem have a more detrimental effect on women than on men (Allotey and Gyapong, 2005; Downs et al., 2011; Hotez and Whitham, 2014; Corno et al., 2020; Engels et al., 2020). In addition, the widespread belief in sub-Saharan regions that FGS is sexually transmitted is a major barrier to seeking treatment (Downs et al., 2011; Corno et al., 2020; Engels et al., 2020). Public perceptions of FGS can affect a woman's position in the family and community, leading to her exclusion from traditional social circles and, in the worst cases, gender-based violence (Allotey and Gyapong, 2005; Corno et al., 2020; Engels et al., 2020). On the other hand, haematuria, a sign of urogenital schistosomiasis, is often perceived as a sign of puberty and virility in boys (Vlassoff and Bonilla, 1994; Kukula et al., 2019; Ayabina et al., 2021).

Sex and gender perspectives in human leishmaniasis

Human leishmaniasis is a sandfly-borne disease caused by different protozoan species of the genus *Leishmania* (World Health Organization, 2010). Leishmaniasis occurs in two principal clinical forms: visceral leishmaniasis (VL) and cutaneous leishmaniasis (CL). There is evidence that both VL and CL are more prevalent in males than in females (World Health Organization, 2010).

The role of sex hormones in influencing the infection level and disease severity has been extensively demonstrated in animal studies, and there exists some evidence for this in humans as well (de Araújo Albuquerque et al., 2021).

From a gender perspective, no gender-related differences in the prevalence of asymptomatic *Leishmania* infection could be described in southern Europe (Ibarra-Meneses et al., 2019; Ortalli et al., 2020). In contrast, studies in sub-Saharan Africa suggest that leishmaniasis may exert a higher burden in men (World Health Organization, 2010). Some researchers have considered that, due to their frequent engagement in outdoor activities, men may be considered at higher risk of exposure to infected insects and thus at higher risk of developing leishmaniasis than women (World Health Organization, 2010). In societies where gendered values put more pressure on women than on men to meet certain beauty standards, CL imposes a greater disease burden on women. CL is a disfiguring disease that often leaves scars on visible body parts (Bilgic-Temel et al., 2019). In countries such as Pakistan or Afghanistan, it has been reported that facial lesions can lead to self-isolation, and to exclusion of women from all aspects of life (Bennis et al., 2018).

The existence of disaggregated data does not provide accurate information on the sex distribution of the disease. In

many endemic areas, access to health care services for women is poor, leading to possible underreporting of leishmaniases cases among females (World Health Organization, 2010). Unsurprisingly, a recent meta-analysis showed that two-thirds of the participants enrolled in clinical trials on VL conducted in the past 40 years were adult males (Dahal et al., 2021).

The changing exposure pattern of monkeypox from a gender perspective

Monkeypox is caused by the *Monkeypox virus* (MPXV) an epitheliotropic orthopoxvirus, endemic in western and central Africa (Essbauer et al., 2009; Tack and Reynolds, 2011). The disease has recently attracted worldwide attention as a growing number of cases is being reported in Europe and North America (The Lancet Infectious Diseases, 2022).

The sex and gender dimensions of this infection are poorly explored. There is a dearth of studies with meaningful data for developing sex- and gender-transformative strategies, guidelines or recommendations for the prevention and control of the spread of MPXV. As an example, from a gender perspective, a study conducted in the Democratic Republic of Congo reported that men appear to be most often affected due to the higher risk of exposure to animals associated with the occupational practices they most engage in (hunting, skinning, and trading), while women are mainly exposed due to domestic duties such as contact with contaminated meat or MPXV-infected family members (Whitehouse et al., 2021). Further studies following Whitehouse et al. (2021), are warranted in different geographies to avoid making unfounded generalizations about the reduced or increased risk of MPXV acquisition.

The 2022 monkeypox outbreak in non-endemic countries is showing novel epidemiological features compared to endemic areas. A recent series of cases suggested that the outbreak was disproportionally affecting white gay and bisexual men in the Northern Hemisphere (Thornhill et al., 2022). As a result of these first publications mass media and public health institutions amplified the notion that MPXV may be acquired through sexual networks (Simões and Bhagani, 2022). On July 2022, the World Health Organization (WHO) declared the global monkeypox outbreak a public health emergency of international concern, and called for prevention strategies amongst gay and bisexual men (Taylor, 2022). The initial reactions by the media and WHO, among other stakeholders, have been received with criticism. The scientific community is wary of these proposed strategies and is conceptualizing alternatives to raise public awareness about monkeypox (Kupferschmidt, 2022). Learning from the experiences of the HIV/AIDS pandemic, gender-blind communication strategies could fuel stigma against LGBTQIA+ communities and create a false risk perception among other non-LGBTQIA+ groups (UNAIDS, 2022).

Discussion

Gender and sex are two different but interweaved entities that need to be considered in every health context, as they clearly affect the potential for infection and the course and severity of infectious diseases (Gay et al., 2021). Evidence-based data is urgently needed to apply a gender- and sex-transformative approach to NZDs prevention and control. However, there is paucity of data on infections causing NZDs, which tend to affect the most vulnerable populations.

This opinion paper focuses on three NZDs, namely schistosomiasis, leishmaniasis and monkeypox, to highlight their relevance in applying a sex and gender perspective to their prevention and control.

Schistosomiasis is a clear example of the existence of sex and gender differences in the manifestation, perception and management of the disease. An example of this is the occupational risk of contracting schistosomiasis, which is generally treated as a men's issue, whereas if a gender perspective was applied, one could assume that women and men are proportionally exposed because of their occupations. On the other hand, genital schistosomiasis is mostly researched as a female disease, although it also affects males.

Studies on leishmaniasis show that from both a sex and gender perspective, males seem more affected than females. Nevertheless, most of the sex data are based on studies enrolling for the most part males (Dahal et al., 2021). Additionally, when addressing the risk of leishmaniasis in the Northern Hemisphere (Ibarra-Meneses et al., 2019; Ortalli et al., 2020) it appears that gender does not play a decisive role in influencing the rate of infection, which could be explained by the different social norms across countries.

In the case of both schistosomiasis and leishmaniasis, it is noteworthy that despite the reported higher risk in men, these diseases place a heavier societal burden on women. The extent of this burden has not been precisely quantified yet. Hence, greater attention from donors and stakeholders in health research should be given to women and gendered minorities in their efforts to addressing the impact of these NZDs.

Monkeypox is an NZD largely ignored in the past (Alakunle and Okeke, 2022). The recent outbreak in non-endemic countries has brought unprecedent attention to the disease. In non-endemic countries, the higher infection rate observed at the start of the global outbreak within the gay and bisexual men, led to the recommendation to implement prevention and screening strategies targeting these specific "communities." However, MPXV is a zoonosis. Hence, the role of animals and the possibility that MPXV might be affecting individuals

regardless of their sexual orientation, should not be overlooked (Haider et al., 2022).

By examining these three NZDs, we identified theoretical and methodological gaps in addressing sex and gender differences. There is a need to apply a holistic methodology combining sex- and gender-oriented approaches with a One Health approach to gain proper insights and tackle NZDs at their sources. Research tools capable of capturing gender-based nuances need to be developed and made available. Medical education should adapt programmes and courses that put these diseases into a gender perspective. Adopting the idea of gender-specific solutions for the management of NZDs may promote a more equitable, safe and effective health care for all. A gender-oriented mindset needs to be also mainstreamed into decision-making to encourage respect and consideration of the diversity of sex and gender identities without promoting stigma (Lancet, 2019).

In conclusion, a sex and gender lens in NZD research can help to understand whether and under what circumstances individuals of any sex or gender identity suffer a greater share of the NZD burden, due to a range of bio-anatomical factors that may act in conjunction with the disproportionate poverty, illiteracy, violence, food insecurity and higher risk of animal-borne pathogen transmission, which affect middle-low-income countries as well as socially-disadvantaged groups in high-income countries. Ultimately, it can maximize the impact of public health interventions and strategies aimed at eliminating some of these diseases by 2030.

Author contributions

DF, SV, and AS contributed to the conceptualization of the manuscript. DF and GZM-P contributed to framing the structure of the manuscript. DF and AR were responsible of the schistosomiasis contribution. SV and MO were responsible of the leishmaniasis contribution. AS and AMDP were responsible of the monkeypox contribution. All authors revised and approved the manuscript before submission.

Funding

This work was partly funded by the German Center for Infection Research (DZIF) through the projects NAMASTE (project number: 8008803819) and VAMS (project number: TI 07.003).

Conflict of interest

The authors declare that the research was conducted in the absence of any commercial or financial relationships that could be construed as a potential conflict of interest.

Publisher's note

All claims expressed in this article are solely those of the authors and do not necessarily represent those of their affiliated organizations, or those of the publisher, the editors and the reviewers. Any product that may be evaluated in this article, or claim that may be made by its manufacturer, is not guaranteed or endorsed by the publisher.

References

Alakunle, E. F., and Okeke, M. I. (2022). Monkeypox virus: a neglected zoonotic pathogen spreads globally. *Nat. Rev. Microbiol.* 20, 507–508. doi: 10.1038/s41579-022-00776-z

Allotey, P., and Gyapong, M. (2005). *The Gender Agenda in the Control of Tropical Diseases : A Review of Current Evidence*. World Health Organization.

Ayabina, D. V., Clark, J., Bayley, H., Lamberton, P. H. L., Toor, J., Hollingsworth, T. D., et al. (2021). Gender-related differences in prevalence, intensity and associated risk factors of Schistosoma infections in Africa: A systematic review and meta-analysis. *PLoS Negl. Trop. Dis.* 15:e0009083. doi: 10.1371/journal.pntd.0009083

Bennis, I., De Brouwere, V., Belrhiti, Z., Sahibi, H., and Boelaert, M. (2018). Psychosocial burden of localised cutaneous Leishmaniasis: a scoping review. *BMC Public Health* 18:358. doi: 10.1186/s12889-018-5260-9

Bilgic-Temel, A., Murrell, D. F., and Uzun, S. (2019). Cutaneous leishmaniasis: A neglected disfiguring disease for women. *Int. J. Womens Dermatol.* 5, 158–165. doi: 10.1016/j.ijwd.2019.01.002

Bustinduy, A. L., Randriansolo, B., Sturt, A. S., Kayuni, S. A., Leutscher, P. D. C., Webster, B. L., et al. (2022). "Chapter One - An update on female and male genital schistosomiasis and a call to integrate efforts to escalate diagnosis, treatment and awareness in endemic and non-endemic settings: The time is now," in: *Advances in Parasitology*, eds D. Rollinson and R. Stothard (Academic Press). doi: 10.1016/bs.apar.2021.12.003

Christinet, V., Lazdins-Helds, J. K., Stothard, J. R., and Reinhard-Rupp, J. (2016). Female genital schistosomiasis (FGS): from case reports to a call for concerted action against this neglected gynaecological disease. *Int. J. Parasitol.* 46, 395–404. doi: 10.1016/j.ijpara.2016.02.006

Connell, R. (2021). *Gender: In World Perspective. 4th Ed.* Hoboken, NJ: Wiley.

Corno, L., Hildebrandt, N., and Voena, A. (2020). Age of marriage, weather shocks, and the direction of marriage payments. *Econometrica* 88, 879–915. doi: 10.3982/ECTA15505

Dahal, P., Singh-Phulgenda, S., Olliaro, P. L., and Guerin, P. J. (2021). Gender disparity in cases enrolled in clinical trials of visceral leishmaniasis: A systematic review and meta-analysis. *PLoS Negl. Trop. Dis.* 15:e0009204. doi: 10.1371/journal.pntd.0009204

de Araújo Albuquerque, L. P., da Silva, A. M., de Araújo Batista, F. M., de Souza Sene, I., Costa, D. L., Costa, C. H. N., et al. (2021). Influence of sex hormones on the immune response to leishmaniasis. *Parasite Immunol.* 43:e12874. doi: 10.1111/pim.12874

Downs, J. A., Mguta, C., Kaatano, G. M., Mitchell, K. B., Bang, H., Simplice, H., et al. (2011). Urogenital Schistosomiasis in women of reproductive age in Tanzania's Lake Victoria region. *Am. J. Trop. Med. Hyg.* 84, 364–369. doi: 10.4269/ajtmh.2011.10-0585

Engels, D., Hotez, P. J., Ducker, C., Gyapong, M., Bustinduy, A. L., Secor, W. E., et al. (2020). Integration of prevention and control measures for female genital schistosomiasis, HIV and cervical cancer. *Bull. World Health Organ.* 98:615. doi: 10.2471/BLT.20.252270

Essbauer, S., Pfeffer, M., and Meyer, H. (2009). Zoonotic poxviruses. *Vet. Microbiol.* 140, 229–236. doi: 10.1016/j.vetmic.2009.08.026

Gay, L., Melenotte, C., Lakbar, I., Mezouar, S., Devaux, C., Raoult, D., et al. (2021). Sexual dimorphism and gender in infectious diseases. *Front. Immunol.* 12:698121. doi: 10.3389/fimmu.2021.698121

Haider, N., Guitian, J., Simons, D., Asogun, D., Ansumana, R., Honeyborne, I., et al. (2022). Increased outbreaks of monkeypox highlight gaps in actual disease burden in Sub-Saharan Africa and in animal reservoirs. *Int. J. Infect. Dis.* 122, 107–111. doi: 10.1016/j.ijid.2022.05.058

Hotez, P., and Whitham, M. (2014). Helminth infections: A new global women's health Agenda. *Obstet. Gynecol.* 123, 155–160. doi: 10.1097/AOG.0000000000000025

Hotez, P. J. (2021). *Forgotten People, Forgotten Diseases: The Neglected Tropical Diseases and Their Impact on Global Health and Development*. *John Wiley & Sons*. doi: 10.1002/9781683673903

Hotez, P. J., and Gurwith, M. (2011). Europe's neglected infections of poverty. *Int. J. Infect. Dis. IJID Off. Publ. Int. Soc. Infect. Dis.* 15, e611–e619. doi: 10.1016/j.ijid.2011.05.006

Ibarra-Meneses, A. V., Carrillo, E., Nieto, J., Sánchez, C., Ortega, S., Estirado, A., et al. (2019). Prevalence of asymptomatic Leishmania infection and associated risk factors, after an outbreak in the south-western Madrid region, Spain, 2015. *Euro. Surveill.* (2019) 24:22. doi: 10.2807/1560-7917.ES.2019.24.22.1800379

Ingersoll, M. A. (2017). Sex differences shape the response to infectious diseases. *PLoS Pathog.* 13, e1006688. doi: 10.1371/journal.ppat.1006688

Kayuni, S., Lampiao, F., Makaula, P., Juziwelo, L., Lacourse, E. J., Reinhard-Rupp, J., et al. (2019). A systematic review with epidemiological update of male genital schistosomiasis (MGS): A call for integrated case management across the health system in sub-Saharan Africa. *Parasite Epidemiol. Control.* 4:e00077. doi: 10.1016/j.parepi.2018.e00077

King, L. (2011). *Neglected Zoonotic Diseases. The Causes and Impacts of Neglected Tropical and Zoonotic Diseases: Opportunities for Integrated Intervention Strategies*. National Academies Press (US). Available online at: https://www.ncbi.nlm.nih.gov/books/NBK62511/ (accessed September 23, 2022).

Klein, S. L. (2004). Hormonal and immunological mechanisms mediating sex differences in parasite infection. *Parasite Immunol.* 26, 247–264. doi: 10.1111/j.0141-9838.2004.00710.x

Kukula, V. A., MacPherson, E. E., Tsey, I. H., Stothard, J. R., Theobald, S., Gyapong, M. A., et al. (2019). major hurdle in the elimination of urogenital schistosomiasis revealed: Identifying key gaps in knowledge and understanding of female genital schistosomiasis within communities and local health workers. Hsieh MH, editor. *PLoS Negl. Trop. Dis.* 13:e0007207. doi: 10.1371/journal.pntd.0007207

Kupferschmidt, K. (2022). Why monkeypox is mostly hitting men who have sex with men. *Science* 376, 1364–1365. doi: 10.1126/science.add5966

Lancet, T. (2019). Feminism is for everybody. *Lancet* 393:493. doi: 10.1016/S0140-6736(19)30239-9

Manandhar, M., Hawkes, S., Buse, K., Nosrati, E., and Magar, V. (2018). Gender, health and the 2030 agenda for sustainable development. *Bull. World Health Organ.* 96, 644–653. doi: 10.2471/BLT.18.211607

McManus, D. P., Dunne, D. W., Sacko, M., Utzinger, J., Vennervald, B. J., Zhou, X. N., et al. (2018). Schistosomiasis. *Nat. Rev. Dis. Primer* 4:13. doi: 10.1038/s41572-018-0013-8

Molyneux, D. H., Asamoa-Bah, A., Fenwick, A., Savioli, L., and Hotez, P. (2021). The history of the neglected tropical disease movement. *Trans. R. Soc. Trop. Med. Hyg.* 115, 169–175. doi: 10.1093/trstmh/trab015

Munisi, D. Z., Buza, J., Mpolya, E. A., and Kinung'hi, S. M. (2016). Intestinal Schistosomiasis among primary schoolchildren in two on-shore communities in Rorya District, Northwestern Tanzania: Prevalence, intensity of infection and associated risk factors. *J. Parasitol. Res.* 2016, 1–11. doi: 10.1155/2016/1859737

Nava-Castro, K., Hernández-Bello, R., Muñiz-Hernández, S., Camacho-Arroyo, I., and Morales-Montor, J. (2012). Sex steroids, immune system, and parasitic infections: facts and hypotheses. *Ann. N. Y. Acad. Sci.* 1262, 16–26. doi: 10.1111/j.1749-6632.2012.06632.x

Ortalli, M., De Pascali, A. M., Longo, S., Pascarelli, N., Porcellini, A., Ruggeri, D., et al. (2020). Asymptomatic Leishmania infantum infection in blood donors living in an endemic area, northeastern Italy. *J. Infect.* 80, 116–120. doi: 10.1016/j.jinf.2019.09.019

Pouramin, P., Nagabhatla, N., and Miletto, M. A. (2020). systematic review of water and gender interlinkages: assessing the intersection with health. *Front. Water*. 2:e00006. doi: 10.3389/frwa.2020.00006

Schistosomiasis. COR-NTD. 2022. (2022). *COR-NTD*. Available online at: https://www.cor-ntd.org/schistosomiasis (accessed 23 September, 2022).

Schneider-Crease, I. A., Blackwell, A. D., Kraft, T. S., Emery Thompson, M., Maldonado Suarez, I., Cummings, D. K., et al. (2021). Helminth infection is associated with dampened cytokine responses to viral and bacterial stimulations in Tsimane forager-horticulturalists. *Evol. Med. Public Health* 9, 349–359. doi: 10.1093/emph/eoab035

Scully, E. P. (2022). Sex, gender and infectious disease. *Nat. Microbiol.* 7, 359–360. doi: 10.1038/s41564-022-01064-5

Sevilimedu, V., Pressley, K. D., Snook, K. R., Hogges, J. V., Politis, M. D., Sexton, J. K., et al. (2017). Gender-based differences in water, sanitation and hygiene-related diarrheal disease and helminthic infections: a systematic review and meta-analysis. *Trans. R. Soc. Trop. Med. Hyg.* 2017:trw080v1. doi: 10.1093/trstmh/trw080

Simões, P., and Bhagani, S. A. (2022). viewpoint: The 2022 monkeypox outbreak. *J. Virus Erad.* 8:100078. doi: 10.1016/j.jve.2022.100078

Standley, C. J., Adriko, M., Besigye, F., Kabatereine, N. B., and Stothard, R. J. (2011). Confirmed local endemicity and putative high transmission of Schistosoma mansoni in the Sesse Islands, Lake Victoria, Uganda. *Parasit Vect.* 4:29. doi: 10.1186/1756-3305-4-29

Tack, D. M., and Reynolds, M. G. (2011). Zoonotic poxviruses associated with companion animals. *Animals* 1, 377–395. doi: 10.3390/ani1040377

Taylor, L. (2022). Monkeypox: WHO declares a public health emergency of international concern. *BMJ* 2022:o1874. doi: 10.1136/bmj.o1874

The Lancet Infectious Diseases (2022). Monkeypox: a neglected old foe. *Lancet Infect. Dis.* 22:913. doi: 10.1016/S1473-3099(22)00377-2

Thornhill, J. P., Barkati, S., Walmsley, S., Rockstroh, J., Antinori, A., Harrison, L. B., et al. (2022). Monkeypox virus infection in humans across 16 countries — April–June 2022. *N. Engl. J. Med.* 2022:NEJMoa2207323. doi: 10.1056/NEJMoa2207323

UNAIDS (2022). *UNAIDS Warns That Stigmatizing Language on Monkeypox Jeopardises Public Health*. Available online at: https://www.unaids.org/en/resources/presscentre/pressreleaseandstatementarchive/2022/may/20220522_PR_Monkeypox (accessed September 23, 2022).

Vlassoff, C., and Bonilla, E. (1994). Gender-related differences in the impact of tropical diseases on women: what do we know? *J. Biosoc. Sci.* 26, 37–53. doi: 10.1017/S0021932000021040

Whitehouse, E. R., Bonwitt, J., Hughes, C. M., Lushima, R. S., Likafi, T., Nguete, B., et al. (2021). Clinical and epidemiological findings from enhanced monkeypox surveillance in Tshuapa Province, Democratic Republic of the Congo during 2011–2015. *J. Infect. Dis.* 223, 1870–1878. doi: 10.1093/infdis/jiab133

World Health Organization (2007). *Addressing Sex and Gender in Epidemic-Prone Infectious Diseases*. Geneva: World Health Organization.

World Health Organization (2010). *Report of a Meeting of the WHO Expert Committee on the Control of Leishmaniases, WHO Tech Rep Ser. 2010:949*. World Health Organization. Available online at: https://apps.who.int/iris/bitstream/handle/10665/44412/WHO_TRS_949_eng.pdf?sequence=1&isAllowed=y (accessed September 23, 2022).

frontiers | Frontiers in Microbiology

TYPE Original Research
PUBLISHED 28 October 2022
DOI 10.3389/fmicb.2022.1022704

OPEN ACCESS

EDITED BY
Beatrice Vitali,
University of Bologna, Italy

REVIEWED BY
Tania Lupoli,
New York University, United States
Innokentii Vishnyakov,
Institute of Cytology (RAS), Russia
Rozhina Elvira,
Kazan Federal University, Russia

*CORRESPONDENCE
Sabrina Curreli
scurreli@ihv.umaryland.edu
Davide Zella
dzella@ihv.umaryland.edu

SPECIALTY SECTION
This article was submitted to Infectious Agents and Disease, a section of the journal Frontiers in Microbiology

RECEIVED 18 August 2022
ACCEPTED 03 October 2022
PUBLISHED 28 October 2022

CITATION
Curreli S, Benedetti F, Yuan W, Munawwar A, Cocchi F, Gallo RC, Sherman NE and Zella D (2022) Characterization of the interactome profiling of *Mycoplasma fermentans* DnaK in cancer cells reveals interference with key cellular pathways.
Front. Microbiol. 13:1022704.
doi: 10.3389/fmicb.2022.1022704

Characterization of the interactome profiling of *Mycoplasma fermentans* DnaK in cancer cells reveals interference with key cellular pathways

Sabrina Curreli[1,2]*, Francesca Benedetti[1,3], Weirong Yuan[1], Arshi Munawwar[1], Fiorenza Cocchi[1,2], Robert C. Gallo[1,2], Nicholas E. Sherman[4] and Davide Zella[1,3]*

[1]Institute of Human Virology, University of Maryland School of Medicine, Baltimore, MD, United States, [2]Department of Medicine, University of Maryland School of Medicine, Baltimore, MD, United States, [3]Department of Biochemistry and Molecular Biology, University of Maryland School of Medicine, Baltimore, MD, United States, [4]Biomolecular Analysis Facility Core, School of Medicine, University of Virginia, Charlottesville, VA, United States

Chaperone proteins are redundant in nature and, to achieve their function, they bind a large repertoire of client proteins. DnaK is a bacterial chaperone protein that recognizes misfolded and aggregated proteins and drives their folding and intracellular trafficking. Some Mycoplasmas are associated with cancers, and we demonstrated that infection with a strain of *Mycoplasma fermentans* isolated in our lab promoted lymphoma in a mouse model. Its DnaK is expressed intracellularly in infected cells, it interacts with key proteins to hamper essential pathways related to DNA repair and p53 functions and uninfected cells can take-up extracellular DnaK. We profile here for the first time the eukaryotic proteins interacting with DnaK transiently expressed in five cancer cell lines. A total of 520 eukaryotic proteins were isolated by immunoprecipitation and identified by Liquid Chromatography Mass Spectrometry (LC-MS) analysis. Among the cellular DnaK-binding partners, 49 were shared between the five analyzed cell lines, corroborating the specificity of the interaction of DnaK with these proteins. Enrichment analysis revealed multiple RNA biological processes, DNA repair, chromatin remodeling, DNA conformational changes, protein-DNA complex subunit organization, telomere organization and cell cycle as the most significant ontology terms. This is the first study to show that a bacterial chaperone protein interacts with key eukaryotic components thus suggesting DnaK could become a perturbing hub for the functions of

important cellular pathways. Given the close interactions between bacteria and host cells in the local microenvironment, these results provide a foundation for future mechanistic studies on how bacteria interfere with essential cellular processes.

KEYWORDS

Mycoplasma fermentans, chaperone protein, DnaK protein, proteomics, cellular pathways

Introduction

DnaK is a conserved heat shock protein expressed in prokaryotic cells. Chaperone proteins are abundant and redundant in nature as they play fundamental functions for the maintenance of the cellular integrity. Indeed, they recognize and assist the folding of newly synthesized proteins, both preventing their aggregation and helping protein trafficking among different cellular compartments (Kim et al., 2013). Structurally DnaK (as well as the correspondent human counterpart family of heat shock proteins HSP70) is composed of two domains: a nucleotide binding domain (NBD) that binds adenosine-tri-phosphate (ATP) and a substrate binding domain (SBD), connected by a flexible linker (Genevaux et al., 2007). By an ATP-regulated process (ATPase activity) mediated by the NBD, the SBD binds a large repertoire of protein clients and confers chaperone function (Calloni et al., 2012) thus allowing the DnaK protein to recognize hydrophobic amino acid residues exposed by unfolded proteins and promote the *de novo* protein folding (Rüdiger et al., 1997). The binding of DnaK to client protein is transient and is driven by two classes of co-chaperones: DnaJ and the nucleotide exchange factor (NEF) (Bracher and Verghese, 2015). DnaJ stimulates the ATPase activity of DnaK, while NEFs promote the exchange of DnaK-bound ADP with ATP. Bacteria, mitochondria and chloroplasts have only one type of NEF called GrpE. In contrast, a large diversity of HSP70 NEFs has been discovered in the eukaryotic cells (Bracher and Verghese, 2015). Although a functioning chaperone complex requires the co-chaperones, DnaK can bind client proteins with an affinity regulated by ATP (Mayer and Gierasch, 2019). Indeed, chaperone proteins have the common ability to bind numerous client proteins (Rüdiger et al., 1997; Van Durme et al., 2009; Mayer and Gierasch, 2019; Ryu et al., 2020). To this regard the proteome of DnaK was previously solved in *Escherichia coli* cells and 700 interacting bacterial proteins were identified (Calloni et al., 2012). It was demonstrated that *E. coli* DnaK enriched proteins included a wide range of proteins with dominant functions associated to bacterial DNA replication, recombination, repair, cell division and chromosome segregation (Calloni et al., 2012).

Though most *Mycoplasma* are extracellular, some are able to invade eukaryotic cells (Yavlovich et al., 2004; Curreli et al., 2021) and several groups (Lo et al., 1993; Baseman et al., 1995; Yavlovich et al., 2004; Hegde et al., 2014), including ours (Curreli et al., 2021), have shown that they can grow intracellularly, indicating that the host invasion contributes to *Mycoplasmas* persistence and pathogenesis. To this regard, *Mycoplasmas* have been associated with some human cancers (Huang et al., 2001), including prostate cancer (Barykova et al., 2011), oral cell carcinoma (Henrich et al., 2014) and non-Hodgkin's lymphoma (NHL) in HIV-seropositive subjects (Ainsworth et al., 2001). Moreover, chromosomal alterations and phenotypic changes have previously been observed *in vitro* in mouse and human cells infected with *Mycoplasma fermentans* subtype *incognitus*, and these aberrations did eventually result in the acquisition of malignant properties, including loss of anchorage dependency, ability to form colonies in soft agar, and tumorigenicity in nude mice (Zhang et al., 2006; Jiang et al., 2008; Namiki et al., 2009). In addition, infections with several *Mycoplasmas* (*fermentans*, *arginini*, *hominis,* and *arthritidis*) inhibit p53 activity and cooperate with Ras in oncogenic transformation, though the responsible bacterial protein has not been identified (Logunov et al., 2008). These findings indicate that, in some cases, *Mycoplasmas* could facilitate tumorigenesis, though no direct carcinogenic role for any *Mycoplasmas* has been demonstrated *in vivo*. Moreover, we have previously shown by phylogenetic amino acid analysis that some other bacteria associated with human cancers (including certain *Mycoplasmas*, *H. pylori* and *F. nucleatum*) have highly related DnaKs, suggesting a possible common mechanism of cellular transformation (Zella et al., 2018). This suggests that *Mycoplasmas*, and perhaps certain other bacteria with closely related DnaK, may have oncogenic activity mediated by common mechanism(s) DnaK-related.

We previously demonstrated that infection with a *M. fermentans* strain isolated in our laboratory from cells from an HIV-seropositive patients promoted lymphoma in a mouse model and that its DnaK interacts with key cellular proteins, including USP10 and PARP1, to hamper essential pathways related to DNA repair and p53 functions (Zella et al., 2018; Benedetti et al., 2020a). We also analyzed Mycoplasma-infected cells showing that DnaK mRNA and DnaK protein are both mainly found in the cytosol (Curreli et al., 2021) and that, similar to eukaryotic HSP70 (Becker et al., 2002;

Abbreviations: PARP1, Poly (ADP-Ribose) Polymerase-1; USP10, Ubiquitin carboxyl-terminal hydrolase 10; LS-MC, Liquid Chromatography Mass Spectrometry.

Theriault et al., 2006), DnaK can be taken up by bystander cells (Zella et al., 2018). It is unclear how the uptake or the release of DnaK inside the cell can affect host functions, though it is clear that identifying the key cellular targets of this bacterial chaperone protein can provide useful information on mechanisms of cellular transformation and possibly uncover alterations of other important cellular pathways.

Here we describe our results based on a proteomics approach aimed at characterizing eukaryotic client proteins by using label-free quantitative proteomics. We identified eukaryotic proteins that bind Mycoplasma DnaK from five different human tumor cell lines, representative of different cancer types. It is worth noting that Mycoplasmas are found in the tumor microenvironment of four tissues, namely gastric, colon adenocarcinoma, lung and prostate cancer (Benedetti et al., 2020b). Furthermore, we selected the fifth cancer line, a neuroblastoma cell line, due to the increasingly important association between gut and brain (Cryan et al., 2019; Muller et al., 2020), and the hypothesis that microbial proteins released by the gut microbiota (which include Mycoplasmas) could influence brain functions and cancers (Mehrian-Shai et al., 2019). We found that Mycoplasma DnaK binds 520 cellular proteins that we characterized based on enrichment and protein-protein interaction analysis. This study is the first to show how a bacteria chaperone protein can affect cellular pathways and it creates a platform for further functional and *in vivo* studies.

Materials and methods

Cell culture, plasmid, and transfection

Gastric adenocarcinoma cells AGS and Prostate adenocarcinoma cells PC3 were growth in F-12K medium (Kaighn's Modification of Ham's F-12 medium). Small cell lung cancer H446 were grown in RPMI-1640 medium. Neuroblastoma SH-SY5Y cells were grown in a 1:1 mixture of Eagle's Minimum Essential medium (EMEM) and F12 medium. Colorectal carcinoma cells HCT116 were grown in McCoy's 5a Medium Modified. All cell lines were purchased from the American Tissue Culture Collection (ATCC, Manassas, VA). The growth media were supplemented with 10% of fetal bovine serum (FBS; Thermo Fisher Scientific, Waltham, MA), 100 U/ml of penicillin, and 100 μg/ml of streptomycin (both from Thermo Fisher Scientific, Waltham, MA). The cells were cultured at 37°C in a humidified atmosphere with 5% CO_2.

The full length DnaK from *M. fermentans* cloned into pcDNA 3.1 Directional/V5-His TOPO vector was previously described (Zella et al., 2018). A pcDNA 3.1/V5-His empty vector was used as a control in the transfection experiments. Transient transfection of the cells was performed with lipofectamine 2000 (Thermo Fisher Scientific, Waltham, MA – #11668) or Fugene HD (Promega, Madison, WI – #E2311), depending on the cell type. Lipofectamine 2000 was used to transfect HCT116 cells. Briefly, three T75 flasks were grown at 80% confluence. Transfection was performed in a mixture containing OptiMEM media (Thermo Fisher Scientific, Waltham, MA, USA), the plasmid DNA containing DnaK-V5-His or without the insert (control) and lipofectamine 2000 and incubated overnight. Two T75 were transfected with DnaK, and 1 T75 was transfected with the control empty vector. Transfected cells were harvested after 48 h. Transfections of AGS, PC3, H446 and SH-SY5Y were performed with Fugene HD. The protocol was similar to the one used for transfection with lipofectamine, with the difference that the mixture containing OptiMEM media (Thermo Fisher Scientific, Waltham, MA), the plasmid DNA containing DnaK-V5-His or without the insert (control) and Fugene HD reagent, were not removed from the cell culture media.

Western blotting

Western blot was performed to verify that the transfection and the immunoprecipitation (IP) were successful and to validate Mass Spectrometry results. When Western blotting was used to verify the effectiveness of the transfection or of the immunoprecipitation, the membranes were probed with a mouse mAb against V5 tag (Thermo Fisher Scientific, Waltham, MA – #R960-25, dilution used 1:1,000) and a mouse mAb against β-actin (Cell Signaling Technology, Danvers, MA – #3700, dilution used 1:1,000). To validate proteins identified by Mass Spectrometry the following antibodies were used in the co-IP experiments: anti-PARP1 (R&D Systems, Minneapolis, MN – #AF-600, concentration used 0.4 μg/ml), anti-KU70 (Cell Signaling Technology, Danvers, MA – #4588, dilution used 1:1,000), anti-KU80 (Cell Signaling Technology, Danvers, MA – #2180, dilution used 1:1,000), anti-LIG3 (Thermo Fisher Scientific, Waltham, MA – #ma1-23191, dilution used 1:500-1:3,000), anti-β-catenin (Cell Signaling Technology, Danvers, MA – #8480, dilution used 1:1,000), anti-SF3B1 (Thermo Fisher Scientific, Waltham, MA – #PA541723, concentration used 1 μg/ml), anti-XRCC1 (Thermo Fisher Scientific, Waltham, MA – #MA1-12640, concentration used 1-2 μg/ml), anti-RPA/p70 (Santa Cruz Biotechnology, Dallas, TX – #SC-28304, dilution used 1:200), anti-DNA-PK (Cell Signaling Technology, Danvers, MA – #12311, dilution used 1:1,000) anti-DHX9 (Abcam, Cambridge, UK – ab26271, concentration used 1 μg/ml), anti-RUVBL2 (Novus Biologicals, Littleton, CO – #NBP2-01764, dilution used 1:500-2,000).

For Western blot analysis, cell monolayers were washed in cold PBS, detached using a scraper, and resuspended in RIPA lysis buffer (Sigma-Aldrich, St. Louis, MO, USA) in the presence of protease inhibitors (Sigma-Aldrich, St. Louis, MO, USA). The protein concentration was measured by the Bradford assay (Bio-Rad, Hercules, CA, USA). Thirty micrograms of protein

were resolved by SDS/PAGE, transferred to a polyvinylidene difluoride (PVDF) membrane using trans-blot turbo transfer system (Bio-Rad), blocked in 5% non-fat dried milk in Tris-Buffered Saline (TBS) and probed overnight with the primary antibody. Blots were incubated with secondary HRP-conjugated antibodies (anti-rabbit IgG, Cell Signaling Technology, Danvers, MA – #7074, dilution used 1:1,000; anti-mouse IgG, Cell Signaling Technology, Danvers, MA – #7076, dilution used 1:1,000), developed using an ECL chemiluminescent substrate kit (Amersham Bioscience, Amersham, United Kingdom), and exposed and acquired using the ChemiDoc MP digital image system (Bio-Rad, Hercules, CA, USA).

Immunoprecipitation

DnaK-V5 transfected cells were harvested at 48 h. After washing the monolayer with cold PBS, cells were detached with a scraper and resuspended in 1 ml of radioimmune precipitation buffer (Cell Signaling Technology, Danvers, MA) containing protease inhibitors (Sigma-Aldrich, St. Louis, MO, USA). Lysates were precleared with 50 μl of Dynabeads magnetic beads for 1 h at 4°C with end-over-end rotation. Non-specifically bound proteins were removed by a magnet. Next, 400 μg of lysate were incubated for 2 h at 4°C with end-over-end rotation with antibody-coated beads by using the IP Dynabeads Protein G Immunoprecipitation Kit (Thermo Fisher Scientific, Waltham, MA – #10007D). Specifically, for each analyzed cell line, four experimental IPs were performed including: a duplicate IP with anti-rabbit V5 Tag antibody (Abcam, Cambridge, United Kingdom – #ab9116, 1.775 mg/ml), one IP with the isotype control rabbit IgG (Abcam, Cambridge, United Kingdom – #ab172730, 1 mg/ml), one IP with anti-rabbit V5 Tag antibody that was pre-incubated with V5 blocking peptide (Sigma-Aldrich, St. Louis, MO – #V7754, 50 μg in the blocking mix). The beads with the bound proteins were collected with a magnet, washed three times with washing buffer and resuspended in precipitation buffer (provided with the kit). Following 10 min incubation at 70°C, the beads were removed from the proteins and resuspended in SDS-PAGE sample buffer. 1/6 of the total immuno-precipitated product was analyzed by SDS-PAGE immunoblot to verify that the IP procedure was successful, while the remaining material was analyzed by Mass Spectrometry.

Liquid chromatography mass spectrometry sample analysis

The gel pieces from the band (2 large slice fractions per sample) were transferred to a siliconized tube and washed in 200 μl 50% methanol. The gel pieces were dehydrated in acetonitrile, rehydrated in 30 μl of 10 mM dithiolthreitol in 0.1 M ammonium bicarbonate and reduced at room temperature for 0.5 h. The DTT solution was removed and the sample alkylated in 30 μl 50 mM iodoacetamide in 0.1 M ammonium bicarbonate at room temperature for 0.5 h. The reagent was removed, and the gel pieces were dehydrated in 100 μl acetonitrile. Next, the acetonitrile was removed, and the gel pieces rehydrated in 100 μl 0.1 M ammonium bicarbonate. The pieces were dehydrated in 100 μl acetonitrile, the acetonitrile was removed, and the pieces completely dried by vacuum centrifugation. The gel pieces were rehydrated in 20 ng/μl trypsin in 50 mM ammonium bicarbonate on ice for 30 min. Any excess enzyme solution was removed and 20 μl 50 mM ammonium bicarbonate added. The sample was digested overnight at 37^{o}C and the peptides formed extracted from the polyacrylamide in a 100 μl aliquot of 50% acetonitrile/5% formic acid. This extract was evaporated to 15 μl for MS analysis. The Liquid chromatography mass spectrometry (LC-MS) system consisted of a Thermo Electron Q Exactive HF mass spectrometer system with an Easy Spray ion source connected to a Thermo 75 μmx 15 cmC18Easy Spray column (through pre-column). 7 μl of the extract was injected and the peptides eluted from the column by an acetonitrile/0.1 M acetic acid gradient at a flow rate of 0.3 μl/min over 2.0 h. The nanospray ion source was operated at 1.9 kV. The digest was analyzed using the rapid switching capability of the instrument acquiring a full scan mass spectrum to determine peptide molecular weights followed by product ion spectra (Top10 HCD) to determine amino acid sequence in sequential scans. This mode of analysis produces approximately 25,000 MS/MS spectra of ions ranging in abundance over several orders of magnitude.

Mass spectrometry data analysis

The data generated from the MS samples were analyzed by database search by using the Sequest search algorithm within Proteome Discoverer 2.4.1 (Thermo Fisher Scientific) against Uniprot Human Proteome database The UniProt Consortium (2017). The Sequest search results were uploaded into the Scaffold 4.11.0 software program (Proteome Software, Inc.) for quantitative data analysis. To ensure the quality of our approach we applied multiple controls and filtering conditions at different stages of the experiments, starting from duplicate experiments performed for each analyzed cell line. The following filters were applied for data analysis: 99% minimum protein ID probability, a minimum number of 2 unique peptides for one protein and a stringent minimum peptide ID probability of 95% (producing a FDR, 1%). The identified protein was removed from the list if detected in the control IPs with the isotype Ig or the anti-V5 Ig performed in the presence of V5 blocking peptide. To be included in the list, both duplicate samples needed to have a spectral count value. Spectral count values of 1 and a mean spectral count less than 5 were removed. Quantification

was label free based upon total spectral counts. Duplicate spectral count list for each identified protein were generated for each cell line. One-way analysis of variance (ANOVA) with Benjamini Ochberg correction (Ferreira and Zwinderman, 2006) was performed with Scaffold software on normalized duplicate spectral counts of proteins differentially expressed between the five cell types, by selecting a p-value of significance $\leq$0.05 and a minimum spectral count value of 3.

Surface plasmon resonance binding analysis of DnaK-DnaK and DnaK-PARP1

Surface plasmon resonance (SPR) binding studies of DnaK-DnaK and DnaK-PARP1 were performed at 25°C on a BIAcore T100 System (BIAcore, Inc., Piscataway, NY). The assay buffer was HBS-EP (10 mM HEPES, 150 mM NaCl, 0.05% surfactant P20, pH 7.4, 3 mM EDTA). DnaK (2274.9 RUs for DnaK-DnaK and 2220 RUs for DnaK-PARP1, respectively) was immobilized on CM5 sensor chips using the amine-coupling chemistry recommended by the manufacturer. Analytes were introduced into the flow cells at 35 μl/min in the running buffer. Association and dissociation were assessed for 120 s and 600 s, respectively for the DnaK-DnaK binding, while 250 s and 600 s, respectively for the DnaK-PARP1 binding analysis. Resonance signals were corrected for non-specific binding by subtracting the background of the control flow-cell. After each analysis, the sensor chip surfaces were regenerated with 10 mM glycine solution (pH 2.0) with MgCl 1M and equilibrated with the buffer before next injection.

Gene enrichment analysis and enrichment clustering

Metascape was used to perform the enrichment analysis and the enrichment clustering (Zhou et al., 2019). The following ontology terms were included in the enrichment analysis: Gene Ontology (GO) Biological Processes (Ashburner et al., 2000), Reactome gene set (Fabregat et al., 2018), Kyoto Encyclopedia of Genes and Genomes (KEGG) Pathway (Kanehisa and Goto, 2000), Canonical pathways (Subramanian et al., 2005), Halmark Gene Set (Liberzon et al., 2015), CORUM (Ruepp et al., 2010) and WikiPathways (Martens et al., 2021). The enrichment analysis applied the hypergeometric statistical tests to identify input proteins that were significantly overexpressed, using a cutoff of 0.01 and an enrichment factor $>$1.5. To account for multiple testing the q-value was calculate by applying the Banjamini-Hochberg procedure (Ferreira and Zwinderman, 2006). The resulting ontology term were hierarchically clustered based on their similarity, by applying a kappa score $>$0.3 (Cohen, 1960). A cluster was represented by the most significant term. An enrichment network was also visualized with Cytoscape (V3.6.1) (Shannon et al., 2003), where each node represents a significant term, and the cluster was represented by terms with the same color. The nodes were linked by an edge based on their similarity score.

Protein-protein interaction network

Metascape was used to assemble protein-protein interaction networks (Zhou et al., 2019). The bioinformatic program used Biogrid database (Oughtred et al., 2021) and applied the MCODE algorithm (Bader and Hogue, 2003) that combines the three most enriched ontology terms. The top 10 most significant MCODES were represented.

Results

Strategy for the identification of proteins binding DnaK transiently expressed in different cancer cell lines

We performed LC-MS analysis from five human cancer cell lines (HCT116, AGS, H446, PC3, SH-SY5Y) transfected with an expression vector transiently expressing *M. fermentans* DnaK-V5. **Supplementary Figure 1** represents the experimental workflow.

We identified 520 proteins across the five cell types (**Figure 1** and **Supplementary Table 1**). The highest number of proteins was found in small cell lung carcinoma (n = 318) and neuroblastoma (n = 292), followed by the colorectal cancer (n = 219), gastric adenocarcinoma cells (n = 141) and finally prostate cancer (n = 137) (**Figure 1A**). A Venn diagram, used to visualize the number of shared and unique proteins obtained from each cell line, indicates that the shared hit in all five analyzed cell lines included 49 proteins (**Figure 1B**). Accordingly, the purple lines from the Circos plot link the proteins that are shared between the five cell lines, therefore showing the overlaps between proteins from different cell lines (**Figure 1C**). The detection of shared hits and overlaps among five different cancer cell types supports the reproducibility of our MS analysis. This finding also suggests that DnaK may have a higher binding affinity for these 49 eukaryotic proteins (listed in **Supplementary Table 2**), given that DnaK could recognize and bind these same 49 proteins from 5 different cell lines. However, due to the different nature of the 49 shared proteins, further studies will be necessary to understand the higher affinity of DnaK for these 49 proteins. On the other hand, we found that unique proteins can bind DnaK in each one of the 5 cell lines, as shown in the Venn diagram (**Figure 1B**) and indicated by the light orange inner arcs in the Circos plot (**Figure 1C**). This lack of concomitant expression could be due to different

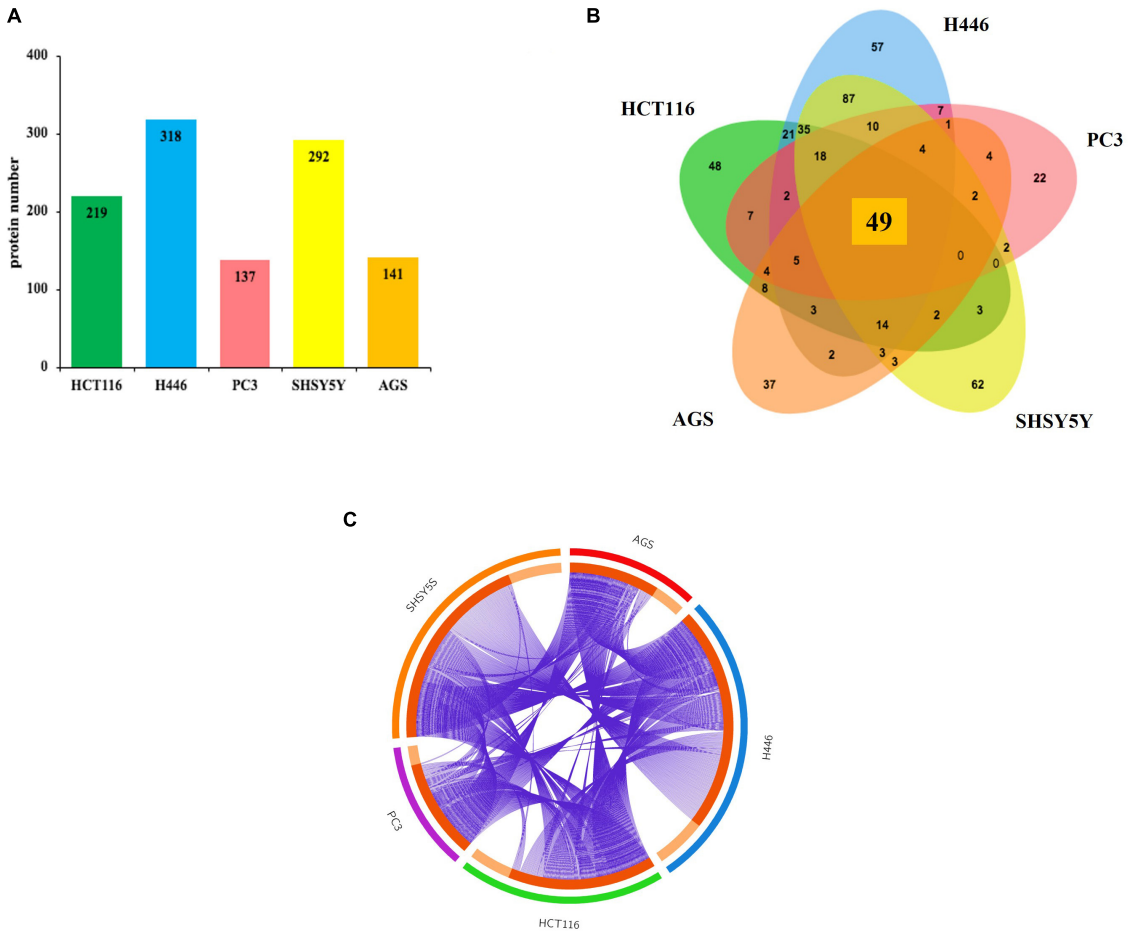

FIGURE 1
Lists the total number of proteins immunoprecipitated by DnaK-V5 and identified by mass spectrometry analysis in each cell type. **(A)** A total of 520 proteins were identified. The histogram indicates the number of hits for each cell type. **(B)** A Venn diagram (http://jvenn.toulouse.inra.fr/app/example.html) visualizes the number of shared and unique proteins obtained from each cell type. Of these, 49 proteins were shared among all five human cell lines analyzed. **(C)** The Circos plot (Krzywinski et al., 2009) shows the overlaps between the proteins from the input lists. On the outside, each arc represents the identity of the five analyzed cell lines (red for AGS, blue for H446, green for HCT116, purple for PC3, and orange for SH-SY5Y); on the inside, each arc represents a protein list, where each protein has a spot on the arc. The dark orange color of the inside arc represents the proteins that appear in multiple cell lines and the light orange color of the inside arc represents proteins that are unique to that cell type list. Purple lines link the proteins that are shared by multiple cell type. The greater the number of purple links and the longer are the inside dark orange arcs. This implies a greater overlap among the proteins from each cell line. A full list of the total 520 isolated proteins is given in **Supplementary Table 1**.

reasons, including tissue specificity, time-expression dependent, lack of sensitivity or differentiation/activation programs specific per each analyzed cell type. However, to simplify our analysis and gain a better understanding of the potential effects of these interactions, we decided to cluster together the proteins of each related pathway.

Bioinformatics analysis for the enriched terms

Enrichment analysis showed that the list of proteins from the five cancer cell lines were overexpressed in 182 GO biological processes terms, 151 Reactome terms, 15 KEGG pathways, 62 CORUM and 7 WikiPathways terms (**Supplementary Tables 1, 2**). The top 20 most significantly enriched terms consisted with pathways related to RNA biological processes (mRNA processing, RNA metabolic process, RNA localization, RNA transport, mRNA translation, ribonucleoprotein complex subunit organization and gene silencing by miRNA, and mRNA splicing), DNA repair, chromatin biology (DNA-protein complexes, chromatin remodeling and chromosome organization) and cell cycle (**Table 1**).

The heatmap of the top 20 enriched terms (**Figure 2A** and **Table 2**) showed that in all the 5 cancer cell lines the ontology terms related to RNA biology were significantly enriched. Small

TABLE 1 Top 20 significant enriched ontology terms in AGS, H446, PC3, HCT116, and SH-SY5Y according to the *p*-value and *q*-value.

GO	Category	Description	Count	%	Log10(P)	Log10(q)
R-HSA-8953854	Reactome Gene Sets	Metabolism of RNA	121	23.27	−83.36	−79
GO:0006402	GO Biological Processes	mRNA catabolic process	87	16.73	−68.75	−64.69
GO:0006412	GO Biological Processes	Translation	77	35.16	−65.12	−61.24
GO:1903311	GO Biological Processes	regulation of mRNA metabolic process	64	12.31	−44.85	−41.91
GO:0022618	GO Biological Processes	ribonucleoprotein complex assembly	57	10.96	−41.89	−39.04
GO:0006338	GO Biological Processes	chromatin remodeling	37	12.67	−36.4	−33.91
GO:0071103	GO Biological Processes	DNA conformation change	54	10.38	−34.64	−32.1
GO:0006281	GO Biological Processes	DNA repair	67	12.88	−33.37	−30.85
CORUM:1332	CORUM	Large Drosha complex	16	5.03	−27.65	−25.49
WP3888	WikiPathways	VEGFA-VEGFR2 Signaling Pathway	52	10	−26.09	−23.67
GO:0006403	GO Biological Processes	RNA localization	40	7.69	−26.01	−23.59
GO:0050684	GO Biological Processes	regulation of mRNA processing	32	6.15	−25.09	−22.68
R-HSA-73894	Reactome Gene Sets	DNA Repair	34	11.64	−22.86	−20.9
GO:0071824	GO Biological Processes	protein-DNA complex subunit organization	39	7.5	−21.95	−19.59
GO:0032200	GO Biological Processes	telomere organization	26	8.18	−20.92	−19
R-HSA-1640170	Reactome Gene Sets	Cell Cycle	57	10.96	−20.45	−18.12
GO:0072331	GO Biological Processes	signal transduction by p53 class mediator	36	6.92	−20.08	−17.76
GO:0051052	GO Biological Processes	regulation of DNA metabolic process	45	8.65	−19.84	−17.52
R-HSA-8878171	Reactome Gene Sets	Transcriptional regulation by RUNX1	34	6.54	−19.59	−17.28
GO:0006302	GO Biological Processes	double-strand break repair	29	9.12	−19.32	−17.46

Count = total number of proteins from the 5 cell lines proteomics list that are included in the corresponding onthology term; % = percentage of proteins from the 5 cell lines proteomics list that are found in the corresponding onthology term; Log10(P) = p-value in Log base 10; Log10(q) = multiple test adjusted p-value in Log base 10 by using the Banjamini-Hochberg procedure.

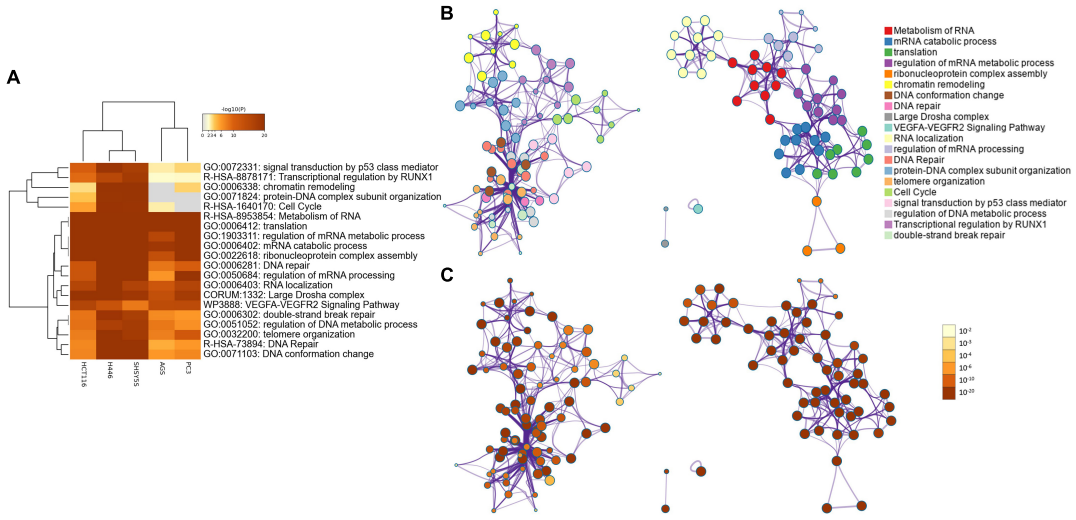

FIGURE 2
(A) Heatmap showing the top 20 enrichment terms across input proteins in the five cell lines, according to the *p*-value. **(B)** Network of enriched ontology clusters colored by cluster ID. A subset of enriched terms was selected based on the best p-values from each of the 20 clusters, and represented as a network plot, visualized by Cytoscape (Shannon et al., 2003). Each node represents an enriched term and is colored by its cluster ID. The 20 cluster IDs are listed on the side. **(C)** Network of enriched ontology clusters colored by *p*-value. The same network shown in **(B)** is represented colored by its p-value. On the side is the *p*-value scale ranging from 10^{-2} to 10^{-20}.

cell lung cancer cells (H446) and neuroblastoma cells (SH-SY5Y) were hierarchically clustered together with a very high significant association for most of the terms. In contrast, the gastric (AGS) and prostate (PC3) adenocarcinoma cell lines clustered together and were not significantly enriched in the GO term of protein-DNA complex subunit organization and

minimally or no significant in the GO term of chromatin remodeling and the Reactome term of cell cycle (**Table 2** and **Figure 2A**).

A network representation of the enriched terms (**Figure 2B**) highlights 2 major subnetworks. One included multiple RNA biological processes while the other subnetwork included chromatin remodeling, DNA conformation change, DNA repair, protein-DNA complex subunit organization, telomere organization, cell cycle, signal transduction by p53, regulation of DNA metabolic process and transcriptional regulation of RUNX1. Two separated terms included the CORUM large Drosha complex and the WikiPathways of VEGFa-VEGFR2 signaling pathway. The networks colored by p-value (**Figure 2C**) highlights how the subnetwork including RNA-related processes was highly significant for all the terms, while the second subnetwork included some terms less significant (e.g., cell cycle and transcriptional regulation by RUNX1).

Protein-protein interaction analysis

To better understand the interplay between the identified proteins, we performed a protein-protein interaction (PPI) network analysis by using Metascape (Zhou et al., 2019). Biologically relevant networks were obtained by applying a Molecular Complex Detection (MCODE) algorithm (Oughtred et al., 2021; **Supplementary Table 3**). Our data show that the most significant interaction networks covered by the proteins binding DnaK include the mRNA splicing network (Log10 *p*-value –88.9), the Nonsense-Mediated Decay (NMD) complex (Log10 *p*-value –68.3) and the DNA repair pathways (Log10 *p*-value –15) (**Figure 3** and **Supplementary Table 3**).

Finally, we confirmed that DnaK forms homodimers, which are believed to represent a more efficient configuration of the protein in its interactions with cellular components. In fact, previous cross-linking experiments demonstrated that DnaK forms a transient dimer upon ATP binding. Biochemical analyses then showed that this dimer is essential for the efficient interaction of the protein with the co-chaperone molecule Hsp40, and in turn allows for efficient DnaK activity (Sarbeng et al., 2015). By using surface plasmon resonance binding analysis we indeed confirmed that DnaK used in our experiments could forms homodimers. Based on our data, kinetic analysis of DnaK-DnaK association yielded a Kd value of $2.956e^{-8}$M (**Figure 4**).

Validation of the mass spectrometry identified proteins implicated in the reactome pathway of DNA repair (R-HSA-73894)

We previously demonstrated the effect of DnaK in decreasing p53 tumor-suppressor activity and its inhibitory effect on PARP1 (Zella et al., 2018). To confirm and expand our

TABLE 2 Top 20 significant clusters of the enriched ontology terms in AGS, H446, PC3, HCT116, and SH-SY5Y according to the *p*-value.

GO	Description	AGS Log10(P)	H446 Log10(P)	HCT116 Log10(P)	PC3 Log10(P)	SH-SY5Y Log10(P)
GO:0072331	signal transduction by p53 class mediator	−2.67	−19.46	−10.47	−3.49	−17.22
R-HSA-8878171	Transcriptional regulation by RUNX1	−2.15	−15.28	−9.14	−2.19	−18.30
GO:0006338	chromatin remodeling	0	−33.60	−3.26	−3.59	−36.40
GO:0071824	protein-DNA complex subunit organization	0	−19.72	−4.10	0	−21.90
R-HSA-1640170	Cell Cycle	−2.60	−19.79	−5.64	0	−19.56
R-HSA-8953854	Metabolism of RNA	−31.07	−73.48	−59.43	−40.64	−64.30
GO:0006412	translation	−20.69	−42.61	−65.12	−23.20	−31.58
GO:0006402	mRNA catabolic process	−19.05	−55.35	−65.18	−25.69	−47.06
GO:1903311	regulation of mRNA metabolic process	−15.37	−37.67	−33.44	−28.60	−34.46
GO:0022618	ribonucleoprotein complex assembly	−13.33	−26.73	−39.63	−23.90	−28.05
GO:0006281	DNA repair	−8.43	−33.06	−12.33	−10.36	−28.74
GO:0050684	regulation of mRNA processing	−6.28	−22.12	−12.48	−20.01	−20.36
GO:0006403	RNA localization	−12.03	−23.19	−15.66	−15.93	−16.29
CORUM:1332	Large Drosha complex	−13.43	−27.65	−20.36	−18.02	−18.84
WP3888	VEGFA-VEGFR2 Signaling Pathway	−14.29	−12.81	−15.99	−14.49	−8.16
GO:0006302	double-strand break repair	−6.98	−19.32	−8.48	−6.10	−17.10
GO:0051052	regulation of DNA metabolic process	−8.23	−16.98	−8.69	−6.59	−18.11
GO:0032200	telomere organization	−7.74	−20.92	−7.88	−11.47	−18.16
R-HSA-73894	DNA Repair	−5.14	−21.64	−7.17	−6.09	−22.86
GO:0071103	DNA conformation change	−6.15	−32.32	−7.38	−7.18	−31.48

Log10(P) = *p*-value in Log base 10.

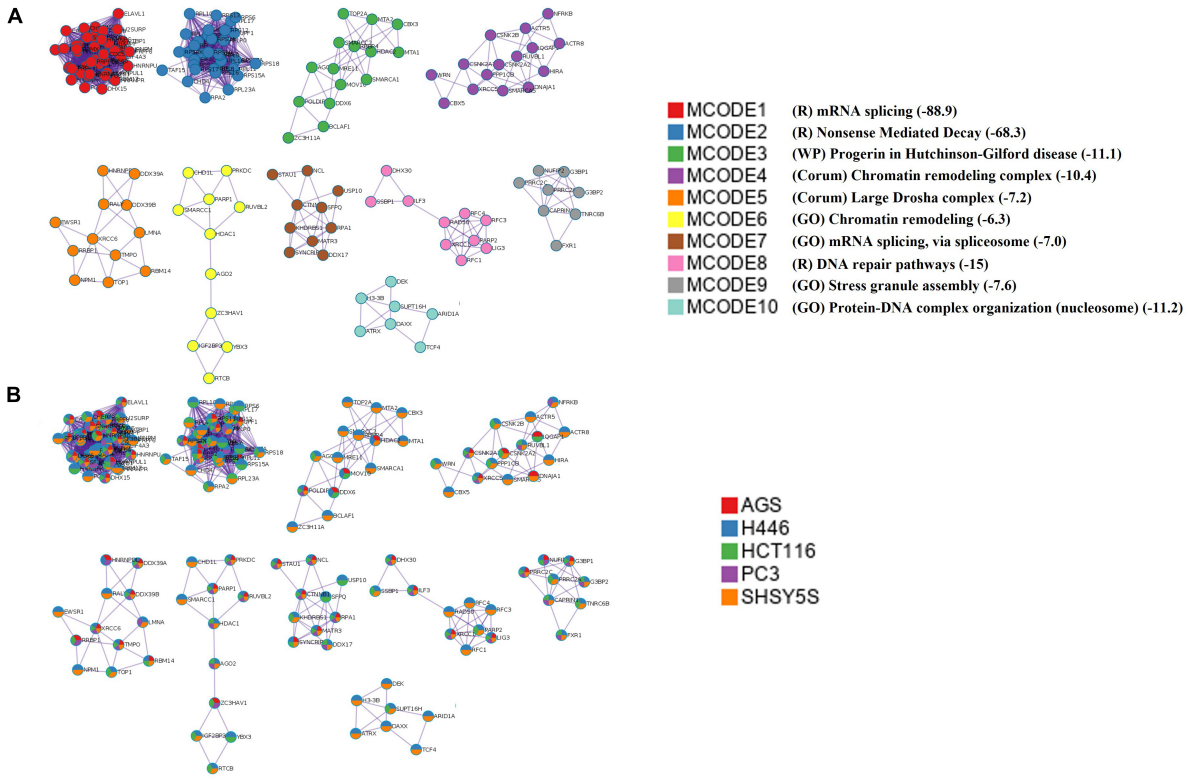

FIGURE 3
Top 10 significant protein-protein interaction networks. **(A)** The top 10 MCODE complexes formed by the 520 proteins from the pulled list of the 5 analyzed cell lines. The PPI included the mRNA splicing pathway (MCODE1 and 7), the nonsense-mediated decay (NMD) (MCODE2), the effect of progerin on the involved genes in Hutchinson-Gilford Progeria Syndrome (MCODE3), the INO80 chromatin remodeling complex (MCODE4), Large Drosha complex (MCODE5), chromatin remodeling complex (MCODE6), DNA repair pathways (MCODE8), stress granule assembly (MCODE9), and protein-DNA complex subunit organization (MCODE10). The mRNA splicing pathway was the most significant. *P*-value in Log 10 are given in parenthesis in the Legend and in **Supplementary Table 3**. In the Legend R = Reactome, WP = WikiPathways, GO = GO term. **(B)** The network nodes are displayed as pie. Color code for pie sector represents a protein list from each of the five analyzed cell lines. The keys codes for the MCODEs shown in this figure are listed in **Supplementary Table 3**, together with their correspondent *p*-value.

findings, we first performed enrichment analysis of both DNA repair pathways from the GO ontology term (GO:0006281) and the reactome (R-HAS-73894). The top 20 significant clusters in all 5 analyzed cell lines are showed in **Table 2**. Next, we sought to explore further the correlation of DnaK with the reactome pathway of the DNA repair (R-HSA-73894). The most abundant proteins were identified from the cell lines of small cell lung carcinoma and neuroblastoma (n = 34 for both cell lines) (**Figure 5A**). The Venn diagram indicates that the shared hits in all five analyzed cell lines included 7 proteins (**Figure 5B**) and the purple lines in the Circos plot visualize the shared hits (**Figure 5C**). Among these proteins (**Figure 5D**), X-Ray Repair Cross Complementing 5 (XRCC5), X-Ray Repair Cross Complementing 6 (XRCC6) and Protein Kinase, DNA-Activated, Catalytic Subunit (PRKDC) are essential components of the DNA double strand repair pathway of Non-Homologous End Joining (NHEJ) (Lieber, 2010). In this contest, the XRCC5-XRCC6 heterodimer plays a central role in binding to the ends of the double strand broken DNA and in recruiting PRKDC (Gottlieb and Jackson, 1993). PRKDC is a Serine/threonine-protein kinase that acts as a sensor of DNA damage and phosphorylates itself and a number of proteins participating in the NHEJ machinery, favoring and promoting the execution of the repair (Drouet et al., 2006).

The remaining shared hits in the 5 cancer cell lines included X-Ray Repair Cross Complementing 1 (XRCC1), PARP1, Replication Protein A1 (RPA1) and DNA ligase 3 (LIG3) (**Figure 5D**). These proteins are known player during multiple DNA repair processes including Base Excision Repair (BER) (Kutuzov et al., 2021), Nucleotide Excision Repair (NER) (Moser et al., 2007, Marteijn et al., 2014) and the double strand repair pathway of Homologous Recombination (HR) (Heyer et al., 2010) Specifically, PARP1 activity is necessary in different steps of the repair process. It is an essential sensor of the DNA damage (Ali et al., 2012) and its catalyzes the addiction of poly(ADP-ribose) (PAR) chains to recruit repair proteins (Jungmichel et al., 2013), including XRCC1 (Masson et al., 1998), in the DNA damage site. XRCC1 acts as a scaffold

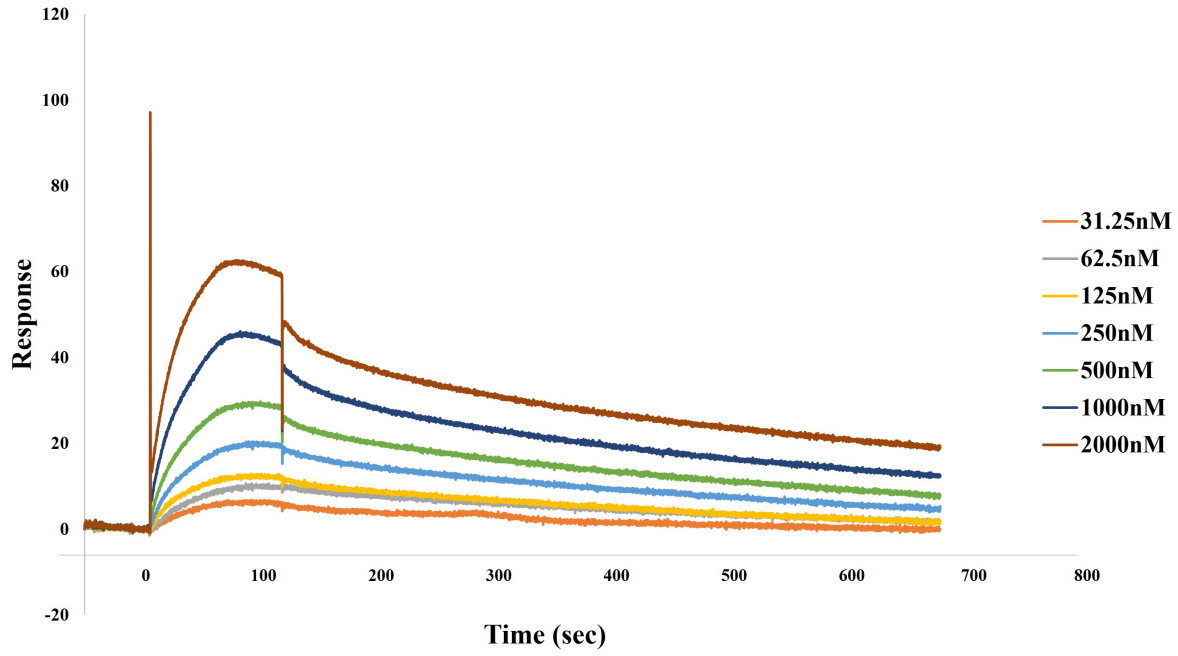

FIGURE 4
Direct binding of DnaK to DnaK (self-binding) as determined by surface plasmon resonance (SPR). Association of DnaK at different concentrations on 2,274.9 response units of DnaK immobilized on a CM5 biosensor chip proceeded at a flow rate of 35 μl/min for 120 s, followed by a 600 s-dissociation in HBS-EP. A preliminary kinetic analysis yielded a Kd value of 2.956e^{-8}M.

protein for the recruitment of factors involved in the repair (Caldecott, 2019), including LIG3 (Nash et al., 1997), that seals the nicked DNA ends (Tomkinson and Sallmyr, 2013). PARP1 has also shown to form a complex with PRKDC and catalyzes its PARylation, that is important for regulating PRKDC activity (Han et al., 2019). Binding of DnaK to these molecular players of the DNA repair pathways may impair the ability of the cell to recognize the damaged DNA and execute the repair, possibly leading to genome instability.

Duplicate spectral counting show that XRCC5, XRCC6 and PARP1 (**Supplementary Figure 2**) where recovered from the IP with high spectral count values (around 200 hits) suggesting they were more abundant in the DnaK's immune-precipitates, while the remaining 4 proteins had less hits. The spectral count of these proteins varied considerably in the five analyzed cell lines and were more abundant in the small cell lung cancer H446 and the neuroblastoma cells SH-SY5Y and constantly reduced in the gastric adenocarcinoma AGS (**Supplementary Figure 2**). Validation analysis was carried out by western blot analysis of DnaK immune-precipitates (**Figure 5E**). The common proteins identified by Mass Spectrometry were detected in all the five cancer cell lines, even if at different levels. Of note, the absence of a band in the IP with the IgG control demonstrates the specificity of the binding (**Figure 5E**). The binding affinity of DnaK to PARP1 was also validated by Surface Plasmon Resonance (SPR) equilibrium analysis, and preliminary kinetic analysis yielded a Kd value of <25 nM (2.501e^{-8}M) (**Supplementary Figure 3**).

Western blot validation of the mass spectrometry identified proteins implicated is the top enriched terms of RNA metabolism, chromatin remodeling and translation

To validate the Mass Spectrometry identified proteins enriched in the top pathways, we performed Western Blot to identify DnaK-bound immunoprecipitated proteins (**Figure 6**). Splicing Factor 3B subunit 1 (SF3B1), a component of the SF3B complex (Cretu et al., 2016) involved in pre-mRNA splicing (**Supplementary Table 4**), was confirmed as a representative factor of the mRNA splicing term (R-HSA-72163). DExH-box helicase 9 (DHX9), a multifunctional nucleic acid helicase (Jain et al., 2010), was validated as a component of various ontology terms including RNA metabolism (R-HSA-8953854), translation (GO:0006412), RNA-mediated gene silencing (CORUM: 1332), as well as DNA repair (R-HSA-73894) (**Supplementary Table 4**). In addition, we validated RuvB-like AAA ATPase-2 (RUVBL2), an enzyme with ATPase and helicase activity (Puri et al., 2007; **Figure 6**). RUVBL2, together with RUVBL1, is a component of various chromatin-remodeling complexes including the

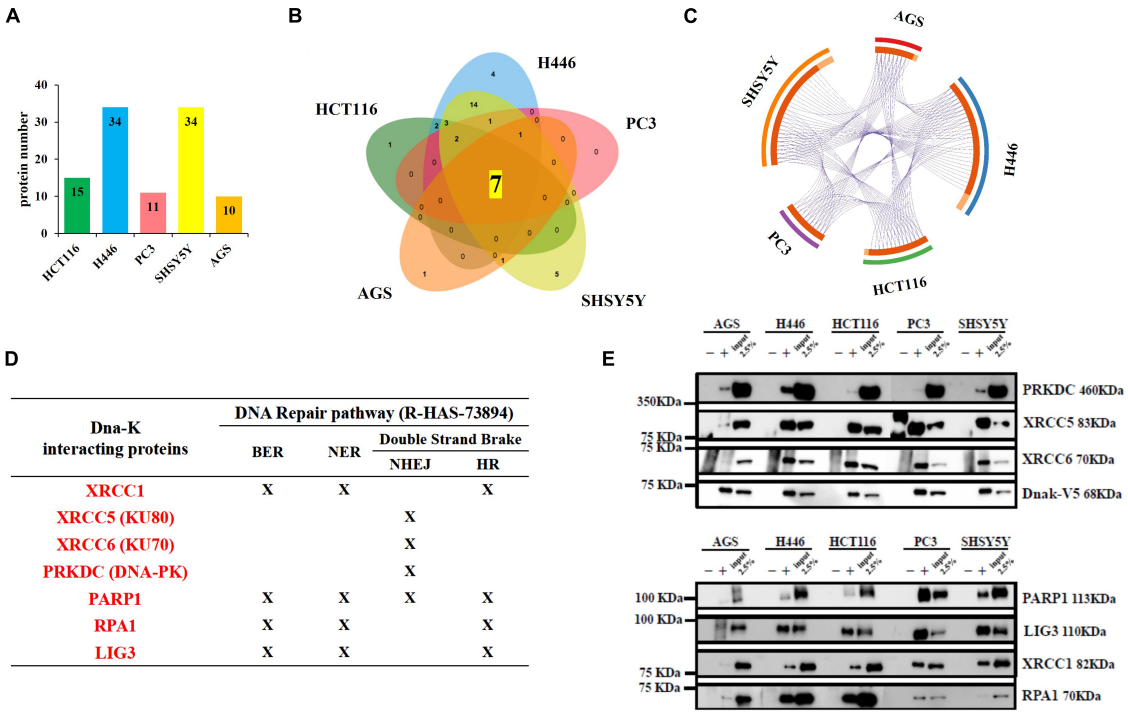

Dna-K interacting proteins	DNA Repair pathway (R-HAS-73894)			
	BER	NER	Double Strand Brake	
			NHEJ	HR
XRCC1	X	X		X
XRCC5 (KU80)			X	
XRCC6 (KU70)			X	
PRKDC (DNA-PK)			X	
PARP1	X	X	X	X
RPA1	X	X		X
LIG3	X	X		X

FIGURE 5
Lists of the total number of proteins immunoprecipitated by DnaK-V5 and identified by mass spectrometry analysis in each cell type that are part of the DNA repair Reactome pathway (R-HSA-73894). **(A)** A total of 34 proteins were identified (see **Supplementary Tables 1, 2**). The histogram indicates the number of hits for each cell type. **(B)** A Venn diagram visualizes the number of shared and unique proteins obtained from each cell type. Of these, 7 proteins were shared among all five human cell lines analyzed. **(C)** The Circos plot shows the overlaps between the proteins from theDNA repair pathway. On the outside, each arc represents the identity of the 5 cell lines (red for AGS, blue for H446, green for HCT116, purple for PC3 and orange for SH-SY5Y); on the inside, each arc represents a protein list, where each protein has a spot on the arc. The dark orange color of the inside arc represents the DNA repair proteins that appear in multiple lists and the light orange color of the inside arc represents DNA repair proteins that are unique to that cell type list. Purple lines link the proteins that are shared by multiple cell types. The greater the number of purple links and the longer are the dark orange arcs. This implies a greater overlap among the protein from each cell line. A full list of the total 34 isolated proteins from the DNA repair Reactome pathway is given in **Supplementary Table 2**. **(D)** Table indicating the membership of the seven proteins in the 4 DNA repair pathways of Base Excision Repair (BER), Nucleotide Excision Repair (NER), Non-Homologous End Joining (NHEJ) and Homologous Recombination (HR). **(E)** Western blot from DnaK immunoprecipitation comparing the five cancer cell lines. On the left side, the Molecular Weight (MW) Marker is indicated. On the right side, the name and MW of each validated protein are given. For each of the 5 cell types, three samples were loaded: the immunoprecipitated DnaK-transfected lysate with the antibody isotype control, the immunoprecipitated DnaK-transfected lysate with anti-V5 antibody and 2.5% load of the DnaK-transfected lysate used for the immunoprecipitations.

Nucleosome Acetyltransferase of Histone 4 (NuA4) histone acetyltransferase complex (Jha et al., 2008). By forming complexes, RUBVL2 regulates the accessibility of the DNA to proteins and therefore plays a critical role in major pathways related to chromatin remodeling, DNA damage response, ribonucleoproteins assembly (GO:0022618), protein-DNA complex subunit organization (GO:0071824) and cell cycle (R-HAS-1640170) (**Supplementary Table 4**; Jha and Dutta, 2009).

Discussion

Some species of Mycoplasmas, including *M. fermentans*, are associated with cancers (Ainsworth et al., 2001; Barykova et al., 2011; Henrich et al., 2014) and we previously demonstrated that Mycoplasma infection promoted lymphoma in a mouse model and its DnaK, a chaperone protein belonging to the HSP70 family, interacts with key cellular proteins to hamper essential pathways related to DNA repair and p53 functions (Zella et al., 2018). Chaperone proteins are fundamental for a correct protein folding, prevent a protein aggregation, and help to remove misfolded and incomplete proteins (Saibil, 2013). Since Mycoplasmas are able to invade eukaryotic cells (Lo et al., 1993; Baseman et al., 1995; Yavlovich et al., 2004; Hegde et al., 2014; Curreli et al., 2021), the release of bacteria components, including DnaK, inside the host cell is likely to contribute to Mycoplasma's pathogenesis and interfere with the maintenance of the normal cell functions. Indeed, we previously demonstrated that upon invasion, DnaK

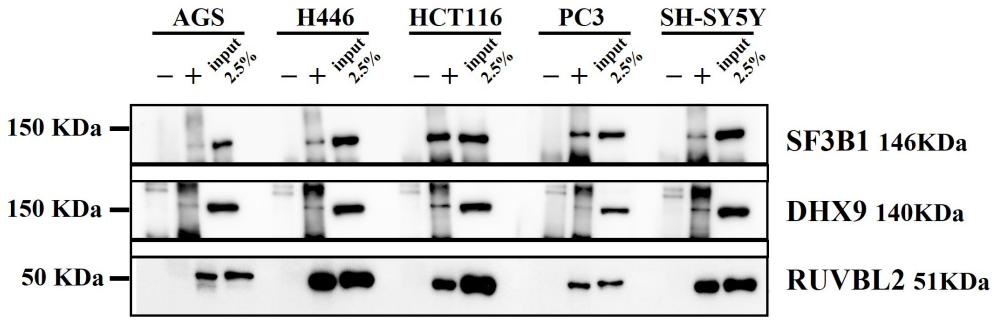

FIGURE 6
Western blot from DnaK immunoprecipitation comparing the five cancer cell lines. On the left side the Molecular Weight (MW) Marker is indicated. On the right side the name and MW of each validated protein are given. For each of the five cell types, three samples were loaded: the immunoprecipitated DnaK-transfected lysate with the antibody isotype control, the immunoprecipitated DnaK-transfected lysate with anti-V5 antibody and 2.5% load of the Dank-transfected lysate used for the immunoprecipitations.

protein is found inside the infected cells (Curreli et al., 2021) and that DnaK is taken up by bystander cells (Zella et al., 2018).

This work stems from our previous efforts in understanding how Mycoplasma DnaK is able to interfere with important cellular pathways. To this regard, we previously demonstrated that DnaK binds to PARP1 and USP10, affecting DNA repair and p53-dependent activities (Zella et al., 2018; Benedetti et al., 2020a). Here we deepen our investigation of DnaK's key cellular targets to gain information about the possible role of DnaK in promoting cellular transformation and altering important cellular functions. For this purpose, we employed a label-free quantitative proteomics approach to identify the eukaryotic proteins binding Mycoplasma's DnaK, upon transient transfection in 5 different human cancer cell lines. We found that DnaK interacts with a total of 520 proteins and their amount number ranges from 137 to 318 depending on the cell line. Our MS analysis showed that the shared hits in all 5 analyzed cell lines included 49 proteins, indicating conserved key target proteins among the analyzed cancer cell lines. On the other hand, the finding of unique proteins binding DnaK in the different cell lines is probably reflective of a cell-specific differentiation program.

The ability to bind a wide array of proteins is a common feature of chaperone proteins (Calloni et al., 2012; Ryu et al., 2020), and 700 interacting proteins were previously isolated from the proteomics analysis of DnaK in *E. coli* (Calloni et al., 2012). Similarly, the proteome of HSP70 and HSC70 (Heat shock cognate 71 kDa protein) was solved in eukaryotic cells and approximately 772 potential interactors were identified (Ryu et al., 2020). Indeed binding of HSP70s to their client proteins have been defined a "selectively promiscuous" process (Mayer and Gierasch, 2019) since chaperones can bind hydrophobic amino acid residues exposed by many unfolded proteins, but not all the proteins in the proteome (Rüdiger et al., 1997). Our current findings that a bacteria chaperone can bind numerous eukaryotic proteins suggest that the previously reported 57% shared sequence similarity (Chiappori et al., 2015) between DnaK and the most common human equivalent HSC70/HSP72 (Kim et al., 2013) might be relevant for the binding. Indeed, members of the HSP70 family of chaperones are involved in some of the most critical functions of the proteostasis network (Mayer and Gierasch, 2019). Our data thus further support the theory that the mechanism of binding proteins by prokaryotic and eukaryotic chaperones has remained evolutionary conserved (Mayer and Gierasch, 2019). To this regard, we are investigating whether the group of identified bacteria-DnaK-interacting human proteins has a significant overlap with the proteins interacting with human HSP70, and the effect of DnaK binding on these client proteins. This could indeed provide with a better understanding of the full scale of potential disruption of cellular pathways that DnaK could promote.

The activity of HSP70/DnaK is regulated by cycles of ATP binding and hydrolysis (Calloni et al., 2012; Nunes et al., 2015), and this in turn allows DnaK interaction with client proteins with an affinity modulated by the ATP itself (Mayer and Gierasch, 2019). However, DnaK has a weak ATPase activity, and like other chaperone proteins, it needs to cooperate with co-chaperones and cellular factors to accelerate ATPase activity and eventually accomplish its proper function (Bracher and Verghese, 2015; Clerico et al., 2015). Since in our experimental system only the bacterial DnaK was expressed, without the respective co-chaperones DnaJ and NEF (Bracher and Verghese, 2015), we evaluated potential partner proteins that could support its functional status. We showed that DnaK binds the protein disulfide isomerase family A member 6 (PDIA6) in all the analyzed cell lines, that is a member of the protein disulfide isomerase (PDI) family (Ellgaard and Ruddock, 2005) with a chaperone activity (Kikuchi et al., 2002). We also found that in the gastric adenocarcinoma cells AGS and neuroblastoma SH-SY5Y cells DnaK binds

DnaJA1, a member of the HSP40 family of molecular co-chaperones (Qiu et al., 2006). DnaJA1 is well known for regulating eukaryotic HSP70 by stimulating ATPase activity thus generating the ADP-bound that interacts stably with the substrates (Qiu et al., 2006). In addition, we showed that DnaK forms homodimers. According to previously published data (Sarbeng et al., 2015), this homodimeric structure is considered more efficient in its ability to control the proper folding of the client proteins. Based on our data, it is thus very likely that Mycoplasma DnaK could indeed exerts its activity inside the eukaryotic host cell by forming homodimers and hijacking cellular co-chaperones like DnaJA1. Further studies are needed to assess the extent and the biological significance of such bindings.

Enrichment analysis revealed a sub-network which comprised ontology terms related to DNA-proteins interactions and included chromatin remodeling, DNA conformation change, DNA repair, protein-DNA complex subunit organization, telomere organization, cell cycle, signal transduction by p53, regulation of DNA metabolic process and transcriptional regulation of RUNX1. All these listed terms are crucial for the maintenance of genomic stability and DNA organization. We choose some of the most important proteins, namely DnaK-binding proteins XRCC5, XRCC6 and PRKDC, known to participate in NHEJ repair process (Lieber, 2010), for by Western blot analysis validation. Similarly, we validated XRCC1, PARP1, RPA1 and LIG3, known molecular participants in the DNA repair processes of BER (Kutuzov et al., 2021), NER (Moser et al., 2007; Marteijn et al., 2014) and HR (Heyer et al., 2010). Binding of DnaK to these regulators of multiple DNA repair pathways may impair the ability of the cell to recognize the damaged DNA and execute the repair, possibly leading to genome instability and predispose the cell to transformation. These data support our previous finding showing that infection of SCID mice with a strain of *M. fermentans* promotes lymphomagenesis, further indicating that interaction of DnaK with proteins involved in DNA repair pathways may have a role in cellular transformation (Zella et al., 2018).

The other major sub-network enriched was comprised of RNA biological processes, including RNA metabolism, mRNA catabolic process, mRNA splicing, nonsense-mediated decay, ranked highest among the ontology terms significant from the list. Those interactions were unexpected since, in contrast to prokaryotes, bacteria do not possess a spliceosome. These findings imply that DnaK could be directly associated with mRNA splicing/processing complexes. This is in agreement with the finding that the eukaryotic HSP70 family member binds and stabilizes a target mRNA independently from its chaperone activity (Kishor et al., 2017). It is also in agreement with a previous study demonstrating that DnaK from *E. coli* can bind AU rich RNAs and that the co-chaperones DnaJ and GrpE can modulate this effect (Zimmer et al., 2001). Consistent with these findings, the implication of DnaK in multiple processes of eukaryotic RNA biology may reduce the performance of the cellular quality control machinery or may interfere with the efficiency of protein translation in the cells infected with the bacteria.

Earlier studies have used proteomics-based analysis to identify networks of protein-protein interaction in several *in vitro* models of infection with the whole infectious agent (Urwyler et al., 2009; Noster et al., 2019; Noto et al., 2019). Our previous observation that binding of DnaK to the target proteins has an inhibitory effect with their function (Zella et al., 2018; Benedetti et al., 2020a) clearly indicates that the intrusion of a bacteria chaperone in the eukaryotic cells may compete with the activity of the eukaryotic chaperones and inhibit the function of the bound proteins. For this reason, we decided to focus our proteomic analysis around DnaK. Protein-protein interaction network analysis indicated that the most significant biological complexes formed by the proteins binding DnaK include: the mRNA splicing network (Log10 *p*-value –88.9), the Nonsense-Mediated Decay (NMD) complex (Log10 *p*-value –68.3) and the DNA repair pathways (Log10 *p*-value –15).

Here we show for the first time that a bacteria chaperone protein interacts with critical components of important cellular pathways in certain human cancer cell lines. Future studies are needed to broaden our analysis to include the specific interactions of DnaK with proteins from different cell types, both of normal and transformed phenotype. Further studies are also needed to both assess the biological outcomes of such interactions and to elucidate the mechanism(s) responsible for any change in client proteins function, whether is through simply direct binding to DnaK or improper folding. This would allow us to better understand the extent of DnaK interference with a number of cellular pathways active at different stages of cell development and differentiation. In addition, the nature of the binding of bacteria DnaK with eukaryotic proteins needs to be investigated. For example, we don't know whether the DnaK-client's bindings are transient, as normally occurs for chaperone proteins (Bracher and Verghese, 2015) or stable, and we don't know the fate or the effect on the activity of the client proteins bound by DnaK.

Overall, the role of *Mycoplasma fermentans* in human diseases, including cancer, has been highlighted by several studies, and this research, together with other previous data (Benedetti et al., 2020b, Benedetti et al., 2021), strongly indicate that this bacterium and others expressing DnaKs similar in amino acid composition and structure may play a more complex role beyond the one of being simple opportunistic bacteria. Given the close interactions between bacteria and host cells in the local microenvironment (Maman and Witz, 2018), these data should help provide the foundation for future

mechanistic studies on how bacteria interfere with essential cellular processes.

Data availability statement

The raw mass spectrometric data files presented in the study are deposited in the PRIDE repository, with the accession number PXD035477 (http://www.ebi.ac.uk/pride/archive/projects/PXD035477).

Author contributions

SC, RCG, and DZ: conceptualization. SC and DZ: data curation. SC: formal analysis. RCG and DZ: funding acquisition. SC, FB, AM, FC, and DZ: investigation. SC and WY: methodology. SC, RCG, and DZ: supervision. SC, FB, AM, and FC: visualization. NS: mass spectrometry. SC: writing – original draft. SC, FB, WY, AM, FC, RCG, NS, and DZ: writing – review and editing. All authors contributed to the article and approved the submitted version.

Acknowledgments

We thank the Biomolecular Analysis Facility in the University of Virginia, School of Medicine for mass spectrometry services.

Conflict of interest

The authors declare that the research was conducted in the absence of any commercial or financial relationships that could be construed as a potential conflict of interest.

Publisher's note

All claims expressed in this article are solely those of the authors and do not necessarily represent those of their affiliated organizations, or those of the publisher, the editors and the reviewers. Any product that may be evaluated in this article, or claim that may be made by its manufacturer, is not guaranteed or endorsed by the publisher.

Author disclaimer

The views expressed are her own and do not represent the views of the Food and Drug Administration or the United States Government.

Supplementary material

The Supplementary Material for this article can be found online at: https://www.frontiersin.org/articles/10.3389/fmicb.2022.1022704/full#supplementary-material

SUPPLEMENTARY FIGURE 1
Experimental workflow. **(A)** Five human cancer cell lines were transfected with DnaK-V5 expression vector. **(B)** Proteins were extracted in non-denaturing conditions and DnaK-V5 expression was validated by Western Blot (WB). **(C)** Precleared lysates were separated in 4 parts to perform immunoprecipitation (IP): 1. IP with immunoglobulin (Ig) isotype control, 2. Duplicate IP with anti-V5 Ig, 3. IP with anti-V5 Ig in the presence of V5 blocking peptide. **(D)** All IP were confirmed by WB and **(E)** samples were tryptic digested and subjected to Mass Spectrometry (MS) for protein identification. **(F)** The identified proteins were analyzed using the Scaffold proteome Software program. **(G)** Further data cleaning was applied to select only proteins commonly present in the duplicate samples, while proteins pulled from the IP with the isotype Ig and the anti-V5 Ig in the presence of V5 blocking peptide were subtracted.

SUPPLEMENTARY FIGURE 2
Quantitative comparison of DnaK-V5-binding proteins and detected by Mass Spectrometry analysis in the five cancer cell lines. Duplicates MS/MS data of proteins binding DnaK-V5 from five cancer cell lines was quantitatively determined by spectra counting in Scaffold software. PARP1, RPA1, LIG3, XRCC1, XRCC5, XRCC6, and PRKDC were chosen to represent common proteins in the 5 cell lines and components of the Reactome pathway of DNA repair (R-HSA-73894). ANOVA statistical analysis with Benjamini Ochberg correction (Ferreira and Zwinderman, 2006), was performed with Scaffold 4 on normalized duplicate spectra counts of proteins differentially expressed between the five cell types, by selecting a p-value of significance <0.05.

SUPPLEMENTARY FIGURE 3
Direct binding of PARP1 to DnaK as determined by surface plasmon resonance (SPR). Association of PARP1 at different concentrations on 2,220 response units of DnaK immobilized on a CM5 biosensor chip proceeded at a flow rate of 35 μl/min for 250 s, followed by a 600 s-dissociation in HBS-EP buffer. A preliminary kinetic analysis yielded a Kd value of <25 nM ($2.501e^{-8}$M).

References

Ainsworth, J. G., Easterbrook, P. J., Clarke, J., Gilroy, C. B., and Taylor-Robinson, D. (2001). An association of disseminated *Mycoplasma fermentans* in HIV-1 positive patients with non-Hodgkin's lymphoma. *Int. J. STD AIDS* 12, 499–504. doi: 10.1258/0956462011923589

Ali, A. A. E., Timinszky, G., Arribas-Bosacoma, R., Kozlowski, M., Hassa, P. O., Hassler, M., et al. (2012). The zinc-finger domains of Parp1 cooperate to recognize DNA strand breaks. *Nat. Struct. Mol. Biol.* 19, 685–692. doi: 10.1038/nsmb.2335

Ashburner, M., Ball, C. A., Blake, J. A., Botstein, D., Butler, H., Cherry, J. M., et al. (2000). Gene ontology: Tool for the unification of biology. the gene ontology consortium. *Nat. Genet.* 25, 25–29. doi: 10.1038/75556

Bader, G. D., and Hogue, C. W. (2003). An automated method for finding molecular complexes in large protein interaction networks. *BMC Bioinform.* 4:2. doi: 10.1186/1471-2105-4-2

Barykova, Y. A., Logunov, D. Y., Shmarov, M. M., Vinarov, A. Z., Fiev, D. N., Vinarova, N. A., et al. (2011). Association of *Mycoplasma hominis* infection with prostate cancer. *Oncotarget* 2, 289–297. doi: 10.18632/oncotarget.256

Baseman, J. B., Lange, M., Criscimagna, N. L., Giron, J. A., and Thomas, C. A. (1995). Interplay between mycoplasmas and host target cells. *Microb. Pathog.* 19, 105–116. doi: 10.1006/mpat.1995.0050

Becker, T., Hartl, F. U., and Wieland, F. (2002). CD40, an extracellular receptor for binding and uptake of Hsp70-peptide complexes. *J. Cell Biol.* 158, 1277–1285. doi: 10.1083/jcb.200208083

Benedetti, F., Cocchi, F., Latinovic, O. S., Curreli, S., Krishnan, S., Munawwar, A., et al. (2020a). Role of Mycoplasma Chaperone DnaK in cellular transformation. *Int. J. Mol. Sci.* 21:1311. doi: 10.3390/ijms21041311

Benedetti, F., Curreli, S., and Zella, D. (2020b). Mycoplasmas-host interaction: Mechanisms of inflammation and association with cellular transformation. *Microorganisms* 8:1351. doi: 10.3390/microorganisms8091351

Benedetti, F., Curreli, S., Gallo, R. C., and Zella, D. (2021). Tampering of viruses and *Bacteria* with Host DNA repair: Implications for cellular transformation. *Cancers* 13:241. doi: 10.3390/cancers13020241

Bracher, A., and Verghese, J. (2015). The nucleotide exchange factors of Hsp70 molecular chaperones. *Front. Mol. Biosci.* 2:10. doi: 10.3389/fmolb.2015.00010

Caldecott, K. W. (2019). XRCC1 protein; Form and function. *DNA Repair* 81:102664. doi: 10.1016/j.dnarep.2019.102664

Calloni, G., Chen, T., Schermann, S. M., Chang, H. C., Genevaux, P., Agostini, F., et al. (2012). DnaK functions as a central hub in the *E. coli* chaperone network. *Cell Rep.* 1, 251–264. doi: 10.1016/j.celrep.2011.12.007

Chiappori, F., Fumian, M., Milanesi, L., and Merelli, I. (2015). DnaK as antibiotic target: Hot spot residues analysis for differential inhibition of the *Bacteria*l protein in comparison with the human Hsp70. *PLoS One* 10:e0124563. doi: 10.1371/journal.pone.0124563

Clerico, E. M., Tilitsky, J. M., Meng, W., and Gierasch, L. M. (2015). How hsp70 molecular machines interact with their substrates to mediate diverse physiological functions. *J. Mol. Biol.* 427, 1575–1588. doi: 10.1016/j.jmb.2015.02.004

Cohen, J. (1960). A Coefficient of agreement for nominal scales. *Educ. Psychol. Meas.* 20, 37–46. doi: 10.1177/001316446002000104

Cretu, C., Schmitzová, J., Ponce-Salvatierra, A., Dybkov, O., De Laurentiis, E. I., Sharma, K., et al. (2016). Molecular architecture of SF3B and structural consequences of its cancer-related mutations. *Mol. Cell* 64, 307–319. doi: 10.1016/j.molcel.2016.08.036

Cryan, J. F., O'riordan, K. J., Cowan, C. S. M., Sandhu, K. V., Bastiaanssen, T. F. S., Boehme, M., et al. (2019). The microbiota-gut-brain axis. *Physiol. Rev.* 99, 1877–2013. doi: 10.1152/physrev.00018.2018

Curreli, S., Tettelin, H., Benedetti, F., Krishnan, S., Cocchi, F., Reitz, M., et al. (2021). Analysis of DnaK expression from a strain of *Mycoplasma fermentans* in infected HCT116 human colon carcinoma cells. *Int. J. Mol. Sci.* 22:3885. doi: 10.3390/ijms22083885

Drouet, J., Frit, P., Delteil, C., De Villartay, J. P., Salles, B., and Calsou, P. (2006). Interplay between Ku, artemis, and the DNA-dependent protein kinase catalytic subunit at DNA ends. *J. Biol. Chem.* 281, 27784–27793. doi: 10.1074/jbc.M603047200

Ellgaard, L., and Ruddock, L. W. (2005). The human protein disulphide isomerase family: Substrate interactions and functional properties. *EMBO Rep.* 6, 28–32. doi: 10.1038/sj.embor.7400311

Fabregat, A., Jupe, S., Matthews, L., Sidiropoulos, K., Gillespie, M., Garapati, P., et al. (2018). The reactome pathway knowledgebase. *Nucleic Acids Res.* 46:D649–D655. doi: 10.1093/nar/gkx1132

Ferreira, J. A., and Zwinderman, A. H. (2006). On the benjamini–hochberg method. *Ann. Stat.* 34, 1827–1849. doi: 10.1214/009053606000000425

Genevaux, P., Georgopoulos, C., and Kelley, W. L. (2007). The Hsp70 chaperone machines of *Escherichia coli*: A paradigm for the repartition of chaperone functions. *Mol. Microbiol.* 66, 840–857. doi: 10.1111/j.1365-2958.2007.05961.x

Gottlieb, T. M., and Jackson, S. P. (1993). The DNA-dependent protein kinase: Requirement for DNA ends and association with Ku antigen. *Cell* 72, 131–142. doi: 10.1016/0092-8674(93)90057-W

Han, Y., Jin, F., Xie, Y., Liu, Y., Hu, S., Liu, X. D., et al. (2019). DNA-PKCS PARYLATION regulates DNA-PK kinase activity in the DNA damage response. *Mol. Med. Rep.* 20, 3609–3616. doi: 10.3892/mmr.2019.10640

Hegde, S., Hegde, S., Spergser, J., Brunthaler, R., Rosengarten, R., and Chopra-Dewasthaly, R. (2014). *In vitro* and *in vivo* cell invasion and systemic spreading of Mycoplasma agalactiae in the sheep infection model. *Int. J. Med. Microbiol.* 304, 1024–1031. doi: 10.1016/j.ijmm.2014.07.011

Henrich, B., Rumming, M., Sczyrba, A., Velleuer, E., Dietrich, R., Gerlach, W., et al. (2014). *Mycoplasma salivarium* as a dominant coloniser of Fanconi anaemia associated oral carcinoma. *PLoS One* 9:e92297. doi: 10.1371/journal.pone.0092297

Heyer, W. D., Ehmsen, K. T., and Liu, J. (2010). Regulation of homologous recombination in eukaryotes. *Annu. Rev. Genet.* 44, 113–139. doi: 10.1146/annurev-genet-051710-150955

Huang, S., Li, J. Y., Wu, J., Meng, L., and Shou, C. C. (2001). Mycoplasma infections and different human carcinomas. *World J. Gastroenterol.* 7, 266–269. doi: 10.3748/wjg.v7.i2.266

Jain, A., Bacolla, A., Chakraborty, P., Grosse, F., and Vasquez, K. M. (2010). Human DHX9 helicase unwinds triple-helical DNA structures. *Biochemistry* 49, 6992–6999. doi: 10.1021/bi100795m

Jha, S., and Dutta, A. (2009). RVB1/RVB2: Running rings around molecular biology. *Mol. Cell* 34, 521–533. doi: 10.1016/j.molcel.2009.05.016

Jha, S., Shibata, E., and Dutta, A. (2008). Human Rvb1/Tip49 is required for the histone acetyltransferase activity of Tip60/NuA4 and for the downregulation of phosphorylation on H2AX after DNA damage. *Mol. Cell Biol.* 28, 2690–2700. doi: 10.1128/MCB.01983-07

Jiang, S., Zhang, S., Langenfeld, J., Lo, S.-C., and Rogers, M. B. (2008). Mycoplasma infection transforms normal lung cells and induces bone morphogenetic protein 2 expression by post-transcriptional mechanisms. *J. Cell. Biochem.* 104, 580–594. doi: 10.1002/jcb.21647

Jungmichel, S., Rosenthal, F., Altmeyer, M., Lukas, J., Hottiger, M. O., and Nielsen, M. L. (2013). Proteome-wide identification of poly(ADP-Ribosyl)ation targets in different genotoxic stress responses. *Mol. Cell* 52, 272–285. doi: 10.1016/j.molcel.2013.08.026

Kanehisa, M., and Goto, S. (2000). KEGG: Kyoto encyclopedia of genes and genomes. *Nucleic Acids Res.* 28, 27–30. doi: 10.1093/nar/28.1.27

Kikuchi, M., Doi, E., Tsujimoto, I., Horibe, T., and Tsujimoto, Y. (2002). Functional analysis of human P5, a protein disulfide isomerase homologue. *J. Biochem.* 132, 451–455. doi: 10.1093/oxfordjournals.jbchem.a003242

Kim, Y. E., Hipp, M. S., Bracher, A., Hayer-Hartl, M., and Ulrich Hartl, F. (2013). Molecular chaperone functions in protein folding and proteostasis. *Annu. Rev. Biochem.* 82, 323–355. doi: 10.1146/annurev-biochem-060208-092442

Kishor, A., White, E. J. F., Matsangos, A. E., Yan, Z., Tandukar, B., and Wilson, G. M. (2017). Hsp70's RNA-binding and mRNA-stabilizing activities are independent of its protein chaperone functions. *J. Biol. Chem.* 292, 14122–14133. doi: 10.1074/jbc.M117.785394

Krzywinski, M., Schein, J., Birol, I., Connors, J., Gascoyne, R., Horsman, D., et al. (2009). Circos: An information aesthetic for comparative genomics. *Genome Res.* 19, 1639–1645. doi: 10.1101/gr.092759.109

Kutuzov, M. M., Belousova, E. A., Kurgina, T. A., Ukraintsev, A. A., Vasil'eva, I. A., Khodyreva, S. N., et al. (2021). The contribution of PARP1, PARP2 and poly(ADP-ribosyl)ation to base excision repair in the nucleosomal context. *Sci. Rep.* 11:4849. doi: 10.1038/s41598-021-84351-1

Liberzon, A., Birger, C., Thorvaldsdóttir, H., Ghandi, M., Mesirov, J. P., and Tamayo, P. (2015). The Molecular signatures database (MSIGDB) hallmark gene set collection. *Cell Syst.* 1, 417–425. doi: 10.1016/j.cels.2015.12.004

Lieber, M. R. (2010). The mechanism of double-strand Dna break repair by the nonhomologous DNA end-joining pathway. *Annu. Rev. Biochem.* 79, 181–211. doi: 10.1146/annurev.biochem.052308.093131

Lo, S. C., Hayes, M. M., Kotani, H., Pierce, P. F., Wear, D. J., Newton, P. B. III, et al. (1993). Adhesion onto and invasion into mammalian cells by mycoplasma penetrans: A newly isolated mycoplasma from patients with AIDS. *Mod. Pathol.* 6, 276–280.

Logunov, D. Y., Scheblyakov, D. V., Zubkova, O. V., Shmarov, M. M., Rakovskaya, I. V., Gurova, K. V., et al. (2008). Mycoplasma infection suppresses p53, activates NF-κB and cooperates with oncogenic Ras in rodent fibroblast transformation. *Oncogene* 27, 4521–4531. doi: 10.1038/onc.2008.103

Maman, S., and Witz, I. P. (2018). A history of exploring cancer in context. *Nat. Rev. Cancer* 18, 359–376. doi: 10.1038/s41568-018-0006-7

Marteijn, J. A., Lans, H., Vermeulen, W., and Hoeijmakers, J. H. (2014). Understanding nucleotide excision repair and its roles in cancer and ageing. *Nat. Rev. Mol. Cell Biol.* 15, 465–481. doi: 10.1038/nrm3822

Martens, M., Ammar, A., Riutta, A., Waagmeester, A., Slenter, D. N., Hanspers, K. R. A. M., et al. (2021). WikiPathways: Connecting communities. *Nucleic Acids Res.* 49:D613–D621. doi: 10.1093/nar/gkaa1024

Masson, M., Niedergang, C., Schreiber, V., Muller, S., Menissier-De Murcia, J., and De Murcia, G. (1998). Xrcc1 is specifically associated with poly(ADP-ribose) polymerase and negatively regulates its activity following DNA damage. *Mol. Cell Biol.* 18, 3563–3571. doi: 10.1128/MCB.18.6.3563

Mayer, M. P., and Gierasch, L. M. (2019). Recent advances in the structural and mechanistic aspects of Hsp70 molecular chaperones. *J. Biol. Chem.* 294, 2085–2097. doi: 10.1074/jbc.REV118.002810

Mehrian-Shai, R., Reichardt, J. K. V., Harris, C. C., and Toren, A. (2019). The gut–brain axis, paving the way to brain cancer. *Trends Cancer* 5, 200–207. doi: 10.1016/j.trecan.2019.02.008

Moser, J., Kool, H., Giakzidis, I., Caldecott, K., Mullenders, L. H., and Fousteri, M. I. (2007). Sealing of chromosomal Dna nicks during nucleotide excision repair requires XRCC1 and DNA ligase III alpha in a cell-cycle-specific manner. *Mol. Cell* 27, 311–323. doi: 10.1016/j.molcel.2007.06.014

Muller, P. A., Schneeberger, M., Matheis, F., Wang, P., Kerner, Z., Ilanges, A., et al. (2020). Microbiota modulate sympathetic neurons via a gut-brain circuit. *Nature* 583, 441–446. doi: 10.1038/s41586-020-2474-7

Namiki, K., Goodison, S., Porvasnik, S., Allan, R. W., Iczkowski, K. A., Urbanek, C., et al. (2009). Persistent exposure to mycoplasma induces malignant transformation of human prostate cells. *PLoS One* 4:e6872. doi: 10.1371/journal.pone.0006872

Nash, R. A., Caldecott, K. W., Barnes, D. E., and Lindahl, T. (1997). Xrcc1 protein interacts with one of two distinct forms of DNA ligase III. *Biochemistry* 36, 5207–5211. doi: 10.1021/bi962281m

Noster, J., Chao, T. C., Sander, N., Schulte, M., Reuter, T., Hansmeier, N., et al. (2019). Proteomics of intracellular *Salmonella enterica* reveals roles of *Salmonella* pathogenicity island 2 in metabolism and antioxidant defense. *PLoS Pathog.* 15:e1007741. doi: 10.1371/journal.ppat.1007741

Noto, J. M., Rose, K. L., Hachey, A. J., Delgado, A. G., Romero-Gallo, J., Wroblewski, L. E., et al. (2019). Carcinogenic *Helicobacter* pylori strains selectively dysregulate the *in vivo* gastric proteome, which may be associated with Stomach Cancer Progression. *Mol. Cell. Proteom.* 18, 352–371. doi: 10.1074/mcp.RA118.001181

Nunes, J. M., Mayer-Hartl, M., Hartl, F. U., and Müller, D. J. (2015). Action of the Hsp70 chaperone system observed with single proteins. *Nat. Commun.* 6:6307. doi: 10.1038/ncomms7307

Oughtred, R., Rust, J., Chang, C., Breitkreutz, B. J., Stark, C., Willems, A., et al. (2021). The Biogrid database: A comprehensive biomedical resource of curated protein, genetic, and chemical interactions. *Protein Sci.* 30, 187–200. doi: 10.1002/pro.3978

Puri, T., Wendler, P., Sigala, B., Saibil, H., and Tsaneva, I. R. (2007). Dodecameric structure and Atpase activity of the human TIP48/TIP49 complex. *J. Mol. Biol.* 366, 179–192. doi: 10.1016/j.jmb.2006.11.030

Qiu, X. B., Shao, Y. M., Miao, S., and Wang, L. (2006). The diversity of the DnaJ/Hsp40 family, the crucial partners for Hsp70 chaperones. *Cell. Mol. Life Sci.* 63, 2560–2570. doi: 10.1007/s00018-006-6192-6

Rüdiger, S., Germeroth, L., Schneider-Mergener, J., and Bukau, B. (1997). Substrate specificity of the DnaK chaperone determined by screening cellulose-bound peptide libraries. *EMBO J.* 16, 1501–1507. doi: 10.1093/emboj/16.7.1501

Ruepp, A., Waegele, B., Lechner, M., Brauner, B., Dunger-Kaltenbach, I., Fobo, G., et al. (2010). Corum: The comprehensive resource of mammalian protein complexes–2009. *Nucleic Acids Res.* 38:D497–D501. doi: 10.1093/nar/gkp914

Ryu, S. W., Stewart, R., Pectol, D. C., Ender, N. A., Wimalarathne, O., Lee, J. H., et al. (2020). Proteome-wide identification of HSP70/HSC70 chaperone clients in human cells. *PLoS Biol.* 18:e3000606. doi: 10.1371/journal.pbio.3000606

Saibil, H. (2013). Chaperone machines for protein folding, unfolding and disaggregation. *Nat. Rev. Mol. Cell Biol.* 14, 630–642. doi: 10.1038/nrm3658

Sarbeng, E. B., Liu, Q., Tian, X., Yang, J., Li, H., Wong, J. L., et al. (2015). A functional DnaK dimer is essential for the efficient interaction with Hsp40 heat shock protein. *J. Biol. Chem.* 290, 8849–8862. doi: 10.1074/jbc.M114.596288

Shannon, P., Markiel, A., Ozier, O., Baliga, N. S., Wang, J. T., Ramage, D., et al. (2003). Cytoscape: A software environment for integrated models of biomolecular interaction networks. *Genome Res.* 13, 2498–2504. doi: 10.1101/gr.1239303

Subramanian, A., Tamayo, P., Mootha, V. K., Mukherjee, S., Ebert, B. L., Gillette, M. A., et al. (2005). Gene set enrichment analysis: A knowledge-based approach for interpreting genome-wide expression profiles. *Proc. Natl. Acad. Sci. U.S.A.* 102, 15545–15550. doi: 10.1073/pnas.0506580102

The UniProt Consortium (2017). UniProt: The universal protein knowledgebase. *Nucleic Acids Res.* 45:D158–D169. doi: 10.1093/nar/gkw1099

Theriault, J. R., Adachi, H., and Calderwood, S. K. (2006). Role of scavenger receptors in the binding and internalization of heat shock protein 70. *J. Immunol.* 177, 8604–8611. doi: 10.4049/jimmunol.177.12.8604

Tomkinson, A. E., and Sallmyr, A. (2013). Structure and function of the DNA ligases encoded by the mammalian LIG3 gene. *Gene* 531, 150–157. doi: 10.1016/j.gene.2013.08.061

Urwyler, S., Nyfeler, Y., Ragaz, C., Lee, H., Mueller, L. N., Aebersold, R., et al. (2009). Proteome analysis of *Legionella* vacuoles purified by magnetic immunoseparation reveals secretory and endosomal Gtpases. *Traffic* 10, 76–87. doi: 10.1111/j.1600-0854.2008.00851.x

Van Durme, J., Maurer-Stroh, S., Gallardo, R., Wilkinson, H., Rousseau, F., and Schymkowitz, J. (2009). Accurate prediction of DnaK-peptide binding via homology modelling and experimental data. *PLoS Comput. Biol.* 5:e1000475. doi: 10.1371/journal.pcbi.1000475

Yavlovich, A., Katzenell, A., Tarshis, M., Higazi, A. A., and Rottem, S. (2004). *Mycoplasma fermentans* binds to and invades HeLa cells: Involvement of plasminogen and urokinase. *Infect. Immun.* 72, 5004–5011. doi: 10.1128/IAI.72.9.5004-5011.2004

Zella, D., Curreli, S., Benedetti, F., Krishnan, S., Cocchi, F., Latinovic, O. S., et al. (2018). Mycoplasma promotes malignant transformation *in vivo*, and its DnaK, a *Bacteria*l chaperone protein, has broad oncogenic properties. *Proc. Natl. Acad. Sci. U.S.A.* 115:E12005–E12014. doi: 10.1073/pnas.1815660115

Zhang, S., Tsai, S., and Lo, S.-C. (2006). Alteration of gene expression profiles during mycoplasma-induced malignant cell transformation. *BMC Cancer* 6:116. doi: 10.1186/1471-2407-6-116

Zhou, Y., Zhou, B., Pache, L., Chang, M., Khodabakhshi, A. H., Tanaseichuk, O., et al. (2019). Metascape provides a biologist-oriented resource for the analysis of systems-level datasets. *Nat. Commun.* 10:1523. doi: 10.1038/s41467-019-09234-6

Zimmer, C., Von Gabain, A., and Henics, T. (2001). Analysis of sequence-specific binding of Rna to Hsp70 and its various homologs indicates the involvement of N- and C-terminal interactions. *Rna* 7, 1628–1637.

frontiers | Frontiers in Microbiology

TYPE Original Research
PUBLISHED 03 November 2022
DOI 10.3389/fmicb.2022.979790

OPEN ACCESS

EDITED BY
Svetlana Khaiboullina,
University of Nevada, Reno,
United States

REVIEWED BY
Anusak Kerdsin,
Kasetsart University Chalermphrakiat Sakon Nakhon Province Campus, Thailand
Nicolás Francisco Cordeiro,
Universidad de la República, Uruguay

*CORRESPONDENCE
Mariela E. Srednik
mariela.srednik@gmail.com

SPECIALTY SECTION
This article was submitted to Infectious Agents and Disease, a section of the journal Frontiers in Microbiology

RECEIVED 27 June 2022
ACCEPTED 02 August 2022
PUBLISHED 03 November 2022

CITATION
Srednik ME, Morningstar-Shaw BR, Hicks JA, Mackie TA and Schlater LK (2022) Antimicrobial resistance and genomic characterization of *Salmonella enterica* serovar Senftenberg isolates in production animals from the United States. *Front. Microbiol.* 13:979790. doi: 10.3389/fmicb.2022.979790

Antimicrobial resistance and genomic characterization of *Salmonella enterica* serovar Senftenberg isolates in production animals from the United States

Mariela E. Srednik*, Brenda R. Morningstar-Shaw, Jessica A. Hicks, Tonya A. Mackie and Linda K. Schlater

National Veterinary Services Laboratories, Animal and Plant Health Inspection Service, United States Department of Agriculture, Ames, IA, United States

In the USA, *Salmonella enterica* subspecies *enterica* serovar Senftenberg is among the top five serovars isolated from food and the top 11 serovars isolated from clinically ill animals. Human infections are associated with exposure to farm environments or contaminated food. The objective of this study was to characterize *S.* Senftenberg isolates from production animals by analyzing phenotypic antimicrobial resistance profiles, genomic features and phylogeny. *Salmonella* Senftenberg isolates (n=94) from 20 US states were selected from NVSL submissions (2014–2017), tested against 14 antimicrobial drugs, and resistance phenotypes determined. Resistance genotypes were determined using whole genome sequencing analysis with AMRFinder and the NCBI and ResFinder databases with ABRicate. Plasmids were detected using PlasmidFinder. Integrons were detected using IntFinder and manual alignment with reference genes. Multilocus-sequence-typing (MLST) was determined using ABRicate with PubMLST database, and phylogeny was determined using vSNP. Among 94 isolates, 60.6% were resistant to at least one antimicrobial and 39.4% showed multidrug resistance. The most prevalent resistance findings were for streptomycin (44.7%), tetracycline (42.6%), ampicillin (36.2%) and sulfisoxazole (32.9%). The most commonly found antimicrobial resistance genes were *aac*(6')-Iaa (100%), *aph*(3")-Ib and *aph*(6)-Id (29.8%) for aminoglycosides, followed by bla_{TEM-1} (26.6%) for penicillins, *sul*1 (25.5%) and *sul*2 (23.4%) for sulfonamides and *tet*A (23.4%) for tetracyclines. Quinolone-resistant isolates presented mutations in *gyr*A and/or *par*C genes. Class 1 integrons were found in 37 isolates. Thirty-six plasmid types were identified among 77.7% of the isolates. Phylogenetic analysis identified two distinct lineages of *S.* Senftenberg that correlated with the MLST results. Isolates were classified into two distinct sequence types (ST): ST14 (97.9%) and ST 185 (2.1%). The diversity of this serotype suggests multiple introductions into animal populations from outside sources. This study provided antimicrobial susceptibility and genomic characteristics of *S.* Senftenberg clinical isolates from production animals in the USA during 2014 to 2017. This study will serve as a base for future studies focused on the phenotypic and molecular

antimicrobial characterization of *S.* Senftenberg isolates in animals. Monitoring of antimicrobial resistance to detect emergence of multidrug-resistant strains is critical.

KEYWORDS

antimicrobial resistance, whole genome sequencing, phylogeny, resistance genes, *Salmonella* Senftenberg

Introduction

Salmonella enterica subsp. *enterica* serovar Senftenberg is commonly isolated from animals and food. This serovar is widely distributed and has been found worldwide. In the USA, *S.* Senftenberg is among the top five serovars isolated from food and among the top 11 serovars isolated from clinically ill animals (Switt, 2019). *S.* Senftenberg and *S.* Montevideo were the most common serotypes found in animal feeds in the USA in 2012 (Li et al., 2012). In Europe, *S.* Senftenberg was found more frequently in poultry flocks than other serotypes and the emergence of this serotype was a cause of concern in 2012 (Boumart et al., 2012). Most *Salmonella* serovars, including *S.* Senftenberg, are tolerant to desiccation and able to colonize and persist in feed mills (Pedersen et al., 2008). Interestingly, *S.* Senftenberg is also a heat-resistant serotype (Doyle and Mazzotta, 1999), which may contribute to persistence in feed and the environment. This can be a source of contamination on farms and in processing environments. Human infections with *S.* Senftenberg are rare and are typically associated with exposure to poultry flocks, farm environments, or contaminated food (Boumart et al., 2012). Worldwide, *S.* Senftenberg has been linked to outbreaks associated with contaminated pistachios, salami, basil, Maradol papayas, peanut butter, alfalfa sprouts and baby cereal (Centers for disease Control and Prevention, 2010, 2016, 2022; US Food and Drug Administration, 2014; Hassan et al., 2019; Switt, 2019; Haendiges et al., 2021).

Although antimicrobial-resistant isolates of *S.* Senftenberg are usually associated with animal sources (Stepan et al., 2011), antimicrobial-resistant human isolates of *S.* Senftenberg have been reported in the USA, and extensively drug-resistant (XDR) strains have been isolated from patients outside of the USA, raising public health concerns (Hendriksen et al., 2013; Veeraraghavan et al., 2019). Infections caused by *S.* Senftenberg range from asymptomatic to severe, and deaths have been associated with the XDR strains of *S.* Senftenberg in China (El Ghany et al., 2016). XDR strains are resistant to all but only one or two categories of antimicrobials, leaving clinicians and veterinarians with few to no treatment options (Magiorakos et al., 2012).

Horizontal transfer of genetic material is important in the spread of MDR. Resistance genes can be inserted in the form of cassettes into integrons; these mobilizable genetic elements are grouped in three classes (class 1, 2 and 3) based on the presence of three different integrases encoded by the *intl*1, *intl*2, *intl*3 genes. Integrons can be mobilized within the chromosome to other regions, or they can be inserted in integrative-conjugative elements and plasmids, which can facilitate the horizontal transfer of resistance genes between bacteria (Stokes and Gillings, 2011).

Since *Salmonella* is associated with outbreaks of foodborne disease, MDR strains pose a risk to public health because of the potential for treatment failures (Nair et al., 2018). Few studies exist on the antimicrobial susceptibility and genetic diversity of *Salmonella* serovar Senftenberg of animal origin. Among all *Salmonella* serotyping submissions received at the NVSL from January 1, 2014, through December 31, 2017, *S.* Senftenberg ranked number eight during 2014 and number 10 during 2015 among clinical isolates, and ranked number one during 2014, 2015, 2016 and number two during 2017 among non-clinical isolates. The objective of this study was to compare phenotypic and genomic resistance data, mechanisms of antimicrobial resistance, plasmid replicons, genetic relatedness, and to characterize *S.* Senftenberg diagnostic isolates recovered from poultry, swine, and cattle in the USA between 2014 and 2017, and to provide useful retrospective information for future studies on *S.* Senftenberg.

Materials and methods

Bacterial isolates

A total of 94 *S.* Senftenberg isolates from swine (n = 50), poultry (n = 24) and cattle (n = 20) were selected from the National Veterinary Services Laboratories (NVSL) *Salmonella* repository isolates archived at room temperature on nutrient agar slants. Samples came from 20 US States (IA = 20, MN = 15, AR = 8, MO = 8, IL = 6, IN = 4, TX = 4, NC = 4, OH = 4, PA = 4, OK = 2, KS = 2, NE = 2, NY = 2, SD = 2, VA = 2, WI = 2, AL = 1, AZ = 1, KY = 1).

Isolates were selected from samples that were submitted to the NVSL for *Salmonella* serotyping, confirmed by classical (Grimont and Weill, 2007) and molecular typing using Luminex xMAP® technology (Dunbar et al., 2015), between the years of 2014 and 2017. The dataset was initially limited to one sample per year per owner. If more than the targeted number of isolates were available, a randomly selected subset of isolates was chosen. The data was then de-identified to remove information other than the animal

species, state of origin, clinical status, and sample type and assigned a unique identifier. *Salmonella* was confirmed using Biotyper software with an autoflex speed™ MALDI-TOF instrument (Bruker Daltonics, Billerica, MA, USA).

Antimicrobial susceptibility testing

All *Salmonella* isolates were tested for antimicrobial susceptibility against 14 class-representative antimicrobial agents using the Sensititre CMV4AGNF plate (Thermo Fisher Scientific, Waltham, MA, USA) including: gentamicin (GEN), streptomycin (STR), amoxicillin/clavulanic acid (AMC), cefoxitin (FOX), ceftriaxone (CRO), meropenem (MEM), sulfisoxazole (SUL), trimethoprim/sulfamethoxazole (SXT), ampicillin (AMP), chloramphenicol (CHL), ciprofloxacin (CIP), nalidixic acid (NAL), azithromycin (AZM), and tetracycline (TET). Results were interpreted using consensus interpretative criteria established by the National Antimicrobial Resistance Monitoring System (US Food and Drug Administration, 2021).

Whole genome sequencing and genome analysis

DNA was extracted using Promega Maxwell® with the Whole Blood DNA kit following manufacturer's instructions. *S.* Senftenberg isolates were subjected to whole genome sequencing using the Illumina MiSeq platform with 2×250 paired-end chemistry and the NexteraXT library preparation kit (Illumina, Inc., San Diego, CA, USA). AMR gene alleles were determined using AMRFinder (Feldgarden et al., 2019) and the NCBI and ResFinder databases (Zankari et al., 2012) using ABRicate[1] with an identity threshold of 80% over ≥60% of the length of the target gene. Integrons were identified using IntFinder 1.0 (Loaiza et al., 2020). Integron classes were mapped using NCBI reference sequences of the *intI*1 (MG785026.1), *intI*2 (MK994977.1) and *IntI*3 (KM194584.1) integrase genes, and resistance genes available in the CARD (Comprehensive Antimicrobial Resistance Database, card.macmaster.ca) database using Geneious Prime v11.0.9 + 11 (Biomatters Ltd., NZ). Plasmid replicons were identified using ABRicate with the PlasmidFinder database (Carattoli et al, 2014). PointFinder was used for analysis of chromosomal structural gene mutations (Zankari et al., 2017). Isolate sequences are publicly available in the NCBI BioProject PRJNA785813.

Multilocus-sequence-typing (MLST) was determined using ABRicate with PubMLST database. The single nucleotide polymorphism (SNP) analysis of all isolates was performed using the NVSL vSNP pipeline[2]. Isolates were separated and analyzed by MLST with the respective reference (*S.* Senftenberg NZ_CP016837 for ST185 and NZ_CP029036 for ST14). A SNP-based phylogenetic tree was generated with RAxML in the vSNP pipeline (Stamatakis, 2014). The k-mer based phylogeny tool kSNP was used to generate a reference-free phylogenetic tree of all the *S.* Senftenberg isolates (Gardner et al., 2015).

Relationship of antimicrobial susceptibility with antimicrobial genes

Each antimicrobial susceptibility interpretation (resistant or susceptible) for each antimicrobial tested was compared with the presence or absence of the corresponding resistance gene or genes and/or chromosomal gene mutations found. Intermediate phenotypes were counted as susceptible in this analysis. Using the phenotypic results as the reference outcome, sensitivity was calculated by dividing the number of isolates that were genotypically resistant by the total number of isolates exhibiting clinical resistance phenotypes. Specificity was calculated by dividing the number of isolates that were genotypically susceptible by the total number of isolates with susceptible phenotypes (McDermott et al., 2016).

Results

Antimicrobial susceptibility testing

Overall, the highest percentage of resistance was found to the following antimicrobials: streptomycin (44.7%), tetracycline (42.6%), ampicillin (36.2%) and sulfisoxazole (32.9%) (Figure 1). All of the *S.* Senftenberg isolates were susceptible to meropenem.

Among all 94 isolates, 60.6% (n = 57) were resistant to at least one antimicrobial and 39.4% (n = 37) isolates were MDR. Among MDR isolates, 60% were from swine, 20% from cattle and 12.5% from poultry. Four isolates from swine showed possible XDR; one isolate was only susceptible to meropenem, one isolate was susceptible to gentamycin and meropenem, and two isolates were susceptible to meropenem and azithromycin (one of which with presence of the macrolide *erm*B gene). Most isolates showed diverse resistance profiles, with the most common resistance profile (AMP, GEN, STR) found in just five isolates. Supplementary Table S1 summarizes the phenotypic resistance profiles and the resistance genes present in *S.* Senftenberg isolates displaying antimicrobial resistance.

Antimicrobial resistance genes and integrons

Antimicrobial resistance genes are shown in Table 1. The most commonly observed was the aminoglycoside acetyltransferase *aac*(6′)-Iaa gene, which was found in all isolates, and the aminoglycoside phosphotransferase *aph*(3″)-Ib and *aph*(6)-Id

1 https://github.com/seeman/abricate/

2 https://github.com/USDA-VS/vSNP

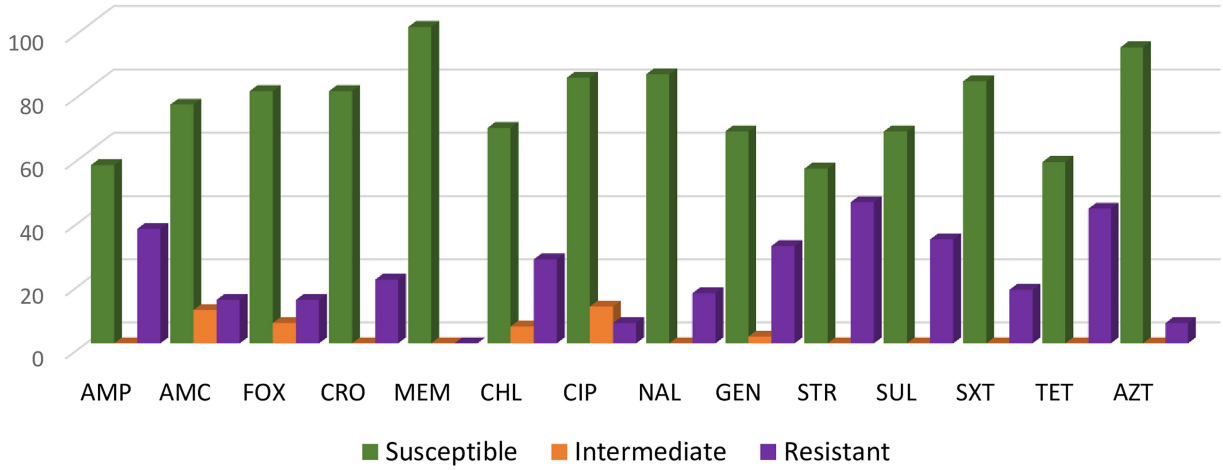

FIGURE 1
Antimicrobial resistance rates of the 94 *Salmonella* Senftenberg isolates. For ciprofloxacin (CIP) isolates categorized as intermediate (MIC 0.12 to 0.5 μg/mL) or resistant (MIC ≥ 1 μg/mL) were defined as having decreased susceptibility to CIP with a MIC ≥ 0.12 μg/mL.

TABLE 1 Antimicrobial resistance genes of the 94 *Salmonella* Senftenberg isolates.

Drug classes	Resistance genes
β-lactams	bla_{TEM-1B} (26.6%), bla_{CMY-2} (14.9%), bla_{SHV-12} (5.3%), bla_{TEM-1A} (1.1%)
Phenicols	*flo*R (14.9%), *cat*A2 (8.5%), *cml*A5 (3.4%), *cml*A1 (1.1%).
Quinolones	*qnr*B2 (6.4%), *qnr*B19 (3.4%), *qnr*B77 (2.1%), *qnr*B6 (1.1%).
Quinolones/Aminoglycosides	*aac*(6′)-Ib-cr (1.1%).
Aminoglycosides	*aac*(6′)-laa (100%), *aph*(3″)-Ib (29.8%), *aph*(6)-Id (29.8%), *aph*(3′)-Ia (23.4%), *aad*A1 (17%), *aad*A2 (15.9%), *aac*(6′)-Ib4 (9.6%), *aac*(6′)-Ib (7.4%), *aac*(6′)-IIc (7.4%), *aac*(3)-II (7.4%), *aac*(3)-*VIa* (7.4%), *ant*(2″)-Ia (7.4%), *aad*A6 (3.4%), *aph*(4)-Ia (3.4%), and others with 1.1%.
Folate pathway inhibitors	*sul*1 (25.5%), *sul*2 (23.4%), *dfr*A19 (6.4%), *dfr*A1 (3.4%), *dfr*A34 (3.4%), *dfr*A12 (2.1%), *dfr*A15 (2.1%), *dfr*A27 (1.1%), *sul*3 (1.1%)
Tetracyclines	*tet*A (23.4%), *tet*B (8.5%), *tet*D (8.5%), 5.3%), *tet*X (1.1%).
Macrolides	*ere*A (6.4%), *mph*A (3.2%), *erm*42 (2.1%), *mph*E (1.1%), *erm*B (1.1%), *msr*E (1.1%).
Ansamycins (Rifamycin)	*arr*-269,927,220 (7.4%), *arr*-3 (1.1%).
Glycopeptides (Bleomycin)	*ble*O (3.2%), *ble*Tn5 (1.1%).
Polymyxins (Colistin)	*mcr*-9.1 (8.5%)

genes seen together in 29.8% (n = 28) of isolates. The *sul*1 gene, a dihydropteroate synthase that is linked to other resistance genes of class 1 integrons and confers resistance to sulfonamides, was found in 25.5% (n = 24) of the isolates; and the *sul*2 gene was observed in 23.4% (n = 22) of the isolates. Resistance to tetracycline was due to the presence of the *tet*A gene that encodes a tetracycline efflux pump, and it was observed in 23.4% (n = 22) of the isolates.

Among beta-lactams, bla_{TEM-1B}, a class A narrow-spectrum beta-lactamase, was the most prevalent beta-lactamase gene (26.6%) conferring resistance to penicillins (ampicillin); but bla_{CMY-2}, a class C beta-lactamase, was the most prevalent beta-lactamase gene (14.9%) against penicillins plus inhibitors (amoxicillin + clavulanic acid) and cephalosporins (cefoxitin, ceftriaxone). The class A extended spectrum beta-lactamases (ESBLs) encoded by the bla_{SHV-12} gene were found in five isolates from swine.

In addition to *aph*(3″)-Ib and *aph*(6)-Id genes, other resistance genes were observed that convey resistance to aminoglycosides, including several integron-encoded aminoglycoside nucleotidyltransferases such as *aad*A1, which was observed in 17% of isolates, *aad*A2, which was observed in 15.9% of isolates, and *aad*A5, *aad*A6, *aad*A12, *aad*A16, and *aad*A25, which were observed in lower frequencies. Resistance genes for gentamicin included several aminoglycoside acetyltransferases encoded by: *aac*(6′)-Ib4 gene in 9.6%; *aac*(6′)-Ib, *aac*(3′)-II, *aac*(6′)-IIc, *aac*(3)-VIa in 7.4%; and *aac*(3)-IVa in 4.3%. The nucleotidyltransferase *ant*(2″)-la gene was found in 7.4%, and the methyltransferase *arm*A gene in one isolate. Six genes conferring resistance to macrolides were found in 13.8% of isolates; the *ere*A gene that encodes an erythromycin esterase was the most frequently identified in 6 isolates, followed by the *mph*A gene that encodes a macrolide 2′-phosphotransferase in 3 isolates. Several resistance genes were found for chloramphenicol; the most frequent was the plasmid or transposon-encoded chloramphenicol exporter *flo*R, which was observed in 14.9% of isolates, followed by *cat*A2 gene, a chloramphenicol O-acetyltransferase, which was observed in 8.5% of isolates. Additional chloramphenicol exporter genes found in lower frequency were *cml*A5 (3.4%) and *cml*A1 (1.1%) genes.

Quinolone-resistance genes were detected in 12 isolates; the most frequent gene was *qnr*B2, a plasmid-mediated quinolone resistance protein, which was observed in 6.4% of isolates, and others in lower frequency: *qnr*B19 in 3.4%, *qnr*B77 in 2.1%, *qnr*B6 in 1.1% and *aac*(6′)-lb-cr in 1.1% of isolates. The *aac*(6′)-lb-cr gene doubly confers resistance to aminoglycoside and fluoroquinolone antibiotics through fluoroquinolone-acetylating activity.

Some isolates presented other genes that confer resistance to antimicrobials that were not included on the panel: the *aph*(3′)-Ia gene conferring resistance to kanamycin was detected in 22 (23.4%) isolates, the mobilized and plasmid-mediated colistin resistance and phosphoethanolamine transferase *mcr*-9.1 gene was detected in eight (8.5%) isolates, the *arr*-269927220, an ADP-ribosyltransferase that confers resistance to rifamycin was detected in seven (7.4%) isolates, and the *arr*-3 gene in one (1.1%) isolate. The *ble*O gene that encodes a bleomycin binding protein was detected in three (3.2%) isolates, and the *ble*Tn5 gene that encodes a bleomycin binding protein BLMT by the *ble* gene on the transposon Tn5 was found in one (1.1%) isolate. Interestingly, the *aac*(6′)-Iaa gene was observed in all isolates using ResFinder databases. The *aac*(6′)-Iaa gene is a chromosomal-encoded aminoglycoside acetyltransferase that confers resistance to tobramycin and kanamycin aminoglycosides. The gene resistance profile varied among the isolates. In addition to antimicrobial resistance genes, we observed the gene *qac*EΔ1, which confers resistance to quaternary ammonium compounds (QAC), in 25 (26.6%) isolates. We also detected the presence of a sulfonamide resistance gene and the presence of the *intl*1 gene, a class 1 integron, in these isolates (Table 2). Among isolates that showed resistance to at least one antimicrobial, 64.9% (n = 37) were positive for *intI*1, but no isolates carried *intI*2 or *intI*3 genes. Class 1 integrons variable regions enclosed one or several gene cassettes containing *aad*A, *drf*A, *flo*R, *aac*(6′)-Ib, *ant*(2′′)-la, and *cml*A. Class 1 integrons were found in different proportions among species source: 78.6% (n = 11) in poultry, 61.1% (n = 22) in swine and 47.1% (n = 4) in cattle isolates (Table 3). The *sul*1 gene, which is often carried in the conserved sequence (3′ CS) of a class 1 integron, was missing in 11 isolates. Ten of these integrons were identified as In48, and carried a resistant gene cassette (*aac*(6)-Ib), the other one was classified as In192, positive for *Intl*1 and carried a *dfr*A15 cassette.

Point mutations

Seventeen isolates exhibited decreased resistance to ciprofloxacin (MIC ≥0.12 μg/ml). Fluoroquinolone-resistance genes were identified in 11 of those isolates. The remaining six isolates did not harbor any resistance genes; however, point mutations were detected in these six isolates. Four isolates showed a point mutation in the *gyr*A (D87N) and *par*C (T57S) genes, and the other two isolates had a mutation in only the *par*C (T57S) gene. Five isolates exhibited resistance to nalidixic acid without any specific quinolone resistance gene present, but in four of these five isolates there were point mutations in *gyr*A and *par*C genes and in only the *par*C gene for one isolate. Interestingly, all the isolates showed mutations in the *par*C gene regardless of phenotypic resistance to nalidixic acid or ciprofloxacin.

Relationship of antimicrobial susceptibility with antimicrobial resistance genes

The association of antimicrobial susceptibility with antimicrobial resistance genes is shown in Table 3. The least discordance among the animal isolates was seen for β-lactams and the most were seen for phenicols.

Antimicrobial resistance by animal species

Antimicrobial resistance varied across isolates from different animal species. Isolates from all animal species showed susceptibility to MEM. Isolates from cattle and swine showed resistance to all other antimicrobials in variable frequency. All poultry isolates were susceptible to AMC, FOX, CRO, AZM, CIP and NAL (Figure 2).

The percentage of isolates that were MDR varied among the different animal species. Sixty percent (30/50) of the isolates from swine were MDR; three were resistant to 12 antimicrobials and one was resistant to 13 antimicrobials, being possible XDR. Fewer isolates from cattle (5/24, 16.6%) and poultry (3/24, 12.5%) were MDR.

Plasmid typing

Antimicrobial resistance genes are often encoded on mobile genetic elements such as plasmids. In this study, 36 plasmid types were identified in 73 (77.7%) isolates. Plasmid profiles differed among each animal species. Thirty-four different plasmids were found among swine isolates, 14 among poultry isolates and 10 among cattle isolates. The most prevalent plasmid was ColRNAI, found in 60.6% of the study isolates: n = 20 (83.3%) in poultry, n = 31 (62%) in swine and n = 6 (30%) in cattle isolates. Other prevalent plasmids were Col440II, present in 35.1% of isolates, Col440I in 24.5% of isolates, RepA1pKPC-CAV1321 in 13.8% of isolates, IncHI2A and IncHI2 in 12.8% of isolates (75% in swine isolates) and others in lower frequency. The presence of the *mcr*-9.1 colistin resistance gene and the presence of the ESBL bla_{SHV-12} gene were correlated with the presence of the two plasmids IncHI2A and IncHI2.

TABLE 2 Antimicrobial resistance genes detected in the variable region of class 1 integrons among *Salmonella* Senftenberg isolates from the USA.

Source	Isolate ID	Integrase	Gene cassettes in the variable region	3' CS	IntFinder 1.0			
					Integron name	Identity (%)	Query/template length (bp)	Accession number
Swine	18–006979-062	*Intl*1	*aad*A2	*qac*EΔ1, *sul*1	In128	99.9	1,009/1,009	AF221903
Swine	18–006979-143	*Intl*1	-	*qac*EΔ1, *sul*1	-			
Swine	18–006979-166	*Intl*1	*ant*(2″)-Ia, *cml*A5	*qac*EΔ1, *sul*1	In571	98.3	3,016/2,999	AB285479
Swine	18–006979-167	*Intl*1	*aad*A1	*qac*EΔ1, *sul*1	-			
Swine	18–006979-173	*Intl*1	-	*qac*EΔ1, *sul*1	-			
Swine	18–012180-030	*Intl*1	*dfr*A15, *aad*A1, *aac*(3)-*VIa*	-	-			
Swine	18–012180-145	*Intl*1	*dfr*A19	*qac*EΔ1, *sul*1	-			
Swine	18–012180-261	*Intl*1	*aad*A7	*qac*EΔ1, *sul*1	In142	99.29	981/981	AF234167
Swine	18–012180-267	*Intl*1	-	*qac*EΔ1, *sul*1	-			
Swine	18–012180-282	*Intl*1	*ant*(2″)-Ia, *aad*A2, *aac*(3)-*VIa*	*qac*EΔ1, *sul*1	In293	100	1,531/1,531	DQ520939
Swine	18–012180-381	*Intl*1	-	*qac*EΔ1, *sul*1	-			
Swine	18–012180-398	*Intl*1	-	-	-			
Swine	18–012180-578	*Intl*1	*dfr*A1	*qac*EΔ1, *sul*1	In363	99.57	1,173/1,172	DQ402098
Swine	18–024125-014	*Intl*1	*aad*A24, *aac*(3)-*VIa*	*qac*EΔ1, *sul*1	In288	99.65	10,493/10,484	FJ621588
Swine	18–024125-062	*Intl*1	*aac*(6′)-Ib-cr, *arr*-3, *dfr*A27, *aad*A16	*qac*EΔ1, *sul*1	In1333	99.74	5,296/5,289	CP017059
Swine	18–024127-046	*Intl*1	*dfr*A12, *aad*A2	*qac*EΔ1, *sul*1	-			
Swine	18–024131-069	*Intl*1	*dfr*A12, *aad*A2	*qac*EΔ1, *sul*1	-			
Swine	18–038875-061	*Intl*1	*ant*(2″)-Ia, *cml*A5	*qac*EΔ1, *sul*1	In571	99.97	2,999/2,999	AB285479
Swine	18–038876-010	*Intl*1	-	*qac*EΔ1, *sul*1	-			
Swine	19–020610-021	*Intl*1	*ant*(2″)-Ia, *aad*A2	*qac*EΔ1, *sul*1	In293	100	1,531/1,531	DQ520939
Swine	19–020610-022	*Intl*1	*aad*A1	*qac*EΔ1, *sul*1	-			
Swine	19–020610-039	*Intl*1	-	*qac*EΔ1, *sul*1	-			
Cattle	18–006979-079	*Intl*1	aadA6, *aac*(3)-*VIa*	*qac*EΔ1, *sul*1	-			
Cattle	18–006979-295	*Intl*1	*aad*A12, *ant*(2″)-Ia, *cml*A5	*qac*EΔ1, *sul*1	-			
Cattle	18–012180-049	*Intl*1	*aac*(6′)-Ib4, *aad*A1	-	In48	98.83	1,032/1,029	AF439785
Cattle	18–038877-071	*Intl*1	-	*qac*EΔ1, *sul*1	-			
Poultry	18–006979-061	*Intl*1	*aac*(6′)-Ib4, *aad*A1	-	In48	98.83	1,032/1,029	AF439785
Poultry	18–012180-524	*Intl*1	*aac*(6′)-Ib4, *aad*A1	-	In48	98.83	1,032/1,029	AF439785
Poultry	18–024128-087	*Intl*1	*ant*(2″)-Ia, *aad*A2	*qac*EΔ1, *sul*1	In293	100	1,531/1,531	DQ520939
Poultry	18–038310-008	*Intl*1	*aad*A1, *aac*(3)-*VIa*	-	In790	99.9	1917/1917	JQ326986
Poultry	18–038310-026	*Intl*1	*aac*(6′)-Ib4, *aad*A1	-	In48	98.83	1,032/1,029	AF439785
Poultry	18–038873-015	*Intl*1	*aac*(6′)-Ib4, *aad*A1	-	In48	98.83	1,032/1,029	AF439785
Poultry	18–038873-077	*Intl*1	*aad*A2	-	In532	99.57	2,568/2,567	AB121039
Poultry	18–038876-062	*Intl*1	*aac*(6′)-Ib4, *aad*A1	-	In48	98.83	1,032/1,029	AF439785
Poultry	18–038877-021	*Intl*1	*aac*(6′)-Ib4, *aad*A1	-	In48	98.83	1,032/1,029	AF439785
Poultry	19–020610-061	*Intl*1	*aac*(6′)-Ib4, *aad*A1	-	In48	98.83	1,032/1,029	AF439785
Poultry	19–021046-006	*Intl*1	*aac*(6′)-Ib4, *aad*A1	-	In48	98.83	1,032/1,029	AF439785

(-) = not detected

10.3389/fmicb.2022.979790

10.3389/fmicb.2022.979790

TABLE 3 Correlation of phenotype susceptibility and genotype.

Drug classes	Phenotype: resistant (R)		Phenotype: susceptible (S)		Sensitivity (%)	Specificity (%)	PPV (%)	NPV (%)
	Genotype: R	Genotype: S	Genotype: R	Genotype: S				
Beta-lactams								
AMP	31	3	1	59	96.9	95.2	91.2	98.3
AMC	12	1	2	79	85.7	98.8	92.3	97.5
FOX	13	0	1	80	92.9	100	100	98.8
CRO	18	1	1	74	94.7	98.7	94.7	98.7
Phenicol								
CHL	21	4	0	69	100	94.5	84.0	100
Quinolones								
CIP	15	2	1	76	93.75	97.4	88.2	98.7
NAL	14	1	2	77	87.5	98.7	93.3	97.5
Aminoglycosides								
GEN	27	2	6	59	81.8	96.7	93.1	90.8
STR	39	3	3	49	92.9	94.2	92.9	94.2
Folate pathway inhibitors								
SUL	27	4	3	60	90.0	93.75	87.1	95.2
SXT	16	0	1	77	94.1	100	100	98.7
Tetracycline								
TET	36	4	1	53	97.3	92.9	90.0	98.1
Macrolide								
AZM	6	0	1	87	85.7	100	100	98.9

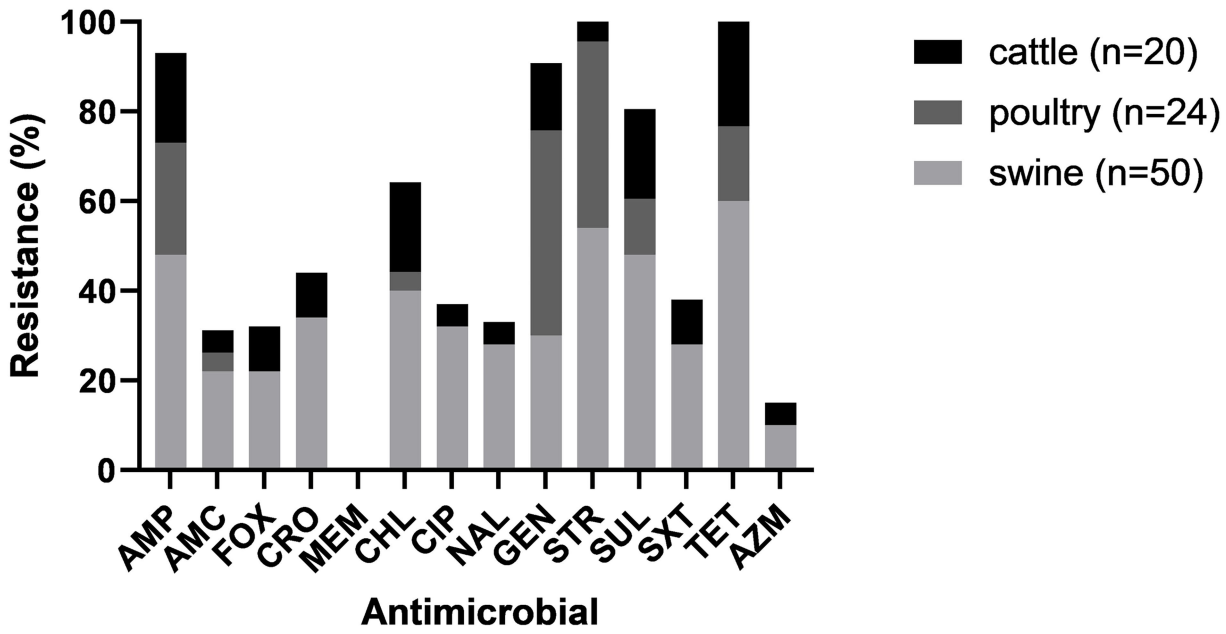

FIGURE 2
Antimicrobial resistance for each drug among cattle, poultry and swine.

MLST and phylogenetic relationships

Isolates were classified into two distinct sequence types (ST) based on MLST analysis from genome sequences. Ninety-two isolates (97.9%) belonged to ST14 and only two isolates (2.1%) belonged to ST185. Both isolates in ST185 were from cattle. ST14 and ST185 share no common alleles at any of the seven loci that define an allelic profile or ST by MLST analysis.

S. Senftenberg is a polyphyletic serovar. Phylogenetic analysis identified two distinct lineages of *S.* Senftenberg in this study that correlated with the MLST results. The smaller clade corresponded to ST185, and the majority of isolates corresponded to ST14 (Supplementary Figure S1).

The addition of closely related representative serotypes from NCBI shows that the two MLST types observed in this study are entirely distinct lineages; and in addition, a third lineage of *S.* Senftenberg which was not observed in this study, becomes visible with isolate NZ_CP007505. This suggests that the serotype designation may not represent a good indicator of the genetic relationships between strains.

The isolates corresponding to ST14 showed a cluster of nine isolates that are significantly divergent from the rest of the isolates. This cluster has accumulated 137 SNPs since sharing a most recent common ancestor with the nearest relatives. Of interest was the presence of common resistance characteristics in this cluster, with eight isolates from poultry and one isolate from cattle showing a similar antimicrobial resistance pattern, resistance genes, class 1 integron, and plasmid profile (Supplementary Figure S2; Table 4). The well differentiated cluster within the ST14 group showed an average distance of 30.8 SNPs (range of 22 to 44 SNP) from a common ancestor.

Discussion

A previous study of animal and human isolates in the USA (Stepan et al., 2011) showed that human strains of *S.* Senftenberg were susceptible to all of the antimicrobials tested, whereas the animal isolates showed a range of resistance, with most isolates being resistant to two or more antimicrobials.

In this study, isolates from swine and cattle showed resistance to 13 antimicrobials in different frequencies, whereas poultry isolates showed resistance to only six antimicrobials tested; these results differ from Stepan et al. (Stepan et al., 2011) where the rate of resistance to antimicrobials was similar across the host species (swine, cattle and poultry). Other important findings of our study were the presence of three isolates from swine resistant to 12 antibiotics and one resistant to 13 antibiotics.

In this study we found two sequence types associated with *S.* Senftenberg (ST14 = 97.8% and ST185 = 2.1%), whereas Stepan et al. (Stepan et al., 2011) found three sequence types (ST14 = 85.7%, ST185 = 13.2% and ST145 = 1%), with ST145 only found in one isolate from swine. The two lineages identified in our study and the branches within the lineage corresponding to ST14 did not show host specificity. This information, combined with the frequent isolation of this serotype from feed, may indicate that the serotype is more likely to be introduced from a common external source rather than circulating long-term within animal populations. In a study in China, El Ghany et al. (El Ghany et al., 2016) identified two phylogenetically distinct clades of *S.* Senftenberg by SNP analysis. Variations were in the *Salmonella* pathogenicity island (SPI)-1 and SPI-2 that exhibited distinct biochemical and phenotypic signatures. Clade 1 isolates comprised three sequence types: ST185, ST217, and ST1751, being single or double locus variants relative to one another. In contrast, clade 2 isolates included only ST14. In our study, the two distinct lineages also differ in the ST. Even though there are other STs observed in other datasets, these STs are single or double locus variants relative to one another.

We observed that there are other serotypes that fall between the two lineages, indicating that they are two completely independent lineages in *S.* Senftenberg and not a single serotype that diverged over time.

As may be expected based on the phylogenetic diversity, resistance patterns among *S.* Senftenberg isolates differ significantly among isolates. In our study, the most common resistance profile was AMP, GEN, STR (n = 5 isolates), whereas Stepan et al. (Stepan et al., 2011) found STR, TET, SXT the most common (n = 4 isolates).

In Veeraraghavan et al. study (Veeraraghavan et al., 2019) beta-lactam resistance was associated with the presence of the $bla_{\text{TEM-1}}$, $bla_{\text{OXA-9}}$, $bla_{\text{CMY-2}}$, and $bla_{\text{NDM-1}}$ genes, resistance to aminoglycosides was associated with five genes, namely *aac*(6′)-Ia, *aac*(6′)-Ib, *aph*(3″)-Ib, *aph*(6′)-Ib and *ant*(2″)-Ia, and sulfonamide resistance was associated with the *sul*1 and *sul*2 genes and resistance to chloramphenicol with the *flor*R gene. In our study, we found $bla_{\text{TEM-1}}$, $bla_{\text{CMY-2}}$ and $bla_{\text{SHV-12}}$. The $bla_{\text{SHV-12}}$ gene, an ESBL that shows resistance to ceftriaxone, was found in five isolates from swine. These five isolates also carried other antimicrobial genes against beta-lactams, aminoglycosides, sulfonamides, tetracyclines and rifamycin: $bla_{\text{TEM-1}}$, *aac*(3)-II, *aac*(6')-IIc, *aac*(6')-Ib, *sul*1, *sul*2, *tet*D, *arr*-269927220, and all of them were positive for IncHI2A, IncHI2, RepA pKPC-CAV1321 plasmids. IncHI2 plasmid replicon has been reported to encode $bla_{\text{SHV-12}}$, the most predominant ESBL within *Enterobacteriaceae* (Liakopoulos et al., 2018), and can be transfer among diverse bacterial population. Expanded monitoring of *Salmonella* from swine for this gene would be appropriate to evaluate the extent of the gene in the U.S. swine population to determine if swine are a significant reservoir of ceftriaxone-resistance. In general, both *aph*(3″)-Ib and *aph*(6)-Id genes were predominantly found in streptomycin-resistant isolates in other MDR *S. enterica* (Cohen et al., 2020) and we found them in 29.8% isolates. Additionally, these 2 genes are found together in an HI type plasmid (McMillan et al., 2019). The *acc*(6′)-Iaa gene that confers resistance to tobramycin, kanamycin and amikacin, and that was found in all our isolates, was previously found in *S.* Typhimurium and *S.* Infantis; but it seems to have no clinical significance and evolutionary advantage (Jovčić et al., 2020). In our study *sul*1 and *sul*2 genes were also associated

10.3389/fmicb.2022.979790

TABLE 4 Antimicrobial resistance profile, integrons and plasmids in the ST14 differentiated group of 9 isolates.

ID isolate	Source	State	Year	Antimicrobial Susceptibility test	Antimicrobial resistance genes	Integrons	Plasmids
19–021046-006	Poultry	IA	2017	AMP, GEN, STR	bla_{TEM-1}, *aac*(6′)-Ib4, *aad*A1, *acc*(6′)-laa	*Intl1*, *aac*(6′)-Ib4, *aad*A1	Col440II, ColRNAI, IncFIB, IncFII.
18–006979-061	Poultry	MO	2014	AMP, GEN, STR	bla_{TEM-1}, *aac*(6′)-Ib4, *aad*A1, *acc*(6′)-laa	*Intl1*, *aac*(6′)-Ib4, *aad*A1	Col440II, Col440I, ColRNAI, IncFIB, IncFII.
18–038873-015	Poultry	MO	2016	GEN, STR	*aac*(6′)-Ib4, *aad*A1, *acc*(6′)-laa	*Intl1*, *aac*(6′)-Ib4, *aad*A1	Col440II, ColRNAI, IncFIB, IncFII.
18–038877-021	Poultry	IA	2017	AMP, GEN, STR	bla_{TEM-1}, *aac*(6′)-Ib4, *aad*A1, *acc*(6′)-laa	*Intl1*, *aac*(6′)-Ib4, *aad*A1	Col440II, ColRNAI, IncFIB, IncFII.
18–024128-065	Poultry	IN	2016	GEN	*acc*(6′)-laa	Not found	Col440II, ColRNAI
18–038310-026	Poultry	IA	2016	GEN, STR	*aac*(6′)-Ib4, *aad*A1	*Intl1*, *aac*(6′)-Ib4, *aad*A1	Col440II, ColRNAI, IncFIB, IncFII.
19–020610-061	Poultry	AR	2017	AMP, GEN, STR	bla_{TEM-1}, *aac*(6′)-Ib4, *aad*A1, *acc*(6′)-laa	*Intl1*, *aac*(6′)-Ib4, *aad*A1	Col440II, ColRNAI, IncFIB, IncFII.
18–012180-524	Poultry	MO	2015	AMP, AMC, GEN	bla_{TEM-1}, *aac*(6′)-Ib4, *aad*A1, *acc*(6′)-laa	*Intl1*, *aac*(6′)-Ib4, *aad*A1	Col440II, ColRNAI, IncFIB, IncFII.
18–012180-049	Cattle	IN	2015	AMP, GEN, STR	bla_{TEM-1}, *aac*(6′)-Ib4, *aad*A1, *acc*(6′)-laa	*Intl1*, *aac*(6′)-Ib4, *aad*A1	Col440II, Col440I, ColpVC

with sulfonamide resistance, and *flo*R gene the most prevalent associated with chloramphenicol resistance, although other genes also were found.

In an XDR *S.* Senftenberg isolate from a human clinical case in India (Veeraraghavan et al., 2019), fluoroquinolone resistance was attributed to substitutions in the *gyr*A (S83Y, D87G) and *par*C (S80I) genes. The *par*C substitution appears to be a characteristic mutation present in quinolone-resistant *S.* Senftenberg isolates from human cases (Whichard et al., 2007). In the Wichard study (Whichard et al., 2007), all *S.* Senftenberg isolates had *par*C mutations (T57S and S80I). We also found *par*C mutations in all isolates; but in contrast to the human isolates, we found S83S and D87N mutations in *gyr*A, and only the T57S mutation in *par*C in the animal isolates. The widespread presence of *par*C mutations without corresponding resistance does not appear to be specific to *S.* Senftenberg strains. One study of serotype Paratyphi (Qian et al., 2020) showed *par*C mutations in all isolates (n = 8) with 7 isolates being susceptible to ciprofloxacin. This clearly illustrates that the presence of mutations does not necessarily correspond to phenotypic resistance (Sáenz et al., 2003). On the other hand, one study in nontyphoidal *S. enterica* isolated from pigs in Thailand showed resistance to fluoroquinolones, either in the presence or absence of genes and/or mutations, and *par*C mutation (T57) was found in 62.4% of the isolates (Poomchuchit et al., 2021).

When we compared our *S.* Senftenberg results with a study that evaluated antimicrobial susceptibility patterns found in other serovars isolated from poultry (Cohen et al., 2020), the percentage of MDR in *S.* Senftenberg from poultry (12.5%) was higher than *S.* Orion (10%) and lower than *S.* Kentucky (97.4%), *S.* Hadar (80%), *S.* Java (75%), *S.* Infantis (60%), *S.* Bredeney (50%), *S.* Montevideo (40%), *S.* Newport (30%), *S.* Virchow (30%), *S.* Blockeley (27.3%), *S.* Muenchen (25%). In MDR swine *Salmonella* isolates, Argüello et al. (Argüello et al., 2018) demonstrated the importance of class 1 integrons and certain genes. In this study, 60% (n = 30) of isolates from swine origin showed MDR, and in 70% (n = 21) of these isolates we observed the presence of a class 1 integron.

The number of plasmids did not correlate with MDR or XDR, as we found isolates with as many as seven or eight plasmids that were resistant to only one or two antibiotics and isolates with only one plasmid with resistance to seven antibiotics.

Of the other genes found in *S.* Senftenberg strains, the presence of the *mcr*-9 gene that confers resistance to colistin was of interest. This is a novel *mcr* homologue detected in MDR colistin-susceptible *Salmonella* Typhimurium isolated from a patient in the USA in 2010 (Carroll et al., 2019). The *mcr*-9 gene was shown to be capable of conferring phenotypic resistance to colistin in numerous genera of *Enterobacteriaceae*, and it is harbored in IncHI2 and/or IncHI2A replicons (Carroll et al., 2019). The Sensititre CMV4AGNF plate did not include colistin, so we were unable to determine if this gene was expressed in the *S.* Senftenberg isolates. However, a set of 57 *Salmonella* isolates, including four *S.* Senftenberg swine isolates used in the current study, were positive for *mcr*-9 when tested using the Sensititre GNX3F plate that contains colistin (unpublished data). Of

the 57 isolates, only one had an MIC of 2 ng/μl (resistant), and the remaining 56 had an MIC of 1 ng/μl or lower (susceptible), with the four isolates from this current study having MIC values equal to or lower than 0.5 ng/μl. These results agree with the report of Tyson et al. (Tyson et al., 2020) affirming that the *mcr*-9 gene in *Salmonella* is not associated with colistin resistance in the USA. All isolates positive for this gene in our study carried two plasmids (IncHI2A and IncHI2), while all other isolates were negative for these two plasmids, so we could associate the presence of these plasmids with the presence of the *mcr*-9 gene. In other studies, the *mcr*-1 gene was found in IncHI2/ST3, IncI2, and IncX4 plasmids in isolates from animals and humans (Stefaniuk and Tyski, 2019).

In addition to antimicrobial resistance genes, antiseptic resistance genes are important because disinfectants are used in farm environments. Benzalkonium chloride is a surface-active QAC (quaternary ammonium compound), and it is used as a farm disinfectant. The *qac*EΔ1 is frequently present in *E. coli* and other enteric bacteria (Zou et al., 2014). In this study 25 isolates carried the *qac*EΔ1 gene that has been identified in mobile genetic elements. The *qac*E and *qac*EΔ1 genes are located on an integron, a *qac*EΔ1 represents a disrupted form of *qac*E that evolved as a result of the insertion of a DNA segment near the 3′ end of the *qac*E gene carrying a *sul*1 sulfonamide resistance determinant (Paulsen et al., 1993). All but one of the *S.* Senftenberg isolates positive for *qac*EΔ1 gene carried the *sul*1 gene. The one exception carried the *sul*2 and *sul*3 genes. We also detected the presence of class 1 integrons in the *qac*EΔ1 positive isolates. Class 1 integrons are associated with an *Intl*1 integrase in the 5′ conserved sequence (CS) and with a 3′ CS conferring resistance to antibiotics (sulfonamides) and bactericidal compounds (quaternary ammonium) of the integron (Deng et al., 2015). Class 1 integrons have previously been detected in *S.* Senftenberg (Vo et al., 2006), but to our knowledge, there are no reports of class 2 or class 3 integrons in this serovar. We found 10 isolates harboring a class 1 integron homologous to the In48 integron (98.83%) that carries the aminoglycoside 6'-N-acetyltransferase (*aac*A4) gene. In our isolates, this integron carried the aminoglycoside N-acetyltransferase *aac*(6′)-Ib4 gene (*aac*(6′)-Ib allele) and the *aad*A1 gene. The frequent use of QAC may facilitate resistance to disinfectants, and QACs may serve as important selective agents in MDR pathogens (Sinwat et al., 2021). In the present study, all *S.* Senftenberg isolates carrying the *qac*EΔ1 gene were MDR.

Concordance between the presence of antimicrobial resistance genes and phenotypic resistance profiles were seen in 98.1% of isolates for the antimicrobials tested. The presence of resistance genes do not necessarily confer phenotypic resistance, and occasionally, an isolate will display antimicrobial resistance without the presence of a known resistance gene (Piddock, 2016). The presence or absence of resistance genes is not enough for the phenomenon of antimicrobial resistance. Mechanisms such as enzyme activation, target modification or protection, regulation of gene expression, or changes in the cell wall can play an important role in the resistance of antimicrobials (Paudyal et al., 2019).

Conclusion

This study provided an analysis of retrospective data of *Salmonella* Senftenberg and information about the antimicrobial susceptibility and genomic characteristics in diagnostic isolates of *S.* Senftenberg from production animals in the USA. This study reports the genotype-phenotype homogeneity and variability of *S.* Senftenberg of animal origin. The ability of *S.* Senftenberg to persist in the environment, to cause disease in various animal species, to be a potential risk of transmission to humans and to harbor resistance to critical antimicrobial and mobile elements capable of dissemination of acquired resistance genes makes *S.* Senftenberg an important public health pathogen. In this study we found that 39.4% of the isolates tested displayed multidrug resistance, and four isolates were potentially extensively drug resistant. This has important implications for both animal and human health, due to possible transmission of MDR bacteria from animal to animal or animal to human (zoonotic), and the difficulty in treatment of resistant bacteria. These data highlight the need to strengthen surveillance to detect the prevalence and transmission of nontyphoidal *Salmonella* species because of the emergence of MDR strains. It is critical to identify the emergence of these strains as early as possible to avoid further dissemination and establish control procedures. This data is useful for future studies on *S.* Senftenberg and to further understand this pathogen as few studies exist on the antimicrobial susceptibility, genotypic profiles and genetic diversity of *Salmonella* Senftenberg of animal origin.

Data availability statement

The datasets presented in this study can be found in online repositories. The names of the repository/repositories and accession number(s) can be found at: https://www.ncbi.nlm.nih.gov/, bioproject/PRJNA785813.

Author contributions

MS and LS: conceptualization. MS and JH: methodology, formal analysis, and visualization. JH: software, formal analysis and validation. MS: investigation and writing – original draft preparation. LS: resources, supervision, project administration and funding acquisition. MS, JH, BM, TM and LS: writing – review and editing. LS: Supervision. All authors contributed to the article and approved the submitted version.

Funding

This project was supported in part by an appointment to the Research Participation Program at the Animal and Plant Health Inspection Service, United States Department of Agriculture, administered by the Oak Ridge Institute for Science and Education

through an interagency agreement between the US Department of Energy and USDA APHIS.

Acknowledgments

We are grateful to Claudia Perea for assistance with the phylogenetic trees.

Conflict of interest

The authors declare that the research was conducted in the absence of any commercial or financial relationships that could be construed as a potential conflict of interest.

Publisher's note

Supplementary material

The Supplementary material for this article can be found online at: https://www.frontiersin.org/articles/10.3389/fmicb.2022.979790/full#supplementary-material

References

Argüello, H., Guerra, B., Rodríguez, I., Rubio, P., and Carvajal, A. (2018). Characterization of antimicrobial resistance determinants and class 1 and class 2 Integrons in *Salmonella enterica* spp., multidrug-resistant isolates from pigs. *Genes (Basel)* 9:256. doi: 10.3390/genes9050256

Boumart, Z., Roche, S. M., Lalande, F., Virlogeux-Payant, I., Hennequet-Antier3, C., Menanteau, P., et al. (2012). Heterogeneity of Persistence of *Salmonella enterica* Serotype Senftenberg strains could explain the emergence of this serotype in poultry flocks. *PLoS One* 7:e35782. doi: 10.1371/journal.pone.0035782

Carattoli, A., Zankari, E., García-Fernández, A., Voldby Larsen, M., Lund, O., Villa, L., et al. (2014). In silico detection and typing of plasmids using PlasmidFinder and plasmid multilocus sequence typing. *Antimicrob. Agents Chemother.* 58, 3895–903. doi: 10.1128/AAC.02412-14

Carroll, L. M., Gaballa, A., Guldimann, C., Sullivan, G., Henderson, L. O., and Wiedmann, M. (2019). Identification of novel mobilized colistin resistance gene *mcr*-9 in a multidrug-resistant, colistin-susceptible *Salmonella enterica* serotype Typhimurium isolate. *MBio* 10, e00853–e00819. doi: 10.1128/mBio.00853-19

Center for Genomic Epidemiology (1998). Technical university of Denmark, Kongens. Lyngby, Denmark. https://cge.cbs.dtu.dk/services/IntFinder-1.0/ (Accessed April 2022).

Centers for disease Control and Prevention (2010). Multistate Outbreak of human *Salmonella* Montevideo infections (final update). Available at: https://www.cdc.gov/Salmonella/2010/montevideo-5-4-2010.html

Centers for Disease Control and Prevention (2016). Multistate outbreak of *Salmonella* Montevideo and *Salmonella* Senftenberg infections linked to wonderful pistachios (final update). Available at: https://www.cdc.gov/Salmonella/montevideo-03-16/index.html

Centers for Disease Control and Prevention, National Center for Emerging and Zoonotic Infectious Diseases (NCEZID), Division of Foodborne, Waterborne, and Environmental Diseases (DFWED) (2022). *Salmonella* Outbreak Linked to Peanut Butter. Available at: https://www.cdc.gov/Salmonella/senftenberg-05-22/index.html

Cohen, E., Davidovich, M., Rokney, A., Valinsky, L., Rahav, G., and Gal-Mor, O. (2020). Emergence of new variants of antibiotic resistance genomic islands among multidrug-resistant *Salmonella enterica* in poultry. *Environ. Microbiol.* 22, 413–432. doi: 10.1111/1462-2920.14858

Deng, Y., Bao, X., Ji, L., Chen, L., Liu, J., Miao, J., et al. (2015). Resistance integrons: class 1, 2 and 3 integrons. *Ann. Clin. Microbiol. Antimicrob.* 14:1. doi: 10.1186/s12941-015-0100-6

Doyle, M. E., and Mazzotta, A. S. (1999). Review of studies on the thermal resistance of *Salmonellae*. *J. Food Prot.* 63, 779–795. doi: 10.4315/0362-028x-63.6.779

Dunbar, S. A., Ritchie, V. B., Hoffmeyer, M. R., Rana, G. S., and Zhang, H. (2015). Luminex(®) multiplex bead suspension arrays for the detection and serotyping of *Salmonella* spp. *Methods Mol. Biol.* 1225, 1–27. doi: 10.1007/978-1-4939-1625-2_1

El Ghany, M. A., Shi, X., Li, Y., Ansari, H. R., Hill-Cawthorne, G. A., Ho, Y. S., et al. (2016). Genomic and phenotypic analyses reveal the emergence of an atypical *Salmonella enterica* Serovar Senftenberg variant in China. *J. Clin. Microbiol.* 54, 2014–2022. doi: 10.1128/JCM.00052-16

Feldgarden, M., Brover, V., Haft, D. H., Prasad, A. B., Slotta, D. J., Tolstoy, I., et al. (2019). Validating the AMRFinder tool and resistance gene database by using antimicrobial resistance genotype-phenotype correlations in a collection of isolates. *Antimicrob. Agents Chemother.* 63, e00483–e00419. doi: 10.1128/AAC.00483-19, published correction appears in *Antimicrob Agents Chemother*. 64(4):e00361-20

Gardner, S. N., Slezak, T., and Hall, B. G. (2015). kSNP3.0: SNP detection and phylogenetic analysis of genomes without genome alignment or reference genome. *Bioinformatics* 31, 2877–2878. doi: 10.1093/bioinformatics/btv271

Grimont, P. A. D., and Weill, F. X. (2007). *Antigenic Formulae of the Salmonella Serovars, 9th Edn*, Geneva: World Health Organization.

Haendiges, J., Davidson, G. R., Pettengill, J. B., Reed, E., Ramachandran, P., Blessington, T., et al. (2019). Genomic evidence of environmental and resident *Salmonella* Senftenberg and Montevideo contamination in the pistachio supply-chain. *PLoS One* 16:e0259471. doi: 10.1371/journal.pone.0259471

Hassan, R., Whitney, B., Williams, D. L., Holloman, K., Grady, D., Thomas, D., et al. (2019). Multistate outbreaks of *Salmonella* infections linked to imported Maradol papayas – United States, December 2016–September 2017. *Epidemiol. Infect.* 147, e265–e268. doi: 10.1017/S0950268819001547

Hendriksen, R. S., Joensen, K. G., Lukwesa-Musyani, K., Leekitcharoenphon, A. P., Nakazwe, R., Aarestrup, F. M., et al. (2013). Extremely drug-resistant *Salmonella enterica* Serovar Senftenberg infections in patients in Zambia. *J. Clin. Microbiol.* 51, 284–286. doi: 10.1128/JCM.02227-12

Jovčić, B., Novović, K., Filipić, B., Velhner, M., Todorović, D., Matović, K., et al. (2020). Genomic characteristics of Colistin-resistant *Salmonella enterica* subsp. *enterica* Serovar Infantis from poultry farms in the republic of Serbia. *Antibiotics (Basel).* 9:886. doi: 10.3390/antibiotics9120886

Liakopoulos, A., van der Goot, J., Bossers, A., Betts, J., Brouwer, M., Kant, A., et al. (2018). Genomic and functional characterisation of IncX3 plasmids encoding bla_{SHV-12} in *Escherichia coli* from human and animal origin. *Sci. Rep.* 8:7674. doi: 10.1038/s41598-018-26073-5

Li, X., Bethune, L. A., Jia, Y., Lovell, R. A., Proescholdt, T. A., Benz, S. A., et al. (2012). Surveillance of *Salmonella* prevalence in animal feeds and characterization of the *Salmonella* isolates by serotyping and antimicrobial susceptibility. *Foodborne Pathog. Dis.* 9, 692–698. doi: 10.1089/fpd.2011.1083

Loaiza, K., Ortega-Paredes, D., Kristofer Johansson, M. H., and Ferrer Florensa, A. (2020). IntFinder: a freely-available user-friendly web tool for detection of class 1 integrons in next-generation sequencing data using k-mer alignment. ECCMID 2020. Available at: https://www.escmid.org/escmid_publications/eccmid_abstract_book

Magiorakos, A., Srinivasan, R. B., Carey, Y., Carmeli, M. E., Falagas, C. G., Giske, S., et al. (2012). Multidrug-resistant, extensively drug-resistant, and pandrug-resistant bacteria: an international expert proposal for interim standard definitions for acquired resistance. *Clin. Microbiol. Infect.* 18, 268–281. doi: 10.1111/j.1469-0691.2011.03570.x

McDermott, P. F., Tyson, G. H., Kabera, C., Chen, Y., Li, C., Folster, J. P., et al. (2016). Whole-genome sequencing for detecting antimicrobial resistance in Nontyphoidal *Salmonella*. *Antimicrob. Agents Chemother.* 60, 5515–5520. doi: 10.1128/AAC.01030-16

McMillan, E. A., Gupta, S. K., Williams, L. E., Jove, T., Hiott, L. M., Woodley, T. A., et al. (2019). Antimicrobial resistance genes, cassettes, and plasmids present in *Salmonella enterica* associated with United States food animals. *Front. Microbiol.* 10:832. doi: 10.3389/fmicb.2019.00832

Nair, V. T., Venkitanarayanan, D. K., and Kollanoor Johny, A. (2018). Antibiotic-resistant *Salmonella* in the food supply and the potential role of antibiotic alternatives for control. *Foods (Basel, Switzerland).* 7:167. doi: 10.3390/foods7100167

Paudyal, N., Pan, H., Elbediwi, M., Zhou, X., Peng, X., Li, X., et al. (2019). Characterization of *Salmonella* Dublin isolated from bovine and human hosts. *BMC Microbiol.* 19:226. doi: 10.1186/s12866-019-1598-0

Paulsen, I. T., Littlejohn, T. G., Rådström, P., Sundström, L., Sköld, O., Swedberg, G., et al. (1993). The 3′ conserved segment of integrons contains a gene associated with multidrug resistance to antiseptics and disinfectants. *Antimicrob. Agents Chemother.* 37, 761–768. doi: 10.1128/AAC.37.4.761

Pedersen, T. B., Olsen, J. E., and Bisgaard, M. (2008). Persistence of *Salmonella* Senftenberg in poultry production environments and investigation of its resistance to desiccation. *Avian Pathol.* 37, 421–427. doi: 10.1080/03079450802216561

Piddock, L. J. (2016). Assess drug-resistance phenotypes, not just genotypes. *Nat. Microbiol.* 1, 16120. doi: 10.1038/nmicrobiol.2016.120

Poomchuchit, S., Kerdsin, A., Chopjitt, P., Boueroy, P., Hatrongjit, R., Akeda, Y., et al. (2021). Fluoroquinolone resistance in non-typhoidal *Salmonella enterica* isolated from slaughtered pigs in Thailand. *J. Med. Microbiol.* 70:001386. doi: 10.1099/jmm.0.001386

Qian, H., Cheng, S., Liu, G., Tan, Z., Dong, C., Bao, J., et al. (2020). Discovery of seven novel mutations of *gyr*B, *par*C and pare in *Salmonella* Typhi and Paratyphi strains from Jiangsu Province of China. *Sci. Rep.* 10:7359. doi: 10.1038/s41598-020-64346-0

Roer, L., Hendriksen, R. S., Leekitcharoenphon, P., Lukjancenko, O., Sommer, K., Hasman, H., et al. (2016). Is the evolution of *Salmonella enterica* subsp. *enterica* linked to restriction-modification systems? *mSystems* 1, e00009–e00016. doi: 10.1128/mSystems.00009-16

Sáenz, Y., Zarazaga, M., Briñas, L., Ruiz-Larrea, F., and Torres, C. (2003). Mutations in *gyr*A and *par*C genes in nalidixic acid-resistant *Escherichia coli* strains from food products, humans and animals. *J. Antimicrob. Chemother.* 51, 1001–1005. doi: 10.1093/jac/dkg168

Sinwat, N., Witoonsatian, K., Chumsing, S., Suwanwong, M., Kankuntod, S., Jirawattanapong, P., et al. (2021). Antimicrobial resistance phenotypes and genotypes of *Salmonella* spp. isolated from commercial duck meat production in Thailand and their minimal inhibitory concentration of disinfectants. *Microb. Drug Resist.* 27, 1733–1741. doi: 10.1089/mdr.2020.0230. Epub 2021 Jun 1

Stamatakis, A. (2014). RAxML version 8: a tool for phylogenetic analysis and post-analysis of large phylogenies. *Bioinformatics* 30, 1312–1313. doi: 10.1093/bioinformatics/btu033

Stefaniuk, E. M., and Tyski, S. (2019). Colistin resistance in Enterobacterales strains – A current view. *Pol. J. Microbiol.* 68, 417–427. doi: 10.33073/pjm-2019-055

Stepan, R. M., Sherwood, J. S., Peterman, S. R., and Logue, C. M. (2011). Molecular and comparative analysis of *Salmonella enterica* Senftenberg from humans and animals using PFGE, MLST and NERMS. *BMC Microbiol.* 11:153. doi: 10.1186/1471-2180-11-153

Stokes, H. W., and Gillings, M. R. (2011). Gene flow, mobile genetic elements and the recruitment of antibiotic resistance genes into gram-negative pathogens. *FEMS Microbiol. Rev.* 35, 790–819. doi: 10.1111/j.1574-6976.2011.00273.x

Switt, A. I. M. D. (2019). *Salmonella* Senftenberg. https://confluence.cornell.edu.

Tyson, G. H., Li, C., Hsu, C. H., Ayers, S., Borenstein, S., Mukherjee, S., et al. (2020). The *mcr*-9 gene of *Salmonella* and *Escherichia coli* is not associated with Colistin resistance in the United States. *Antimicrob. Agents Chemother.* 64, e00573–e00520. doi: 10.1128/AAC.00573-20

US Food and Drug Administration (2014). FDA investigation summary—multistate outbreak of *Salmonella* Senftenberg infections associated with pistachios from a California roaster. Available at: http://wayback.archive-it.org/7993/20171114154922/, https://www.fda.gov/Food/RecallsOutbreaksEmergencies/Outbreaks/ucm386377.htm.

US Food and Drug Administration (2021). Interpretative Criteria for Susceptibility Testing. Available at: https://fda.gov/animal-veterinary/national-antimicrobial-resistance-monitoring-system/resources (Accessed August 2021).

Veeraraghavan, B., Jacob, J. J., Prakash, J. A. J., Pragasam, A. K., Neeravi, A., Narasimman, V., et al. (2019). Extensive drug resistant *Salmonella enterica* serovar Senftenberg carrying bla_{NDM} encoding plasmid p5558 (IncA/C) from India. *Pathogens Global Health* 113, 20–26. doi: 10.1080/20477724.2019.1574112

Vo, A. T. T., van Duijken, E., Fluit, A. C., Wannet, W. J. B., Verbruggen, A. J., Maas, H. M. E., et al. (2006). Antibiotic resistance, integrons and *Salmonella* genomic island 1 among non-typhoidal *Salmonella* serovars in The Netherlands. *Int. J. Antimicrob. Agents* 28, 172–179. doi: 10.1016/j.ijantimicag.2006.05.027

Whichard, J. M., Gay, K., Stevenson, K. E., Joyce, K. J., Cooper, K. L., Omondi, M., et al. (2007). Human *Salmonella* and concurrent decreased susceptibility to quinolones and extended-Spectrum Cephalosporins. *Emerg. Infect. Dis.* 13, 1681–1688. doi: 10.3201/eid1311.061438

Yasir, M., Farman, M., Shah, M. W., Jiman-Fatni, A. A., Othman, N. A., Almasaudi, S. B., et al. (2020). Genomic and antimicrobial resistance genes diversity in multidrug CTX-M-positive isolates of *Escherichia coli* at a health care facility in Jeddah. *J. Infect. Public Health* 13, 94–100. doi: 10.1016/j.jiph.2019.06.011

Zankari, E., Allesøe, R., Joensen, F. G., Cavaco, L. M., Lund, O., and Aarestrup, F. M. (2017). PointFinder: a novel web tool for WGS-based detection of antimicrobial resistance associated with chromosomal point mutations in bacterial pathogens. *J. Antimicrob. Chemother.* 72, 2764–2768. doi: 10.1093/jac/dkx217

Zankari, E., Hasman, H., Cosentino, S., Vestergaard, M., Rasmussen, S., Lund, O., et al. (2012). Identification of acquired antimicrobial resistance genes. *J. Antimicrob. Chemother.* 67, 2640–2644. doi: 10.1093/jac/dks261

Zou, L., Meng, J., McDermott, P. F., Wang, F., Yang, Q., Cao, G., et al. (2014). Presence of disinfectant resistance genes in *Escherichia coli* isolated from retail meats in the USA. *J. Antimicrob. Chemother.* 69, 2644–2649. doi: 10.1093/jac/dku197

frontiers | Frontiers in Microbiology

TYPE Opinion
PUBLISHED 04 November 2022
DOI 10.3389/fmicb.2022.1039188

OPEN ACCESS

EDITED BY
Svetlana Khaiboullina,
University of Nevada, Reno,
United States

REVIEWED BY
Punit Kaur,
All India Institute of Medical
Sciences, India

*CORRESPONDENCE
Manish Kumar
manish@south.du.ac.in
Neelja Singhal
neelja@south.du.ac.in

SPECIALTY SECTION
This article was submitted to
Infectious Agents and Disease,
a section of the journal
Frontiers in Microbiology

RECEIVED 07 September 2022
ACCEPTED 17 October 2022
PUBLISHED 04 November 2022

CITATION
Garg A, Singhal N and Kumar M (2022)
Investigating the eukaryotic host-like
SLiMs in microbial mimitopes and their
potential as novel drug targets for
treating autoimmune diseases.
Front. Microbiol. 13:1039188.
doi: 10.3389/fmicb.2022.1039188

Investigating the eukaryotic host-like SLiMs in microbial mimitopes and their potential as novel drug targets for treating autoimmune diseases

Anjali Garg, Neelja Singhal* and Manish Kumar*

Department of Biophysics, University of Delhi South Campus, New Delhi, India

KEYWORDS

motif mimicry, short linear motifs (SLiMs), autoimmunity, mimitopes, drug targets

Introduction

The host genetics play an important role in the induction of autoimmune response against self-antigens however; several epidemiological and molecular evidences suggest microbial pathogens (viruses and bacteria) are the principal environmental triggers of autoimmunity (Fujinami, 2001; Ascherio and Munger, 2007; Libbey and Fujinami, 2010; Tarakhovsky and Prinjha, 2018; Lester et al., 2019). Reportedly, four main criteria have been associated with molecular mimicry and the underlying human disease, (i) epidemiological evidence associating a pathogen with a disease, (ii) presence of antibodies and/or immune cells against the specific antigens related with the disease, (iii) cross-reactivity of antibodies or immune cells of the host with microbial antigens and, (iv) reproduction by the antigen of the disease process *in vivo* or *in vitro* (Ang et al., 2004; Johnson et al., 2017).

Microbes can exhibit four types of molecular mimicry with the host proteins, (i) sequential or structural similarities with the proteins or protein-domains, (ii) similarities with the protein-structures without sequence homology, (iii) architectural similarities with the binding surfaces without sequence homology (interface mimicry) and, (iv) similarities with the short linear motifs (SLiMs) of the proteins (motif mimicry) (Xue et al., 2014; Dolan et al., 2015). SLiMs are short stretches of amino acids (3–10 amino acids) which are functionally diverse and mediate various signaling and protein-protein interactions (PPIs) (Davey et al., 2012; Dinkel et al., 2014; Garg et al., 2022). One another important functional component of a protein is molecular recognition features (MoRFs) 5–25 amino acid long. They are present in the structurally disordered region of protein hence disordered. But once MoRFs binds to the their partner, they attain a well-developed structure (Vacic et al., 2007; Yan et al., 2016). Reportedly, several viruses and bacteria propagate and sustain themselves inside the host by mimicking SLiMs of the host proteins (Sámano-Sánchez and Gibson, 2020).

PPIs and cell signaling play a pivotal role in the functioning of cellular life. Hence, mimicry of the host proteins involved in PPIs and cell signaling greatly helps microbes in modulating/disrupting the host defense mechanisms. Moreover, substitution of microbial proteins in the host PPI networks eventually shifts the paradigm of host-pathogen interactions in the favor of the pathogen. Several eukaryotic host-like SLiMs have been reported in viral proteins which helps in their entry inside the host cell and modulation of host cellular pathways related to transcription regulation, cell cycle, immune response etc. (Davey et al., 2011; Garamszegi et al., 2013; Hagai et al., 2014). Similarly, several eukaryotic host-like SLiMs have also been reported in bacterial proteins which helps them to interfere with signaling pathways involving protein tyrosine kinases (TKs) and mitogen-activated protein kinases (MAPKs), tyrosine phosphorylation etc., (Higashi et al., 2002; Frese et al., 2006; Li et al., 2007; Zhu et al., 2007; Sámano-Sánchez and Gibson, 2020). The emergence of antibiotic resistance in pathogens necessitates discovery of new anti-infective therapies. Recently, protein-based immune-modulatory molecules or drugs which can disrupt the host-pathogen PPIs have been proposed as a novel anti-infective therapy (Sámano-Sánchez and Gibson, 2020). Such therapeutics can interfere with the host-pathogen SLiM-mediated interactions and create a hostile and non-conducive host environment for the survival of the pathogen. Though, mimicry of the eukaryotic host-like SLiMs has been recognized as an important mechanism underlying microbial pathogenicity, presence and characteristics of host-like SLiMs have not been studied in the mimicry peptides (mimitopes) of bacteria and viruses experimentally associated with autoimmune diseases. Thus, the present study was conducted to discern if the experimentally verified microbial mimitopes underlying various autoimmune diseases exhibit motif mimicry with the host and potentially modulate the host PPIs. Additionally, the evolutionary pressure on microbial mimitopes was also determined. This is the first report on potential of autoimmunity-related microbial mimitopes in modulating host protein-protein interactions and their evolutionary characteristics.

Materials and methods

Retrieval of experimentally validated mimicry proteins from miPepBase

In the present study, the information on bacterial, viral and the host mimicry proteins was retrieved from a database of experimentally verified mimicry proteins, miPepBase (updated version assessed on January 2021). The database collates information about only the experimentally verified mimicry proteins/peptides and autoimmune diseases, thereof (Garg et al., 2017).

Investigating the presence of eukaryotic host-like SLiMs in microbial mimicry proteins and mimitopes

The presence of eukaryotic host-like SLiMs in the microbial mimicry proteins and mimitopes was predicted using ANCHOR (Dosztányi et al., 2009). A eukaryotic host-like SLiM was considered to be present in the microbial mimitope if at least half of the amino acid of mimitopes overlapped with the SLiM region.

Molecular evolutionary analyses of microbial mimitopes

The putative homologous/orthologous sequence of microbial mimicry proteins were identified using BLAST search against NCBI non-redundant (NR) protein database. To obtain a sequence homologous to each microbial protein, the NR database was searched using the microbial protein as query. Search results with query coverage of $\geq$80 and atleast 80% sequence identity were selected as the criteria for homology and used for further evolutionary analyses. The Orthologous protein clusters of each mimicry protein were aligned using ClustalW version 2 (Larkin et al., 2007). The corresponding gene sequences of these proteins were also aligned on the basis of their codons using pal2nal (Suyama et al., 2006). The ratio between the rate of non-synonymous substitution to the rate of synonymous substitution ($\omega = d\mathrm{N}/d\mathrm{S}$) was used as a measure of the strength of selection pressure acting on a protein-coding gene. Assuming synonymous mutations are subjected to almost strictly neutral selection, the $\omega < 1$, $\omega = 1$, and $\omega > 1$ represent negative selection, neutral evolution, and positive Darwinian selection, respectively (Yang, 2002). To compute the dN/dS ratio for each amino acid of the microbial mimitope, a site-specific model of the likelihood method was used using the codeml module of the PAML package (Yang, 2007).

Result and discussion

Microbial mimicry of the host peptides has been implicated in several autoimmune diseases like multiple sclerosis (Wekerle and Hohlfeld, 2003), type 1 diabetes mellitus (Coppieters et al., 2012), autoimmune uveitis (Wildner and Diedrichs-Möhring, 2003), encephalomyelitis (Phelan et al., 2020), inflammatory bowel disease (Biank et al., 2007; Yusung and Braun, 2014), Crohn's disease (Cunha-Neto and Kalil, 2014; Polymeros et al., 2014), sarcoidosis, etc.

Motif mimicry of the eukaryotic host-like SLiMs has been associated with the pathogenicity of several bacteria and viruses because it helps them to hijack the host processes by rewiring the host PPI networks, signaling pathways, post-translational

modifications etc., (Davey et al., 2012; Dinkel et al., 2014). Since, SLiMs are abundantly present in cell signaling and PPI network proteins, drugs targeting SLiM-regulated cellular processes have been proposed as novel therapeutics against bacterial and viral infections (Davey et al., 2011; Via et al., 2015; Sámano-Sánchez and Gibson, 2020). Thus, the present study was conducted to discern if the mimicry peptides (experimentally verified as responsible for autoimmune diseases; collated in miPepBase) contain the functional modules of PPIs, SLiMs and can be explored as novel drug targets.

A total of 150 bacterial mimicry proteins with their corresponding 28 host proteins and, 34 viral mimicry proteins with their corresponding 22 host mimicry proteins were retrieved from the miPepBase. The bacterial and their corresponding host mimicry proteins were named as Bacterial-set proteins. The viral and their corresponding host mimicry proteins were named as Viral-set proteins. The Bacterial-set proteins were involved in 16, while the Viral-set proteins were involved in 12 different types of autoimmune diseases. The detailed information of the host and pathogen, UniProtKB ID and name of the mimicry-protein(s), mimitope sequences, associated autoimmune diseases, and source of information (Pubmed ID) is provided in Supplementary Table 1.

During infection, the pathogens repurpose the host cells in a manner which is conducive to their own survival, proliferation and helpful for evading the host immunity. Thus, if the host cells can be rewired to the uninfected state or the one that is close to it, the disease progression can be halted or slowed down. Thus, drugs/molecules which can inhibit either (i) interactions between microbial host-like SLiMs and host PPI networks or, (ii) the metabolic chokepoints of these PPI networks or, (iii) nodes in the regulatory networks upstream or downstream of the hijacked host-SLiMs can be explored as novel therapeutics. Also termed as host-directed therapy, this approach has proved useful in combating many viruses and bacteria (Sámano-Sánchez and Gibson, 2020). The classical examples of host-directed therapy are the chemical inhibition of the proteasomal pathway which resulted in reduced viral loads in dengue infection and, RNA interference (RNAi) against some human proteins which inhibited replication of HIV and hepatitis C virus (Schwegmann and Brombacher, 2008). Our results revealed that the eukaryotic host-like SLiMs were abundant in the microbial mimicry proteins because 41 bacterial and 20 viral mimicry proteins showed the presence of SLiMs (Supplementary Table 2). On the contrary, only a few microbial mimitopes overlapped with the eukaryotic host-like SLiMs. Of the total 155 bacterial mimitopes, 10 bacterial mimitopes showed SLiMs and of the 43 viral mimitopes only 4 viral mimitopes had SLiMs (Table 1). This suggests that the most of the microbial mimitopes implicated in autoimmune diseases could not potentially rewire the host PPI networks for their own benefit. And, their pathology might have only the autoimmune component due to cross reactivity between the microbial epitopes and host peptides. However, the microbial mimitopes of ten bacteria and three viruses overlapped with the eukaryotic host-like SliMs (Table 1). Seven mimitopes, one each of *Agrobacterium tumefaciens*, *Yersinia enterocolitica, Escherichia coli, Propionibacterium freudenreichii, Streptococcus mutans, Lactobacillus johnsonii, Bifidobacterium longum* and two each of *Mycobacterium leprae* and Group A streptococcus showed the presence of eukaryotic host-like SLiMs in their mimitopes. Among the viruses, one mimitope of Herpes simplex virus and Herpes virus saimiri and two mimitopes of Epstein Barr virus had host-like SLiMs (Table 1). This suggests that these peptide regions might not only be responsible for inducing autoimmune diseases in the host by exhibiting epitope mimicry with the host, motif mimicry of the host-like SLiMs might also aid these bacteria and viruses in interrupting the host cell signaling and PPI networks.

Evaluation of the selection pressure on the microbial mimitopes revealed that 77.85% of the bacterial and 83.54% of the viral amino acids were under negative selection pressure ($\omega < 1$), implying that microbial mimtopes were generally conserved or had a low mutation rate. Comas et al., reported that the T cell epitopes of *M. tuberculosis* were highly conserved which might be a distinct evolutionary strategy of a highly successful pathogen as *M. tuberculosis* for immune subversion (Comas et al., 2010). This suggests that other pathogens might also employ a similar strategy for a sustained survival inside the host. However, analysis of the microbial mimitopes which overlapped with the eukaryotic host-like SLiMs revealed that only 46.75% of the bacterial mimitopes and 25% of the viral mimitopes were under negative selection pressure ($\omega < 1$) (Table 1; Supplementary Figure 1). This observation can be explained by the fact that SLiMs are in disordered regions of the proteins hence, the rate of mutation is high and these regions are usually under a positive selection pressure (Uyar et al., 2014). In past we have also shown that low complexity regions of proteins are not always disordered (Kumari et al., 2015).

Conventionally, autoimmune diseases like systemic lupus erythematosus, encephalomyelitis, multiple sclerosis etc., are treated using immunomodulators or immunosuppressants which only try to cure the symptoms but do not eliminate the etiological agent which continues to proliferate inside the host and interfering with vital cellular process(es). On the contrary, protein-based immune-modulatory molecules/drug molecules designed to inhibit the mimitopes (or eukaryotic host-like SLiMs) might also disrupt the host-pathogen PPIs. This implies that inhibitors of microbial mimitopes (or eukaryotic host-like SLiMs) identified in this study would not only help in treating the pathogen-associated autoimmune disease but also eliminate the etiopathological agent associated with the disease.

Finally, the repertoire of mimitopes discovered in this study suggests new paradigms underlying autoimmune diseases and the etiopathology associated with the infection. Such knowledge can provide important clues for the discovery

TABLE 1 Detailed information about the microbial mimitopes which overlapped with the eukaryotic host-like SliMs.

Sr. No.	Name and Uniprot id of the host mimicry protein (in parenthesis)	Autoimmune disease	Associated microbe	Name and Uniprot id of the microbial mimicry protein	Sequence of the microbial mimitope*	Position of the mimitope [Start-End]	Number of amino acids in the microbial mimitope	Number of amino acids in mimitope which show negative selection ($\omega < 1$)
1	Myelin basic protein of Mouse [P04370]	Encephalomyelitis	*Agrobacterium tumefaciens*	Replicating protein [P15394]	**AAQNRPSGPRK**	200–210	11	0
			Yersinia enterocolitica	YsaN [O30438]	**ANQTRPADIAA**	445–455	11	0
			Propionibacterium freudenreichii	Uroporphyrinogen III methyltransferase [Q51720]	**AHHVRPPALVV**	227–237	11	0
			Herpes simplex virus	Viral transcription factor ICP4 [P08392]	**AAQARPRPVAV**	790–800	11	0
			Herpes virus saimiri	Uncharacterized protein [Q80BM4]	**AAQRRPSRPFR**	125–135	11	11
2	Myelin basic protein of Cattle [P02687]	Leprosy	*Mycobacterium leprae*	50S ribosomal L2 [O32984]	**VSPWGKPEGRTR KPNKSSNK**	247–266	20	17
			Mycobacterium leprae	50S ribosomal L2 [O32984]	EQA**NINWGKA GRMRWKGKRP**	200–219	20	20
3	HEAE encephalitogen from myelin basic protein of rat [P02688]	Multiple Sclerosis	*Lactobacillus johnsonii*	FtsY [Q74IQ0]	**ESAEEVTTEDEQ**ER	125–138	14	5
4	Ro protein of human [P10155]	Systemic lupus erythematosus	Epstein Barr virus	Epstein_Barr virus nuclear antigen_1 (EBNA_1) [Q3KSS4]	**GGSGSG PRHRDGVRR**	58–72	15	0
5	Human skeletal myosin protein [P12883]	NA	*Escherichia coli*	Colicin protein [P02978]	**KAFQE**AEQR	148–156	9	8
6	SmD protein of human [P63162]	Systemic lupus erythematosus	Epstein Barr virus	Epstein_Ban nuclear antigen_1 (EBNA_1) [G0YSX7]	**PPPGRRP**	11–17	7	0
7	Human skeletal myosin protein [Q9UKX3]	Juvenile dermatomyositis	Group A streptococcus	M5 [P49054]	**ALEKLNK**EL	287–295	9	9
8	Myelin basic protein of rabbit [P25274]	Multiple Sclerosis	*Streptococcus mutans*	Permease [Q8DUP2]	**KTYGTLPSQD**	143–152	10	10
		Multiple Sclerosis	*Bifidobacterium longum*	Hypothetical [Q8G3X4]	**TNYGALPGSI**	9–18	10	10

*SLiM regions in the microbial mimitopes are shown in bold face.

10.3389/fmicb.2022.1039188

of new drugs/protein-based immune-modulatory molecules against the pathogens.

Author contributions

NS and MK conceived and designed the study. AG performed the work, prepared the illustrations, and wrote initial draft manuscript. All authors contributed to the critical analysis and revision, analyzed the results, and wrote the final versions of manuscript.

Funding

The work was carried out using the resources funded by the Indian Council of Medical Research [Grant Nos: VIR(25)/2019/ECD-1 and ISRM/12(33)/2019]. AG was supported by ICMR-JRF scheme [Grant Number: 3/1/3 J.R.F.-2016/LS/HRD-(32262)]. NS was supported by CSIR Senior Research Associateship (Scientists' Pool Scheme) [Grant Number: 13(9089-A)/2019-Pool].

Conflict of interest

The authors declare that the research was conducted in the absence of any commercial or financial relationships that could be construed as a potential conflict of interest.

Publisher's note

Supplementary material

The Supplementary Material for this article can be found online at: https://www.frontiersin.org/articles/10.3389/fmicb.2022.1039188/full#supplementary-material

References

Ang, C. W., Jacobs, B. C., and Laman, J. D. (2004). The Guillain-Barré syndrome: a true case of molecular mimicry. *Trends Immunol.* 25, 61–66. doi: 10.1016/j.it.2003.12.004

Ascherio, A., and Munger, K. L. (2007). Environmental risk factors for multiple sclerosis. Part II: noninfectious factors. *Ann. Neurol.* 61, 504–513. doi: 10.1002/ana.21141

Biank, V., Broeckel, U., and Kugathasan, S. (2007). Pediatric inflammatory bowel disease: clinical and molecular genetics. *Inflamm. Bowel Dis.* 13, 1430–1438. doi: 10.1002/ibd.20213

Comas, I., Chakravartti, J., Small, P. M., Galagan, J., Niemann, S., Kremer, K., et al. (2010). Human T cell epitopes of *Mycobacterium tuberculosis* are evolutionarily hyperconserved. *Nat. Genet.* 42, 498–503. doi: 10.1038/ng.590

Coppieters, K. T., Wiberg, A., and von Herrath, M. G. (2012). Viral infections and molecular mimicry in type 1 diabetes. *APMIS* 120, 941–949. doi: 10.1111/apm.12011

Cunha-Neto, E., and Kalil, J. (2014). Molecular mimicry and chagas' disease. *Mol. Mimicry Microb. Autoimmun.* doi: 10.1128/9781555818074.ch18

Davey, N. E., Travé, G., and Gibson, T. J. (2011). How viruses hijack cell regulation. *Trends Biochem. Sci.* 36, 159–169. doi: 10.1016/j.tibs.2010.10.002

Davey, N. E., Van Roey, K., Weatheritt, R. J., Toedt, G., Uyar, B., Altenberg, B., et al. (2012). Attributes of short linear motifs. *Mol. Biosyst.* 8, 268–281. doi: 10.1039/C1MB05231D

Dinkel, H., Van Roey, K., Michael, S., Davey, N. E., Weatheritt, R. J., Born, D., et al. (2014). The eukaryotic linear motif resource ELM: 10 years and counting. *Nucleic Acids Res.* 42, D259–D266. doi: 10.1093/nar/gkt1047

Dolan, P. T., Roth, A. P., Xue, B., Sun, R., Dunker, A. K., Uversky, V. N., et al. (2015). Intrinsic disorder mediates hepatitis C virus core-host cell protein interactions: HCV Core MoRFs target cellular proteins. *Protein Sci.* 24, 221–235. doi: 10.1002/pro.2608

Dosztányi, Z., Mészáros, B., and Simon, I. (2009). ANCHOR: web server for predicting protein binding regions in disordered proteins. *Bioinformatics* 25, 2745–2746. doi: 10.1093/bioinformatics/btp518

Frese, S., Schubert, W.-D., Findeis, A. C., Marquardt, T., Roske, Y. S., Stradal, T. E. B., et al. (2006). The phosphotyrosine peptide binding specificity of Nck1 and Nck2 Src homology 2 domains. *J. Biol. Chem.* 281, 18236–18245. doi: 10.1074/jbc.M512917200

Fujinami, R. S. (2001). Viruses and autoimmune disease – two sides of the same coin? *Trends Microbiol.* 9, 377–381. doi: 10.1016/S0966-842X(01)02097-2

Garamszegi, S., Franzosa, E. A., and Xia, Y. (2013). Signatures of pleiotropy, economy and convergent evolution in a domain-resolved map of human–virus protein–protein interaction networks. *PLoS Pathog.* 9, e1003778. doi: 10.1371/journal.ppat.1003778

Garg, A., Dabburu, G. R., Singhal, N., and Kumar, M. (2022). Investigating the disordered regions (MoRFs, SLiMs and LCRs) and functions of mimicry proteins/peptides in silico. *PLoS ONE* 17, e0265657. doi: 10.1371/journal.pone.0265657

Garg, A., Kumari, B., Kumar, R., and Kumar, M. (2017). miPepBase: a database of experimentally verified peptides involved in molecular mimicry. *Front. Microbiol.* 8, 2053. doi: 10.3389/fmicb.2017.02053

Hagai, T., Azia, A., Babu, M. M., and Andino, R. (2014). Use of host-like peptide motifs in viral proteins is a prevalent strategy in host-virus interactions. *Cell Rep.* 7, 1729–1739. doi: 10.1016/j.celrep.2014.04.052

Higashi, H., Tsutsumi, R., Fujita, A., Yamazaki, S., Asaka, M., Azuma, T., et al. (2002). Biological activity of the Helicobacter pylori virulence factor CagA is determined by variation in the tyrosine phosphorylation sites. *Proc. Natl. Acad. Sci. USA.* 99, 14428–14433. doi: 10.1073/pnas.222375399

Johnson, T. P., Tyagi, R., Lee, P. R., Lee, M.-H., Johnson, K. R., Kowalak, J., et al. (2017). Nodding syndrome may be an autoimmune reaction to the parasitic worm Onchocerca volvulus. *Sci. Transl. Med.* 9, eaaf6953. doi: 10.1126/scitranslmed.aaf6953

Kumari, B., Kumar, R., and Kumar, M. (2015). Low complexity and disordered regions of proteins have different structural and amino acid preferences. *Mol. Biosyst.* 11, 585–594. doi: 10.1039/C4MB00425F

Larkin, M. A., Blackshields, G., Brown, N. P., Chenna, R., McGettigan, P. A., McWilliam, H., et al. (2007). Clustal W and clustal X version 2.0. *Bioinformatics* 23, 2947–2948. doi: 10.1093/bioinformatics/btm404

Lester, P. J., Buick, K. H., Baty, J. W., Felden, A., and Haywood, J. (2019). Different bacterial and viral pathogens trigger distinct immune responses in a globally invasive ant. *Sci. Rep.* 9, 5780. doi: 10.1038/s41598-019-41843-5

Li, H., Xu, H., Zhou, Y., Zhang, J., Long, C., Li, S., et al. (2007). The phosphothreonine lyase activity of a bacterial type III effector family. *Science*. 315, 1000–1003. doi: 10.1126/science.1138960

Libbey, J. E., and Fujinami, R. S. (2010). Potential triggers of MS. *Results Probl. Cell Differ*. 51, 21–42. doi: 10.1007/400_2008_12

Phelan, J., Grabowska, A. D., and Sepúlveda, N. (2020). A potential antigenic mimicry between viral and human proteins linking myalgic encephalomyelitis/chronic fatigue syndrome (ME/CFS) with autoimmunity: the case of HPV immunization. *Autoimmun. Rev.* 19, 102487. doi: 10.1016/j.autrev.2020.102487

Polymeros, D., Tsiamoulos, Z. P., Koutsoumpas, A. L., Smyk, D. S., Mytilinaiou, M. G., Triantafyllou, K., et al. (2014). Bioinformatic and immunological analysis reveals lack of support for measles virus related mimicry in Crohn's disease. *BMC Med.* 12, 139. doi: 10.1186/s12916-014-0139-9

Sámano-Sánchez, H., and Gibson, T. J. (2020). Mimicry of short linear motifs by bacterial pathogens: a drugging opportunity. *Trends Biochem. Sci.* 45, 526–544. doi: 10.1016/j.tibs.2020.03.003

Schwegmann, A., and Brombacher, F. (2008). Host-directed drug targeting of factors hijacked by pathogens. *Sci. Signal.* 1, re8. doi: 10.1126/scisignal.129re8

Suyama, M., Torrents, D., and Bork, P. (2006). PAL2NAL: robust conversion of protein sequence alignments into the corresponding codon alignments. *Nucleic Acids Res.* 34, W609–W612. doi: 10.1093/nar/gkl315

Tarakhovsky, A., and Prinjha, R. K. (2018). Drawing on disorder: how viruses use histone mimicry to their advantage. *J. Exp. Med.* 215, 1777–1787. doi: 10.1084/jem.20180099

Uyar, B., Weatheritt, R. J., Dinkel, H., Davey, N. E., and Gibson, T. J. (2014). Proteome-wide analysis of human disease mutations in short linear motifs: neglected players in cancer? *Mol. Biosyst.* 10, 2626–2642. doi: 10.1039/C4MB00290C

Vacic, V., Oldfield, C. J., Mohan, A., Radivojac, P., Cortese, M. S., Uversky, V. N., et al. (2007). Characterization of molecular recognition features, MoRFs, and their binding partners. *J. Proteome Res.* 6, 2351–2366. doi: 10.1021/pr07 01411

Via, A., Uyar, B., Brun, C., and Zanzoni, A. (2015). How pathogens use linear motifs to perturb host cell networks. *Trends Biochem. Sci.* 40, 36–48. doi: 10.1016/j.tibs.2014.11.001

Wekerle, H., and Hohlfeld, R. (2003). Molecular mimicry in multiple sclerosis. *N. Engl. J. Med*. 349, 185–186. doi: 10.1056/NEJMcibr035136

Wildner, G., and Diedrichs-Möhring, M. (2003). Autoimmune uveitis induced by molecular mimicry of peptides from rotavirus, bovine casein and retinal S-antigen. *Eur. J. Immunol.* 33, 2577–2587. doi: 10.1002/eji.200324058

Xue, B., Blocquel, D., Habchi, J., Uversky, A. V., Kurgan, L., Uversky, V. N., et al. (2014). Structural disorder in viral proteins. *Chem. Rev.* 114, 6880–6911. doi: 10.1021/cr4005692

Yan, J., Dunker, A. K., Uversky, V. N., and Kurgan, L. (2016). Molecular recognition features (MoRFs) in three domains of life. *Mol. Biosyst.* 12, 697–710. doi: 10.1039/C5MB00640F

Yang, Z. (2002). Inference of selection from multiple species alignments. *Curr. Opin. Genet. Dev.* 12, 688–694. doi: 10.1016/S0959-437X(02)00348-9

Yang, Z. (2007). PAML 4: phylogenetic analysis by maximum likelihood. *Mol. Biol. Evol.* 24, 1586–1591. doi: 10.1093/molbev/msm088

Yusung, S., and Braun, J. (2014). Molecular mimicry, inflammatory bowel disease, and the vaccine safety debate. *BMC Med.* 12, 166. doi: 10.1186/s12916-014-0166-6

Zhu, Y., Li, H., Long, C., Hu, L., Xu, H., Liu, L., et al. (2007). Structural insights into the enzymatic mechanism of the pathogenic MAPK phosphothreonine lyase. *Mol. Cell* 28, 899–913. doi: 10.1016/j.molcel.2007.11.011

frontiers | Frontiers in Microbiology

TYPE Original Research
PUBLISHED 17 November 2022
DOI 10.3389/fmicb.2022.1016895

OPEN ACCESS

EDITED BY
Svetlana Khaiboullina,
University of Nevada,
Reno, United States

REVIEWED BY
Alexandra Irrgang,
Bundesanstalt für Risikobewertung (BfR),
Germany
Prasanth Manohar,
Zhejiang University-University
of Edinburgh Institute,
China
Shangshang Qin,
Zhengzhou University,
China

*CORRESPONDENCE
Patricia Alba
patricia.alba@izslt.it

SPECIALTY SECTION
This article was submitted to
Infectious Agents and Disease,
a section of the journal
Frontiers in Microbiology

RECEIVED 11 August 2022
ACCEPTED 10 October 2022
PUBLISHED 17 November 2022

CITATION
Carfora V, Diaconu EL, Ianzano A,
Di Matteo P, Amoruso R, Dell'Aira E,
Sorbara L, Bottoni F, Guarneri F,
Campana L, Franco A, Alba P and
Battisti A (2022) The hazard of
carbapenemase (OXA-181)-producing
Escherichia coli spreading in pig and veal
calf holdings in Italy in the genomics era:
Risk of spill over and spill back between
humans and animals.
Front. Microbiol. 13:1016895.
doi: 10.3389/fmicb.2022.1016895

The hazard of carbapenemase (OXA-181)-producing *Escherichia coli* spreading in pig and veal calf holdings in Italy in the genomics era: Risk of spill over and spill back between humans and animals

Virginia Carfora[1], Elena Lavinia Diaconu[1], Angela Ianzano[1], Paola Di Matteo[1], Roberta Amoruso[1], Elena Dell'Aira[1], Luigi Sorbara[1], Francesco Bottoni[1], Flavia Guarneri[2], Laura Campana[3], Alessia Franco[1], Patricia Alba[1]* and Antonio Battisti[1]

[1]Department of General Diagnostics, National Reference Laboratory for Antimicrobial Resistance, Istituto Zooprofilattico Sperimentale del Lazio e Della Toscana "M. Aleandri", Rome, Italy, [2]Sede Territoriale di Brescia, Laboratorio Diagnostica Generale, Istituto Zooprofilattico Sperimentale Della Lombardia e Dell'Emilia-Romagna "Bruno Ubertini", Brescia, Italy, [3]Agenzia Tutela Della Salute, Brescia, Italy

Carbapenemase-producing Enterobacterales (CPE) are considered a major public health issue. In the frame of the EU Harmonized AMR Monitoring program conducted in Italy in 2021, 21 epidemiological units of fattening pigs (6.98%; 95% CI 4.37–10.47%; 21/301) and four epidemiological units of bovines <12months (1.29%; 95% CI 0.35–3.27%, 4/310) resulted positive to OXA-48-like-producing *E. coli* (*n*=24 OXA-181, *n*=1 OXA-48). Whole Genome Sequencing (WGS) for in-depth characterization, genomics and cluster analysis of OXA-181-(and one OXA-48) producing *E. coli* isolated, was performed. Tracing-back activities at: (a) the fattening holding of origin of one positive slaughter batch, (b) the breeding holding, and (c) one epidemiologically related dairy cattle holding, allowed detection of OXA-48-like-producing *E. coli* in different units and comparison of further human isolates from fecal samples of farm workers. The OXA-181-producing isolates were multidrug resistant (MDR), belonged to different Sequence Types (STs), harbored the IncX and IncF plasmid replicons and multiple virulence genes. Bioinformatics analysis of combined Oxford Nanopore Technologies (ONT) long reads and Illumina short reads identified $bla_{OXA-181}$ as part of a transposon in IncX1, IncX3, and IncFII fully resolved plasmids from 16 selected *E. coli*, mostly belonging to ST5229, isolated during the survey at slaughter and tracing-back activities. Although human source could be the most likely cause for the introduction of the $bla_{OXA-181}$-carrying IncX1 plasmid in the breeding holding, concerns arise from carbapenemase OXA-48-like-producing *E. coli* spreading in 2021 in Italian fattening pigs and, to a lesser extent, in veal calf holdings.

KEYWORDS

carbapenem-resistant Enterobacterales, OXA-48-like carbapenemases, OXA-181 carbapenemases, long-read sequencing, Whole Genome Sequencing, plasmids, pig, bovine

Introduction

Carbapenemase-producing Enterobacterales (CPE) are considered a major public health issue and Class D carbapenemases are the main causes of carbapenem resistance among *A. baumannii* and Enterobacterales isolated from human infections in many countries (Pitout et al., 2019). These enzymes show activity against amino-, carboxy-, and ureidopenicillins and narrow-spectrum cephalosporins (e.g., cephalothin), and they also have limited activities against broad-spectrum cephalosporins (especially ceftazidime) and most beta-lactam inhibitors (Pitout et al., 2019). The group II OXA carbapenemases is composed by the OXA-48-related variants (OXA-48-like beta-lactamases). The OXA-181, differing by four aminoacid substitutions from OXA-48, is the most common OXA-48-like variant so far identified (Pitout et al., 2019).

Mobilization and transfer of OXA-48-like beta-lactamases from the chromosome of *Shewanella* spp. onto conjugative plasmids of other bacterial species has been likely associated to mobile genetic elements (MGEs), as the composite transposon Tn1999, responsible for the spread of this antimicrobial resistance (AMR) gene to Enterobacterales (Potron et al., 2011b). The current international spread of $bla_{\text{OXA-181}}$ among Enterobacterales has been mainly associated to the insertion of the element IS*Ecp1*, which is situated within Tn2013 upstream of $bla_{\text{OXA-181}}$ and the ΔlysR-Δere (downstream $bla_{\text{OXA-181}}$), located on different plasmids mainly belonging to the ColE2, IncX3, IncN1, and IncT replicon types (Potron et al., 2011a). The presence of IS*Ecp1* has been previously reported to facilitate the acquisition of ESBL genes such as $bla_{\text{CTX-M-15}}$ (Poirel et al., 2008).

In humans, $bla_{\text{OXA-181}}$ was first described in Enterobacterales isolates from Indian patients (Potron et al., 2011a) and over the next 3 years (2012–2014), it spread also in Europe, Asia, and Africa (Ruppé et al., 2014; Lunha et al., 2016; Ouédraogo et al., 2016), with the majority of isolates being co-producers of NDM-1 and having a travel history to the Indian sub-continent (Ruppé et al., 2014). Indeed, the Indian sub-continent has been considered a reservoir of all types of carbapenemases, including OXA-181 (Nordmann and Poirel, 2014). Since 2014, OXA-181 was further detected worldwide (Rojas et al., 2017). OXA-48-like carbapenemases, although their true burden is likely underestimated at global level due to the difficulty in their detection (Boyd et al., 2022), already represent a great clinical and public health concern, since they are the cause of considerable case-fatality rates in infected patients (Bakthavatchalam et al., 2016).

In Europe, the genetic environment (IncT-type plasmid) of a $bla_{\text{OXA-181}}$ was described in a *Citrobacter freundii* human isolate co-producing NDM-1 (Villa et al., 2013). In Italy, one OXA-181-producing *E.coli* co-harboring $bla_{\text{CTX-M-15}}$, $bla_{\text{CMY-2}}$, and *qnrS1* genes was described from the rectal swab of a human patient (Piazza et al., 2018), and one from a pediatric patient, associated with $bla_{\text{NDM-5}}$ (Marchetti et al., 2020). The *E. coli* IncX3 plasmid named pKP_BO_OXA181 from an Italian patient was also submitted to Genbank in 2017 (GenBank accession number MG228426).

In companion animals, $bla_{\text{OXA-181}}$ was recently reported in extraintestinal Pathogenic *Escherichia coli* in a dog from Portugal (Brilhante et al., 2020) and in *E. coli* isolated in rectal swabs from hospitalized dogs in Switzerland (Nigg et al., 2019). To date, indeed, there are only very limited findings on OXA-48-and OXA-48-like producing *Enterobacteriaceae* in livestock. In Egypt, $bla_{\text{OXA-48}}$ and $bla_{\text{OXA-181}}$ were identified in different *E. coli* isolates from healthy dairy cattle (Braun et al., 2016).

$bla_{\text{OXA-181}}$ was detected with $bla_{\text{CMY-2}}$, *qnrS1*, *arm*A, and *mcr*-1 in *E. coli* associated to diarrhea and oedema disease in two pigs sampled in Italy (Pulss et al., 2017). However, in this latter case description, there is no further information on the presence and prevalence of $bla_{\text{OXA-181}}$ in related commensal *E.coli*, nor tracing back investigations have been performed to hypothesize possible transmission routes of $bla_{\text{OXA-181}}$.

The aims of this study are: (i) to describe the results of the EU Harmonized AMR Monitoring program conducted in 2021 of OXA-181-(and one OXA-48-) producing *E. coli* isolated mainly from caecal samples in pigs and, to a lesser extent in bovines <12 months, and the tracing back investigations conducted after the first positive case at slaughter; (ii) to investigate by WGS analysis the molecular mechanisms responsible for the mobilization and spread of $bla_{\text{OXA-181}}$ gene in food-producing animals and in-contact humans, performing *in silico* typing, determination of $bla_{\text{OXA-48}}$-like genetic context and full reconstruction of the plasmids where the $bla_{\text{OXA-181}}$ gene(s) were located; and (iii) to study the genomic epidemiology of $bla_{\text{OXA-48}}$-like *E. coli* and assess the genetic relationships among isolates from animal and human hosts carriers detected at the holding of origin of the positive slaughter batch and at epidemiologically related pig and dairy holdings.

Materials and methods

Sampling and isolate identification

In the frame of the Harmonized European Monitoring for AMR (EU Decision 2013/652[1] and 2020/1729[2]) conducted in Italy in 2021, 301 caecal content samples from fattening pigs and 310 caecal content samples from bovine animals under 1 year of age

1 https://eur-lex.europa.eu/legal-content/EN/TXT/PDF/?uri=CELEX:32013D0652&from=EN

2 https://eur-lex.europa.eu/legal-content/EN/TXT/PDF/?uri=CELEX:32020D1729&from=EN

were collected. These samples obtained from randomly selected epidemiological units at slaughterhouses, were stratified according to EFSA Technical specifications[3] in Italian regions accounting for >80% on the national throughput of pork and veal meat. Epidemiological unit for fattening pigs and bovines <12 months was the slaughter batch (animals raised together in the same holding of origin).

Beside the results of the survey at slaughter, here we report the results of samples taken by the Competent Authorities (Veterinary Services) in the context of the tracing back and sampling activity in relation to the first positive fattening holding. In this context, fresh fecal samples from the floor of the boxes (of the holdings) where the animals were kept, were taken at (a) the fattening holding of origin of the first positive slaughter batch; (b) the holding providing weaners to the above fattening holding; and (c) one epidemiologically related dairy cattle holding. Additionally, two human fecal samples from one worker and the owner at breeding holding (holding b) only, were voluntary made available through the Local Health Competent Authorities (after giving informed consent to participate in the study).

According to the protocol of the European Union Reference Laboratory for Antimicrobial Resistance,[4] all samples were cultured by the isolation method specific for CPE using selective media for CR *E. coli*. Briefly, caecal or fecal samples (depending on whether it was monitoring at slaughter or tracing back investigation), were cultured in buffered peptone water at 1:10 (w/v) concentration and incubated at 37°C overnight. 10 µl of the pre-enrichment broth was plated in selective media bi plate for CPE (CHROMID™CARBA SMART; bioMérieux) and incubated overnight at 37°C. One suspected OXA-48-like-producing colony from each sample was isolated on blood agar plates and identified as *bla*$_{\text{OXA-48}}$(like)-positive *E. coli* by specific screening PCRs (Poirel et al., 2011). Confirmed *bla*$_{\text{OXA-48}}$(like)-positive *E. coli* isolates were in-depth characterized.

Antimicrobial susceptibility testing

Antimicrobial susceptibility testing was performed as minimum inhibitory concentration (MIC) determination by broth microdilution, using the EU consensus 96-well microtiter plates (Trek Diagnostic Systems, Westlake, OH, United States). The following antimicrobials were tested, as reported in the EU Decision 2020/1729/EU: amikacin, ampicillin, azithromycin, cefotaxime, ceftazidime, chloramphenicol, ciprofloxacin, colistin, gentamicin, meropenem, nalidixic acid, sulfamethoxazole, tetracycline, tigecycline, trimethoprim (first panel) and cefepime, cefotaxime, cefotaxime + clavulanic acid, cefoxitin, ceftazidime, ceftazidime + clavulanic acid, ertapenem, imipenem, meropenem, and temocillin (second panel). Dilution ranges and interpretation of MIC values using epidemiological cutoffs (ECOFFs) were performed according to the EU Decision 2020/1729/EU and to the EFSA manual published in 2021 [European Food Safety Authority (EFSA) et al., 2021]. For carbapenems and temocillin, results were also interpreted according to EUCAST[5] clinical breakpoints (Table 1). *Escherichia coli* ATCC 25922 was used as quality control strain.

The results of AST were further compared with the AMR genotypes to determine if the phenotypic resistance patterns were confirmed by the presence of the corresponding AMR genes.

Library preparation and whole genome sequencing

The *bla*$_{\text{OXA-48}}$(like)-positive isolates obtained from pigs at slaughter and from the tracing back activity after the first positive fattening holding, were investigated by WGS analysis.

DNA extraction and library preparation were performed according to Alba et al. (2021). Briefly, genomic DNA was extracted using the QIAamp DNA Mini Kit (Qiagen, Hilden, Germany) following the manufacturer's protocol. Libraries for short reads pair-end sequencing were prepared using the NexteraXT DNA library preparation kit (Illumina, Inc., San Diego, CA, United States) and sequenced on an Illumina platform (MiSeq).

In parallel, libraries of 16 selected isolates, with five of them obtained from pigs at slaughter (Table 2) and 11 isolated in the frame of the tracing back investigations (Table 3) were prepared

3 https://efsa.onlinelibrary.wiley.com/doi/epdf/10.2903/j.efsa.2020.6364

4 https://www.eurl-ar.eu/CustomerData/Files/Folders/21-protocols/530_esbl-ampc-cpeprotocol-version-caecal-v7-09-12-19.pdf

5 www.eucast.org

TABLE 1 Epidemiological cutoffs (ECOFFs) and clinical breakpoints for carbapenems and temocillin, with number (nR) and percentage (%) of *E. coli* resistant isolates from the survey at slaughter.

	R (ECOFF)	R (CB)	nR/tot (%) ECOFF	nR/tot (%) CB
ETP (ertapenem)	>0,06	>0,5	25/25(**100%**)	7/25 (28%)
IMI (imipenem)	>0,5	>4	5/25 (20%)	5/25(20%)
MER (meropenem)	>0,125	>8	13/25 (52%)	0/25 (0%)
TRM (temocillin)	>16	>16	25/25(**100%**)	25/25(**100%**)

R, resistance; CB, Clinical breakpoint; ECOFF, Epidemiological cut-off; nR/tot, number of resistant isolates/total of isolates from the survey at slaughter.

TABLE 2 Metadata and genomic characteristics of the OXA-48(like) producing *E. coli* obtained from the samples collected from the survey at slaughter.

Isolate ID	Region	Host	Production type	ST	Serotype	Carbapenemase type	AMR genes	Inc Plasmid replicons	Chromosomal Point Mutations	Phenotypic AMR pattern	Sample accession number
21019054–1*	C	Pig	Fattening	48	O70:H11	OXA-181	*aad*A2[$] $bla_{OXA-181}$ bla_{TEM-1B} *cml*A1[$] *dfr*A12 *mef*(B) *sul*3 *tet*(A)[$] *tet*(M)[$]	IncX3 IncY		CHL, TMP, SMX, TET, AMP, ETP, FEP, and TRM	ERS12773674
21034263–1*	D	Pig	Fattening	5229	-:H51	OXA-181	*aac*(3)-IId[$] *aad*A17[$] *ant*(3″)-Ia[$] $bla_{OXA-181}$ *cml*A1[$] *dfr*A12 *flo*R[$] *lnu*(F) *sul*2 *sul*3 *tet*(A)[$] *tet*(M) [$]	IncFIC(FII) IncX1	*gyr*A p.D87N *par*C p.S80I	CHL, GEN, NAL, TMP, SMX, TET, AMP, CIP, ETP, MER, and TRM	ERS12773675
2105491–1*	C	Pig	Fattening	10	O101; O9a:H9	OXA-181	*aph*(3″)-Ib *aph*(6)-Id $bla_{OXA-181}$ bla_{TEM-1B} *dfr*A5 *qnr*S1 *sit*ABCD[$] *sul*2	IncFII IncX3		TMP, SMX, AMP, CIP, MER, ETP, IMI, FOT, FEP, and TRM	ERS12773676
21055959–1*	D	Pig	Fattening	5229	-:H51	OXA-181	*aac*(3)-IId[$] *aad*A17[$] *ant*(3″)-Ia[$] $bla_{OXA-181}$ bla_{TEM-1B} *cml*A1[$] *dfr*A12 *flo*R[$] *lnu*(F) *qnr*S1 *sul*2 *sul*3 *tet*(A)[$] *tet*(M)[$]	IncFIC(FII) IncX3	*gyr*A p.D87N *par*C p.S80I	CHL, GEN, NAL, TMP, SMX, TET, AMP, CIP, ETP, IMI, MER, FEP, FOT, FOX, and TRM	ERS12773677
21066975–1*	C	Pig	Fattening	5229	-:H51	OXA-181	*aac*(3)-IId[$] *aad*A17[$] *ant*(3″)-Ia[$] $bla_{OXA-181}$ bla_{TEM-1B} *cml*A1[$] *dfr*A12 *flo*R[$] *lnu*(F) *sul*2 *sul*3 *tet*(A)[$] *tet*(M)[$]	IncFIC(FII) IncX1	*gyr*A p.D87N *par*C p.S80I	CHL, GEN, NAL, TMP, SMX, TET, AMP, CIP, ETP, FOT, and TRM	ERS12773678
21076969–1	C	Pig	Fattening	3489	O153:H25	OXA-181	*aac*(3)-IId[$] *aph*(3″)-Ia $bla_{CTX-M-55}$ $bla_{OXA-181}$[#] *cml*A1[$] *dfr*A12 *flo*R[$] *fos*A3 *lnu*(F)[$] *qnr*S1 *rmt*B *sul*2 *sul*3 *tet*(A)[$] *tet*(M)[$]	IncFIB(AP001918) IncFIC(FII) IncFII(pHN7A8) IncX3[#]	*par*C p.S80I	CHL, GEN, NAL, TMP, SMX, TET, AMP, CIP, AMK, ETP, MER, FEP, FOT, TAZ, and TRM	ERS12773679
21080958–1	C	Pig	Fattening	5229	-:H51	OXA-181	*aac*(3)-IId[$] $bla_{OXA-181}$ *cml*A1[$] *dfr*A12 *flo*R[$] *lnu*(F) *sul*2 *sul*3 *tet*(A)[$] *tet*(M) [$]	IncFIB(AP001918) IncFIC(FII) IncX1	*gyr*A p.D87N *par*C p.S80I	CHL, GEN, NAL, TMP, SMX, TET, AMP, CIP, ETP, IMI, MER, FOT, and TRM	ERS12773680

(Continued)

10.3389/fmicb.2022.1016895

TABLE 2 (Continued)

Isolate ID	Region	Host	Production type	ST	Serotype	Carbapenemase type	AMR genes	Inc Plasmid replicons	Chromosomal Point Mutations	Phenotypic AMR pattern	Sample accession number
21088819–1	D	Pig	Fattening	117	-:H4	OXA-181	*aac*(3)-IId[§] *aph*(3″)-Ib *aph*(6)-Id $bla_{OXA-181}$[#] bla_{TEM-1B} *dfr*A17 *qnr*S1 *sit*ABCD[§] *tet*(A) [§]	IncFIB(AP001918) IncFIC(FII) IncX3[#]	*gyr*A p.S83L	GEN, NAL, TMP, TET, AMP, CIP, ETP, and TRM	ERS12773681
21094270–1	C	Bovine	Beef	5229	-:H51	OXA-181	*aac*(3)-IId[§] *aph*(3″)-Ia $bla_{OXA-181}$ *cml*A1[§] *dfr*A12 *flo*R[§] *lnu*(F) *qnr*S1 *sul*2 *sul*3 *tet*(B) *tet*(M)[§]	IncFIB(AP001918) IncFIC(FII) IncX3	*gyr*A p.D87N *par*C p.S80I	TMP, SMX, TET, AMP, CIP, FOT, ETP, MER, TAZ, and TRM	ERS12773682
21097167–1	C	Pig	Fattening	542	-:H38	OXA-181	*aad*A2[§] *aph*(6)-Id *aph*(3″)-Ib[§] $bla_{OXA-181}$[#] bla_{TEM-1B} *cml*A1[§] *dfr*A1[§] *sul*1[§] *sul*3 *tet*(B)	IncFIB(pHCM2) IncFII(pCRY)[#] IncX1 IncY		CHL, TMP, SMX, TET, AMP, MER, ETP, FEP, and TRM	ERS12773683
21100090–1	C	Pig	Fattening	410	-:H9	OXA-181	*aac*(3)-IVa[§] *aad*A2[§] *aph*(3″)-Ia *aph*(3″)-Ib[§] *aph*(4)-Ia *aph*(6)-Id bla_{CARB-2} $bla_{OXA-181}$ *cml*A1[§] *dfr*A16 *flo*R[§] *sul*3 *tet*(A)[§]	IncFIA(HI1) IncI1-I(Alpha) IncR IncX1 IncY	*gyr*A p.D87N *par*C p.S80I *par*E p.S458A	CHL, GEN, NAL, TMP, SMX, TET, AMP, CIP, ETP, MER, FEP, and TRM	ERS12773684
21100098–1	D	Pig	Fattening	410	O159:H28	OXA-181	*aac*(3)-IIa *aad*A2[§] *aph*(3″)-Ib *aph*(3″)-Ia $bla_{OXA-181}$ bla_{TEM-1A} *cat*A1[§] *cml*A1[§] *dfr*A12 *flo*R[§] *mef*(C)[§] *mph*(A)[§] *mph*(G) *qnr*S1 *sul*2[§] *tet*(B) *tet*(M) [§]	IncFIB(AP001918) IncFIC(FII) IncI1-I(Alpha) IncX3	*gyr*A p.D87N *par*C p.S80I *par*E p.S458A	CHL, GEN, AZI, NAL, TMP, SMX, TET, AMP, CIP, ETP, and TRM	ERS12773685
21102457–1	C	Pig	Fattening	38	O86:H30	OXA-48	*aac*(3)-IId[§] *aad*A5 bla_{OXA-48} bla_{TEM-1B} *cat*A1[§] *dfr*A17 *mph*(A)[§] *sul*1[§] *tet*(D)		*gyr*A p.S83A	GEN, AZI, NAL, TMP, SMX, TET, AMP, CIP, MER, ETP, IMI, FEP, FOT, and TRM	ERS12773686

(Continued)

10.3389/fmicb.2022.1016895

TABLE 2 (Continued)

Isolate ID	Region	Host	Production type	ST	Serotype	Carbapenemase type	AMR genes	Inc Plasmid replicons	Chromosomal Point Mutations	Phenotypic AMR pattern	Sample accession number
21109909–1	C	Pig	Fattening	5229	O76:H51	OXA-181	*aac*(3)-IId[§] *aph*(3″)-Ia $bla_{OXA-181}$[#] bla_{TEM-1B} *cat*A2[§] *cml*A1[§] *dfr*A12 *flo*R[§] *lnu*(F) *sul*2 *sul*3 *tet*(A)[§] *tet*(M)[§]	IncFIB(AP001918) IncFIC(FII) IncX3[#]	*gyr*A p.D87N *par*C p.S80I	CHL, GEN, NAL, TMP, SMX, TET, AMP, CIP, ETP, FOT, and TRM	ERS12773687
21110411–1	A	Pig	Fattening	/	-:H10	OXA-181	*aac*(3)-IIa *aph*(3″)-Ib[§] *aph*(6)-Id bla_{DHA-1} $bla_{OXA-181}$[§] bla_{TEM-1B} *cat*A1[§] *dfr*A17 *dfr*A1[§] *flo*R[§] *mph*(A)[§] *qnr*B4 *sul*1[§] *sul*3	IncFII IncX3 IncY		CHL, GEN, AZI, TMP, SMX, AMP, CIP, ETP, FOT, FOX, TAZ, and TRM	ERS12773688
21112463–1	C	Pig	Fattening	5229	-:H45	OXA-181	*aac*(3)-IId[§] bla_{CMY-2} $bla_{OXA-181}$ bla_{TEM-30} *cml*A1[§] *dfr*A12 *flo*R[§] *lnu*(F) *sul*2 *sul*3 *tet*(A)[§] *tet*(M)[§]	IncFIB(AP001918) IncFIC(FII) IncFII(pCoo) IncI1-I(Alpha) IncX1	*gyr*A p.D87N *par*C p.S80I	CHL, GEN, NAL, TMP, SMX, TET, AMP, CIP, MER, ETP, IMI, FEP, FOT, FOX, TAZ, and TRM	ERS12773689
21112465–1	E	Pig	Fattening	542	O167:H20	OXA-181	*aac*(3)-IVa[§] *aad*A2[§] *aph*(3″)-Ia *aph*(4)-Ia $bla_{OXA-181}$[#] bla_{TEM-1B} *cml*A1 *dfr*A1[§] *flo*R[§] *mph*(B) *sul*1[§] *sul*3 *tet*(A)[§] *tet*(M)[§]	IncFIB(AP001918) IncFIC(FII) IncX1 IncX3[#]		CHL, GEN, NAL, TMP, SMX, TET, AMP, CIP, MER, ETP, FEP, FOX, and TRM	ERS12773690
21116039–1	B	Bovine	Beef	5229	-:H9	OXA-181	*aac*(3)-IId[§] *aph*(3″)-Ia $bla_{OXA-181}$ bla_{TEM-1B} *cml*A1[§] *dfr*A12 *flo*R[§] *lnu*(F) *sul*2 *sul*3 *tet*(A)[§] *tet*(M) [§]	IncFIB(AP001918) IncFIC(FII) IncX1	gyrA p.D87N parC p.S80I	CHL, GEN, NAL, TMP, SMX, TET, AMP, CIP, MER, ETP, FEP, and TRM	ERS12773691
21122716–1	C	Pig	Fattening	5229	-:H51	OXA-181	*aac*(3)-IId[§] $bla_{OXA-181}$ bla_{TEM-1B} *cml*A1[§] *dfr*A12 *flo*R[§] *lnu*(F) *sul*2 *sul*3[§] *tet*(A)[§] *tet*(M) [§]	IncFIB(AP001918) IncFIC(FII) IncX1	*gyr*A p.D87N *gyr*A p.S83L *par*C p.S80I	CHL, GEN, NAL, TMP, SMX, TET, AMP, CIP, MER, ETP, and TRM	ERS12773692

(Continued)

10.3389/fmicb.2022.1016895

TABLE 2 (Continued)

Isolate ID	Region	Host	Production type	ST	Serotype	Carbapenemase type	AMR genes	Inc Plasmid replicons	Chromosomal Point Mutations	Phenotypic AMR pattern	Sample accession number
21126335–1	C	Bovine	Beef	542	O163:H20	OXA-181	*aph(3″)-Ib*[§] *aph(6)-Id* $bla_{OXA-181}$ bla_{TEM-1B} *catA1*[§] *dfrA1*[§] *floR*[§] *lnu(G)* *qnrS1 sul3 tet(B)*	IncFIB(AP001918) IncFIC(FII) IncX3 IncY		CHL, NAL, TMP, SMX, TET, AMP, CIP, ETP, FEP, and TRM	ERS12773693
21127652–1	C	Pig	Fattening	218	-:H38	OXA-181	*aadA2*[§] *aph*(3″)-Ib[§] *aph*(6)-Id $bla_{OXA-181}$[#] bla_{TEM-1B} *cml*A1[§] *dfr*A12 *sul3 tet*(B)	IncR IncX3[#]		CHL, TMP, SMX, TET, AMP, ETP, and TRM	ERS12773694
21130011–1	D	Bovine	Beef	10	O13/O129;O13/O135:H48	OXA-181	*aac*(3)-IIa *aac*(3)-IVa[§] *ant*(3″)-Ia[§] *aph*(3″)-Ib[§] *aph*(4)-Ia *aph*(6)-Id $bla_{CTX-M-1}$ $bla_{OXA-181}$ *flo*R[§] *lnu*(G) *mph*(A)[§] *qnr*S1 *sul*1[§] *tet*(A)[§] *tet*(B) *tet*(M)[§]	IncFIA(HI1) IncFIB(AP001918) IncFIC(FII) IncHI1A IncHI1B(R27) IncX3		CHL, GEN, SMX, TET, AMP, CIP, ETP, FEP, FOT, TAZ, and TRM	ERS12773695
21133286–1	B	Pig	Fattening	48	O8:H11	OXA-181	*aac*(3)-IVa[§] *aph*(3″)-Ia *aph*(4)-Ia $bla_{OXA-181}$ bla_{TEM-1B} *flo*R[§] *qnr*S1 *tet*(A)[§] *tet*(M)[§]	IncFIB(AP001918) IncFIC(FII) IncX1 IncX3		CHL, GEN, NAL, TET, AMP, CIP, ETP, and TRM	ERS12773696
21135758–1	B	Pig	Fattening	7461	O112ab:H38	OXA-181	$bla_{OXA-181}$ *qnr*S1	IncX3	gyrA p.S83L	NAL, AMP, CIP, MER, ETP, and TRM	ERS12773697
21137340–1	B	Pig	Fattening	101	O82:H8	OXA-181	*aph*(3″)-Ib[§] *aph*(6)-Id[§] $bla_{OXA-181}$ *dfr*A1 *qnr*S1 *sit*ABCD[§] *sul2 tet*(B)	IncB/O/K/Z_2 IncFIA IncFIB(AP001918) IncFIC(FII) IncFII(pCTU2) IncX3		TMP, SMX, TET, AMP, CIP, ETP, and TRM	ERS12773698

*ONT-sequenced.
[#]located on the same contig.
[§]ResFinder identity or coverage < 100%.
CHL, chloramphenicol; GEN, gentamicin; AZI, azithromycin; NAL, nalidixic acid; TMP, trimethoprim; COL, colistin; SUL, sulfamethoxazole; TET, tetracycline; AMP, ampicillin; CIP, ciprofloxacin; AMK, amikacin; MER, meropenem; FOT, cefotaxime; TAZ, ceftazidime; TGC, tigecycline; ETP, ertapenem; IMI, imipenem; FEP, cefepime; FOX, cefoxitin; and TRM, temocillin.

10.3389/fmicb.2022.1016895

TABLE 3 Metadata and genomic characteristics of the OXA-181 producing *Escherichia coli* obtained from the samples collected in the context of the tracing- back activities after the first OXA-181-producing *E. coli* isolate detection.

Isolate ID	Host	Production type	Sampling site	ST	Serotype	AMR genes	Inc plasmid replicons	Sample accession number
21019054–1	Pig	Fattening	Slaughterhouse	48	O70:H11	*aad*A2[§] $bla_{OXA-181}$ bla_{TEM-1B} *cml*A1[§] *dfr*A12 *mef*(B) *sul*3 *tet*(A)[§] *tet*(M)[§]	IncX3 IncY	ERS12773674
21041921–5	Pig	Fattening	Pen 1 (box 5)	5229	O76:H51	*aac*(3)-IId[§] *ant*(3″)-Ia[§] *aph*(3″)-Ia[§] $bla_{OXA-181}$ bla_{TEM-1B} *flo*R[§] *lnu*(F) *sul*2 *sul*3 *tet*(A)[§]	IncFIC(FII) IncX1	ERS12841964
21041921–11	Pig	Fattening	Pen 1 (box 11)	5229	-:H51	*aad*A2[§] $bla_{CTX-M-1}$ $bla_{OXA-181}$ bla_{TEM-1B} *cml*A1[§] *dfr*A12 *flo*R[§] *mph*(A)[§] *sul*2 *sul*3 *tet*(M)[§]	IncFIC(FII) IncX1	ERS12841965
21058774–1	Pig	Breeding	Gestation Unit	224	O8:H23	*aac*(3)-IIa *aac*(3)-IVa[§] *aad*A5 *aph*(3″)-Ia *aph*(4)-Ia *arm*A $bla_{OXA-181}$ bla_{TEM-1A} *dfr*A17 *mef*(C)[§] *mph*(G) *sul*1[§]	IncFII IncI1-I(Alpha) IncX1 IncY	ERS12841966
21058774–11	Pig	Breeding	Farrowing Unit (pen)	5229	O76:H51	*aac*(3)-IId[§] *ant*(3″)-Ia[§] *aph*(3″)-Ia $bla_{OXA-181}$ bla_{TEM-1B} *flo*R[§] *lnu*(F) *sul*2 *sul*3 *tet*(A)[§]	IncFIC(FII) IncX1	ERS12841967
21058774–16	Pig	Breeding	Weaner Unit "A"	1494	O9a:-	*aac*(3)-IId[§] *aad*A2[§] $bla_{OXA-181}$ bla_{TEM-1B} *dfr*A12 *flo*R[§] *lnu*(F)[§] *sul*3 *tet*(A)[§] *tet*(B) *tet*(M)[§]	IncFIA(HI1) IncFIB(K) IncFII(pCRY) IncR IncX1	ERS12841968
21058774–18	Pig	Breeding	Weaner Unit "B"	5229	O76:H51	*aac*(3)-IId[§] *ant*(3″)-Ia[§] *aph*(3″)-Ia $bla_{OXA-181}$ bla_{TEM-1B} *flo*R[§] *lnu*(F) *sul*2 *sul*3 *tet*(A)[§]	IncFIB(AP001918) IncFIC(FII) IncX1	ERS12841969
21058774–20	Pig	Breeding	Weaner Unit "C"	5229	O76:H51	*aac*(3)-IId[§] *ant*(3″)-Ia[§] *aph*(3″)-Ia $bla_{OXA-181}$ bla_{TEM-1B} *flo*R[§] *lnu*(F) *sul*2 *sul*3 *tet*(A)[§]	IncFIC(FII) IncX1	ERS12841970
21058774–21	Pig	Breeding	Finisher Unit	5229	O76:H51	*aac*(3)-IId[§] *ant*(3″)-Ia[§] *aph*(3″)-Ia $bla_{OXA-181}$ bla_{TEM-1B} *flo*R[§] *lnu*(F) *sul*2 *sul*3 *tet*(A)[§]	IncFIC(FII) IncX1	ERS12841971
21067608–2	Human	N.A.	N.A.	5229	O101:H9	*aac*(3)-IId[§] *aad*A5 *aph*(3″)-Ib *aph*(6)-Id $bla_{OXA-181}$ bla_{TEM-1B} *cat*A1[§] *dfr*A17 *flo*R[§] *mph*(A)[§] *sul*1[§] *sul*2 *tet*(B)	IncFII IncX1	ERS12841972
21067608–3	Human	N.A.	N.A.	744	O76:H51	*aac*(3)-IId[§] *ant*(3″)-Ia[§] *aph*(3″)-Ia $bla_{OXA-181}$ bla_{TEM-1B} *flo*R[§] *lnu*(F) *sul*2 *sul*3	IncFIC(FII) IncX1	ERS12841973

(Continued)

TABLE 3 (Continued)

Isolate ID	Host	Production type	Sampling site	ST	Serotype	AMR genes	Inc plasmid replicons	Sample accession number
21067610–3	Bovine	Dairy		5229	O76:H51	*aac*(3)-IId[§] *ant*(3″)-Ia[§] *aph*(3″)-Ia $bla_{OXA-181}$ bla_{TEM-1B} *flo*R[§] *lnu*(F) *sul2 sul3 tet*(A)[§]	IncFIC(FII) IncX1	ERS12841974

[§]ResFinder identity or coverage < 100%.

with the rapid barcoding kit (SQK-RBK004) and sequenced using the nanopore-based MinION device (ONT; Branton et al., 2008).

Bioinformatics analysis

Illumina raw reads were analyzed using an internal pipeline for assembly, which includes the following tools: FastQC,[6] Trimmomatic (Bolger et al., 2014), Spades (Bankevich et al., 2012), and Quast (Gurevich et al., 2013). Molecular characterization was performed on all the assembled genomes with the MLST tool[7] for Multilocus Sequence Typing (MLST) analysis and with the ABRicate tool[8] using the Genomic Epidemiology (CGE) databases (last update 22/04/2022) of ResFinder (with a threshold of 95% for coverage and identity) and PointFinder[9] for the detection of the genetic basis of AMR to confirm the AMR phenotypes, PlasmidFinder[10] for plasmid replicon typing, SerotypeFinder[11] for *in silico* serotyping and VirulenceFinder[12] for virulotyping. Additionally, the VF database[13] was used for virulence gene detection.

For the samples subjected to both short and long reads sequencing, high accuracy basecalling was performed on long-reads obtained from the MinION device according to the ONT workflow. A hybrid (Illumina-ONT) assembly was performed using the Unicycler pipeline (Wick et al., 2017) with the default parameters (Diaconu et al., 2020). Assemblies from the OXA-181 producing isolates recovered during the monitoring were compared using the Mashtree algorithm (Katz et al., 2019). The assemblies obtained were annotated using the Bakta tool (Schwengers et al., 2021). Additionally, a manual curation for the obtained annotation was also performed. All the obtained plasmid sequences were compared calculating the average nucleotide identity (ANI) for the alignment coverage and identity, using the BLAST algorithm (Goris et al., 2007; Supplementary Table 1).

Representative hybrid assemblies of the different plasmids harboring $bla_{OXA-181}$, were compared by BLAST, using both the stand alone tool and the on-line tool against the nr/nt database. After that, assemblies of the IncX3 plasmids detected in this study were compared with selected IncX3 plasmid sequences obtained from publicly available databases with more than 80% of identity: FDAARGOS_433 (CP023897) from Canada, pAMA1167 (CP024806) from Denmark, pOXA 181_29144 (KX523903) from Czech Republic, pSTIB_IncX3_OXA_181 = IncX3_OXA_181 (MG570092) from Lebanon, pOXA181 IHIT35346 (KX894452) from Italy, pKBN10P04869C (CP026476) from South Korea, pKP_BO_OXA181 (MG228426) from Italy, and NZ_CP040399.1 from India. The complete sequence of the IncX3 plasmid pMOL4791 from sample ID 21054791 (accession number ERS12413439) was used as reference.

Similarly, our IncX1 plasmid sequences were compared with publicly available databases using the IncX1 plasmid pMOL6975 from sample ID 21066975 (accession number ERS12413440). Results were represented using BRIG (Alikhan et al., 2011) or using the R[14] package ggplot2 version 3.3.6.9000.

Results

OXA-48-like producing *Escherichia coli* prevalence at slaughterhouse

Overall, $n = 21$ out of 301 caecal samples of fattening pigs (6.98%; 95% CI 4.37–10.47%) and $n = 4$ out of 310 bovines <12 months (1.29%; 95% CI 0.35- 3.27%) resulted positive to OXA-48-like-producing *E. coli* ($n = 24$ OXA-181, $n = 1$ OXA-48).

6 https://www.bioinformatics.babraham.ac.uk/projects/fastqc/
7 https://github.com/tseemann/mlst
8 https://github.com/tseemann/abricate
9 https://cge.cbs.dtu.dk/services/ResFinder/
10 https://cge.cbs.dtu.dk/services/PlasmidFinder/
11 https://cge.cbs.dtu.dk/services/SerotypeFinder/
12 https://cge.cbs.dtu.dk/services/VirulenceFinder/
13 http://www.mgc.ac.cn/VFs/
14 https://www.r-project.org

Antimicrobial susceptibility testing

The complete results and interpretation of AST performed on the 25 OXA-48-like-producing *E. coli* obtained from the survey at slaughter, are reported in Supplementary Table 1 and Table 2. The isolates presented a MDR resistance profile ranging from a pattern of minimum four resistances (beta-lactams, carbapenems, fluoroquinolones, and trimethoprim, 1/25, 4.0%) up to a pattern of eight resistances (carbapenems, fluoroquinolones, aminoglycosides, sulphonamides, tetracyclines, trimethoprim, phenicols, all beta-lactams or macrolides 3/25, 12.0%). As for the carbapenem resistance phenotypes, all of them showed microbiological resistance to ertapenem and 13/25 (52%) to meropenem, while 5/25 (20%) showed microbiological and clinical resistance to imipenem. All of them were also microbiologically and clinically resistant to the semi-synthetic betalactam antibiotic temocillin (Table 1). Additionally, 17/25 (68%) isolates, were concomitantly resistant to aminoglycosides, with all of them showing resistance to gentamicin and one also to amikacin (ID 21076969–1). Moreover, some isolates were also resistant to certain Highest Priority Critically Important antimicrobials (HPCIAs), with almost (22/25, 88%) all being resistant to ciprofloxacin and 3/25 (12%) also to azithromycin. Four isolates were Extended-Spectrum Cephalosporins (ESC)-R, being resistant to cefotaxime and ceftazidime, while elevated MICs for cefotaxime slightly above the CUTOFF (mode = 0.5 mg/L) were observed in other five isolates.

Bionformatics analysis of OXA-48-(like)-producing *Escherichia coli* from the survey at slaughter (short-read sequencing)

Genomic characterization of the 24 OXA-181 and one OXA-48 producing isolates indicated that the OXA-181-producing isolates presented a high degree of Sequence Types (STs) diversity, although nine out of 25 isolates belonged to ST5229.

According to the results of SerotypeFinder, the isolates belonged to different serotypes (Table 2), and none of them belonged to the most relevant serogroups associated to Shiga-Toxin *E. coli* (STEC) infections in humans. Two isolates (IDs 21058774–1, 21133286–1) belonged to the serogroup O8, which is frequently found in the intestinal pathogenic *E. coli* (inPEC) pathotype implicated in post-weaning diarrhea in swine. However, in these isolates, the genes encoding the fimbriae F4, F5, F6, and F41 and F4, F18ac, which are typical of this pathotype (Luppi, 2017; Yang et al., 2019), were lacking.

As for the results of the virulence-associated determinants detected by VirulenceFinder and VF database, almost all isolates harbored the curli fimbriae (*csgA*) and the type 1 fimbriae (*fim*H), while only some of them presented at least one of the following virulence genes: *fim*A, *ast*A encoding the enteroaggregative *E. coli* heat-stable enterotoxin 1 (EAST1), *pap*C, *iuc*D, *pic*, and *hly*F. Of these, only one isolate (ID 21088819) harbored all the above mentioned genes except for *fim*A. However, none of these genes indicated the presence of a specific *E. coli* pathotype. Three isolates, 21054791, 21088819, and 21137340, presented the gene *sit*ABCD, and one of them (21088819) presented also *kat*P, both responsible for resistance to hydrogen peroxide.

In general, the AMR genotypes were in agreement with the MDR phenotypic resistance patterns (Table 2).

As for the MDR phenotypes including resistance to HPCIAs, two of the four ESC-R isolates, (IDs 21076969 and 21130011) were confirmed ESBL producers, harboring $bla_{\text{CTX-M-55}}$ and $bla_{\text{CTX-M-1}}$, respectively, while isolates with IDs 21110411 and 21112463, had an AmpC profile, presenting $bla_{\text{CMY-2}}$ and $bla_{\text{DHA-1}}$ genes, respectively. As for the 22 ciprofloxacin resistant isolates, 15 of them presented some chromosomal mutations associated with (fluoro)quinolone resistance, *gyr*A p.D87N or p.S83A, *par*C p.S80I, or *par*E p.S458A. Moreover, 12 isolates presented the transferable quinolone resistance (*qnr*) genes *qnr*S1 and one isolate *qnr*B4. In six cases, these *qnr* genes were found together with chromosomal mutations associated to (fluoro)quinolone resistance. One isolate presented a (fluoro)quinolone resistance phenotype (ciprofloxacin MIC value of 16 mg/L), but did not harbor any related known accessory resistance gene or chromosomal point mutation. The OXA-48-producing isolate presented the following AMR genes profile: *aac*(3)-IId, *aadA5*, $bla_{\text{OXA-48}}$, $bla_{\text{TEM-1B}}$, *catA1*, *dfrA17*, *mph*(A), *sul1*, and *tet*(D).

Additionally, all 17 gentamicin-resistant isolates harbored at least one of the corresponding gentamicin resistance genes as *aac*(3)-IId, *aac*(3)-IVa, and *aac*(3)-IIa. One of them (ID 21076969–1) showing phenotypic resistance to amikacin presented also the corresponding gene *rmt*B, responsible for phenotypic resistance to amikacin and gentamicin (Figure 1; Table 2).

The results of PlasmidFinder analysis revealed the presence of different plasmid replicons (Figure 1; Table 2) with IncX (IncX1 and IncX3) and IncF types being the most represented in the 25 isolates. In five isolates $bla_{\text{OXA-181}}$ was located on the same contig of the IncX3 replicon and in one isolate, on the same contig of IncFII (Figure 1; Table 2). Differently, the OXA-48-producing isolate (21102457–1) did not contain any plasmid replicon.

The results of the Mash analysis are represented in Figure 1. The Mash clusterization indicated the presence of a non-clonal population of OXA-48-like producing *E. coli* in the dataset analyzed. The clusters were distributed according to the different Clonal Complexes (CCs) and STs. No clear region or host species correlation was observed.

Bionformatics analysis of OXA-181-producing *Escherichia coli* from tracing-back activities (short-read sequencing)

A total of 11 OXA-181 producing *E. coli* were obtained from 11 samples collected from different sampling sites within the studied holdings in the context of the tracing back activities

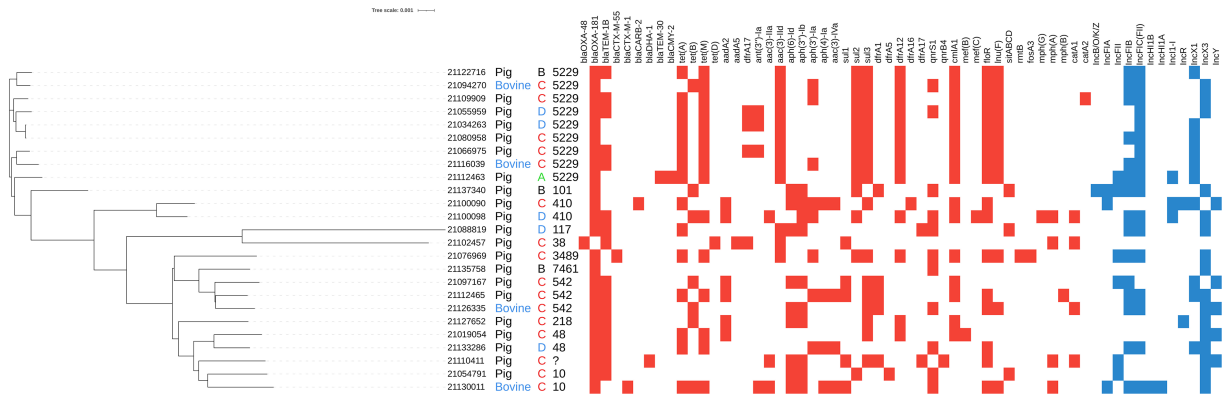

FIGURE 1
Mash clusterization of the complete genome, resistome and plasmidome of the 25 OXA-181-producing *Escherichia coli* isolated from caecal samples collected at slaughterhouse during the monitoring activities. From left to right: isolate ID, host (pig in black letters, bovine in blue letters), region anonymized and ST. Colored squares indicate the presence of resistance genes (red squares) and plasmid replicons (blue squares).

related to the *E. coli* isolate 21019054–1 detected from the survey at slaughter (Table 3).

In detail, two isolates were obtained from fecal samples collected from the fattening holding of origin, six from different units of the breeding holding providing weaners, one from an epidemiologically related dairy cattle holding, and two from human samples taken from the worker and owner at the breeding holding. As for the results of molecular characterization, eight out of 11 isolates were classified as ST5229 whereas the other ones were classified as ST224, ST1494, and ST744. None of them belonged to ST48, the ST to which the first positive isolate at slaughterhouse belonged. The results of the *in silico* serotype determination were almost in agreement with the STs, being the serotype most represented O76:H51, associated with ST5229.

All presented a MDR gene profile and, at least, two different plasmid types (Table 3).

Full reconstruction of the $bla_{OXA-181}$-carrying plasmids by hybrid (short and long-read) assembly approach

The complete sequence of 16 plasmids harboring $bla_{OXA-181}$ was obtained through the hybrid (Illumina–ONT) assembly approach. In the studied OXA-181 producing *E. coli* population, $bla_{OXA-181}$ was confirmed to be located in different type of plasmids, according to the incompatibility group classification: IncX3 (in three isolates from the survey at slaughter) IncX1 (in two isolates from the survey at slaughter and 10 isolates from tracing-back activities) and IncFII (in one isolate from tracing-back activities). In all the three plasmid types, $bla_{OXA-181}$ was part of a transposon with a similar general structure, which in all IncX1 plasmids resulted identical (Figure 2). Coverage and identity values obtained comparing all the 16 fully resolved plasmids are reported in Supplementary Table 1.

The size of the IncX3 plasmids from the ID21019054, ID21055959, and ID21054791 isolates were 51,982; 57,195, and 57,650 bp, respectively. Using the plasmid from ID 21054791 (pMOL4791) as reference, all three resolved plasmids IncX3 harboring $bla_{OXA-181}$ were very similar with 100% identity but 90–91% coverage (Supplementary Table 1). The two larger plasmids contained also the resistance gene *qnr*S. The *rep*B gene was located in the region 5931..6944 and *rep*A in 44413..45373, being truncated in the plasmid from ID21054791. Most of the genes found were involved in the stabilization, replication and conjugation of the plasmids, except the resistance genes and the different ISS sequences. The complete sequences of our three IncX3 plasmids from *E. coli* isolates (IDs 21019054, 21054791, and 21055959) shared a similarity of 99% with only 89% of the plasmid covered, when compared with publicly available IncX3 plasmids containing $bla_{OXA-181}$ using Blast (Figure 3).

At least, two IncX3 plasmids (IDs 21019054, 21055959) resolved in this study harbored a gene encoding a membrane transport protein (*yheS*) together with a DNA invertase. These genes were located in the "extra region" which was not present in the plasmids previously published. As for all the 12 IncX1 plasmids resolved in the present work, their size range was 57,694–58,897 bp and the largest one was used as reference (ID 21066975; pMOL6975). These plasmids were all almost identical between them with a 98-99% coverage and 99-100% sequence identity (Supplementary Table 1) and no similar IncX1 plasmids were found in public available databases. Our IncX1 plasmids contained mainly the genes involved in their maintenance, replication and conjugation (Figure 4). All harbored $bla_{OXA-181}$ in a transposon (19869..28757), that also contained *rep*A and *ere*A, and flanked by *tn*3 and IS6. This IncX1 plasmid also presented a type II toxin/antitoxin system, with the toxin of the RelE/StbE family and its antitoxin RelB (9784..10306).

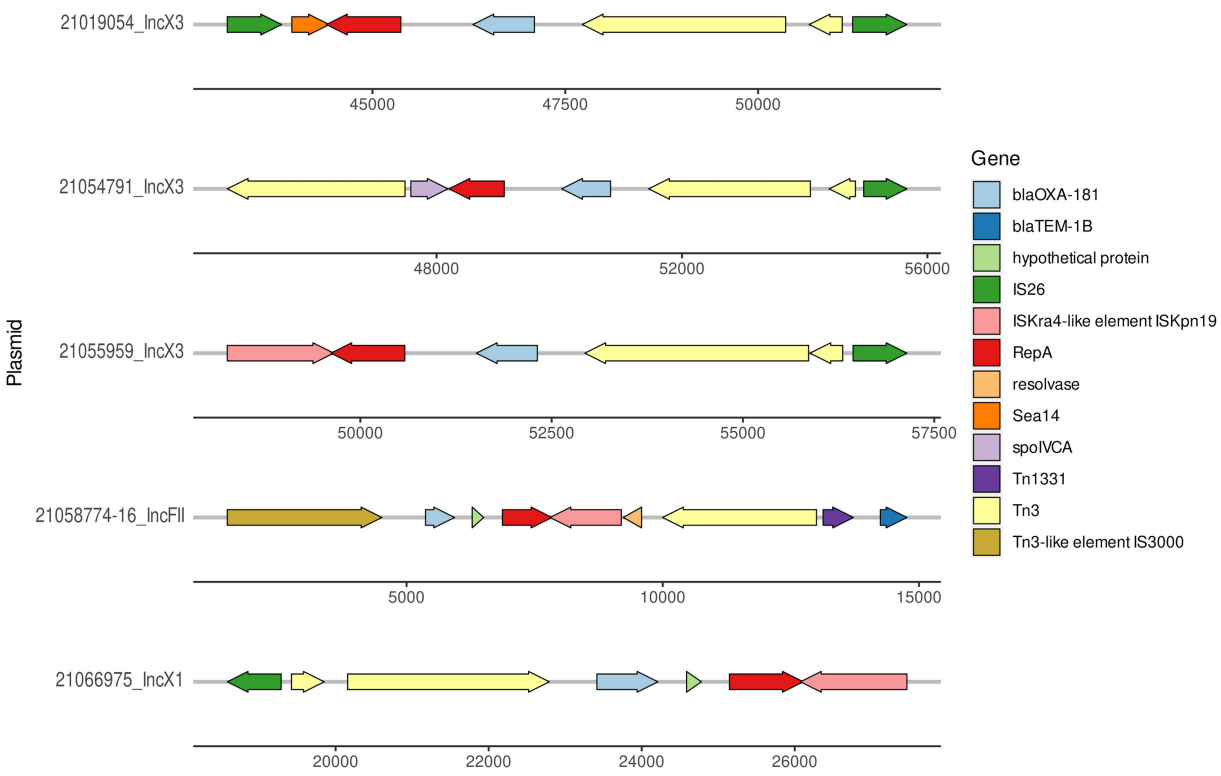

FIGURE 2
Graphical representation of the region where *bla*$_{OXA-181}$ was located in the three IncX3 plasmids, one representative IncX1 (pMOL6975) from ID21066975 (accession number ERS12413440) and IncFII (21058774–16) plasmids.

Discussion

In the last years, *bla*$_{OXA-181}$ has been detected not only in hospitals, but also in community settings, and occasionally also in animals (livestock, companion animals, and wildlife) and in the environment (Mairi et al., 2018). According to the EU-harmonized AMR monitoring program conducted in EU Member States using selective media for CRE, the occurrence of carbapenemase-producing *E. coli* and *Salmonella* spp. among livestock epidemiological Units in Europe has so far remained very sporadic. Indeed, only three *E.coli* isolates from Germany harboring *bla*$_{VIM-1}$ (pig meat; Irrgang et al., 2019), *bla*$_{OXA-48}$ (fattening pig; Irrgang et al., 2020a), *bla*$_{GES-5}$ (fattening pig; Irrgang et al., 2020b), and one presumptive CR *E. coli* isolate from Romania, were detected in 2018 and 2019 [European Food Safety Authority (EFSA) and European Center for Disease Prevention and Control (ECDC), 2021]. In previous years (2015–2017), very similar results were also obtained, with only three *E. coli* from broilers and broiler meat in Romania confirmed as *bla*$_{OXA-162}$ carriers [European Food Safety Authority (EFSA) and European Center for Disease Prevention and Control (ECDC), 2019; Bortolaia et al., 2021]. Prior to the findings described in this study, voluntary monitoring of CRE isolates conducted in Italy since 2014 revealed for the first time in 2019 the presence of only one *bla*$_{NDM-4}$ positive *E.coli* from an Italian sample taken at slaughter (Diaconu et al., 2020). Conversely, thanks to the AMR monitoring activities conducted in 2021, we have witnessed for the first time the spread of OXA-181 producing isolates spreading in holdings of fattening pigs (estimated around 7%) and veal calves (around 2%), farmed in four contiguous Italian regions and provinces. This has been most likely facilitated by the intensive trade patterns occurring throughout the national territory, which is typical of these animal productions also across the EU [European Food Safety Authority (EFSA), 2010]. In our study, MLST analysis revealed a dominant ST (ST5229) in the pig and veal calf holdings in three out of the five Italian regions involved. Noteworthy, we detected the same ST also during the tracing back activities in the fattening holdings of origin, in different units of the same breeding holding, in the epidemiologically related dairy cattle holding and also in one of the two positive workers at the breeding holding (Table 3). To the best of our knowledge, *E. coli* ST5229 isolates have never been reported to harbor *bla*$_{OXA-48}$-(like) genes. This ST has been previously described in *E.coli* harboring multiple AMR genes (e.g., *mcr* and ESBL genes) isolated from pig samples in different Asian countries (Li et al., 2021; Truong et al., 2021). Conversely, we observed that the same plasmids of three different Inc. groups carrying the *bla*$_{OXA-181}$ gene in the same transposon structure were harbored by different STs. This feature is indicative of the mobilization of *bla*$_{OXA-181}$

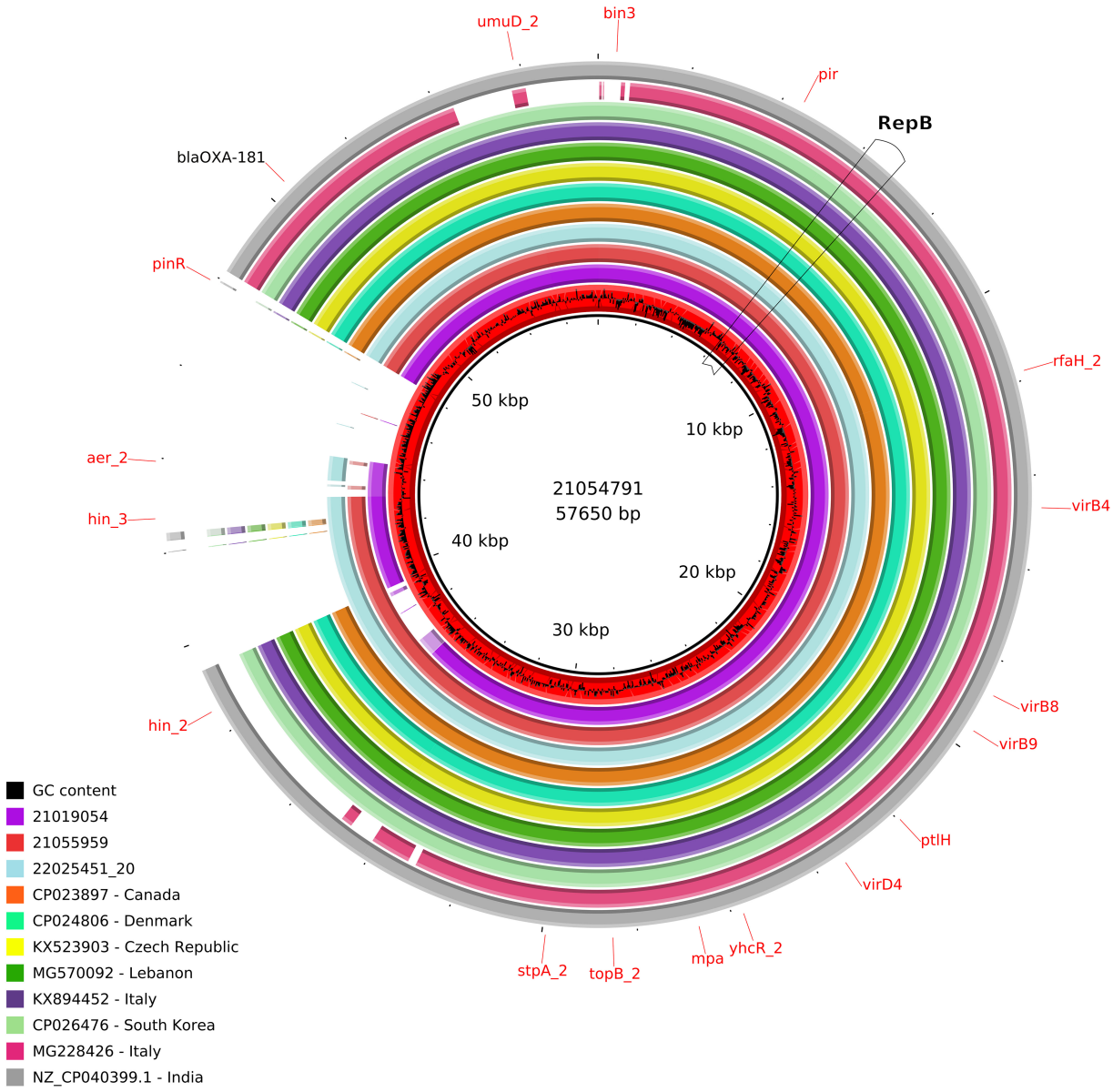

FIGURE 3
Comparison of the IncX3 plasmids obtained in this study and publicly available IncX3 plasmids containing $bla_{OXA-181}$. From the inner circle, the plasmids represented were the following: red: ID21054791 used as reference (accession number ERS12413439), including the CG content graph (sequenced in this study, *Escherichia coli*, caecal content, pig 2021), violet: ID21019054 (sequenced in this study, *E. coli*, pig caecal content 2021), light red: ID21055959 (sequenced in this study, *E. coli*, pig caecal content, 2021), turquoise: ID22025451_20 (sequenced at the Italian NRL-AR; *Citrobacter freundii*, pig feces, 2022), orange: FDAARGOS_433 (CP023897, Canada, *E. coli*, human, 2017), hospital green: pAMA1167_OXA_181 (CP024806, Denmark, *E. coli*, human, 2017), yellow: pOXA_181_29144 (KX523903, Czech Republic, *Klebsiella pneumoniae*, human, 2016), green: pSTIB_IncX3_OXA_181 (MG570092, Lebanon, *E. coli*, human, 2016), purple: pOXA181 IHIT35346 (KX894452, isolated in Italy, *E. coli*, pig, 2016), light green: pKBN10P04869C (CP026476, South Korea, *E. coli*, human, 2017), pink: pKP_BO_OXA181 (MG228426, Italy, *E. coli*, human, 2017), and gray: (NZ_CP040399.1, India, *E. coli*, human, 2016).

region and its likely horizontal transfer among different plasmid types and hosts. Accordingly, the massive and rapid dissemination of $bla_{OXA-181}$ in the studied holdings could be the result of the combined effect of clonal spread and horizontal gene transfer.

Overall, clonal dissemination in humans has been previously reported to play a minor role in the spread of OXA-48-like carbapenemases, although certain high-risk clones of *Klebsiella pneumoniae* and *Escherichia coli* have been associated with the global spread of OXA-48, OXA-181, OXA-232, and OXA-204 carbapenemases in humans (Pitout et al., 2019). Among *E. coli* isolates, ST410 has been described as the most common high-risk global clone associated with $bla_{OXA-181}$ in human patients, usually carried by IncX3 plasmid types (Pitout et al., 2019). Similarly, in

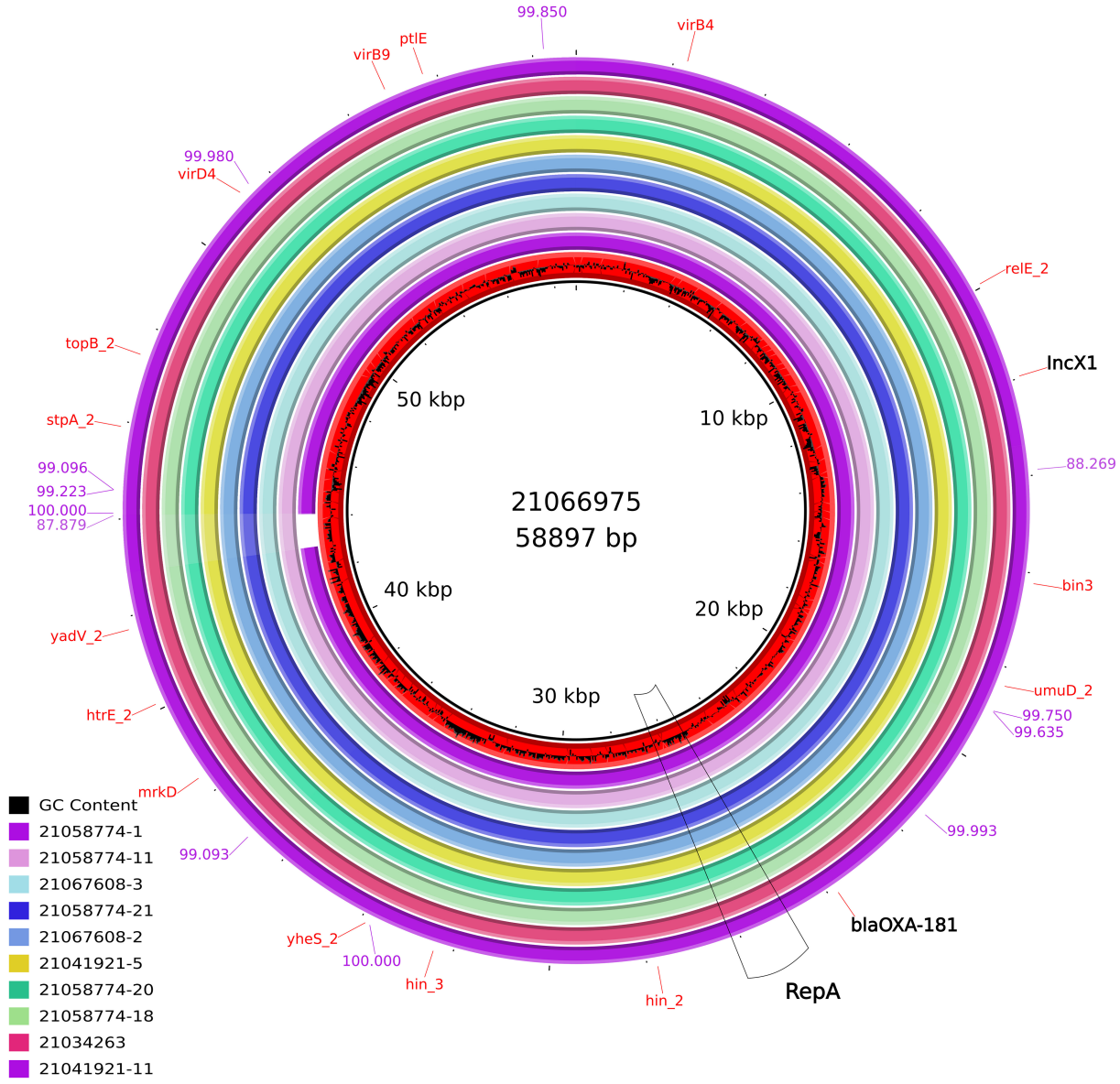

FIGURE 4
Comparison of the IncX1 plasmids from *E.coli* obtained in this study containing $bla_{OXA-181}$. From the inner circle, the plasmids represented were: ID21066975 used as reference (accession number ERS12413440, *Escherichia coli,* pig, caecal content at slaughterhouse) ID21058774-1 (Breeding pig), ID21058774-11 (Breeding pig), ID21067608-3 (Human), ID21058774-21 (Breeding pig), ID21067608-2 (Human), ID21041921-5 (Fattening pig), ID21058774-20 (Breeding pig), ID21058774-18 (Breeding pig), ID21034263-1 (pig, caecal content at slaughterhouse), and ID21041921-11 (Fattening pig). The bluish values indicate the % of identity of one IncX1 complete sequence (ID 21041921–11) compared with the reference sequence ID 21066975.

animals this clone was also detected in 24 hospitalized pets in Switzerland (Nigg et al., 2019) and from a dog in Portugal (Brilhante et al., 2020). In our study, OXA-181 producing *E. coli* belonging to ST410 were identified in two caecal samples coming from two fattening pig holdings located in regions B and C (IDs 21100090–1 and 21100098–1) and this represents the first report of this high-risk clone associated with $bla_{OXA-181}$ in livestock. This finding is of concern, as this clone has been reported to promote not only the spread of $bla_{OXA-181}$, but also the spread of different carbapenem-resistant genes as bla_{NDM}, bla_{KPC-2}, and CTX-M-type extended-spectrum β-lactamase genes in clinical settings of different countries (Qin et al., 2018).

We have detected $bla_{OXA-181}$ in three different plasmid types (IncX1, IncX3, and IncF types), which in most cases did not carry other AMR genes. However, almost all isolates showed a MDR profile and harbored the corresponding AMR genes, including co-resistance to HPCIAs (fluoroquinolones, macrolides, and third and fourth generation cephalosporins). Hence, these findings are of particular concern as they underline the co-occurrence, within the same isolate, of different plasmid types harboring multiple

AMR genes, including those encoding resistance to last-resort drugs that are spread across the animal-human interface.

Moreover, the co-occurrence of different plasmids could facilitate the mobilization of the transposon containing $bla_{OXA-181}$ to other MDR carrying plasmids or the fusion of these plasmids into a mosaic plasmid (Zheng et al., 2013).

In our study, we have detected $bla_{OXA-181}$ in a composite transposon, in different *E. coli* isolated from pig and veal calf holdings of four Italian regions. So far, the global spread of $bla_{OXA-181}$ among Enterobacterales in humans has been reported to be mainly caused by the same insertion element IS*Ecp1* situated within the Tn2013 transposon located on various plasmid backbones (Pitout et al., 2019). Additionally, it should be noted that we detected $bla_{OXA-181}$ also in the same IncX3 plasmid of a MDR, AmpC producing (CMY-34-type) *C. freundii* (Figure 3). This isolate was also beta-lactam, fluoroquinolone and phenicol resistant, and was detected in the same pig holding which tested positive for OXA-181 producing MDR *E. coli* during the survey at slaughter in 2021 (data not shown). This finding provides the observational evidence that an identical OXA-181-positive plasmid (100% coverage and identity with the plasmid of ID 21019054) was shared between two Enterobacterales species isolated from the same porcine fecal sample. Moreover, in this study we have demonstrated that the same transposon containing $bla_{OXA-181}$, could be found in plasmids belonging to at least three different Inc. groups, confirming that this gene may be itself mobilizable through transposable elements and could be introduced in different plasmid scaffolds.

This mobile structure was found to be identical to those previously detected in other IncX3 plasmids from *E. coli* isolated from human and occasional animal sources in different countries worldwide, and also in different Enterobacterales species as *Klebsiella pneumoniae* (Figure 3). In addition, the genetic environment of the $bla_{OXA-181}$ gene observed in our plasmids was identical in approximately 80% of the sequence.

As for the IncX1 plasmids, to our knowledge, similar plasmids carrying $bla_{OXA-181}$ have never been described before in Enterobacterales, as our IncX1 plasmids shared only an approximately 50% of identity with publicly available IncX1 sequences. In the isolates under study, this IncX1 plasmid is almost the same (99-100% identity), including the IncX1 plasmid found in OXA-181 producing *E. coli* from humans. In addition, IncX1 seems to be more stable than IncX3 probably because of the presence of the RelE/StbE toxin family and its antitoxin RelB in IncX1, as previously reported (Jensen and Gerdes, 1995). Overall, our study highlights that these plasmids can be efficiently harbored by *E. coli* ST/lineages frequently detected in fecal samples from pigs, calves and humans, and it is likely they are part of the "normal" intestinal microbiota of healthy food-producing animals, including those sent for slaughter. These findings are of public health importance due to the "opportunistic" nature and MDR attitude of Enterobacterales, which are a major threat in healthcare-related infections.

Although OXA-181 is a stronger carbapenemase than OXA-48, imipenem and meropenem MICs values are usually lower than for *K. pneumoniae* carbapenemase (KPC)-producing or Metallo-Beta-Lactamase (MBL)-positive isolates, and often remain apparently "susceptible" to some carbapenems according to current clinical EUCAST and CLSI breakpoints. However, the phenotypes of the OXA-181 producing isolates under study were unequivocally resistant to ertapenem (and temocillin), while only 13/25 (52%) tested microbiologically resistant to meropenem and 5/25 (20%) microbiologically and clinically resistant to imipenem (Table 1). Indeed, detection of carbapenemases of the OXA-48 family in clinical settings may be challenging, as previously reviewed (Kidd et al., 2020), because they usually show a modest hydrolytic activity against carbapenems that could also vary in relation to the different OXA-48-like enzymes. Moreover, clinical practice demonstrates how the *in vitro* susceptibility against carbapenems may not predict the success for the treatment of OXA-48-like producing Enterobacterales. In this regard, OXA-48-like producing Enterobacterales are most likely underreported, as they could be hard to identify without targeted molecular analysis. Other factors, including bacterial species, enzyme expression, membrane permeability, and any other resistance mechanisms, may contribute to the resistance phenotype (Kidd et al., 2020). Overall, these aspects are of particular concern, not only for the clinical relevance of Enterobacterales encoding for OXA-181 and in general for OXA-48-like carbapenemases, in human medicine, where high case-fatality rates have been observed in healthcare-associated infections (Cuzon et al., 2011; Navarro-San Francisco et al., 2013; Rodríguez et al., 2021), but also in the context of possible transmission events and spread (of isolates and MGEs) that can occur between animals and humans.

In conclusion, carbapenem-resistant Enterobacterales are still uncommon in animals worldwide and so far have been considered very sporadic in the EU. However, the findings of our population and genomic studies underline how their continuous and specific monitoring in the EU in food-producing animals and along the food chain is of a great relevance, despite carbapenems are among beta-lactams that have never been authorized for veterinary use. Indeed, the extensive use of other antimicrobials, as well as the continuous oral usage of aminopenicillins, besides selecting for extended-spectrum cephalosporin resistance (Cavaco et al., 2008), may be of selective advantage also for the spread of carbapenemases in animal primary productions, following their introduction from human or human-related sources. These findings in the animal productions sector should further increase the awareness of this hidden threat for human health. In our study, possible transmission pathways among farms, between animals and in-contact humans were investigated, and point to a human source as the most likely cause for the introduction of the OXA-181 carrying plasmid (IncX1 type) in the breeding holding where initial tracing-back activities were conducted. Whatever the initial source, we have provided evidence that these CRE have been amplified within the intensive animal production

systems, especially in pigs. The spread of CRE in food-producing animals is of particular concern in a "One Health" perspective, since it may soon represent an important and additional source of CRE exposure for humans along the food chain. In this regard, specific integrated policies for risk mitigation are needed, in order to reduce the burden of MDR carbapenemase-producing bacteria in humans and minimize the impact of any possible animal and environmental reservoirs.

Data availability statement

Illumina raw reads of the 36 isolates and ONT raw reads from 16 selected isolates analyzed in this study, were submitted to the European Nucleotide Archive (http://www.ebi.ac.uk/ena) under the study accession number PRJEB54630. The single sample accession numbers of each isolate are reported in Table 2 and 3.

Ethics statement

Human fecal samples from workers and owners were voluntary made available through the Local Health Competent Authorities, after giving informed consent to participate in the study. This work does not contain experimentation with animals. As reported in the main text, the studied samples were collected from (1) caecal samples, taken by the Competent Authorities (Veterinary Services) after the slaughtering (for food) in the frame of the harmonized European Monitoring for Antimicrobial resistance (EU Decision 2013/652 and 2020/1729) or (2) fresh fecal samples taken by the Competent Authorities (Veterinary Services) on the floor of the boxes (of the holdings) where the animals were kept.

Author contributions

AF, VC, PA, and AB conceived and designed the experiments. FG and LC performed tracing-back activities. AI, PD, LS, ED, and RA performed the experiments. FB and ELD managed the data. ELD, PA, VC, AF, and AB analyzed the data. VC, PA, ELD, AF, and AB wrote the paper. All authors contributed to the article and approved the submitted version.

Funding

This work was funded partly by the Italian Ministry of Health (Ricerca Corrente, grant N° IZSLT - PRC202002). The genomic work on the use of the combined approach of short and long-read sequencing to resolve the OXA-181-carrying plasmids was conducted in the framework of the Full Force project, supported by the European Union's Horizon 2020 Research and Innovation programme under grant agreement No 773830: One Health European Joint Programme.

Acknowledgments

The authors wish to thank Carmela Buccella, Roberta Onorati, Fabiola Feltrin, Angelo Giacomi, Fiorentino Stravino, Gessica Cordaro, Manuela Iurescia, and Tamara Cerci from Istituto Zooprofilattico Sperimentale del lazio e Toscana "M. Aleandri" for their technical support; Giuseppe Merialdi, DVM, Giovanni Alborali, DVM, Silvia Bellini, DVM from Istituto Zooprofilattico Sperimentale della Lombardia e dell'Emilia—Romagna "Bruno Ubertini," Italy; and Antonio Vitali, DVM, Francesco Brescianini, DVM, Veterinary Officers at ATS Brescia, for providing technical support in the tracing back activities at holding level. The authors also wish to thank Loredana Candela, DVM, General Direction of Animal Health and Veterinary Medicinal Products, Italian Ministry of Health, for networking and facilitating investigations at holding level.

Conflict of interest

The authors declare that the research was conducted in the absence of any commercial or financial relationships that could be construed as a potential conflict of interest.

Publisher's note

All claims expressed in this article are solely those of the authors and do not necessarily represent those of their affiliated organizations, or those of the publisher, the editors and the reviewers. Any product that may be evaluated in this article, or claim that may be made by its manufacturer, is not guaranteed or endorsed by the publisher.

Supplementary material

The Supplementary material for this article can be found online at: https://www.frontiersin.org/articles/10.3389/fmicb.2022.1016895/full#supplementary-material

References

Alba, P., Taddei, R., Cordaro, G., Fontana, M. C., Toschi, E., Gaibani, P., et al. (2021). Carbapenemase IncF-borne bla_{NDM-5} gene in the *E. coli* ST167 high-risk clone from canine clinical infection, Italy. *Vet. Microbiol.* 256:109045. doi: 10.1016/j.vetmic.2021.109045

Alikhan, N. F., Petty, N. K., Ben Zakour, N. L., and Beatson, S. A. (2011). BLAST ring image generator (BRIG): simple prokaryote genome comparisons. *BMC Genomics* 12:402. doi: 10.1186/1471-2164-12-402

Bakthavatchalam, Y. D., Anandan, S., and Veeraraghavan, B. (2016). Laboratory detection and clinical implication of Oxacillinase-48 like Carbapenemase: the hidden threat. *J. Global Infect. Dis.* 8, 41–50. doi: 10.4103/0974-777X.176149

Bankevich, A., Nurk, S., Antipov, D., Gurevich, A. A., Dvorkin, M., Kulikov, A. S., et al. (2012). SPAdes: a new genome assembly algorithm and its applications to single-cell sequencing. *J. Comput. Biol.* 19, 455–477. doi: 10.1089/cmb.2012.0021

Bolger, A. M., Lohse, M., and Usadel, B. (2014). Trimmomatic: a flexible trimmer for Illumina sequence data. *Bioinformatics* 30, 2114–2120. doi: 10.1093/bioinformatics/btu170

Bortolaia, V., Ronco, T., Romascu, L., Nicorescu, I., Milita, N. M., Vaduva, A. M., et al. (2021). Co-localization of carbapenem ($bla_{OXA-162}$) and colistin (*mcr*-1) resistance genes on a transferable IncHI2 plasmid in Escherichia coli of chicken origin. *J. Antimicrob. Chemother.* 76, 3063–3065. doi: 10.1093/jac/dkab285

Boyd, S. E., Holmes, A., Peck, R., Livermore, D. M., and Hope, W. (2022). OXA-48-like β-lactamases: global epidemiology, treatment options, and development pipeline. *Antimicrob. Agents Chemother.* 66:e0021622. doi: 10.1128/aac.00216-22

Branton, D., Deamer, D. W., Marziali, A., Bayley, H., Benner, S. A., Butler, T., et al. (2008). The potential and challenges of nanopore sequencing. *Nat. Biotechnol.* 26, 1146–1153. doi: 10.1038/nbt.1495

Braun, S. D., Ahmed, M. F., El-Adawy, H., Hotzel, H., Engelmann, I., Weiß, D., et al. (2016). Surveillance of extended-Spectrum Beta-lactamase-producing *Escherichia coli* in dairy cattle farms in the Nile Delta. *Front. Microbiol.* 7:1020. doi: 10.3389/fmicb.2016.01020

Brilhante, M., Menezes, J., Belas, A., Feudi, C., Schwarz, S., Pomba, C., et al. (2020). OXA-181-producing Extraintestinal pathogenic *Escherichia coli* sequence type 410 isolated from a dog in Portugal. *Antimicrob. Agents Chemother.* 64, e02298–e02219. doi: 10.1128/AAC.02298-19

Cavaco, L. M., Abatih, E., Aarestrup, F. M., and Guardabassi, L. (2008). Selection and persistence of CTX-M-producing *Escherichia coli* in the intestinal flora of pigs treated with amoxicillin, ceftiofur, or cefquinome. *Antimicrob. Agents Chemother.* 52, 3612–3616. doi: 10.1128/AAC.00354-08

Cuzon, G., Ouanich, J., Gondret, R., Naas, T., and Nordmann, P. (2011). Outbreak of OXA-48-positive carbapenem-resistant Klebsiella pneumoniae isolates in France. *Antimicrob. Agents Chemother.* 55, 2420–2423. doi: 10.1128/AAC.01452-10

Diaconu, E. L., Carfora, V., Alba, P., Di Matteo, P., Stravino, F., Buccella, C., et al. (2020). Novel IncFII plasmid harboring bla_{NDM-4} in a carbapenem-resistant *Escherichia coli* of pig origin, Italy. *J. Antimicrob. Chemother.* 75, 3475–3479. doi: 10.1093/jac/dkaa374

European Food Safety Authority (EFSA) (2010). Analysis of the baseline survey on the prevalence of methicillin-resistant Staphylococcus aureus (MRSA) in holdings with breeding pigs, in the EU, 2008, part B: factors associated with MRSA contamination of holdings; on request from the European Commission. *EFSA J.* 8:1597. doi: 10.2903/j.efsa.2010.1597

European Food Safety Authority (EFSA), Amore, G., Beloeil, P.-A., Garcia Fierro, R., Guerra, B., Papanikolaou, A., et al. (2021). Manual for reporting 2021 antimicrobial resistance data within the framework of directive 2003/99/EC and decision 2020/1729/EU. EFSA supporting publication 2021:EN-6652. 31pp.

European Food Safety Authority (EFSA) and European Center for Disease Prevention and Control (ECDC) (2019). The European Union summary report on antimicrobial resistance in zoonotic and indicator bacteria from humans, animals and food in 2017. *EFSA J.* 17:e05598. doi: 10.2903/j.efsa.2019.5598

European Food Safety Authority (EFSA) and European Center for Disease Prevention and Control (ECDC) (2021). The European Union summary report on AntimicrobialResistance in zoonotic and indicator bacteria from humans, animals and food in 2018/2019. *EFSA J.* 19:6490. doi: 10.2903/j.efsa.2021.6490

Goris, J., Konstantinidis, K. T., Klappenbach, J. A., Coenye, T., Vandamme, P., and Tiedje, J. M. (2007). DNA-DNA hybridization values and their relationship to whole-genome sequence similarities. *Int. J. Syst. Evol. Microbiol.* 57, 81–91. doi: 10.1099/ijs.0.64483-0

Gurevich, A., Saveliev, V., Vyahhi, N., and Tesler, G. (2013). QUAST: quality assessment tool for genome assemblies. *Bioinformatics* 29, 1072–1075. doi: 10.1093/bioinformatics/btt086

Irrgang, A., Pauly, N., Tenhagen, B. A., Grobbel, M., Kaesbohrer, A., and Hammerl, A. J. A. (2020a). Spill-over from public health? First detection of an OXA-48-producing Escherichia coli in a German pig farm. *Microorganisms* 8:855. doi: 10.3390/microorganisms8060855

Irrgang, A., Tausch, S. H., Pauly, N., Grobbel, M., Kaesbohrer, A., and Hammerl, J. A. (2020b). First detection of GES-5-producing *Escherichia coli* from livestock-an increasing diversity of Carbapenemases recognized from German pig production. *Microorganisms* 8:1593. doi: 10.3390/microorganisms8101593

Irrgang, A., Tenhagen, B.-A., Pauly, N., Schmoger, S., Kaesbohrer, A., and Hammerl, J. A. (2019). Characterization of VIM-1-Producing *E. coli* isolated from a German fattening pig farm by an improved isolation procedure. *Front. Microbiol.* 10:2256. doi: 10.3389/fmicb.2019.02256

Jensen, R. B., and Gerdes, K. (1995). Programmed cell death in bacteria: proteic plasmid stabilization systems. *Mol. Microbiol.* 17, 205–210. doi: 10.1111/j.1365-2958.1995.mmi_17020205.x

Katz, L. S., Griswold, T., Morrison, S. S., Caravas, J. A., Zhang, S., Bakker, H., et al. (2019). Mashtree: a rapid comparison of whole genome sequence files. *J. Open Source Software* 4:1762. doi: 10.21105/joss.01762

Kidd, J. M., Livermore, D. M., and Nicolau, D. P. (2020). The difficulties of identifying and treating Enterobacterales with OXA-48-like carbapenemases. *Clin. Microbiol. Infect.* 26, 401–403. doi: 10.1016/j.cmi.2019.12.006

Li, R., Du, P., Zhang, P., Li, Y., Yang, X., Wang, Z., et al. (2021). Comprehensive genomic investigation of coevolution of mcr genes in *Escherichia coli* strains via Nanopore sequencing. *Global Chall.* 5:2000014. doi: 10.1002/gch2.202000014

Lunha, K., Chanawong, A., Lulitanond, A., Wilailuckana, C., Charoensri, N., Wonglakorn, L., et al. (2016). High-level carbapenem-resistant OXA-48-producing *Klebsiella pneumoniae* with a novel OmpK36 variant and low-level, carbapenem-resistant, non-porin-deficient, OXA-181-producing *Escherichia coli* from Thailand. *Diagn. Microbiol. Infect. Dis.* 85, 221–226. doi: 10.1016/j.diagmicrobio.2016.03.009

Luppi, A. (2017). Swine enteric colibacillosis: diagnosis, therapy and antimicrobial resistance. *Porcine Health Manag.* 3:16. doi: 10.1186/s40813-017-0063-4

Mairi, A., Pantel, A., Sotto, A., Lavigne, J. P., and Touati, A. (2018). OXA-48-like carbapenemases producing E*nterobacteriaceae* in different niches. *Eur. J. Clin. Microbiol. Infect. Dis.* 37, 587–604. doi: 10.1007/s10096-017-3112-7

Marchetti, V. M., Bitar, I., Mercato, A., Nucleo, E., Bonomini, A., Pedroni, P., et al. (2020). Complete nucleotide sequence of plasmids of two *Escherichia coli* strains carrying bla_{NDM-5} and bla_{NDM-5} and $bla_{OXA-181}$ from the same patient. *Front. Microbiol.* 10:3095. doi: 10.3389/fmicb.2019.03095

Navarro-San Francisco, C., Mora-Rillo, M., Romero-Gómez, M. P., Moreno-Ramos, F., Rico-Nieto, A., Ruiz-Carrascoso, G., et al. (2013). Bacteraemia due to OXA-48-carbapenemase-producing Enterobacteriaceae: a major clinical challenge. *Clin. Microbiol. Infect.* 19, E72–E79. doi: 10.1111/1469-0691.12091

Nigg, A., Brilhante, M., Dazio, V., Clément, M., Collaud, A., Gobeli Brawand, S., et al. (2019). Shedding of OXA-181 carbapenemase-producing *Escherichia coli* from companion animals after hospitalization in Switzerland: an outbreak in 2018. *Euro Surveill.* 24:1900071. doi: 10.2807/1560-7917.ES.2019.24.39.1900071

Nordmann, P., and Poirel, L. (2014). The difficult-to-control spread of carbapenemase producers among Enterobacteriaceae worldwide. *Clin. Microbiol. Infect.* 20, 821–830. doi: 10.1111/1469-0691.12719

Ouédraogo, A. S., Compain, F., Sanou, M., Aberkane, S., Bouzinbi, N., Hide, M., et al. (2016). First description of IncX3 plasmids carrying $bla_{OXA-181}$ in *Escherichia coli* clinical isolates in Burkina Faso. *Antimicrob. Agents Chemother.* 60, 3240–3242. doi: 10.1128/AAC.00147-16

Piazza, A., Comandatore, F., Romeri, F., Pagani, C., Floriano, A. M., Ridolfo, A., et al. (2018). First report of an ST410 OXA-181 and CTX-M-15 coproducing *Escherichia coli* clone in Italy: a whole-genome sequence characterization. *Microb. Drug Resist.* 24, 1207–1209. doi: 10.1089/mdr.2017.0366

Pitout, J. D. D., Peirano, G., Kock, M. M., Strydom, K. A., and Matsumura, Y. (2019). The global ascendency of OXA-48-type Carbapenemases. *Clin. Microbiol. Rev.* 33, e00102–e00119. doi: 10.1128/CMR.00102-19

Poirel, L., Naas, T., and Nordmann, P. (2008). Genetic support of extended-spectrum beta-lactamases. *Clin. Microbiol. Infect.* 14, 75–81. doi: 10.1111/j.1469-0691.2007.01865.x

Poirel, L., Walsh, T. R., Cuvillier, V., and Nordmann, P. (2011). Multiplex PCR for detection of acquired carbapenemase genes. *Diagn. Microbiol. Infect. Dis.* 70, 119–123. doi: 10.1016/j.diagmicrobio.2010.12.002

Potron, A., Nordmann, P., Lafeuille, E., Al Maskari, Z., Al Rashdi, F., and Poirel, L. (2011a). Characterization of OXA-181, a carbapenem-hydrolyzing class D beta-lactamase from *Klebsiella pneumoniae*. *Antimicrob. Agents Chemother.* 55, 4896–4899. doi: 10.1128/AAC.00481-11

Potron, A., Poirel, L., and Nordmann, P. (2011b). Origin of OXA-181, an emerging carbapenem-hydrolyzing oxacillinase, as a chromosomal gene in *Shewanella xiamenensis*. *Antimicrob. Agents Chemother.* 55, 4405–4407. doi: 10.1128/AAC.00681-11

Pulss, S., Semmler, T., Prenger-Berninghoff, E., Bauerfeind, R., and Ewers, C. (2017). First report of an *Escherichia coli* strain from swine carrying an OXA-181 carbapenemase and the colistin resistance determinant MCR-1. *Int. J. Antimicrob. Agents* 50, 232–236. doi: 10.1016/j.ijantimicag.2017.03.014

Qin, S., Cheng, J., Wang, P., Feng, X., and Liu, H. M. (2018). Early emergence of OXA-181-producing *Escherichia coli* ST410 in China. *J. Glob. Antimicrob. Resist.* 15, 215–218. doi: 10.1016/j.jgar.2018.06.017

Rodríguez, O. L., Sousa, A., Pérez-Rodríguez, M. T., Martínez-Lamas, L., Suárez, R. L., Martínez, C. T., et al. (2021). Mortality-related factors in patients with

OXA-48 carbapenemase-producing *Klebsiella pneumoniae* bacteremia. *Medicine* 100:e24880. doi: 10.1097/MD.0000000000024880

Rojas, L. J., Hujer, A. M., Rudin, S. D., Wright, M. S., Domitrovic, T. N., Marshall, S. H., et al. (2017). NDM-5 and OXA-181 Beta-lactamases, a significant threat continues to spread in the Americas. *Antimicrob. Agents Chemother.* 61, e00454–e00417. doi: 10.1128/AAC.00454-17

Ruppé, E., Armand-Lefèvre, L., Estellat, C., El-Mniai, A., Boussadia, Y., Consigny, P. H., et al. (2014). Acquisition of carbapenemase-producing *Enterobacteriaceae* by healthy travelers to India, France, February 2012 to march 2013. *Euro Surveill.* 19:20768. doi: 10.2807/1560-7917.es2014.19.14.20768

Schwengers, O., Jelonek, L., Dieckmann, M. A., Beyvers, S., Blom, J., and Goesmann, A. (2021). Bakta: rapid and standardized annotation of bacterial genomes via alignment-free sequence identification. *Microb. Genom.* 7:000685. doi: 10.1099/mgen.0.000685

Truong, D. T. Q., Hounmanou, Y. M. G., Dang, S. T. T., Olsen, J. E., Truong, G. T. H., Tran, N. T., et al. (2021). Genetic comparison of ESBL-producing Escherichia coli from workers and pigs at Vietnamese pig farms. *Antibiotics* 10:1165. doi: 10.3390/antibiotics10101165

Villa, L., Carattoli, A., Nordmann, P., Carta, C., and Poirel, L. (2013). Complete sequence of the IncT-type plasmid pT-OXA-181 carrying the $bla_{OXA-181}$ carbapenemase gene from *Citrobacter freundii*. *Antimicrob. Agents Chemother.* 57, 1965–1967. doi: 10.1128/AAC.01297-12

Wick, R. R., Judd, L. M., Gorrie, C. L., and Holt, K. E. (2017). Unicycler: resolving bacterial genome assemblies from short and long sequencing reads. *PLoS Comput. Biol.* 13:e1005595. doi: 10.1371/journal.pcbi.1005595

Yang, G. Y., Guo, L., Su, J. H., Zhu, Y. H., Jiao, L. G., and Wang, J. F. (2019). Frequency of Diarrheagenic virulence genes and characteristics in *Escherichia coli* isolates from pigs with diarrhea in China. *Microorganisms.* 7:308. doi: 10.3390/microorganisms7090308

Zheng, J., Peng, D., Ruan, L., and Sun, M. (2013). Evolution and dynamics of megaplasmids with genome sizes larger than 100 kb in the Bacillus cereus group. *BMC Evol. Biol.* 13:262. doi: 10.1186/1471-2148-13-262

Frontiers in Microbiology

Explores the habitable world and the potential of microbial life

The largest and most cited microbiology journal which advances our understanding of the role microbes play in addressing global challenges such as healthcare, food security, and climate change.

Discover the latest Research Topics

See more →

Frontiers

Avenue du Tribunal-Fédéral 34
1005 Lausanne, Switzerland
frontiersin.org

Contact us

+41 (0)21 510 17 00
frontiersin.org/about/contact